Title
GPCR-biased control of the endocytic network by β-arrestin

Author
Barsi-Rhyne, Benjamin

Publication Date
2022

Peer reviewed|Thesis/dissertation

GPCR-biased control of the endocytic network by β-arrestin

by
Benjamin Barsi-Rhyne

DISSERTATION
Submitted in partial satisfaction of the requirements for degree of
DOCTOR OF PHILOSOPHY

in

Biochemistry and Molecular Biology

in the

GRADUATE DIVISION
of the
UNIVERSITY OF CALIFORNIA, SAN FRANCISCO

Approved:

DocuSigned by:
Robert Edwards
91579E192F544AF...

Robert Edwards
Chair

DocuSigned by:
Mark von Zastrow
D4C...

Mark von Zastrow

DocuSigned by:
Aashish Manglik
...414...

Aashish Manglik

DocuSigned by:
Adam Frost
A1BE03C1C9924A7...

Adam Frost

Committee Members

Dedication & Acknowledgements

The text of this dissertation includes a reprint of “Catalytic activation of β-arrestin by GPCRs" as it appears in *Nature* 557.7705 (2018): 381-386, a preprint that is under review at Cell (Janetzko, Kise et al 2022 bioRxiv), and one manuscript being prepared for submission (Barsi-Rhyne, Manglik, and von Zastrow). Two additional studies that Benjamin Barsi-Rhyne contributed to, one published in Nature Communications. 2016 Mar 18; 7:11046 and another published in Science. 2020 Dec 18;370(6523):1473-1479, were excluded as they were beyond the scope of this dissertation.

The coauthors, Mark von Zastrow and Aashish Manglik, directed and supervised the research described in this dissertation. Benjamin Barsi-Rhyne provided the experimentation and manuscript preparation for much of the following dissertation, which includes substantial and comparable contribution to that of other dissertations in Pharmacology and Cell Biology. Collaborative contributions from others are specified on the title pages of the relevant chapters.

-Mark von Zastrow, M.D., Ph.D. & Aashish Manglik, M.D., Ph.D.

This work would not have been possible without the scientific and moral support from many colleagues, friends, and family members.

First and foremost, I must acknowledge my adviser, Mark von Zastrow. He is a tireless supporter of his trainees, and I am lucky to count myself among them. His infectious curiosity and excitement for science made even the hardest periods of graduate school manageable. I will always be thankful for his mentorship, which provided space to become more independent while giving me support during crucial periods. Mark is an exceptional scientist whose brilliance, kindness, and generosity have had a tremendous impact on our understanding of cell biology and the people who study it.

Aashish Manglik, my co-adviser, was always incredibly supportive and gave new energy to my graduate studies. His training exposed me to an entirely new set of techniques, and I hope I absorbed some of his rigorous, creative, and efficient approach to science. We had many wonderful conversations and he provided me with many excellent opportunities to pursue interesting questions.

The von Zastrow lab was an amazing place to receive my graduate training. Rubbing elbows with many excellent lab members helped me to grow as a scientist, a colleague, and a friend. The postdoctoral fellows taught me many things and could always be counted on to bring good humor, creativity, and helpful advice to our many discussions. Braden Lobingier was incredibly helpful and generous with his time. I cannot believe he let me bug him with questions multiple times a day for years. Damien Jullié approached his science with endurance, intensity, and good humor that I'm still trying to emulate. Miriam Stöber was a positive force in the lab

who was always tuned into my science and asked me many thought provoking questions. Nina Tsevtanova was, and still is, the most efficient scientist I have ever met. Emily Blythe is an exceptional and thorough scientist who is fearless in her approach. I enjoyed our many discussions about the challenges and joys of science and of life. Yasunori Uchida, Rita Fagan, and Nicole Fisher were wonderful to have in the lab and made working there a lot of fun.

The von Zastrow graduate students became some of my best friends. Grace Peng was always there when I needed emotional support and knew when exactly when a dose of tough love was called for. She is one of the funniest and most engaging people I have ever met. Kelsie Eichel, my rotation mentor, helped me gain confidence as a scientist and could always be counted on to appreciate my dark humor and to go on adventures. André Lazar was a source of many hilarious conversations and for commiseration when necessary. Joy Li was a wonderful bench mate whose positive attitude, curiosity, and lemon jam made for many good times. Brian Wysolmerski was a great colleague and coffee partner. Max Thompson was a fantastic mentee who always had highly entertaining riffs. Alison Leaf and Kate Varandas, the senior graduate students when I joined the lab, were exceptionally welcoming and doled out many pieces of shrewd advice that helped me gain my footing.

The Manglik lab was my second home, and I couldn't have asked for a more welcoming group of people. Christian Billesbølle and Jiahao Liang, the only lab members when I joined, helped me in countless ways and were always great fun to be around. Christian is a talented and thoughtful scientist who taught me much about working with proteins. Jiahao was always having a great time in lab. I miss his positive energy. Ishan Deshpande always made time to talk to me about my science and provided helpful feedback. Julian Harris, a truly remarkable

graduate student, taught me more about scientific communication and teaching than anyone else. Nick Hoppe, Bryan Faust, and Chase Webb were always engaging whether we were in the lab or pursuing outdoor adventures.

UCSF was a wonderful place to be a graduate student. My thesis committee, in addition to Mark and Aashish, included Adam Frost and Robert Edwards. They both gave me wonderful pieces of advice in science and in preparing for life after graduate school. Their outside perspectives were critical in shaping the direction of my project and how to communicate it to a broad audience.

My fellow Tetrad students were like a large family who provided me with support and companionship countless times. Among them I'm most thankful for Karen Cheng, Aditya Anand, Kelsey Haas, Elise Nunez, Madeline Keenan, Valentina Garcia, and Nairi Hartooni. I could not have asked for better friends.

Finally, I dedicate this thesis to my wife, Kristine Miller; my parents, James Rhyne and Dana Barsi; my siblings, Nick Barsi-Rhyne, Daniel Rhyne, and Rachel Barsi; as well as my in-laws, Eileen Zefting and Rod Miller. I certainly would not have made it through graduate school without their constant love and support.

Abstract

GPCR-biased control of the endocytic network by β-arrestin

by

Benjamin Barsi-Rhyne

This thesis focuses on the signaling and trafficking functions of β-arrestins, which are critical regulators and transducers for the large G protein-coupled receptor (GPCR) family. The introductory chapter will briefly cover GPCR biology, how the β-arrestins were discovered, the current understanding of the GPCR/β-arrestin complex and how it affects the core β-arrestin functions of desensitization, internalization, and β-arrestin-mediated signaling. The second chapter describes a new cellular mechanism for β-arrestin function termed 'catalytic activation' where β-arrestins briefly bind to GPCRs, become activated, and then remain active after dissociation. The third chapter explores the role of phosphoinositides in β-arrestin conformation and function. The fourth chapter will discuss new approaches to understanding the conformational states of β-arrestins. The fifth chapter describes a new mechanism of β-arrestin–mediated trafficking and provides a framework for understanding how β-arrestins transduce receptor-specific functions. The final chapter summarizes some major advances, discusses how these fit with the established findings, and suggests future directions.

Table of Contents

List of Figures

List of Tables

Chapter 1: Introduction

1.1 Overview

This thesis is focuses on the β-arrestins, a pair of proteins that are critical to the regulation and signal transduction of G protein-coupled receptors (GPCRs). This introductory chapter will briefly describe how GPCRs are essential to human physiology, the discovery of arrestins, how the arrestin/GPCR complex is formed, recent structural insights, and the classical understanding of β-arrestins' role in GPCR signal attenuation, their role in GPCR trafficking, and a current view of arrestin-mediated signaling.

1.2 The relevance of G protein-coupled receptors

Cells are the fundamental unit of life. They produce molecules and sequester them away from the environment where they organize them into intricate structures. One type of molecule, receptors, are key to cell and organismal survival because they detect and respond to changes in the extracellular environment. A family of receptors, called G protein-coupled receptors, are one of the largest cell surface receptor families and because of their diversity they can detect a wide variety of physical and chemical stimuli. Their localization to the plasma membrane, the structure that defines the boundary of a cell, exposes receptor segments to both the extracellular and intracellular environment, thereby allowing them to directly detect and convert an external stimulus into an intracellular response. The ability of GPCRs to carry out this function across a range of cell types places them at important regulatory points of nearly every physiological process, whether it is the perception of the environment by enabling sight, smell, and taste; regulating homeostatic processes such as immunity and blood pressure; and even modulating mood and behavior. As such, misfunction of GPCRs often leads to disease. Luckily, studying GPCRs has allowed for the development of many therapeutics that directly act on these receptors or their downstream signaling pathways.

Most GPCR signaling is initiated when a ligand binds to the extracellular surface of a receptor, resulting in a conformational change that is propagated to its intracellular face. This shape change can be recognized by intracellular effector proteins such as heterotrimeric G proteins and β-arrestins, which together determine much of the downstream cellular response. For G proteins, the activated receptor acts as a guanine nucleotide exchange factor (GEF), an enzyme that promotes exchange of GDP for GTP at the G_{α} subunit, thereby activating it and triggering its dissociation from $G_{\beta\gamma}$ subunits. Once dissociated, G protein subunits can then go

on to activate downstream proteins that produce second messenger responses, such as changing ion concentration or initiating kinase cascades, that ultimately determine the behavior of the cell. This system is also exquisitely sensitive to extracellular stimuli as G protein activation can occur multiple times at a single activated GPCR, allowing for a small stimulus to produce a greatly amplified intracellular response. The response, if left unchecked, would prevent the cell from responding to other stimuli, so cells apply additional regulation. For GPCRs, the main regulators are the arrestins.

1.3 A brief history of arrestins

If heterotrimeric G proteins were discovered as the activators of downstream GPCR signaling, arrestin, as its name implies, was discovered as a signal inactivator. The founding member of the arrestin family, originally called 'retinal S antigen' and now referred to as visual arrestin or arrestin-1, was found to bind tightly to light activated and phosphorylated rhodopsin, a light sensitive GPCR in the retina, thereby preventing heterotrimeric G protein association and desensitizing rhodopsin. Shortly thereafter, visual arrestin was found to serve a similar function for the phosphorylated beta-2 adrenergic receptor (β2AR), although only at much higher concentrations than for rhodopsin. This finding and the discovery that the kinase responsible for β2AR phosphorylation attenuated signaling when crudely prepared but not when purified, led to the hypothesis that a protein analogous to visual arrestin was responsible for the majority of β2AR signal desensitization (Benovic, Kuhn et al. 1987). A search for this protein, using visual arrestin sequence as a probe against cDNA, yielded a protein that was named β-arrestin due to its ability to efficiently desensitize phosphorylated β2ARs (Lohse, Benovic et al. 1990). A couple of years later a second β-arrestin, currently referred to as β-arrestin-2 or arrestin-3, was discovered through a similar approach (Attramadal, Arriza et al. 1992). The final member of the arrestin family to be discovered, cone arrestin or arrestin-4, controls signaling from the color opsins in cone cells of the retina (Craft, Whitmore et al. 1994).

All four members of the arrestin family are similar in their sequence and structures but differ considerably in their expression, receptor specificity, and functions. The most restricted, visual arrestin or arrestin-1, physiologically regulates only rhodopsin, while the least restrictive, β-arrestin-1 and -2, regulate hundreds of GPCRs across most tissues and have the additional functions of promoting signaling and GPCR trafficking (Gurevich and Gurevich 2019). The

desensitization function, which is common to all arrestins, is due to their ability to bind tightly to activated and phosphorylated GPCRs. They can do this because the general arrestin structure, which contains two lobes made of β-sandwich domains that are connected by a hinge and central crest, have a shape that complements the intracellular face of GPCRs. The GPCR transmembrane bundle accepts a portion of the central crest and the phosphorylated cytoplasmic tail that binds a groove in the arrestin N-lobe (Shukla 2013). While highly similar in structure and sequence, the arrestins diverge at their C-terminus, which all extend from the C-lobe and bind to the same N-lobe groove as the GPCR cytoplasmic tail (Hirsch, Schubert et al. 1999, Han, Gurevich et al. 2001). The C-terminus of β-arrestins, unlike the visual arrestins, contains binding sites for clathrin and AP2β, giving them the unique ability to promote GPCR internalization through clathrin-mediated endocytosis (Goodman, Krupnick et al. 1996, Laporte, Oakley et al. 2000, Moaven, Koike et al. 2013). This final point, and an update to the classical understanding it represents, is further discussed in chapters two, five, and six in this thesis.

1.4 The GPCR/arrestin complex

Arrestin association with an activated GPCR, whether stable or very transient (see chapter 2), is required for arrestins to exert their effects on receptor signaling and trafficking. Much of our understanding of the GPCR/arrestin complex stems from biochemical studies of the visual system where arrestin binds to light-activated and phosphorylated rhodopsin (Rh) to form a tight (~3-4 nM) complex (Bayburt, Vishnivetskiy et al. 2011). Initial experiments showed that small amounts of R/arrestin complex could be detected with either phosphorylated or light-activated rhodopsin, but tight complex formation required both (Gurevich and Benovic 1992). This suggested a multisite binding mechanism and led to the proposal that arrestin has two sensors – one for conformationally activated Rh and the other for Rh attached phosphates. Multiple biochemical and structural studies over following decades have supported this proposal and refined our understanding of both the GPCR activation sensor, the arrestin finger loop that probes GPCR transmembrane bundle and other areas facing the receptor, and the phosphate sensor, a groove in the N-lobe, basally associated with the arrestin C-terminus, that binds the phosphorylated receptor cytoplasmic tail (2014). We have also come to understand that arrestin undergoes significant conformational transitions upon rhodopsin binding to these sensors (Gurevich and Gurevich 2004, Kang 2015). The combination of multisite binding, and the arrestin conformational transitions it produces, allows arrestin to bind specifically and with high affinity to activated and phosphorylated rhodopsin thereby blocking further G protein association and arresting signaling.

Both the receptor activation (finger loop) and phosphorylation sensors (N-lobe groove), as well as other sensors not found in visual arrestin (see chapter 3), are conserved in the β-arrestins. Unlike in visual arrestin, these sensors in β-arrestin allow for an unusual level of promiscuity.

The β-arrestins bind to and regulate hundreds of distinct GPCRs that differ, sometimes substantially, in the makeup of their transmembrane core as well as in the number and distribution of phosphates that decorate their intracellular surface. Despite the promiscuity of the β-arrestins, formation of the GPCR/β-arrestin complex is thought to be largely like that observed for the visual system. A notable exception is that receptor binding to phosphate sensor in β-arrestins triggers exposure of clathrin-coated pit binding motifs, that are absent in visual arrestin, allowing β-arrestin to promote receptor accumulation into the clathrin-coated pit and subsequent receptor internalization (see chapter 5) (Tian, Kang et al. 2014). Discovery of this endocytic function led directly to initial and striking observations of how GPCRs leverage the promiscuity of β-arrestins to produce receptor-specific effects. An early example of this was the observation that some receptors remain associated with β-arrestin after receptor endocytosis and appear to resensitize slowly, called 'Class B' GPCRs, while others dissociate rapidly and resensitize quickly, 'Class A' GPCRs (Oakley, Laporte et al. 1999, Oakley, Laporte et al. 2000). Further investigation showed that this difference could be explained by the distinct phosphorylation patterns on receptors that produce strong (Class B) or weak (Class A) engagement of the β-arrestin phosphorylation sensor (Oakley, Laporte et al. 2001). These results showed that receptor-specific differences in the β-arrestin/GPCR complex could produce distinct downstream signaling effects.

Around this time, β-arrestin-mediated signaling was discovered (Luttrell, Ferguson et al. 1999) and was later proposed to promote kinase activation independently of G protein signaling (Wei, Ahn et al. 2003). β-arrestins are believed to do this by scaffolding multiple members of a kinase pathway, such as cRaf/MEK/ERK, thereby promoting signaling by bringing pathway members together in space and time (Gurevich and Gurevich 2014, Gurevich and Gurevich 2018). Here

again, the receptor phosphorylation pattern appears to play a role. Differences in GRK2/3- or GRK5/6-mediated receptor phosphorylation and their associated differences in β-arrestin-mediated signaling led to the proposal of receptor phosphorylation 'barcodes'(Nobles 2011). According to this model, differences in this barcode, either at different receptors or at the same receptor but with different agonists, produce different β-arrestin active conformations, some that produce β-arrestin-mediated signaling and others that do not. While the G protein independence of β-arrestin-mediated signaling has become controversial (see chapter 1.7) (Gurevich and Gurevich 2018), the hypothesis that distinct receptor phosphorylation barcodes can produce distinct β-arrestin active states has gained significant support. Recent experiments in living cells showed that receptor-specific β-arrestin 'conformational signatures' correlate with β-arrestin-mediated signaling (Lee 2016) and others have linked distinct phosphorylation patterns to distinct signaling outcomes (Bouzo-Lorenzo 2016, Sente, Peer et al. 2018). In addition, biophysical experiments, done with multiple distinct receptor phosphopeptides, showed that β-arrestins can adopt multiple active conformations that may be linked to different signaling effects (Yang 2015, Nuber 2016, Mayer, Damberger et al. 2019).

Much of our understanding of the GPCR/arrestin complex, and the functions its formation enables, has focused on the role of receptor phosphorylation and its interaction with the β-arrestin phosphorylation sensor. By contrast, how the β-arrestin activation sensor interacts with the GPCR core and whether it produces distinct functional effects has not been studied until recently.

Two studies have shown that the GPCR core can promote β-arrestin activation without co-engagement of the GPCR cytoplasmic tail (Eichel, Jullié et al. 2018, Latorraca, Wang et al.

2018). One of these, the subject of chapter two, demonstrated that β-arrestins can be catalytically activated (i.e., remain active after GPCR dissociation), a form of activation that is linked to a novel type of β-arrestin-mediated signaling (Eichel, Jullié et al. 2016).

Yet other studies have suggested that some GPCR transmembrane bundles do not engage the β-arrestin activation sensor but remain bound purely by association with the β-arrestin phosphate sensor (Shukla 2014, Thomsen, Plouffe et al. 2016, Cahill, Thomsen et al. 2017). The functional consequence of this type of complex, called the hanging orientation, is that β-arrestins cannot sterically occlude G protein binding. This finding may explain earlier observations of sustained G protein signaling from multiple GPCRs (Calebiro, Nikolaev et al. 2009, Ferrandon, Feinstein et al. 2009).

Taken together, the observations described here, and many other studies that escaped mention, show that the β-arrestin/GPCR complex is essential for producing and regulating many trafficking and signaling functions. They also underscore how the promiscuity of β-arrestins has been leveraged by the large GPCR family to 'program' β-arrestin function in a highly receptor-specific manner. The following sections will briefly describe structural advances in understanding GPCR/β-arrestin complexes and a current view of β-arrestins core functions: desensitization, internalization, and signaling.

1.5 Structural understanding of arrestin

The first structure of an inactive arrestin revealed that the overall molecular architecture consisted of two convex lobes, made of β-sandwich domains, connected by a hinge, and suggested a site for activated and phosphorylated rhodopsin binding in the N-lobe (Granzin, Wilden et al. 1998). Additional insight into the inactive conformation was gained upon release of an additional structure showing that the arrestin C-terminus is bound to the N-lobe where it stabilizes a polar core network of interactions, an arrangement that is conserved in the β-arrestins (Hirsch, Schubert et al. 1999). Transition from the inactive to active conformation was visualized upon the release of two structures, one of a naturally occurring truncation of visual arrestin (p44) and another of a phosphopeptide bound β-arrestin-1 stabilized by a Fab (fragment antigen binding). Both showed that the two lobes of arrestins twist relative to each other (Kim, Hofmann et al. 2013, Shukla, Manglik et al. 2013). Together, along other papers not mentioned here, these structural insights led to the current model of arrestin activation. It says that the phosphorylated GPCR cytoplasmic tail binds to a groove in the N-lobe of arrestins, breaking the polar core, displacing the arrestin C-terminus, and causing an inter-lobe twist of roughly 15-20°.

While these findings describe in high structural detail the role of the arrestin phosphate sensor, a similar level of understanding for the arrestin activation sensor was has only recently started to emerge. It turns out that this sensor is distributed along the receptor facing surface in arrestins (Latorraca, Wang et al. 2018) and was observed first in a arrestin/GPCR structure consisting of visual arrestin and rhodopsin (Kang 2015). This structure showed that the arrestin finger loop inserts into the open transmembrane bundle of the GPCR (a caveat of this structure is that it is a fusion protein of a pre-activated arrestin and rhodopsin).

In the past two years, multiple β-arrestin/GPCR structures have been published showing a few interesting structural features. One of β-arrestin-1 and NTSR1 shows that β-arrestin is rotated relative to the arrestin/rhodopsin structure by about 90° (Yin, Li et al. 2019), suggesting a mechanism by which GPCRs with phosphorylated ICL3s can bind and activate β-arrestins. The second, a M2R-V2R chimeric receptor bound to β-arrestin-1 in lipid nanodiscs, showed that the β-arrestin C-edge can be inserted into the membrane (Staus, Hu et al. 2020), suggesting a cooperative interaction between the receptor and membrane to enhance β-arrestin binding. A third, NTSR1/β-arrestin-1 in a micelle, showed that a $PI_{(4,5)}P_2$ molecule can bridge the receptor/arrestin interface (Huang, Masureel et al. 2020), suggesting additional regulation (see chapter 3). Importantly, this structure is currently the only β-arrestin/GPCR structure not stabilized by Fab30. Finally, a fourth structure of a β1AR/V2R chimeric receptor bound to β-arrestin-1 and the biased agonist formoterol showed a slightly different agonist binding pose when compared to the same receptor bound G protein, suggesting that agonists could be specifically designed to achieve β-arrestin bias (Lee, Warne et al. 2020). Interestingly, all these GPCRs are in different poses relative to β-arrestin-1, suggesting that there is some flexibility in GPCR/β-arrestin binding interface. Surprisingly, despite these differences, β-arrestin-1 adopts a similar degree of N/C-lobe twist regardless of the bound receptor and whether Fab30 is present. Although, this may be biased by the presence of Fab30 in three-quarters of the structures. In contrast to the similar β-arrestin conformations across these receptors, some phosphopeptide bound β-arrestin structures have shown conformational differences (i.e., less twist or other smaller changes) (Min, Yoon et al. 2020, He, Xiao et al. 2021).

Taken together, these findings represent major advances in understanding GPCR/arrestin function through structure. Currently, the only solved receptor/arrestin structures are those that form tight complexes, a limitation that will hopefully be overcome in future studies.

1.6 β-arrestin–mediated desensitization

Our understanding of arrestins ability to turn off G protein signaling also stems from the visual system where signaling is abolished through multisite phosphorylation of rhodopsin and subsequent binding by visual arrestin. As visual arrestin and heterotrimeric G protein share a binding site at the transmembrane core of the receptor, tight binding by visual arrestin sterically hinders further G protein activation (Wilden, Wust et al. 1986, Wilden 1995). This model was later extended beyond the visual system, where the many non-rhodopsin GPCRs can be phosphorylated by other kinases and subsequently bound by the β-arrestins at the plasma membrane (Krasel, Bunemann et al. 2005).

Internalization by β-arrestins, a function absent in visual arrestin, was thought to promote further down regulation of receptor signaling. Recently this paradigm has started to shift, as a few GPCRs have been reported to produce sustained G protein signaling despite remaining bound by β-arrestins after their internalization (Calebiro, Nikolaev et al. 2009, Ferrandon, Feinstein et al. 2009, Feinstein, Yui et al. 2013, Thomsen, Plouffe et al. 2016). This is apparently possible because β-arrestins can adopt distinct poses upon binding to a certain class of GPCR (Shukla 2014, Thomsen, Plouffe et al. 2016, Cahill, Thomsen et al. 2017, Nguyen, Thomsen et al. 2019). The fully engaged and desensitization competent complex forms when β-arrestins bind both the transmembrane core of the receptor and its phosphorylated cytoplasmic tail. The non-desensitizing complex, by contrast, engages only the phosphorylated cytoplasmic tail, leaving the transmembrane core open for heterotrimeric G protein binding. This second complex, termed the ‘super-complex,’ is a simple explanation for how β-arrests can desensitize some receptors and do not desensitize others.

1.7 β-arrestin–mediated GPCR endocytosis and trafficking

β-arrestins are unique among arrestins in that they are required for agonist-promoted internalization of most GPCRs (Ahn, Nelson et al. 2003, Kohout, Nicholas et al. 2004). The first evidence of this was the observation that mutation of β2AR phosphorylation sites or truncation of its cytoplasmic tail drastically reduced receptor internalization, then called sequestration, and that this defect could be overcome by overexpression of either β-arrestin-1 or -2 (Ferguson, Downey et al. 1996). The interactions responsible for their endocytic function became clear when β-arrestins were shown to bind clathrin and the AP2 β-appendage, which are major components of clathrin-coated pits, through sites in the β-arrestin C-terminus that are not present in visual arrestin (Goodman, Krupnick et al. 1996, Krupnick, Goodman et al. 1997, Laporte, Oakley et al. 2000). Under basal conditions the C-terminus is bound to the N-lobe of β-arrestin, which prevents the CHC and AP2β sites from engaging their partners (Han, Gurevich et al. 2001). This N-lobe site is also responsible for binding the phosphorylated receptor cytoplasmic tail (Nobles, Guan et al. 2007, Shukla 2013), leading to a model in which the phosphorylated GPCR cytoplasmic tail displaces the β-arrestin C-terminus, freeing it to engage its partners at the clathrin-coated pit (Schmid, Ford et al. 2006, Kang, Kern et al. 2009). Once GPCRs are clustered into CCPs, clathrin-mediated endocytosis, a constitutive process, remodels the plasma membrane to produce nascent GPCR containing endosomes that can be subsequently trafficked to multiple cellular locations, ultimately being recycled back to the plasma membrane, or degraded by lysosomes. β-arrestins also appear to control intracellular GPCR trafficking (Oakley, Laporte et al. 1999, Oakley, Laporte et al. 2000), although, how they do prevent recycling is yet to dissected. Factors other than those mentioned above have been also implicated in β-arrestin–mediated endocytosis, such as PI4K, ARF6/ARNO, NSF, the μ

subunit of AP2, PIP5K1A, and others, but their precise roles remain less clear (Tian, Kang et al. 2014).

1.8 β-arrestin–mediated signaling

β-arrestins have also been proposed to serve as signal transducers themselves. The first evidence for this function was the observation that β-arrestins associate with c-Src (cellular Src), a member of the non-receptor tyrosine kinases, upon agonist stimulation of the β2AR and produces a downstream ERK (extracellular signal-regulated kinase), member of the MAP kinase family, response. Later, β-arrestins were shown to scaffold multiple MAPK pathway members (McDonald, Chow et al. 2000, Luttrell, Roudabush et al. 2001). These pathways were proposed to be G protein signaling independent (Wei, Ahn et al. 2003)(Shenoy et al 2006), a claim that has since become controversial. A study utilizing CRISPR/Cas9 and pertussis toxin to produce “zero functional G” cells showed that ERK1/2 activation was not dependent on β-arrestin (Grundmann, Merten et al. 2018). An additional study demonstrated little to no effect on β2AR promoted ERK1/2 phosphorylation upon knockout of both β-arrestins (O’Hayre et al 2017). More recently, a study with conducted with multiple independently derived β-arrestin double knockout cell lines reaffirmed that β-arrestins were involved in ERK1/2 phosphorylation (Luttrell, Wang et al. 2018). Importantly, the experiments that cast doubt on the independence of β-arrestin-mediated signaling did not directly test the hypothesis that β-arrestins can scaffold MAPK pathway members, a hypothesis that is supported by multiple studies (Peterson and Luttrell 2017). As it stands now, β-arrestin–mediated signaling is perhaps best understood as way to amplify kinase signaling cascades initiated by G proteins, though these cascades may differ across cells line or native systems.

1.9 References

(2014). Arrestins - Pharmacology and Therapeutic Potential, Springer, Berlin, Heidelberg.

Ahn, S., et al. (2003). Desensitization, internalization, and signaling functions of beta-arrestins demonstrated by RNA interference. *Proc Natl Acad Sci U S A 100*(4): 1740-1744. 10.1073/pnas.262789099

Attramadal, H., et al. (1992). Beta-arrestin2, a novel member of the arrestin/beta-arrestin gene family. *J Biol Chem 267*(25): 17882-17890.

Bayburt, T. H., et al. (2011). Monomeric rhodopsin is sufficient for normal rhodopsin kinase (GRK1) phosphorylation and arrestin-1 binding. *J Biol Chem 286*(2): 1420-1428. 10.1074/jbc.M110.151043

Benovic, J. L., et al. (1987). Functional desensitization of the isolated beta-adrenergic receptor by the beta-adrenergic receptor kinase: potential role of an analog of the retinal protein arrestin (48-kDa protein). *Proc Natl Acad Sci U S A 84*(24): 8879-8882. 10.1073/pnas.84.24.8879

Bouzo-Lorenzo, M. (2016). Distinct phosphorylation sites on the ghrelin receptor, GHSR1a, establish a code that determines the functions of ß-arrestins. *Sci. Rep. 6*. 10.1038/srep22495

Cahill, T. J., et al. (2017). Distinct conformations of GPCR–β-arrestin complexes mediate desensitization, signaling, and endocytosis. *Proc. Natl. Acad. Sci. U. S. A. 114*(10): 2562-2567. 10.1073/pnas.1701529114

Calebiro, D., et al. (2009). Persistent cAMP-signals triggered by internalized G-protein-coupled receptors. *PLoS Biol 7*(8): e1000172. 10.1371/journal.pbio.1000172

Craft, C. M., et al. (1994). Cone arrestin identified by targeting expression of a functional family. *J Biol Chem 269*(6): 4613-4619.

Eichel, K., et al. (2018). Catalytic activation of β-arrestin by GPCRs. *Nature 557*(7705): 381-386. 10.1038/s41586-018-0079-1

Eichel, K., et al. (2016). β-Arrestin drives MAP kinase signalling from clathrin-coated structures after GPCR dissociation. *Nat. Cell Biol. 18*(3): 303-310. 10.1038/ncb3307

Feinstein, T. N., et al. (2013). Noncanonical control of vasopressin receptor type 2 signaling by retromer and arrestin. *J. Biol. Chem. 288*(39): 27849-27860. 10.1074/jbc.M112.445098

Ferguson, S. S., et al. (1996). Role of beta-arrestin in mediating agonist-promoted G protein-coupled receptor internalization. *Science 271*(5247): 363-366. 10.1126/science.271.5247.363

Ferrandon, S., et al. (2009). Sustained cyclic AMP production by parathyroid hormone receptor endocytosis. *Nat. Chem. Biol. 5*(10): 734-742. 10.1038/nchembio.206

Ferrandon, S., et al. (2009). Sustained cyclic AMP production by parathyroid hormone receptor endocytosis. *Nat Chem Biol 5*(10): 734-742. 10.1038/nchembio.206

Goodman, O. B., et al. (1996). β-Arrestin acts as a clathrin adaptor in endocytosis of the β2-adrenergic receptor. *Nature 383*(6599): 447-450. 10.1038/383447a0

Granzin, J., et al. (1998). X-ray crystal structure of arrestin from bovine rod outer segments. *Nature 391*(6670): 918-921. 10.1038/36147

Grundmann, M., et al. (2018). Lack of beta-arrestin signaling in the absence of active G proteins. *Nat. Commun. 9*(1): 341. 10.1038/s41467-017-02661-3

Gurevich, V. V. and J. L. Benovic (1992). Cell-free expression of visual arrestin. Truncation mutagenesis identifies multiple domains involved in rhodopsin interaction. *J Biol Chem 267*(30): 21919-21923.

Gurevich, V. V. and E. V. Gurevich (2004). The molecular acrobatics of arrestin activation. *Trends Pharmacol Sci 25*(2): 105-111. 10.1016/j.tips.2003.12.008

Gurevich, V. V. and E. V. Gurevich (2014). Overview of different mechanisms of arrestin-mediated signaling. *Curr. Protoc. Pharmacol. 67*. 10.1002/0471141755.ph0210s67

Gurevich, V. V. and E. V. Gurevich (2018). Arrestin-mediated signaling: Is there a controversy? *World J Biol Chem 9*(3): 25-35. 10.4331/wjbc.v9.i3.25

Gurevich, V. V. and E. V. Gurevich (2019). GPCR Signaling Regulation: The Role of GRKs and Arrestins. *Front Pharmacol 10*: 125. 10.3389/fphar.2019.00125

Han, M., et al. (2001). Crystal structure of β-arrestin at 1.9 A: possible mechanism of receptor binding and membrane translocation. *Structure 9*. 10.1016/S0969-2126(01)00644-X

He, Q. T., et al. (2021). Structural studies of phosphorylation-dependent interactions between the V2R receptor and arrestin-2. *Nat Commun 12*(1): 2396. 10.1038/s41467-021-22731-x

Hirsch, J. A., et al. (1999). The 2.8 A crystal structure of visual arrestin: a model for arrestin's regulation. *Cell 97*. 10.1016/S0092-8674(00)80735-7

Huang, W., et al. (2020). Structure of the neurotensin receptor 1 in complex with beta-arrestin 1. *Nature 579*(7798): 303-308. 10.1038/s41586-020-1953-1

Kang, D. S., et al. (2009). Structure of an arrestin2-clathrin complex reveals a novel clathrin binding domain that modulates receptor trafficking. *J Biol Chem 284*(43): 29860-29872. 10.1074/jbc.M109.023366

Kang, Y. (2015). Crystal structure of rhodopsin bound to arrestin by femtosecond X-ray laser. *Nature 523*. 10.1038/nature14656

Kim, Y. J., et al. (2013). Crystal structure of pre-activated arrestin p44. *Nature 497*(7447): 142-146. 10.1038/nature12133

Kohout, T. A., et al. (2004). Differential desensitization, receptor phosphorylation, beta-arrestin recruitment, and ERK1/2 activation by the two endogenous ligands for the CC chemokine receptor 7. *J Biol Chem 279*(22): 23214-23222. 10.1074/jbc.M402125200

Krasel, C., et al. (2005). Beta-arrestin binding to the beta2-adrenergic receptor requires both receptor phosphorylation and receptor activation. *J Biol Chem 280*(10): 9528-9535. 10.1074/jbc.M413078200

Krupnick, J. G., et al. (1997). Arrestin/clathrin interaction. Localization of the clathrin binding domain of nonvisual arrestins to the carboxy terminus. *J Biol Chem 272*(23): 15011-15016. 10.1074/jbc.272.23.15011

Laporte, S. A., et al. (2000). The interaction of β-arrestin with the AP-2 adaptor is required for the clustering of β2-adrenergic receptor into clathrin-coated pits. *J. Biol. Chem. 275*(30): 23120-23126.

Latorraca, N. R., et al. (2018). Molecular mechanism of GPCR-mediated arrestin activation. *Nature 557*(7705): 452-456. 10.1038/s41586-018-0077-3

Lee, M. H. (2016). The conformational signature of β-arrestin2 predicts its trafficking and signalling functions. *Nature 531*. 10.1038/nature17154

Lee, Y., et al. (2020). Molecular basis of β-arrestin coupling to formoterol-bound β1-adrenoceptor. *Nature 583*(7818): 862-866. 10.1038/s41586-020-2419-1

Lohse, M. J., et al. (1990). beta-Arrestin: a protein that regulates beta-adrenergic receptor function. *Science 248*(4962): 1547-1550. 10.1126/science.2163110

Luttrell, L. M., et al. (1999). Beta-arrestin-dependent formation of beta2 adrenergic receptor-Src protein kinase complexes. *Science 283*(5402): 655-661. 10.1126/science.283.5402.655

Luttrell, L. M., et al. (2001). Activation and targeting of extracellular signal-regulated kinases by beta-arrestin scaffolds. *Proc Natl Acad Sci U S A 98*(5): 2449-2454. 10.1073/pnas.041604898

Luttrell, L. M., et al. (2018). Manifold roles of β-arrestins in GPCR signaling elucidated with siRNA and CRISPR/Cas9. *Sci. Signal. 11*(549). 10.1126/scisignal.aat7650

Mayer, D., et al. (2019). Distinct G protein-coupled receptor phosphorylation motifs modulate arrestin affinity and activation and global conformation. *Nat Commun 10*(1): 1261. 10.1038/s41467-019-09204-y

McDonald, P. H., et al. (2000). Beta-arrestin 2: a receptor-regulated MAPK scaffold for the activation of JNK3. *Science 290*(5496): 1574-1577. 10.1126/science.290.5496.1574

Min, K., et al. (2020). Crystal Structure of beta-Arrestin 2 in Complex with CXCR7 Phosphopeptide. *Structure 28*(9): 1014-1023 e1014. 10.1016/j.str.2020.06.002

Moaven, H., et al. (2013). Visual arrestin interaction with clathrin adaptor AP-2 regulates photoreceptor survival in the vertebrate retina. *Proc Natl Acad Sci U S A 110*(23): 9463-9468. 10.1073/pnas.1301126110

Nguyen, A. H., et al. (2019). Structure of an endosomal signaling GPCR–G protein–β-arrestin megacomplex. *Nat. Struct. Mol. Biol. 26*(12): 1123-1131. 10.1038/s41594-019-0330-y

Nobles, K. N. (2011). Distinct phosphorylation sites on the β(2)-adrenergic receptor establish a barcode that encodes differential functions of β-arrestin. *Sci. Signal. 4*. 10.1126/scisignal.2001707

Nobles, K. N., et al. (2007). The active conformation of β-arrestin1: direct evidence for the phosphate sensor in the N-domain and conformational differences in the active states of β-arrestins1 and -2. *J. Biol. Chem. 282*. 10.1074/jbc.M611483200

Nuber, S. (2016). β-Arrestin biosensors reveal a rapid, receptor-dependent activation/deactivation cycle. *Nature 531*. 10.1038/nature17198

Oakley, R. H., et al. (1999). Association of β-arrestin with G protein-coupled receptors during clathrin-mediated endocytosis dictates the profile of receptor resensitization. *J. Biol. Chem. 274*(45): 32248-32257.

Oakley, R. H., et al. (2001). Molecular determinants underlying the formation of stable intracellular G protein-coupled receptor-β-arrestin complexes after receptor endocytosis. *J. Biol. Chem. 276*(22): 19452-19460.

Oakley, R. H., et al. (2000). Differential affinities of visual arrestin, beta arrestin1, and beta arrestin2 for G protein-coupled receptors delineate two major classes of receptors. *J. Biol. Chem. 275*. 10.1074/jbc.M910348199

Peterson, Y. K. and L. M. Luttrell (2017). The diverse roles of arrestin scaffolds in G protein-coupled receptor signaling. *Pharmacol. Rev. 69*. 10.1124/pr.116.013367

Schmid, E. M., et al. (2006). Role of the AP2 beta-appendage hub in recruiting partners for clathrin-coated vesicle assembly. *PLoS Biol 4*(9): e262. 10.1371/journal.pbio.0040262

Sente, A., et al. (2018). Molecular mechanism of modulating arrestin conformation by GPCR phosphorylation. *Nat. Struct. Mol. Biol. 25*(6): 538-545. 10.1038/s41594-018-0071-3

Shukla, A. K. (2013). Structure of active β-arrestin-1 bound to a G-protein-coupled receptor phosphopeptide. *Nature 497*. 10.1038/nature12120

Shukla, A. K. (2014). Visualization of arrestin recruitment by a G-protein-coupled receptor. *Nature 512*. 10.1038/nature13430

Shukla, A. K., et al. (2013). Structure of active β-arrestin-1 bound to a G-protein-coupled receptor phosphopeptide. *Nature 497*(7447): 137-141. 10.1038/nature12120

Staus, D. P., et al. (2020). Structure of the M2 muscarinic receptor-beta-arrestin complex in a lipid nanodisc. *Nature 579*(7798): 297-302. 10.1038/s41586-020-1954-0

Thomsen, A. R. B., et al. (2016). GPCR-G Protein-β-Arrestin Super-Complex Mediates Sustained G Protein Signaling. *Cell 166*(4): 907-919. 10.1016/j.cell.2016.07.004

Tian, X., et al. (2014). beta-arrestins and G protein-coupled receptor trafficking. *Handb Exp Pharmacol 219*: 173-186. 10.1007/978-3-642-41199-1_9

Wei, H., et al. (2003). Independent beta-arrestin 2 and G protein-mediated pathways for angiotensin II activation of extracellular signal-regulated kinases 1 and 2. *Proc Natl Acad Sci U S A 100*(19): 10782-10787. 10.1073/pnas.1834556100

Wilden, U. (1995). Duration and amplitude of the light-induced cGMP hydrolysis in vertebrate photoreceptors are regulated by multiple phosphorylation of rhodopsin and by arrestin binding. *Biochemistry 34*(4): 1446-1454. 10.1021/bi00004a040

Wilden, U., et al. (1986). Rapid affinity purification of retinal arrestin (48 kDa protein) via its light-dependent binding to phosphorylated rhodopsin. *FEBS Lett 207*(2): 292-295. 10.1016/0014-5793(86)81507-1

Yang, F. (2015). Phospho-selective mechanisms of arrestin conformations and functions revealed by unnatural amino acid incorporation and (19)F-NMR. *Nat. Commun. 6*. 10.1038/ncomms9202

Yin, W., et al. (2019). A complex structure of arrestin-2 bound to a G protein-coupled receptor. *Cell Res 29*(12): 971-983. 10.1038/s41422-019-0256-2

Chapter 2: Catalytic activation of β-arrestin by GPCRs

Benjamin Barsi-Rhyne contributed data to Figs. 2.5 and S2.7 and provided consultation during experimental design and paper writing process. Most of the experiments were conceived and executed by Kelsie Eichel (UCSF) in the laboratory of Mark von Zastrow (UCSF). Additional contributions were made by Damien Jullié (UCSF) also in the laboratory of Mark von Zastrow (UCSF), Naomi R. Latorraca (Stanford University) in the laboratory of Ron Dror (Stanford University), Mathieu Masureel (Stanford University) in the laboratory of Brian Kobilka (Stanford University), and Jean Baptiste Sibarita (IINS, Bordeaux).

2.1 Abstract

β-arrestins are critical regulator and transducer proteins for G protein-coupled receptors (GPCRs). Cellular β-arrestin function is presently thought to require stable and stoichiometric GPCR/β-arrestin scaffold complex formation driven by the phosphorylated GPCR tail. We demonstrate a distinct and additional mechanism that does not require stable GPCR/β-arrestin scaffolding or the GPCR tail. Instead, it is activated by transient engagement of the GPCR core that destabilizes a conserved inter-domain charge network in β-arrestin. This promotes capture of β-arrestin at the plasma membrane and accumulation in clathrin-coated endocytic structures (CCSs) after GPCR dissociation, requiring a series of β-arrestin interactions with membrane phosphoinositides and CCS lattice proteins. β-arrestin clustering in CCSs without its upstream activating GPCR is associated with a β-arrestin-dependent component of the cellular ERK (Extracellular signal-regulated kinase) response. These results delineate a discrete mechanism of cellular β-arrestin function that is activated catalytically by GPCRs.

2.2 Introduction

GPCRs, the largest family of signaling receptors, regulate essentially every physiological process and comprise an important class of drug targets ((Rosenbaum, Rasmussen et al. 2009); (Lohse, Benovic et al. 1990); (Kang, Tian et al. 2014); (Pierce, Premont et al. 2002)). GPCR-mediated signaling and regulatory events occur primarily through interactions of the receptor with two classes of transducer protein, heterotrimeric G proteins and β-arrestins. β-arrestins were discovered through their ability to prevent coupling of G proteins to GPCRs and are now known to support additional functions, including endocytosis of GPCRs, mediated by clathrin-coated structures, and downstream signaling, mediated by MAP (mitogen-activated protein) kinase cascades (Gurevich and Gurevich 2006, 2014). A long-standing view is that all of these functions occur from a stable and stoichiometric GPCR–β-arrestin complex, the formation of which requires β-arrestin binding to the phosphorylated GPCR tail (Gurevich and Gurevich 2006, Shukla, Xiao et al. 2011). There is emerging evidence that GPCR–β-arrestin complexes can vary in structure but, nevertheless, present concepts of cellular β-arrestin function require the formation of a GPCR–β-arrestin complex driven largely by the phosphorylated GPCR tail (Kumari, Srivastava et al. 2016, Lee, Appleton et al. 2016, Nuber, Zabel et al. 2016, Cahill, Thomsen et al. 2017, Kumari, Srivastava et al. 2017).

Recently, β-arrestin-2 was found to mediate MAP kinase signaling by accumulating in CCSs in response to ligand-dependent activation of the β1-adrenergic GPCR (β1AR) but without co-accumulation of the β1AR. This ability of β-arrestin-2 to operate separately from its activating GPCR is not consistent with the present mechanistic understanding and remains unexplained. Here we show that such ‘action at a distance’ behavior is widespread. We delineate a distinct,

GPCR tail-independent mechanism of cellular β-arrestin activation in which transient engagement of the GPCR acts catalytically.

2.3 Results

Separate trafficking of β-arrestin

We verified separate trafficking of β-arrestin-2 in HEK 293 cells co-expressing recombinant β1ARs using total internal reflection fluorescence (TIRF) microscopy. The β-adrenergic agonist isoproterenol produced rapid and robust accumulation of β-arrestin-2 in CCSs without detectable co-accumulation of β1AR (Fig. 2.1a, b). Nevertheless, trafficking of β-arrestin-2 to CCSs was dependent on ligand-induced β1AR activation, as it was greatly reduced by the β1-selective antagonist CGP 20712A (Extended Data Fig. 2.1a) or in HEK 293 cells that did not express recombinant β1ARs (Extended Data Fig. 2.1b). In H9c2 cells, which natively express β1ARs at higher levels (Branco, Pereira et al. 2011), either isoproterenol or the β1-selective agonist dobutamine activated β-arrestin trafficking through endogenous receptors (Extended Data Fig. 1c) and the β1-selective antagonist CGP 20712A inhibited this (Extended Data Fig. 2.1d). We also found that β-arrestin-1 (also known as arrestin-2) is capable of separate accumulation in CCSs (Extended Data Fig. 2.1e–g), establishing generality across β-arrestin isoforms.

The β2-adrenergic receptor (β2AR) is a homologous GPCR that co-accumulates with β-arrestin in CCSs (Barak, Ferguson et al. 1997, Santini, Gaidarov et al. 2002, Puthenveedu and von Zastrow 2006). We verified this by TIRF microscopy in HEK 293 cells expressing FLAG-tagged β2ARs at levels around tenfold higher than endogenous levels (Fig. 2.1c, d, Extended Data Fig. 2.1h). We considered the possibility that β2ARs can also activate β-arrestin trafficking separately from the receptor, but that this capacity is obscured by the natural tendency of β2ARs to co-traffic. Indeed, when laterally immobilized to prevent receptor accumulation in CCSs (Mondin, Labrousse et al. 2011, Eichel, Jullié et al. 2016),FLAG–β2AR still promoted

rapid accumulation of β-arrestin-2 in CCSs (Fig. 2.1e, f, Extended Data Fig. 2.1i, j). Furthermore, when not immobilized, both β1AR and β2AR produced super-stoichiometric accumulation of β-arrestin-2 in CCSs relative to receptor (around 28- and 4-fold, respectively; Extended Data Fig. 2.1k–m). Moreover, a limited survey of family A GPCRs suggested that such differential activation of β-arrestin trafficking is broadly conserved across GPCRs as well as across β-arrestin isoforms (Extended Data Fig. 2.2).

Activation by GPCR core interaction

Canonical GPCR–β-arrestin scaffolding requires the receptor cytoplasmic tail and is driven by phosphorylation of the tail (Xiao, Shenoy et al. 2004, Nobles, Guan et al. 2007, Shukla, Manglik et al. 2013). By contrast, the β1AR cytoplasmic tail was not required to activate β-arrestin trafficking. β-arrestin accumulation in CCSs was unaffected by nearly complete removal of the GPCR cytoplasmic tail (415T, Extended Data Fig. 2.3a, b). This was also true for β2ARs after a similarly extensive tail truncation (341T, Fig. 2.2a, b), as well as after a less extensive truncation (365T) that was previously shown to abrogate β2AR–β-arrestin scaffold complex formation (Nuber, Zabel et al. 2016) (Extended Data Fig. 2.3c–e).

In principle, GPCRs could promote tail-independent trafficking of β-arrestin through activation of a downstream G-protein-linked signaling pathway. We found that this was not the case, as GPCR-activated β-arrestin-2 accumulation in CCSs did not depend on selectivity for G protein coupling, and trafficking activated by the Gi-coupled D2 dopamine receptor (DRD2) was unaffected by pertussis toxin (Extended Data Fig. 2.3f–h), consistent with a recent report (McCorvy et al. 2018). Further, receptor-independent activation of adenylyl cyclase using forskolin did not promote (or block) β-arrestin-2 trafficking (Extended Data Fig. 2.3i–k). Rather,

the discrete β-arrestin trafficking behavior required direct binding of the ligand-activated GPCR, because a mutant β-arrestin-2 that is unable to bind GPCRs (Gimenez, Babilon et al. 2014) did not accumulate in CCSs (Extended Data Table 1; Extended Data Fig. 2.3l–n). β-arrestin has been shown to engage GPCRs weakly through a ligand-dependent interaction that does not require the phosphorylated receptor tail (Violin, Ren et al. 2006). We hypothesized that transient binding is sufficient to activate β-arrestin trafficking and is mediated by the GPCR core. To test this, we focused on DRD2 because it has a short cytoplasmic tail and yet robustly activates β-arrestin trafficking to CCSs (Extended Data Fig. 2.2g–i). A mutation in the core of DRD2 that specifically disrupts coupling of the receptor to β-arrestin (DRD2(G protein) (Peterson, Pack et al. 2015)) prevented ligand-dependent stimulation of β-arrestin trafficking to CCSs (Fig. 2.2c–e), establishing a critical role for the interaction with the receptor core.

We next investigated how engagement with the receptor core affects the activation of β-arrestin trafficking by focusing on a polar region in β-arrestin that is located proximal to the conserved finger loop and is thought to directly contact the ligand-activated GPCR core(Shukla, Westfield et al. 2014, Cahill, Thomsen et al. 2017). We identified three charged residues in this 'finger-loop-proximal' region that produce constitutive β-arrestin-2 accumulation in CCSs when mutated to alanine (R77A, K78A, D79A; Fig. 2.3a, b). When analyzed using a statistical metric of β-arrestin clustering validated against a previously described constitutively active β-arrestin construct (polar core mutant (Gurevich 1998); Extended Data Table 1, Extended Data Fig. 2.4a, b), these finger-loop-proximal alanine substitutions produced a comparably strong constitutive activation phenotype (Extended Data Fig. 2.4b). The finger-loop-proximal charge mutations also increased ligand-independent interaction of β-arrestin with the clathrin-associated adaptor protein-2 (AP-2; Extended Data

Fig. 2.4c–e), providing biochemical evidence for constitutive activation of β-arrestin. Individual substitution of finger-loop-proximal charged residues was sufficient to produce ligand-independent accumulation of β-arrestin-2 in CCSs, with the K78A mutation having the largest effect (Extended Data Fig. 2.4b, f–h). Further, mutating K78 to arginine (K78R) rather than alanine did not produce constitutive activation (Extended Data Fig. 2.4b, i). Together, these results suggest that K78 stabilizes β-arrestin in its inactive (cytoplasmic) state through a charge interaction positioned at the GPCR core-binding interface.

To investigate how these residues may affect β-arrestin function, we focused on β-arrestin-1, because more structural data are available for this isoform than for β-arrestin-2 and mutating the corresponding residues in β-arrestin-1 produced constitutive accumulation in CCSs (Fig. 2.3c). Crystal structures of putative inactive (Extended Data Fig. 2.5a left, middle) and active (Extended Data Fig. 2.5a right) forms of β-arrestin-1 reveal that the finger-loop-proximal charged residues are located within an extensive network of polar residues spanning the N and C domains of β-arrestin. In both inactive and active structures, R76 may interact with D78 (corresponding to R77 and D79 in β-arrestin-2) but there is no obvious binding partner for K77 (K78 in β-arrestin-2), even though point mutation of this residue produced the strongest constitutive phenotype. We used molecular dynamics simulations to identify acidic residues that might interact with K77. In inactive-state simulations, K77 sometimes formed an intramolecular salt bridge with E313 in the C domain, but this interaction rarely formed in active-state simulations (Fig. 2.3d, Extended Data Fig. 2.5b). This interaction may have been overlooked previously because E313 interacts with R188 on another β-arrestin molecule in the crystal lattice, probably owing to lattice packing (Extended Data Fig. 2.5c). Both K77 and E313 are conserved in β-arrestin-2 (K78 and E314, Extended Data Fig. 2.5d) and, in both β-arrestin

isoforms, separation of N and C domains is thought to accompany β-arrestin activation (Shukla, Manglik et al. 2013, Chen, Perry et al. 2017, Scheerer and Sommer 2017). Therefore, we hypothesized that K77/78 and E313/314 occasionally form a salt bridge that stabilizes the inactive state of β-arrestin by favoring tighter interactions between the N and C domains. Charge mutation of E314 (E314K) also produced ligand-independent accumulation of β-arrestin-2 in CCSs (Fig. 2.3e). Further, mutating both residues (K78E/E314K) to restore the putative ionic interaction by charge swap reversed this constitutive phenotype (Fig. 2.3e). Together, these findings suggest that the finger-loop-proximal charged residues function as part of an interdomain interaction network that maintains β-arrestin in its inactive cytoplasmic form and is destabilized by interaction with the GPCR core.

Capture after GPCR dissociation

For β-arrestin to traffic to CCSs after dissociating from its upstream activating GPCR, additional partner(s) must engage and stabilize β-arrestin at the plasma membrane. We focused on several known candidates (Extended Data Table 1, Extended Data Fig. 2.6a, b). Mutating a conserved phosphoinositide binding determinant in the β-arrestin C domain that was previously mapped and implicated in β-arrestin trafficking (Gaidarov, Krupnick et al. 1999) prevented ligand-induced accumulation of β-arrestin-2 at the plasma membrane and in CCSs (lipid mutant, Fig. 2.4a–i, Extended Data Fig. 6c, d). We demonstrated biochemically that binding of phosphatidylinositol 4,5-bisphosphate (PtdIns(4,5)P2) to this determinant is sufficient to partition β-arrestin out of the solution phase (Extended Data Fig. 2.6e, f). This phosphoinositide-binding determinant is specific to β-arrestins, but a lipid-anchoring region in the C domain was recently identified in visual arrestin (also known as arrestin-1)(Lally, Bauer et al. 2017). Mutating the homologous residues in β-arrestin-2 did not prevent accumulation at

the plasma membrane or in CCSs (Extended Data Table 1, Extended Data Fig. 2.6g, h). Mutating previously identified clathrin (Goodman, Krupnick et al. 1996) and AP-2 (Laporte, Oakley et al. 2000) binding determinants (CCS mutant) in the C terminus of β-arrestin prevented β-arrestin-2 from accumulating in CCSs without blocking accumulation at the plasma membrane (Extended Data Table 1, Fig. 2.4j–l, Extended Data Fig. 2.6i). Mutating the phosphoinositide binding determinant together with clathrin and AP-2 binding determinants blocked β-arrestin-2 accumulation at the plasma membrane altogether, the same phenotype that resulted from mutating only the phosphoinositide binding determinant (lipid and CCS mutant, Fig. 2.4m–o, Extended Data Fig. 2.6j). Similar results were obtained using the β1AR rather than β2AR as the activating GPCR (Extended Data Fig. 2.6k–ac). Further, mutating the phosphoinositide binding determinant prevented the constitutive trafficking phenotype produced by finger-loop-proximal charge mutations in β-arrestin-2 (Extended Data Fig. 2.6ad, ae). These results indicate that β-arrestin is stabilized at the plasma membrane after dissociating from its activating GPCR through a series of non-GPCR interactions.

Whereas the phosphoinositide binding determinant was essential for β1AR- or β2AR-dependent trafficking of β-arrestin-2 to CCSs, it was not required for accumulation of β-arrestin-2 in CCSs produced by a chimeric construct of β2AR containing the tail region of the V2 vasopressin receptor (β2AR–V2R chimaera), a GPCR that is known to form a highly stable tail-dependent GPCR–β-arrestin scaffold complex (Oakley, Laporte et al. 1999) (Extended Data Fig. 2.7a–c). Independently verifying this difference, depleting PtdIns(4,5)P2 from the plasma membrane using phenylarsine oxide (PAO) (Santos, Naal et al. 2013) blocked the ability of β2AR but not that of the β2AR–V2R chimaera to activate trafficking of wild-type β-arrestin-2 to CCSs (Extended Data Fig. 2.7d–g). Thus, phosphoinositide binding to β-arrestin appears to be

required specifically for trafficking of β-arrestin to CCSs after it dissociates from its upstream activating GPCR, but not for trafficking to CCSs while bound in a sufficiently stable GPCR–β-arrestin scaffold complex.

Dynamics in the plasma membrane

We next investigated the discrete trafficking mechanism using single-particle tracking–photoactivated localization microscopy (sptPALM (Manley, Gillette et al. 2008), Fig. 2.5a–d, Extended Data Fig. 2.8a–e, Supplementary Videos 1–4). β-arrestin-2 diffusion profiles exhibited two major peaks when activated by the β2AR. A mobile fraction ($D > 10^{-2}$ μm^2 s^{-1}; log $D >$ −2) overlapped the major diffusion peak of the β2AR, and also that of a lipid probe (PH-PLCδ1) that is known to diffuse freely in the plasma membrane (Hammond, Sim et al. 2009) (Fig. 2.5e, Extended Data Fig. 2.8f–h). An immobile fraction ($D \leq 10^{-2}$ μm^2 s^{-1}; log $D \leq -2$), consistent with the mobility of CCSs was also observed (Liu, Loerke et al. 2009), and the density of immobile β-arrestin-2 molecules was significantly higher within a CCS mask compared to the rest of the plasma membrane. This was true irrespective of whether β-arrestin-2 trafficking was activated by the β1AR or β2AR (9.3 and 6.0-fold enrichment, respectively; n = 11 and 9 cells, respectively, from three independent experiments; P = 0.0004 and 0.0016, respectively; statistical significance calculated using a two-tailed unpaired t-test). Destabilizing clathrin and AP-2 interactions using the β-arrestin-2 CCS mutant shifted the distribution into the mobile peak, irrespective of whether β-arrestin-2 recruitment was activated by the β1AR or β2AR (Fig. 2.5f, g, Extended Data Fig. 2.8i–l, Supplementary Videos 5, 6), confirming that the immobile fraction of β-arrestin-2 molecules largely represents those bound to the CCS lattice. This suggests that disrupting CCS binding displaces β-arrestin towards an association with a

diffusive partner on the plasma membrane. Consistent with this, β-arrestin-2 molecules present within CCSs were essentially immobile after activation by either the β1AR or β2AR (log D = −2.3 and −2.7, respectively; Extended Data Fig. 2.8m–p). Trajectories of both β1AR and β2AR populated CCSs, but β2ARs were preferentially immobilized (log D = −2.3) there, whereas β1ARs remained largely mobile (log D = −1.6). Together, these results indicate that β-arrestin is similarly immobilized in CCSs irrespective of whether (β2AR) or not (β1AR) the activating GPCR is also immobilized there.

Stability of β-arrestin capture

Our results support a working model in which the ligand-activated GPCR acts catalytically to activate β-arrestin trafficking (Extended Data Fig. 2.8q). β-arrestin is subsequently captured and stabilized at the plasma membrane after dissociating from its activating GPCR through a series of non-GPCR interactions that ultimately produce β-arrestin accumulation at CCSs. For this discrete mechanism to be energetically feasible, these non-GPCR interactions must be relatively stable. Indeed, fluorescence recovery after photobleaching (FRAP) demonstrated that β-arrestin-2 accumulated in CCSs exchanges very slowly (half time of equilibrium, t1/2 > 60 s), whether (β2AR) or not (β1AR) the GPCR stimulating β-arrestin accumulation in CCSs co-accumulated (Fig. 2.5h–j, Extended Data Fig. 2.8r). Notably, this duration of β-arrestin association with the CCS is comparable to the lifetime of individual CCSs (Eichel, Jullié et al. 2016). Thus CCSs have the capacity to act both as ‘sinks’ to stabilize β-arrestin at the plasma membrane after GPCR dissociation and as ‘drivers’ of the discrete trafficking mechanism through β-arrestin dissociation from the plasma membrane coupled to endocytic scission of (Eichel, Jullié et al. 2016).

Catalysis and scaffolding co-exist

We believe that distinct catalytic and scaffold-driven mechanisms of GPCR-regulated β-arrestin trafficking are likely to coexist in vivo, with the tendency of a particular GPCR to engage one mechanism relative to the other tuned by the affinity of its tail for β-arrestin (Extended Data Fig. 2.9a). The β1AR appears to be a relatively pure example of a GPCR that activates β-arrestin trafficking primarily through the catalytic mechanism and with very little co-trafficking. The β2AR– V2R chimera favors co-trafficking in a tail-dependent scaffold complex, with trafficking of β-arrestin to CCSs not requiring phosphoinositide binding. The β2AR has a mixed trafficking behavior, producing super-stoichiometric trafficking of β-arrestin to CCSs that is dependent on phosphoinositide binding, yet also co-trafficking to CCSs through interaction of the phosphorylated receptor tail with β-arrestin. Manipulations that enhance GPCR tail binding to β-arrestin can further increase β2AR co-trafficking to CCSs and also cause β1AR to co-traffic (Extended Data Fig. 2.9b–e), emphasizing the tunability of this system.

2.4 Discussion

These results reveal a new framework of cellular β-arrestin activation but raise many additional questions. One is whether catalytic activation of β-arrestin produces a similar or different conformational state relative to β-arrestin that traffics in a tail-dependent GPCR–β-arrestin scaffold complex. Tail-dependent GPCR–β-arrestin complex formation is thought to promote an open β-arrestin conformation defined by displacement of the C terminus of β-arrestin. Determinants of binding to clathrin and AP-2 that are required for β-arrestin accumulation in CCSs are in the C terminus; therefore, β-arrestin that accumulates in CCSs via the catalytic activation mechanism is likely to be in an open conformation. However, it is not known whether other conformational features of β-arrestin are similar or different between the mechanisms. The accompanying Letter by Latorraca et al. (Latorraca, Wang et al. 2018) provides insight into this question by demonstrating through molecular dynamics analysis not only that the GPCR core can promote conformational activation of arrestins, but also that arrestins can frequent conformations similar to those found in the GPCR tail-bound complex once the arrestin C terminus is dissociated, even without the GPCR being bound. Another important goal is to resolve individual steps more fully in the catalytic activation mechanism and determine their kinetics. For example, β-arrestin trafficking could involve additional steps such as transactivation or binding to the phosphorylated tail of another GPCR. Much also remains unknown about the functional consequences of GPCR-catalyzed β-arrestin trafficking. β1ARs are known to promote β-arrestin-dependent ERK signaling by activating β-arrestin trafficking to CCSs without the receptor (Eichel, Jullié et al. 2016); we verified this using a CRISPR knockout approach (O'Hayre, Eichel et al. 2017) (Extended Data Fig. 2.9f, g). The β2AR is unlike the β1AR in that it tends to co-traffic to CCSs with β-arrestin; and β2AR did not produce a strong β-arrestin-dependent component of ERK activation using this assay, when examined in parallel

and with matched receptor expression levels (Extended Data Fig. 2.9h, i). Therefore, we anticipate that the presently delineated catalytic mechanism of cellular β-arrestin activation, by enabling β-arrestin to traffic to CCSs separately from its upstream activating GPCR, is likely to have widespread physiological significance.

2.5 Materials and Methods

Cell culture, expression constructs, and transfections.

HEK 293, COS-1, and H9c2 cells (ATCC authenticated lines CRL-1573, CRL-1650 and CRL 1446, respectively) were cultured in complete growth Dulbecco's modified Eagle's medium (DMEM, Gibco) supplemented with 10% fetal bovine serum (UCSF Cell Culture Facility). Cell line cultures were free of mycoplasma contamination. Transfections were carried out using Lipofectamine 2000 for cDNA according to the manufacturer's protocol. Cells were transfected 48 h before experiments.

N-terminally FLAG-tagged versions of the human β1AR, β2AR, μ-opioid receptor (MOR) and κ-opioid receptor (KOR) were previously described (Cao, Deacon et al. 1999, Temkin, Lauffer et al. 2011). Super ecliptic pHluorin–β2AR was previously described (Yudowski, Puthenveedu et al. 2006). β1AR and β2AR tagged N-terminally with photoactivatable mCherry (PAmCherry–β1AR, PAmCherry–β2AR) was generated using PCR and homology-directed ligation (In-Fusion HD Cloning kit, Clontech). DRD2 was a gift from D. Grandy (Oregon Health & Science University). DRD2 (G protein) was prepared as previously described (Peterson, Pack et al. 2015) by inserting a gBlock gene fragment (IDT) containing the desired mutations with restriction sites BamHI and BstEII (NEB) into the wild-type DRD2 plasmid. The β2AR–V2R chimaera (Oakley, Laporte et al. 2000) was a gift from M. Caron. β1AR–β2AR C tail, β1AR–V2R C tail, β2AR–β1AR C tail were generated using PCR and homology-directed ligation (In-Fusion HD Cloning kit, Clontech). N-terminally FLAG-tagged β1AR(415T) was generated from FLAG–β1AR using site-directed mutagenesis (Phusion Site-Directed Mutagenesis Kit, Thermo Scientific) to create a deletion after residue 415. N-terminally FLAG-tagged β2AR(341T) and FLAG-tagged β2AR(365T), which were previously described (Bouvier, Hausdorff et al. 1988,

Krasel, Bünemann et al. 2005), were prepared by PCR site-directed mutagenesis (Phusion Site-Directed Mutagenesis Kit, Thermo Scientific). β2AR with an N-terminal FLAG tag and a C-terminal GFP tag was generated by inserting a gBlock (IDT) containing a C-terminal fragment of β2AR, a 12 base pair linker and GFP using EcoRV and PshAI (NEB).

β-arrestin-2–GFP, β-arrestin-2–mApple and β-arrestin-2–PAmCherry were previously described (Barak, Ferguson et al. 1997, Eichel, Jullié et al. 2016). β-arrestin-1–mVenus was a gift from R. Sunahara (University of California, San Diego). Specific β-arrestin-2–GFP mutations are described in detail in Extended Data Table 1. All β-arrestin-2–GFP finger- loop-proximal mutants were created by inserting a gBlock (IDT) containing the desired mutations into the β-arrestin-2–GFP wild-type plasmid using restriction sites HindIII and BbvCI (NEB). β-arrestin-2–GFP(E314K) and β-arrestin-2–GFP (K77E/E314K) were created using site-directed mutagenesis (Phusion Site-Directed Mutagenesis Kit, Thermo Scientific) from the wild-type β-arrestin-2–GFP or β-arrestin-2–GFP (K77E) construct, respectively. β-arrestin-2–GFP lipid-binding mutant was previously described (Gaidarov, Krupnick et al. 1999) and was created by inserting a gBlock (IDT) containing the desired mutations into the β-arrestin-2–GFP wild-type plasmid using restriction sites BbvCI and AhdI (NEB). β-arrestin-2–GFP CCS mutant and β-arrestin-2–PAmCherry CCS mutant were created by inserting a gBlock (IDT) containing the desired mutations into the β-arrestin-2–GFP and β-arrestin-2–PAmCherry plasmids, respectively, using restriction sites BlpI and ApaI (NEB). β-arrestin-2–GFP lipid and CCS mutant and β- arrestin-2–GFP lipid and finger-loop-proximal mutant constructs were created by inserting a gBlock (IDT) containing the desired mutations into the β-arrestin-2–GFP CCS mutant plasmid and β-arrestin-2–GFP finger-loop-proximal mutant construct, respectively, using restriction sites BbvCI and AhdI (NEB). β-arrestin-2–GFP(L191G/F192G) was created using site-directed

mutagenesis (Phusion Site-Directed Mutagenesis Kit, Thermo Scientific) from the wild type β-arrestin-2–GFP. β-arrestin-1–mVenus finger-loop-proximal mutant was cloned by inserting a gBlock (IDT) containing the desired mutation into the β-arrestin-1–mVenus wild-type plasmid using restriction sites BamHI and SphI (NEB). β-arrestin-2–GFP KNC mutant, which has been previously described and shown to be defective in binding to GPCRs (Gimenez, Babilon et al. 2014), was subcloned into β-arrestin-2–GFP from a β-arrestin-2 expression plasmid (a gift from V. Gurevich). NAV3β–arrestin-1(1–393) in pGEX4T was generated from a previously described construct (Nobles, Guan et al. 2007) and contains an N-terminal GST tag, 3C cleavage site and AVI tag. NAV3β–arrestin-1(1–393) lipid-binding mutant was created by inserting a gBlock (IDT) containing the desired mutations into the NAV3β– arrestin-1(1–393) using restriction sites EcoRI and NcoI (NEB).

Clathrin–dsRed, clathrin–GFP and clathrin–TagBFP were previously described (Merrifield, Feldman et al. 2002, Puthenveedu and von Zastrow 2006, Eichel, Jullié et al. 2016). GRK2–TagBFP was created by PCR amplifying GRK2, which was a gift from J. Benovic (Thomas Jefferson University), and subcloning into the pTagBFP vector (Evrogen) using NheI and SacII (NEB). PAmCherry–PLCδ1-PH was subcloned from GFP–PLCδ1-PH (Stauffer, Ahn et al. 1998), a gift from T. Meyer (addgene plasmid #21179), using BspEI and EcoRI (NEB).

Live cell TIRF microscopy imaging

TIRF microscopy was performed at 37 °C using a Nikon Ti-E inverted microscope equipped for through-the-objective TIRF microscopy and outfitted with a temperature-, humidity- and CO2-controlled chamber (Okolab). Images were obtained with an Apo TIRF 100 ×, 1.49 numerical aperture objective (Nikon) with solid-state 405, 488, 561 and 647 nm lasers (Keysight

Technologies). An Andor iXon DU897 EMCCD camera controlled by NIS-Elements 4.1 software was used to acquire image sequences every 2 s for 10 min. Unless indicated otherwise, live-cell microscopy assays were performed using HEK 293 cells. Cells were transfected as indicated according to the manufacturer's protocol 48 h before imaging and then plated on poly-l-lysine (0.0001%, Sigma) coated 35-mm glass-bottomed culture dishes (MatTekCorporation) 24h before imaging. Cells were labelled with monoclonal FLAG antibody (M1) (1:1000, Sigma F-3040) conjugated to Alexa Fluor 647 dye (Life Technologies) for 10 min at 37 °C before imaging, washed, and imaged live in DMEM without phenol red (UCSF Cell Culture Facility) supplemented with 30 mM HEPES, pH 7.4 (UCSF Cell Culture Facility). Cells were treated with bath application of the indicated agonist at time 0 s for experiments shown as time courses. At least three independent experiments were performed for all live-cell TIRF microscopy imaging.

TIRF microscopy image analysis.

Quantitative image analysis was performed on unprocessed images using ImageJ and Fiji software (Schindelin, Arganda-Carreras et al. 2012, Schneider, Rasband et al. 2012). To quantify change in β-arrestin fluorescence over time in TIRF microscopy images, which was reported as plasma membrane recruitment, fluorescence values were measured over the entire stack in a region of interest (ROI) corresponding to the cell. Fluorescence values of the ROI were normalized to initial fluorescence values before agonist addition. Minimal bleed-through and photobleaching was verified using single-labeled and untreated samples, respectively. Line scan analysis of receptor, β-arrestin, or clathrin fluorescence from the shown line were carried out using the Fiji plot profile function to measure pixel values from this line. For calculations of fluorescence enrichment into CCSs, a mask of CCSs was generated using a

thresholded average image of the clathrin channel. Enrichment at CCSs for receptor and arrestin was measured as the difference between the average fluorescence in the mask and average fluorescence outside of the thresholded structures. Clustering index was determined using the skew statistical measurement applied to fluorescence intensity values of β-arrestin–GFP pixels in a ROI corresponding to the cell.

Fluorescence recovery after photobleaching

FRAP was performed at 37 °C using a Nikon Ti inverted spinning disk confocal microscope (Yokogawa CSU- W1) equipped with a temperature-, humidity- and CO2-controlled chamber (Okolab). Images were obtained with a Plan Apo VC 100 ×, 1.4 NA objective (Nikon) with 488-, 561- and 640-nm solid-state lasers (Keysight Technologies). An Andor Zyla 4.2 sCMOS camera controlled by MicroManager 2.0 software was used to acquire image sequences. A Rapp Optoelectronic UGA-40 photobleaching system was used to photo bleach β-arrestin-2–GFP on a small area of the plasma membrane with a 473-nm laser (Vortran). Cells were imaged every 2 s for 10 min to monitor fluorescence recovery after photobleaching. All quantitative image analysis was performed on unprocessed images using ImageJ software. The clustering index was calculated for the photobleached and unbleached areas of identical size in the same cell. Photobleaching experiments were performed at least three independent times.

Quantitative live-cell sptPALM

Cells were transfected as indicated according to the manufacturer's protocol 48 h before imaging and then plated on poly-l-lysine (0.0001%, Sigma) coated 35-mm glass-bottomed culture dishes (MatTek Corporation) 24 h before imaging. Results were obtained with at least three independent experiments, except for the analysis of PAmCherry–β1AR diffusion

coefficients profile. For experiments to investigate the diffusion coefficient profile of PAmCherry-tagged receptors, lipid sensor, β-arrestin-2, or control cells without PAmCherry protein expression, cells were surface-labeled with M1–Alexa Fluor 488 and experiments were performed blind regarding the transfection condition. For experiments to localize receptors or β-arrestin behavior relative to CCSs, cells were incubated for 10 min with 100-nm TetraSpeck microspheres (Thermo Fisher), and imaging was performed blind regarding transfection condition. sptPALM experiments were performed at 37 °C using a Nikon Ti-E inverted microscope equipped with TIRF illumination and outfitted with a temperature-, humidity- and CO2-controlled chamber (Okolab). Cells were imaged in a solution containing 135 mM NaCl, 5 mM KCl, 0.4 mM $MgCl_2$,1.8 mM $CaCl_2$, 20 mM HEPES and 5 mM d-glucose, adjusted to pH 7.4, 1 min after addition of 10 μM isoproterenol. Images were acquired with a PL-Apo TIRF 100 ×, 1.49 NA objective (Nikon) with solid-state 405-, 488-, 561- and 647-nm lasers (Keysight Technologies) as light sources. An Andor iXon DU897 EMCCD camera controlled by NIS-Elements 4.1 software was used to acquire stacks of 5,000 images with continuous activation by 405-nm light and imaging by 561-nm laser. Single-molecule image sequences were acquired in streaming mode at 45 Hz in a 256 × 256-pixel area (40 × 40-μm field of view). For colocalization experiments, a clathrin–GFP image was acquired at the end of the sptPALM image series.

Single-molecule fluorescent spots were localized and tracked over time using a combination of wavelet-based segmentation and simulated-annealing tracking algorithms as previously described (Rossier, Octeau et al. 2012, Nair, Hosy et al. 2013). The software package used to derive quantitative data on protein localization and dynamics is custom written, operating as a plug-in running within the MetaMorph software (Molecular Devices) environment. The mean

square displacement (MSD) and diffusion coefficient (*D*) were calculated for every trajectory as follows. For every trajectory of *N* data points (coordinates $x(t)$, $y(t)$ at times $t = 0$ to $N\Delta t$ with Δt = 22 ms), the mean square displacement (MSD) for time intervals $\tau = n \times \Delta t$ is calculated using the formula

$$\sum_{i=1}^{N-n} \frac{[x((i+n)\times\Delta t) - x(i\times\Delta t)]^2 + [y((i+n)\times\Delta t) - y(i\times\Delta t)]^2}{N-n}$$

D was then extracted by linear fit on the first four time points of the MSD curves using the formulae $\mathrm{MSD}(\tau) = \langle r^2 \rangle(\tau) + a = 4D\tau + a$, in which a is the ordinate at the origin of the linear fit due to the precision accuracy in the localization process. The bin at $10^{-5}\,\mu m^2\,s^{-1}$ represents trajectories for which calculation of $D \leq 10^{-5}\,\mu m^2\,s^{-1}$.

To define the diffusion profile across the different conditions, we included only trajectories longer than six points. To consider false detections due to non-specific single-molecule signals, we computed an average histogram of diffusion coefficients from trajectories obtained by imaging cells without PAmCherry expression, using the same parameters described previously. The variability of the number of localizations and diffusion profiles of non-specific single-molecule signal was very low. For each cell exhibiting at least five times more trajectories than the average false-detection count, the histogram of false detections was subtracted from the distribution of diffusion coefficients. Histograms of diffusion coefficients were computed by normalizing the number of trajectories for each bin by the total number of trajectories after false-detection subtraction. We considered trajectories with $D \leq 10^{-2}\,\mu m^2\,s^{-1}$ as

immobile and used this criterion for evaluation of statistical significance using a two-tailed *t*-test.

For analysis of localization of trajectories relative to CCPs, single-particle tracking movies as well as diffraction limited clathrin-GFP images were aligned with subpixel accuracy using a Gaussian fitting on the Tetraspeck microsphere signal as fiduciary marker. Trajectories of more than eight points were used to generate the super-resolution images with a pixel size of 19.6 nm (zoom 8 × compared to the acquired data) and compute the diffusion coefficients as described above. A series of super-resolution images was generated displaying reconstructed individual trajectories, localization density of mobile molecules ($D \geq 10^{-2}\,\mu m^2\,s^{-1}$), immobile molecules ($D \leq 10^{-2}\,\mu m^2\,s^{-1}$), or diffusion coefficient maps. Diffusion coefficient maps were computed by averaging in each pixel the diffusion coefficients from all the trajectories detected in the corresponding pixel. Images of CCSs were zoomed 8 × before alignment and overlaid with the super-resolution images. A binary mask of the CCSs was generated using ImageJ (NIH) by thresholding and eroding by two pixels the 8 × zoomed image of the clathrin mask after bandpass filtering in the Fourier domain. This mask was used in combination with the super-resolution images to calculate the average diffusion coefficient as well as the density of localization with respect to the CCSs.

ERK1/2 activation assays.

Western blot analysis was used to measure activation of ERK1/2. Previously described parental HEK 293 and β-arrestin CRISPR knockout HEK 293 cell lines (O'Hayre, Eichel et al. 2017) were transfected with empty vector control, FLAG–β1AR or FLAG–β2AR expression constructs. Cells were serum starved for 18 h before the assay, incubated with 10 μM

isoproterenol for the indicated times at 37 °C, and then washed on ice with ice-cold PBS. Cells were directly lysed in sample buffer (NuPAGE LDS Sample Buffer (Life Technologies), 100 mM dithiothreitol), sonicated three times for 10 s, boiled, separated by SDS–PAGE (Life Technologies) and transferred to a nitrocellulose membrane that was blocked with TBS Odyssey blocking buffer (LI-COR) for one hour at room temperature and then incubated overnight at 4°C with a mouse ERK1/2 primary antibody (1:2,000, Cell Signaling 4696) and a rabbit phosphorylated-ERK1/2 primary antibody (1:2,000, Cell Signaling 4370). Membranes were washed three times for 5 min in TBS-Tween (0.1% v/v) and incubated with a IRDye 680-labeled anti-rabbit secondary antibody (1:5,000, LI-COR 926-68073) and an IRDye 800-labeled anti-mouse secondary antibody (1:5,000, LI-COR 926-32212) for one hour at room temperature. Membranes were washed three times for 5 min in TBS-Tween (0.1% v/v), imaged using an Odyssey Infrared Imaging System (LI-COR) in the linear range and quantified by measuring band intensity, background subtracting, and normalizing the phosphorylated ERK1/2 band intensity to the total ERK1/2 band intensity. Data are shown as fraction of the maximum response observed across all conditions in each experiment. Five independent experiments were performed for each condition.

Co-immunoprecipitation.

Cells expressing indicated constructs were grown to confluency in 10-cm dishes, and 48 h after transfection, cells were washed twice with reaction buffer (PBS, 30 mM HEPES, pH 7.4) and then crosslinked with 2 mM DSP (Thermo Scientific) for 30 min at room temperature with gentle agitation. The crosslinking reaction was stopped by addition of 20 mM Tris, pH 7.5 for 15 min. Cells were collected, pelleted by centrifugation, lysed on ice for 10 min in 500 µl ice-cold lysis buffer (0.2% Triton X-100, 150 mM NaCl, 25 mM KCl, 10 mM Tris pH 7.4, and 1 mM

EDTA supplemented with a standard protease inhibitor mixture (Roche Applied Science)) and then cleared by centrifugation (14,000*g* for 15 min at 4 °C). Samples were incubated overnight at 4 °C with anti-GFP antibody covalently linked to sepharose beads (1:3, Abcam ab69314), washed with lysis buffer three times, and incubated with SDS sample buffer (Invitrogen) supplemented with 100 mM dithiothreitol to elute proteins. Samples were then separated by SDS– PAGE (Life Technologies) and transferred to a nitrocellulose membrane that was blocked with TBS Odyssey blocking buffer (LI-COR) for one hour at room temperature and then incubated overnight at 4 °C with a mouse β-adaptin primary antibody (1:250, BD Biosciences 610382) and a rabbit GFP primary antibody (1:500, Thermo Fisher Scientific A-11122). Membranes were washed three times for 5 min in TBS-Tween (0.1% v/v) and incubated with an IRDye 680-labelled anti-rabbit secondary antibody (1:5,000, LI-COR 926-68073) and an IRDye 800-labelled anti-mouse secondary antibody (1:5,000, LI-COR 926-32212) for one hour at room temperature. Membranes were washed three times for 5 min in TBS-Tween (0.1% v/v), imaged using an Odyssey Infrared Imaging System (LI-COR) in the linear range and quantified by measuring band intensity, background subtracting, and normalizing the AP-2-immunoprecipitated band intensity to the GFP-bead band intensity. Three independent experiments were performed.

Purification of β-arrestin-1.

N-terminally GST-tagged rat β-arrestin-1 (amino acids 1–393) constructs in the pGEX4T vector were transformed into BL21-CodonPlus (DE3)-RIPL cells (Agilent). Cultures were grown at 37 °C to an absorbance ($A_{600\ nm}$) of 0.6 in Terrific broth and then equilibrated to 16 °C. GST-β-arrestin-1 expression was induced with 0.1 mM isopropyl 1-thio-β-d-galactopyranoside overnight at this temperature, and cells were collected by centrifugation at 6,000*g*. Pellets were

resuspended with cold lysis buffer (50 mM HEPES pH 8.2, 150 mM NaCl, 2 mM DTT, protease inhibitors, 1 mM EDTA). Cells were lysed by passage through an Emulsiflex press (Avestin) and cleared by centrifugation at 40,000*g* for 50 min. The clarified supernatant was incubated with GST-4B resin (GE Healthcare) for 2 hours at 4 °C, and then washed two times with five column volumes of wash buffer (50 mM HEPES pH7.4, 150 mM NaCl, 2 mM DTT). The GST resin with bound GST–β-arrestin-1 was resuspended in two column volumes of wash buffer, and the GST fusion protein was cleaved with 0.1 mg of 3C protease per ml of GST resin overnight at 4 °C. The supernatant and first wash fraction were pooled and centrifuged at 40,000*g* for 30 min. The cleared supernatant was filtered with a 0.45-μm filter, concentrated to 500 μl and gel-filtered using a Superose 6 10/300 GL column (GE Life Science). β-Arrestin-1 was eluted in gel filtration buffer (30 mM HEPES, 150 mM NaCl, 2 mM $MgCl_2$, 5% glycerol). Fractions were analyzed by SDS–PAGE and fractions containing β-arrestin-1 were pooled and concentrated, flash-frozen in liquid N_2, and stored at −80 °C.

Lipid bead binding.

Equal amounts of purified wild-type or lipid-binding mutant β-arrestin-1 protein were incubated with PtdIns (4,5)P_2-coated beads (Echelon) for two hours at room temperature in wash/binding buffer (10 mM HEPES, pH 7.4, 0.25% NP-40, 150 mM NaCl). Samples were then washed three times with wash/ binding buffer. To elute proteins, equal volumes of 2 × Laemmli sample buffer were added and samples were incubated at 95 °C for 5 min. Samples were then separated by SDS–PAGE (Life Technologies) and transferred to a nitrocellulose membrane that was blocked with TBS Odyssey blocking buffer (LI-COR) for one hour at room temperature and then incubated for one hour at room temperature with a mouse anti-β-arrestin primary antibody (1:500, Santa Cruz Biotechnology sc-13140). Membranes were washed three times for 5 min in

TBS-Tween (0.1% v/v) and incubated with an IRDye 800-labeled anti-mouse secondary antibody (1:5,000, LI-COR 926-32212) for one hour at room temperature. Membranes were washed three times for 5 min in TBS-Tween (0.1% v/v), imaged using an Odyssey Infrared Imaging System (LI-COR) in the linear range, and quantified by measuring band intensity and subtracting background intensity. Four independent experiments were performed.

Molecular dynamics simulations.

We analyzed sets of molecular dynamics simulations for each of two conditions: (1) simulations initiated from the inactive-state β-arrestin-1 crystal structure (PDB ID: 1G4M, chain A), and (2) simulations initiated from the active-state β-arrestin-1 crystal structure bound to the phosphorylated C-tail of the V2 vasopressin receptor (PDB ID: 4JQI). For the latter condition, we removed the co-crystallized Fab30 antibody fragment. We performed six simulations for each condition. For each simulation, initial atom velocities were assigned randomly and independently. These simulations correspond to simulations 40 to 51 in Supplementary Table 1 of the accompanying Letter (Latorraca, Wang et al. 2018), which also provides details regarding simulation setup and simulation protocols.

Simulations were visualized and analyzed using Visual Molecular Dynamics (VMD) (Humphrey, Dalke et al. 1996). Simulations were inspected visually for interactions that formed in the inactive state but not the active state. We noticed that Glu313 occasionally formed a salt bridge with Lys77 in the inactive state, persisting for up to hundreds of nanoseconds. We quantified the frequency of salt bridge formation by calculating the minimum distance between polar heavy atoms of Lys77 and Glu313 across all simulations under each condition.

Statistical analysis

Quantitative data are expressed as the mean and error bars represent the standard error of the mean (s.e.m.) unless otherwise indicated. Scatter plots are overlaid with mean and s.e.m. Statistical significance between conditions was analyzed using a two-tailed *t*-test or with Welch's correction for unequal variance and a one-way ANOVA ($\alpha = 0.05$) calculated using Prism 7.0 (GraphPad Software). $^{*}P < 0.05$; $^{**}P < 0.01$; $^{***}P < 0.001$ when compared with control or no-treatment conditions. All experiments showing representative data were repeated at least three independent times with similar results. Independent experiments represent independent biological replicates.

2.5 References

(2014). Arrestins - Pharmacology and Therapeutic Potential, Springer, Berlin, Heidelberg.

Barak, L. S., et al. (1997). A beta-arrestin/green fluorescent protein biosensor for detecting G protein-coupled receptor activation. *J Biol Chem 272*(44): 27497-27500. 10.1074/jbc.272.44.27497

Bouvier, M., et al. (1988). Removal of phosphorylation sites from the beta 2-adrenergic receptor delays onset of agonist-promoted desensitization. *Nature 333*(6171): 370-373. 10.1038/333370a0

Branco, A. F., et al. (2011). Isoproterenol cytotoxicity is dependent on the differentiation state of the cardiomyoblast H9c2 cell line. *Cardiovasc. Toxicol. 11*(3): 191-203. 10.1007/s12012-011-9111-5

Cahill, T. J., et al. (2017). Distinct conformations of GPCR–β-arrestin complexes mediate desensitization, signaling, and endocytosis. *Proc. Natl. Acad. Sci. U. S. A. 114*(10): 2562-2567. 10.1073/pnas.1701529114

Cao, T. T., et al. (1999). A kinase-regulated PDZ-domain interaction controls endocytic sorting of the beta2-adrenergic receptor. *Nature 401*(6750): 286-290. 10.1038/45816

Chen, Q., et al. (2017). Structural basis of arrestin-3 activation and signaling. *Nat. Commun. 8*(1): 1427. 10.1038/s41467-017-01218-8

Eichel, K., et al. (2016). β-Arrestin drives MAP kinase signalling from clathrin-coated structures after GPCR dissociation. *Nat. Cell Biol. 18*(3): 303-310. 10.1038/ncb3307

Gaidarov, I., et al. (1999). Arrestin function in G protein-coupled receptor endocytosis requires phosphoinositide binding. *EMBO J. 18*(4): 871-881. 10.1093/emboj/18.4.871

Gimenez, L. E., et al. (2014). Mutations in arrestin-3 differentially affect binding to neuropeptide Y receptor subtypes. *Cell. Signal. 26*(7): 1523-1531. 10.1016/j.cellsig.2014.03.019

Goodman, O. B., et al. (1996). β-Arrestin acts as a clathrin adaptor in endocytosis of the β2-adrenergic receptor. *Nature 383*(6599): 447-450. 10.1038/383447a0

Gurevich, E. V. and V. V. Gurevich (2006). Arrestins: ubiquitous regulators of cellular signaling pathways. *Genome Biol. 7*(9): 236. 10.1186/gb-2006-7-9-236

Gurevich, V. V. (1998). The selectivity of visual arrestin for light-activated phosphorhodopsin is controlled by multiple nonredundant mechanisms. *J. Biol. Chem. 273*(25): 15501-15506. 10.1074/jbc.273.25.15501

Gurevich, V. V. and E. V. Gurevich (2006). The structural basis of arrestin-mediated regulation of G-protein-coupled receptors. *Pharmacol. Ther. 110*(3): 465-502. 10.1016/j.pharmthera.2005.09.008

Hammond, G. R. V., et al. (2009). Reversible binding and rapid diffusion of proteins in complex with inositol lipids serves to coordinate free movement with spatial information. *J. Cell Biol. 184*(2): 297-308. 10.1083/jcb.200809073

Humphrey, W., et al. (1996). VMD: visual molecular dynamics. *J. Mol. Graph. 14*(1): 33-38, 27-38. 10.1016/0263-7855(96)00018-5

Kang, D. S., et al. (2014). Role of β-arrestins and arrestin domain-containing proteins in G protein-coupled receptor trafficking. *Curr. Opin. Cell Biol. 27*: 63-71. 10.1016/j.ceb.2013.11.005

Krasel, C., et al. (2005). β-Arrestin binding to the β2-adrenergic receptor requires both receptor phosphorylation and receptor activation. *J. Biol. Chem. 280*(10): 9528-9535.

Kumari, P., et al. (2016). Functional competence of a partially engaged GPCR–β-arrestin complex. *Nat. Commun. 7*(1): 1-16. 10.1038/ncomms13416

Kumari, P., et al. (2017). Core engagement with β-arrestin is dispensable for agonist-induced vasopressin receptor endocytosis and ERK activation. *Mol. Biol. Cell 28*(8): 1003-1010. 10.1091/mbc.E16-12-0818

Lally, C. C. M., et al. (2017). C-edge loops of arrestin function as a membrane anchor. *Nat. Commun. 8*: 14258. 10.1038/ncomms14258

Laporte, S. A., et al. (2000). The interaction of β-arrestin with the AP-2 adaptor is required for the clustering of β2-adrenergic receptor into clathrin-coated pits. *J. Biol. Chem. 275*(30): 23120-23126.

Latorraca, N. R., et al. (2018). Molecular mechanism of GPCR-mediated arrestin activation. *Nature 557*(7705): 452-456. 10.1038/s41586-018-0077-3

Lee, M.-H., et al. (2016). The conformational signature of β-arrestin2 predicts its trafficking and signalling functions. *Nature 531*(7596): 665-668. 10.1038/nature17154

Liu, A. P., et al. (2009). Global and local regulation of clathrin-coated pit dynamics detected on patterned substrates. *Biophys. J. 97*(4): 1038-1047. 10.1016/j.bpj.2009.06.003

Lohse, M. J., et al. (1990). beta-Arrestin: a protein that regulates beta-adrenergic receptor function. *Science 248*(4962): 1547-1550. 10.1126/science.2163110

Manley, S., et al. (2008). High-density mapping of single-molecule trajectories with photoactivated localization microscopy. *Nat. Methods 5*(2): 155-157. 10.1038/nmeth.1176

Merrifield, C. J., et al. (2002). Imaging actin and dynamin recruitment during invagination of single clathrin-coated pits. *Nat. Cell Biol. 4*(9): 691-698. 10.1038/ncb837

Mondin, M., et al. (2011). Neurexin-neuroligin adhesions capture surface-diffusing AMPA receptors through PSD-95 scaffolds. *J. Neurosci. 31*(38): 13500-13515. 10.1523/JNEUROSCI.6439-10.2011

Nair, D., et al. (2013). Super-resolution imaging reveals that AMPA receptors inside synapses are dynamically organized in nanodomains regulated by PSD95. *J. Neurosci. 33*(32): 13204-13224. 10.1523/JNEUROSCI.2381-12.2013

Nobles, K. N., et al. (2007). The active conformation of β-arrestin1: direct evidence for the phosphate sensor in the N-domain and conformational differences in the active states of β-arrestins1 and-2. *J. Biol. Chem. 282*(29): 21370-21381.

Nuber, S., et al. (2016). β-Arrestin biosensors reveal a rapid, receptor-dependent activation/deactivation cycle. *Nature 531*(7596): 661-664. 10.1038/nature17198

O'Hayre, M., et al. (2017). Genetic evidence that β-arrestins are dispensable for the initiation of β2-adrenergic receptor signaling to ERK. *Sci. Signal. 10*(484). 10.1126/scisignal.aal3395

Oakley, R. H., et al. (1999). Association of β-arrestin with G protein-coupled receptors during clathrin-mediated endocytosis dictates the profile of receptor resensitization. *J. Biol. Chem. 274*(45): 32248-32257.

Oakley, R. H., et al. (2000). Differential affinities of visual arrestin, βarrestin1, and βarrestin2 for G protein-coupled receptors delineate two major classes of receptors. *J. Biol. Chem. 275*(22): 17201-17210.

Peterson, S. M., et al. (2015). Elucidation of G-protein and β-arrestin functional selectivity at the dopamine D2 receptor. *Proc. Natl. Acad. Sci. U. S. A. 112*(22): 7097-7102. 10.1073/pnas.1502742112

Pierce, K. L., et al. (2002). Seven-transmembrane receptors. *Nat. Rev. Mol. Cell Biol. 3*(9): 639-650. 10.1038/nrm908

Puthenveedu, M. A. and M. von Zastrow (2006). Cargo regulates clathrin-coated pit dynamics. *Cell 127*(1): 113-124. 10.1016/j.cell.2006.08.035

Rosenbaum, D. M., et al. (2009). The structure and function of G-protein-coupled receptors. *Nature 459*(7245): 356-363. 10.1038/nature08144

Rossier, O., et al. (2012). Integrins β1 and β3 exhibit distinct dynamic nanoscale organizations inside focal adhesions. *Nat. Cell Biol. 14*(10): 1057-1067. 10.1038/ncb2588

Santini, F., et al. (2002). G protein–coupled receptor/arrestin3 modulation of the endocytic machinery. *J. Cell Biol. 156*(4): 665-676. 10.1083/jcb.200110132

Santos, M. d. S., et al. (2013). Inhibitors of PI(4,5)P2 synthesis reveal dynamic regulation of IgE receptor signaling by phosphoinositides in RBL mast cells. *Mol. Pharmacol. 83*(4): 793-804. 10.1124/mol.112.082834

Scheerer, P. and M. E. Sommer (2017). Structural mechanism of arrestin activation. *Curr. Opin. Struct. Biol. 45*: 160-169. 10.1016/j.sbi.2017.05.001

Schindelin, J., et al. (2012). Fiji: an open-source platform for biological-image analysis. *Nat. Methods 9*(7): 676-682. 10.1038/nmeth.2019

Schneider, C. A., et al. (2012). NIH Image to ImageJ: 25 years of image analysis. *Nat. Methods 9*(7): 671-675. 10.1038/nmeth.2089

Shukla, A. K., et al. (2013). Structure of active β-arrestin-1 bound to a G-protein-coupled receptor phosphopeptide. *Nature 497*(7447): 137-141. 10.1038/nature12120

Shukla, A. K., et al. (2014). Visualization of arrestin recruitment by a G-protein-coupled receptor. *Nature 512*(7513): 218-222. 10.1038/nature13430

Shukla, A. K., et al. (2011). Emerging paradigms of β-arrestin-dependent seven transmembrane receptor signaling. *Trends Biochem. Sci. 36*(9): 457-469. 10.1016/j.tibs.2011.06.003

Stauffer, T. P., et al. (1998). Receptor-induced transient reduction in plasma membrane PtdIns(4,5)P2 concentration monitored in living cells. *Curr. Biol. 8*(6): 343-346. 10.1016/s0960-9822(98)70135-6

Temkin, P., et al. (2011). SNX27 mediates retromer tubule entry and endosome-to-plasma membrane trafficking of signalling receptors. *Nat. Cell Biol. 13*(6): 715-721. 10.1038/ncb2252

Violin, J. D., et al. (2006). G-protein-coupled Receptor Kinase Specificity for β-Arrestin Recruitment to the β2-Adrenergic Receptor Revealed by Fluorescence Resonance Energy Transfer *. *J. Biol. Chem. 281*(29): 20577-20588. 10.1074/jbc.M513605200

Xiao, K., et al. (2004). Activation-dependent conformational changes in β-arrestin 2. *J. Biol. Chem. 279*(53): 55744-55753.

Yudowski, G. A., et al. (2006). Distinct modes of regulated receptor insertion to the somatodendritic plasma membrane. *Nature Neuroscience 9*(5): 622-627. 10.1038/nn1679

2.6 Figures

Figure 2.1 Discrete mode of GPCR-activated cellular β-arrestin trafficking is broadly conserved

(a–d) Live cell TIRF microscopy images showing (a) FLAG–β1AR (blue) or (c) FLAG–β2AR (blue), β-arrestin-2–GFP (green) and clathrin-light-chain–DsRed (red) before and after 10 μM isoproterenol treatment. Average enrichment at CCSs after 10 μM isoproterenol treatment for (b) FLAG–β1AR (d) FLAG–β2AR (n=14 and 15 cells, respectively, from 3 independent experiments, data shown as mean ± s.e.m.). (e) Live cell TIRF microscopy images of HEK 293 cells co-expressing super ecliptic pHluorin–β2AR (blue), β-arrestin-2–mApple (green), and clathrin-light-chain–TagBFP (red) before and after 10 μM isoproterenol treatment. (f) Timelapse of individual pre-existing CCSs from panel e. Scale bars, 5 μm. (a, c, e, f) show representative images from 3 independent experiments.

Figure 2.2 β-arrestin trafficking activation requires the GPCR core but not the GPCR cytoplasmic tail

(a) Live cell TIRF microscopy images of COS-1 cells co-expressing FLAG–β2AR truncated at the 341st amino acid (341T, blue), β-arrestin-2–GFP (green) and clathrin-light-chain–DsRed (red) before and after 10 μM isoproterenol treatment. (b) Maximum β-arrestin-2–GFP enrichment at CCSs in cells treated with 10 μM isoproterenol and co-expressing the indicated FLAG–β2AR (n=11 cells from 3 independent experiments, p=0.5634 using a two-tailed unpaired t test). (c) Live cell TIRF microscopy images showing FLAG–DRD2 G protein biased mutant (G protein, blue), β-arrestin-2–GFP (green) and clathrin-light-chain–DsRed (red) before and after 10 μM quinpirole treatment. (d) Average (data shown as mean ± s.e.m.) and (e) maximum enrichment of β-arrestin-2–GFP into CCSs in cells expressing wild-type (green) or G protein biased mutant versions (gray) of FLAG-DRD2 and treated with 10 μM quinpirole (n=11 (WT) and 14 (G protein) cells from 3 independent experiments, p=0.013 using a two-tailed unpaired t test using Welch's correction). (a) and (c) show representative images from 3 independent experiments. Scatter plots show overlay of mean and s.e.m. Scale bars, 5 μm. * $p < 0.05$

Figure 2.3 β-arrestin activation is inhibited by a polar network in a region proximal to the β-arrestin finger loop

(a) Representative live cell TIRF microscopy images (from 3 independent experiments) showing FLAG–β2AR (blue), clathrin-light-chain–DsRed (red), and wild-type (top, green) or finger loop proximal mutant (bottom, green) β-arrestin-2–GFP without agonist treatment. Clustering index measuring constitutive activation of the indicated (b) β-arrestin-2–GFP or (c) β-arrestin-1–mVenus constructs without agonist treatment (n=12 cells from 3 independent experiments, $p<0.0001$ and 0.0008, respectively, using a two-tailed unpaired t test). (d) Snapshot from molecular dynamics simulations of inactive-state β-arrestin-1 in which K77 and E313 occasionally form a stable salt bridge. This salt bridge formed 6% of the time in inactive-state simulations (six simulations totaling 26.7 μs); it may form more frequently on longer timescales. It formed in only a few frames of active-state simulations (0.2% of the time across six simulations totaling 29.3 μs in length). (e) Clustering index of the indicated β-arrestin-2–GFP construct without agonist treatment. Statistics were calculated using a two-tailed unpaired t test (for K78E, n=12 cells from 3 independent experiments, $p = 0.0003$; for E314K, n=12 cells from 3 independent experiments, $p<0.0001$. Scatter plots show overlay of mean and s.e.m. Scale bars, 5 μm. *** $p < 0.001$.

Figure 2.4 Phosphoinositide binding is required to capture β-arrestin at the plasma membrane after GPCR dissociation

Representative live cell TIRF microscopy images (from 3 independent experiments) showing FLAG–β2AR, the indicated β-arrestin-2–GFP construct, and clathrin-light-chain–DsRed. Shown are β-arrestin images false-colored to indicate fluorescence intensity, maximum fluorescence enrichment at CCSs, and normalized average plasma membrane (PM) β-arrestin-2–GFP fluorescence (shown as mean ± s.e.m), respectively, from cells co-expressing FLAG–β2ARs without isoproterenol treatment (a–c), and the following β-arrestin-2–GFP constructs with 10 μM isoproterenol treatment: wild-type (d–f), lipid mutant (g–i), CCS mutant (j–l), and CCS and lipid mutant (m–o); n=12 cells per condition. Wild-type β-arrestin-2–GFP maximum enrichment in panel h is replotted from panel e and panel n is replotted from panel k. Statistics were calculated using a two-tailed unpaired t test with Welch's correction. For (h) n=12 and 11 cells, respectively, from 3 independent experiments and p=0.0006. For (k) n=10 cells from 3 independent experiments and p=0.0102. For (n) n=10 cells from 3 independent experiments and p=0.0022. Extended Data Table 1 provides detailed description of β-arrestin mutations. Scatter plots show overlay of mean and s.e.m. scale bars, 5 μm. ** $p < 0.01$; *** $p < 0.001$.

Figure 2.5 Single particle tracking-photoactivated localization microscopy (sptPALM) analysis of GPCR and β-arrestin dynamics and stable β-arrestin binding at CCSs

(a–d) Representative images (from at least 3 independent experiments) of (a) photoactivatable (PA) mCherry-β1AR (green) or (b) PAmCherry-β2AR (green) trajectories and (c) PAmCherry-β-arrestin-2 trajectories (green) with β1AR expression or (d) PAmCherry-β-arrestin-2 (green) trajectories with β2AR expression from sptPALM analysis overlaid with a clathrin marker (red) after 10 μM isoproterenol treatment. (e) False positive corrected diffusion coefficients (D) of PAmCherry-β2AR, β-arrestin-2-PAmCherry, and PAmCherry-PLCδ1-PH in live cells after 10 μM isoproterenol treatment (n=13, 21, and 8 cells, respectively). β-arrestin-2-PAmCherry and PAmCherry-PLCδ1-PH were co-expressed individually with FLAG-β2AR. False positive corrected distribution of diffusion coefficients (D) of β-arrestin-2-PAmCherry wild-type and CCS mutant when co-expressed with (f) FLAG-β1AR (n=13 and 17 cells, respectively, from 3 independent experiments; statistical significance of the immobile fractions was calculated using a two-tailed unpaired t test, $p<0.0001$) or (g) FLAG-β2AR (n=21 and 10 cells, respectively, from 3 independent experiments; statistical significance of the immobile fractions was calculated using a two-tailed unpaired t test, $p=0.002$) β-arrestin-2-PAmCherry diffusion coefficient profiles when activated by the β2AR are replotted from panel e. (h) COS-1 cells co-expressing FLAG-β2AR, β-arrestin-2-GFP (green), and clathrin-light-chain-DsRed (red) were treated with 10 μM isoproterenol for 3 minutes before β-arrestin-2-GFP photobleaching. Shown are representative images (from 3 independent experiments) of the photobleached area. β-arrestin-2 clustering index over the course of the photobleaching experiment in cells co-expressing activated (i) FLAG-β1AR (n=12 cells from 3 independent experiments) or (j) FLAG-β2AR (n=15 and 13 cells for unbleached and photobleached conditions, respectively, from 3 independent experiments). Data are shown as mean ± s.e.m. Scale bars, 0.5 μm.

Extended Data Figure 2.1 Verification of GPCR-specificity of the discrete β-arrestin trafficking mechanism, demonstration that this mechanism produces super-stoichiometric β-arrestin accumulation in CCSs and that its activation does not require the GPCR tail

(a) Average β-arrestin-2–GFP enrichment at CCSs in cells expressing FLAG-β1AR after the following treatments: 10 μM isoproterenol (green, n=14 cells), 15-minute pretreatment with 10 μM CGP 20712A and 10 μM isoproterenol treatment (red, n=12 cells), 10 μM CGP 20712A alone (gray, n=12 cells). Data shown for the 10 μM isoproterenol condition are replotted from Figure 2.1b. (b) Maximum β-arrestin-2–GFP enrichment at CCSs in HEK 293 cells transfected with the indicated receptor or empty vector and treated with 10 μM isoproterenol. (c) β-arrestin-2–GFP enrichment at CCSs in H9c2 cells without GPCR overexpression and treated with 10 μM isoproterenol or 10 μM dobutamine (n=5 or 4 cells, respectively, from 2 independent experiments). (d) β-arrestin-2–GFP enrichment at CCSs in H9c2 cells without GPCR overexpression and treated as indicated (n=12 cells). (e) Live cell TIRF microscopy images (representative of n=3 independent experiments) showing FLAG–β1AR (blue), β-arrestin-1–mVenus (green) and clathrin-light-chain–DsRed (red) before and after 10 μM isoproterenol treatment. (f) Enrichment into CCSs (n=7 cells from 3 independent experiments). (g) Maximum β-arrestin-1–mVenus enrichment at CCSs in HEK 293 cells transfected with FLAG-β1AR or empty vector and treated with 10 μM isoproterenol (n=7 and 11 cells from 3 independent experiments, p=0.0023 using an unpaired t test with Welch's correction). (h) Average β-arrestin-2–GFP enrichment at CCSs in cells expressing FLAG-β2AR after the following treatments: 10 μM isoproterenol (green, n=15 cells), 15-minute pretreatment with 10 μM ICI 118,551 and then 10 μM isoproterenol treatment (red, n=14 cells), 10 μM ICI 118,551 (gray, n=12). Data shown for the 10 μM isoproterenol condition are replotted from Figure 2.1d.

(i) Fluorescence intensity profiles from lines shown in Figure 2.1e. (j) Time-dependent correlation coefficient of line scans across cells derived from immobilization experiments shown in Figure 2.1g, h; n=3). (k) Live cell TIRF microscopy images (representative of n=3 independent experiments) showing FLAG–β2AR-GFP and clathrin-light-chain–DsRed (red) before and after 10 μM isoproterenol treatment. Fluorescence from the Alexa647 conjugated FLAG antibody shown in blue and GFP fluorescence shown in green. (l) Difference in GFP and Alexa647 fluorescence enrichment at CCSs in cells co-expressing FLAG-β1ARs (red), FLAG-β2ARs (blue) and β-arrestin-2-GFP or FLAG-β2AR-GFP (black). Cells were labeled with Alexa647 conjugated FLAG antibody for 10 minutes prior to live cell imaging. Data were derived from the experiments shown in Figure 2.1a, b (blue line, n=14 cells from 3 independent experiments), Figure 2.1c, d (red line, n=15 cells from 3 independent experiments), and Extended Data Figure 2.1k (black line n=12 cells from 3 independent experiments). (m) Plot of β-arrestin/GPCR stoichiometry calculated from the data displayed in panel k, calibrated according to the doubly labeled FLAG-β2AR-GFP reference construct defining 1:1 stoichiometry (For β1AR and β2AR, n=14 and 15 cells, respectively, from 3 independent experiments). A correction index was calculated by dividing GFP fluorescence by Alexa647 (FLAG) fluorescence in CCSs. This correction index was then applied to receptor and β-arrestin-2 enrichment in CCSs to determine β-arrestin-2/GPCR stoichiometry throughout the time course. Images were captured continuously at 0.5 Hz and stoichiometry values over the time course were calculated using a rolling average with 50-frame window size. Scale bar, 5 μm. Scatter plots show overlay of mean and s.e.m. (a, d, h, j, l) show data as mean ± s.e.m. ** $p < 0.01$

Extended Data Figure 2.2 Additional demonstration that multiple GPCRs can activate the discrete β-arrestin trafficking mechanism

(a) Live cell TIRF microscopy images showing FLAG–mu opioid receptor (MOR, blue), β-arrestin-2–GFP (green) and clathrin-light-chain–DsRed (red) before and after 10 μM DAMGO treatment. (b) Average FLAG-MOR and β-arrestin-2–GFP enrichment at CCSs after treatment with 10 μM DAMGO (n=12 cells). (c) Maximum β-arrestin-2–GFP enrichment at CCSs for HEK 293 cells expressing FLAG-MOR or empty vector and treated with 10 μM DAMGO (n=12 cells per condition from 3 independent experiments; p=<0.0001 using a two-tailed unpaired t test with Welch's correction). (d) Live cell TIRF microscopy images showing FLAG–kappa opioid receptor (KOR, blue), β-arrestin-2–GFP (green) and clathrin-light-chain–DsRed (red) before and after 10 μM dynorphin treatment. (e) Enrichment into CCSs after bath application of 10 μM dynorphin (n=18 cells). (f) Maximum β-arrestin-2–GFP enrichment at CCSs in HEK 293 cells expressing FLAG-KOR or empty vector and treated with 10 μM dynorphin (n=18, 13 cells, respectively, from 3 independent experiments; p=0.0028 using a two-tailed unpaired t test with Welch's correction). (g) Live cell TIRF microscopy images showing FLAG–DRD2 (blue), β-arrestin-2–GFP (green) and clathrin-light-chain–DsRed (red), before and after 10 μM quinpirole treatment. (h) Enrichment into CCSs after bath application of 10 μM quinpirole (n=12 cells). (i) Maximum β-arrestin-2–GFP enrichment at CCSs in cells expressing FLAG-DRD2 or untransfected and treated with 10 μM quinpirole (n=11, 12 cells from 3 independent experiments; p=0.0095 using a two-tailed unpaired t test with Welch's correction). (a, d, g) show representative images from 3 independent experiments. (b, e, h) show data as mean ± s.e.m. Scatter plots show overlay of mean and s.e.m. Scale bars, 5 μm. * $p < 0.05$; ** $p < 0.01$; *** $p < 0.001$

Extended Data Figure 2.3 Direct interaction with the GPCR, but not the GPCR cytoplasmic tail, is required for β-arrestin trafficking activation

(a) Live cell TIRF microscopy images showing FLAG–β1AR truncated at the 415th amino acid (415T, blue), β-arrestin-2–GFP (green) and clathrin-light-chain–DsRed (red) before and after 10 μM isoproterenol treatment. (b) Maximum β-arrestin-2–GFP enrichment at CCSs after 10 μM isoproterenol for cells co-expressing the indicated FLAG–β1AR receptor (n=10, 12 cells, respectively, from 3 independent experiments, p=0.5825 calculated using a two-tailed unpaired t test). (c) Live cell TIRF microscopy images showing FLAG–β2AR truncated at the 365th amino acid (365T, blue), β-arrestin-2–GFP (green) and clathrin-light-chain–DsRed (red) before and after 10 μM isoproterenol treatment. (d) Maximum β-arrestin-2–GFP enrichment at CCSs in HEK 293 cells treated with 10 μM isoproterenol and either transfected with FLAG-β2AR or empty vector (n=11, 13 cells, respectively, from 3 independent experiments, p=0.0269 calculated using a two-tailed unpaired t test with Welch's correction). (e) Maximum β-arrestin-2–GFP enrichment at CCSs for cells co-expressing the indicated FLAG–β2AR receptor and treated with 10 μM isoproterenol (n=12 cells from 3 independent experiments, p=0.0606 calculated using a two-tailed unpaired t test). (f) Live cell TIRF microscopy images showing FLAG–DRD2 (blue), β-arrestin-2–GFP (green) and clathrin-light-chain–DsRed (red) before and after 10 μM quinpirole treatment. (g) Initial enrichment in CCSs before 10 μM quinpirole treatment and (h) maximum enrichment after 10 μM quinpirole treatment (n=12 cells from 3 independent experiments; p=0.19 and 0.4873, respectively, using a two-tailed unpaired t test). (i) Live cell TIRF microscopy images showing FLAG–β1AR (blue), β-arrestin-2–GFP (green) and clathrin-light-chain–DsRed (red) before and after 5 μM forskolin (fsk) treatment. (j) Initial enrichment in CCSs before 5 μM forskolin (fsk) treatment and (k) maximum enrichment after 5 μM fsk treatment (n=12 cells from 3 independent experiments; p=0.6325 and 0.0971,

respectively, using a two-tailed unpaired t test). (l) Live cell TIRF microscopy images showing FLAG–β2AR (blue), β-arrestin-2–GFP KNC mutant (green) and clathrin-light-chain–DsRed (red before and after 10 μM isoproterenol treatment. (m) Initial enrichment in CCSs before 10 μM isoproterenol treatment and (n) maximum enrichment after 10 μM isoproterenol (n=9 (WT) or 8 (KNC) cells from 3 independent experiments; p=0.6681(m) and p=0.001 (n) using a two-tailed unpaired t test with Welch's correction). (a, c, f, I, l) show representative images from 3 independent experiments. Scatter plots show overlay of mean and s.e.m. Scale bars, 5 μm. * $p < 0.05$, ** $p < 0.01$

Extended Data Figure 2.4 Additional verification that charge mutations in the finger loop-proximal region of β-arrestin finger loop produce a constitutive activation phenotype

(a) Live cell TIRF microscopy images showing FLAG–β2AR, clathrin-light-chain–DsRed (red), and the polar core mutant of β-arrestin-2–GFP (green) in the absence of agonist treatment. (b) Clustering index of β-arrestin-2–GFP for the indicated construct in the absence of agonist treatment. Statistical significance was calculated using a two-tailed unpaired t test with Welch's correction (polar core mutant: n=12 cells from 3 independent experiments, $p<0.0001$; finger loop proximal mutant: n=16 cells from 3 independent experiments $p<0.0001$; R77A: n=12 cells from 3 independent experiments, $p=0.0403$; K78A: n=12 cells from 3 independent experiments, $p=0.0016$). WT and finger loop proximal mutant data replotted from Figure 2.3b. (c) Association of β-arrestin-2–GFP constructs with the adaptin beta subunit of AP-2 in the absence of agonist treatment. Molecular mass markers (in kDa) are shown on the right side of blots. For gel source data, see Supplementary Figure 2.1. The representative Western blots in panel c are representative of 3 independent experiments, quantified in (d), and shown as AP-2/GFP intensity in the immunoprecipitation conditions (n=3 independent experiments, $p=0.0218$ using a two-tailed unpaired t test). (e) Measurement of β-arrestin-2–GFP construct expression in cell lysates from panel c. (f–i) Live cell TIRF microscopy images showing FLAG–β2AR, clathrin-light-chain–DsRed (red), and β-arrestin-2–GFP with the indicated point mutations (green) in the absence of agonist treatment. Detailed description of β-arrestin mutations are provided in Extended Data Table 1. (a, f–i) show representative images from 3 independent experiments. Scatter plots show overlay of mean and s.e.m. Scale bars, 5 μm. * $p < 0.05$; ** $p < 0.01$; *** $p < 0.001$

Extended Data Figure 2.5 Molecular dynamics simulations suggest that finger loop-proximal charged residues stabilize β-arrestin in an inactive state

(a) Crystal structures of β-arrestin-1 (left) in an inactive (middle) and active (right) conformation reveal an extensive network of polar residues proximal to the finger loop involving residues R76, K77 and D78. (b) Histogram of distances between K77 and E313 in simulations of inactive arrestin (blue) and active arrestin (pink), showing frequency of K77-E313 salt bridge formation. The K77-E313 distance corresponds to the minimum distance between polar heavy atoms on the two residues' side chains. A separation distance of less than 3.0 Å corresponds to formation of the salt bridge. For the six simulations started from the inactive state, the salt bridge formed 1.1%, 5.7%, 6.3%, 17.6%, 1.0%, and 2.0% of the time, respectively (simulation lengths were 4.7 μs, 3.1 μs, 2.9 μs, 5.1 μs, 5.2 μs, and 5.7 μs, respectively). For the six simulations started from the active state, the salt bridge formed 0.02%, 0.04%, 0.0%, 1.1%, 0.0%, and 0.0% of the time, respectively (simulation lengths were 5.0 μs, 5.0 μs, 4.7 μs, 4.8 μs, 4.8 μs, and 5.0 μs, respectively). (c) Inactive state crystal structure of β-arrestin-1 in which E313 interacts with R188 on a different β-arrestin-1 molecule in the crystal lattice. (d) Sequence alignment of arrestins showing conservation of residues R76, K77, D78, and E313. Detailed description of β-arrestin mutations are provided in

Extended Data Figure 2.6 Verification that the conserved phosphoinositide binding determinant in the β-arrestin C-domain is specifically required for the catalytic trafficking mechanism and operates upstream of clathrin and AP-2 binding interactions

Graphical representation of β-arrestin interaction domains without (a) and with (b) βAR activation by isoproterenol. (c) Live cell TIRF microscopy images showing FLAG–β2AR (blue), β-arrestin-2-GFP (green), and clathrin-light-chain–DsRed (red) before and after 10 μM isoproterenol treatment. (d) Live cell TIRF microscopy images showing FLAG–β2AR (blue), β-arrestin-2-GFP lipid mutant (green), and clathrin-light-chain–DsRed (red) before and after 10 μM isoproterenol treatment. (e) Representative western blot (from 4 independent experiments) of purified wild-type and lipid mutant versions of β-arrestin-1(1-393) immunoprecipitation with PIP2-coated agarose beads and quantified in (f) as percent of input protein (n=4 independent experiments, p=0.0142 using a two-tailed unpaired t test). For gel source data, see Supplementary Figure 2.1. (g) Live cell TIRF microscopy images showing FLAG–β2AR (blue), β-arrestin-2-GFP (F191G, L192G) lipid anchor mutant (green), and clathrin-light-chain–DsRed (red) before and after 10 μM isoproterenol treatment. (h) Maximum β-arrestin-2–GFP enrichment at CCSs in cells expressing the indicated β-arrestin-2–GFP construct and treated with 10 μM isoproterenol (n=12 cells from 3 independent experiments; p=0.9227 calculated using a two-tailed unpaired t test). (i) Live cell TIRF microscopy images showing FLAG–β2AR (blue), β-arrestin-2-GFP CCS mutant (green), and clathrin-light-chain–DsRed (red) before and after with 10 μM isoproterenol. (j) Representative images of HEK 293 cells co-expressing FLAG–β2AR (blue), β-arrestin-2-GFP lipid and CCS mutant (green), and clathrin-light-chain–DsRed (red) before and after with 10 μM isoproterenol. Representative β-arrestin images false colored to indicate fluorescence intensity, maximum fluorescence enrichment at CCSs, and normalized average plasma membrane (PM) β-arrestin-2–GFP fluorescence (data shown as

mean ± s.e.m.), respectively, from cells co-expressing FLAG–β1ARs (n=12 cells per condition) without isoproterenol treatment (k–m), and the following β-arrestin-2–GFP constructs with 10 μM isoproterenol treatment: wild-type (n–p), lipid mutant (q–s), CCS mutant (t–v), and CCS and lipid mutant (w–y). Wild-type β-arrestin-2–GFP maximum enrichment at CCSs shown in panels r, u, x is replotted from panel o. Live cell TIRF microscopy images showing cells before and after 10 μM isoproterenol treatment and co-expressing FLAG–β1AR (blue), clathrin-light-chain–DsRed (red), and the following GFP labeled versions of β-arrestin-2 (green): (z) wild-type, (aa) lipid mutant, and (ab) CCS mutant, and (ac) CCS and lipid mutant. (ad) Live cell TIRF microscopy images showing FLAG-β2AR and the indicated β-arrestin-2-GFP construct in the absence of agonist treatment. (ae) Clustering index of β-arrestin-2–GFP for the indicated construct in the absence of agonists treatment. Detailed description of β-arrestin mutations are provided in Extended Data Table 1. (c, d, g, i, j, k, n, q, t, w, z, aa, ab, ac, ad) show representative images from 3 independent experiments. For (r, u, x) n=12 cells from 3 independent experiments; statistical significance was calculated using an unpaired t test with Welch's correction, p=0.0007, 0.0018, and 0.0012, respectively. For (ae), statistical significance was calculated using an unpaired t test with Welch's correction, n=12 (WT) and 16 (finger loop proximal mutant) from 3 independent experiments, p<0.0001; n=12 (WT) and 15 (finger loop proximal & lipid mutant) from 3 independent experiments, p=0.5464). WT and finger loop proximal mutant data replotted from Figure 2.3b. Scatter plots show overlay of mean and s.e.m. Scale bars, 5 μm. ** $p < 0.01$

Extended Data Figure 2.7 Phosphoinositide binding is essential for catalytic activation of β-arrestin trafficking but is dispensable for trafficking mediated by the scaffold mechanism

(a) Live cell microscopy images of HEK 293 cells co-expressing FLAG–β2AR-V2R C tail (blue), β-arrestin-2-GFP CCS mutant (green), and clathrin-light-chain–DsRed (red) before and after with 10 μM isoproterenol treatment. (b) Normalized plasma membrane (PM) fluorescence of β-arrestin-2–GFP lipid mutant in cells co-expressing FLAG–β2AR-V2R (n=12 cells from 3 independent experiments) when treated with 10 μM isoproterenol. (c) Maximum β-arrestin-2–GFP enrichment at CCSs in cells expressing indicated β-arrestin-2–GFP construct before and after activation of FLAG-β2AR-V2R C tail with 10 μM isoproterenol (n=10, 12 cells, respectively, from 3 independent experiments; p=0.6433 using a two-tailed unpaired t test). (d) Live cell microscopy images of COS-1 cells co-expressing FLAG–β2AR (blue), β-arrestin-2-GFP (green), and clathrin-light-chain–DsRed (red) that have been pre-treated for 1 hour with 1 μM phenylarsine oxide (PAO) or vehicle (DMSO) before 10 μM isoproterenol treatment. (e) Normalized average fold over initial β-arrestin-2–GFP fluorescence in cells co-expressing FLAG–β2AR when pre-treated for 1 hour with 1 μM phenylarsine oxide (PAO) before 10 μM isoproterenol treatment (n=12 cells from 3 independent experiments). (f) Live cell microscopy images of COS-1 cells co-expressing FLAG–β2AR-V2R C tail (blue), β-arrestin-2-GFP (green), and CLC-dsRed (red) that have been pre-treated for 1 hour with 1 μM phenylarsine oxide (PAO) before 10 μM isoproterenol treatment. (g) Normalized average fold over initial β-arrestin-2–GFP fluorescence in cells co-expressing FLAG–β2AR or FLAG–β2AR-V2R when pre-treated for 1 hour with 1 μM phenylarsine oxide (PAO) before 10 μM isoproterenol treatment (n=12 cells from 3 independent experiments). (a, d, f) show representative images from 3 independent

experiments. (b, e, g) show data as mean ± s.e.m. Scatter plots show overlay of mean and s.e.m.

Extended Data Figure 2.8 sptPALM controls and mean square displacement (MSD) plots and cellular model

(a) Representative image of a clathrin mask (green) generated from a CLC-GFP image (red). Representative diffusion maps overlaid with the clathrin mask for HEK 293 cells and treated with 10 μM isoproterenol expressing (b) PAmCherry-β1AR, (c) PAmCherry-β2AR, (d) β-arrestin-2-PAmCherry co-expressed with FLAG-β1AR, (e) β-arrestin-2-PAmCherry co-expressed with FLAG-β2AR (f) Distribution of diffusion coefficients (D) of false positive detections from HEK 293 cells expressing FLAG-β2AR and imaged under standard sptPALM acquisition conditions to determine contribution of false positive detections in the experimental setup and analysis. (g) Distribution of diffusion coefficients (D) of PAmCherry-β2AR, PAmCherry-PLCδ1-PH, and β-arrestin-2-PAmCherry in live cells imaged at 37°C after treatment with 10 μM isoproterenol (n=13, 21, and 8 cells, respectively). Black lines show diffusion coefficient profiles that have not been corrected for false positive detections, showing limited contribution to the profiles. β-arrestin-2-PAmCherry and PAmCherry-PLCδ1-PH were co-expressed individually with FLAG-β2AR. (h) Average MSD plots derived from sptPALM analysis of PAmCherry-β1AR and PAmCherry-β2AR trajectories in HEK 293 cells treated with 10 μM isoproterenol (n=8 and 13 cells, respectively). (i) Distribution of diffusion coefficients (D) of β-arrestin-2-PAmCherry wild-type and CCS mutant when co-expressed with FLAG-β1AR in live HEK 293 cells imaged at 37°C after treatment with 10 μM isoproterenol (n=13 and 17 cells, respectively). Black lines show diffusion coefficient profiles that have not been corrected for false positive detections, showing limited contribution to the profiles. (j) Average MSD plots derived from sptPALM analysis of β-arrestin-2-PAmCherry wild-type and CCS mutant trajectories in cells co-expressing FLAG-β1AR and treated with 10 μM isoproterenol (n=13 and 17 cells, respectively). (k) Distribution of diffusion coefficients (D) of β-arrestin-2-PAmCherry wild-type and CCS

mutant when co-expressed with FLAG-β2AR in live cells imaged at 37°C after treatment with 10 μM isoproterenol (n=21 and 10 cells, respectively). Black lines show diffusion coefficient profiles that have not been corrected for false positive detections, showing limited contribution to the profiles. β-arrestin-2-PAmCherry diffusion coefficient profiles when activated by the β2AR are replotted from panel d. (l) Average MSD plots derived from sptPALM analysis of β-arrestin-2-PAmCherry wild-type and CCS mutant trajectories in HEK 293 cells co-expressing FLAG-β2AR and treated with 10 μM isoproterenol (n=21 and 10 cells, respectively). (m) Immobile and (n) mobile β-arrestin-2-PAmCherry trajectory detections overlaid with a clathrin marker (red) in live cells co-expressing FLAG-β1AR after 10 μM isoproterenol treatment. (o) Immobile and (p) mobile β-arrestin-2-PAmCherry trajectory detections overlaid with a clathrin marker (red) in live cells co-expressing FLAG-β2AR after 10 μM isoproterenol treatment. Trajectory detections are false colored based on the density of detections at each pixel. Error bars represent s.e.m; in some cases, error bars are smaller than the height of the symbol and, therefore, not shown. Scale bars, 500 nm for sptPALM images. (q) Proposed cellular pathway for catalytic activation of β-arrestin. (r) Representative microscopy images of COS-1 cells co-expressing FLAG-β2AR, β-arrestin-2-GFP (green), and clathrin-light-chain-DsRed (red) that were treated with 10 μM isoproterenol for 3 minutes. Then, β-arrestin-2-GFP was photobleached in the indicated yellow region (shown in inset; insets are also shown in Figure 2.5h). (a, b, c, d, e, m, n, o, p, and r) show representative examples from at least 3 independent experiments. (f–l) show data as mean ± s.e.m; in some cases, error bars are smaller than the height of the symbol and, therefore, not shown. Scale bars, 500 nm for sptPALM images; 5 μm for FRAP larger images and 0.5 μm for the insets.

Extended Data Figure 2.9 Differences in the bioenergetics of catalytic versus scaffold mechanisms of regulated β-arrestin trafficking and β-arrestin-dependent activation of ERK1/2 promoted by catalytic activation

(a) Schematic depicting the proposed co-existence of catalytic and scaffolding mechanisms of β-arrestin trafficking tuned according to tail binding affinity, emphasizing the difference in tail versus core interactions (shaded boxes). The tail interaction, requiring GPCR phosphorylation (Rp) drives the scaffold mechanism through its essential role in stable GPCR/β-arrestin complex formation. The core interaction mediates catalysis by providing a kinetically favorable path for β-arrestin to remain captured at the PM irrespective of GPCR dissociation. Such capture requires phosphoinositide binding to the β-arrestin C-domain, explaining why the phosphoinositide requirement is specific to the catalytic mechanism and can be overcome by formation of a sufficiently sufficient stable scaffold complex requiring the phosphorylated GPCR tail. Primary energy inputs maintaining each proposed trafficking cycle are indicated by red arrows. The present results identify a specific requirement of the catalytic mechanism for phosphoinositide binding to the C-domain, but they do not exclude binding also in the scaffold complex (which we think is likely). We also cannot presently rule out the possible existence of additional interaction(s) in the catalytic mechanism, such as phosphoinositide binding also to the β-arrestin N-domain that has the potential to displace the β-arrestin C-terminus24. (b) Representative images (from 3 independent experiments) before and after 10 μM isoproterenol treatment of cells expressing chimeric FLAG-tagged β1AR-V2Rs and imaged live with TIRF microscopy. Profiles of FLAG-β2AR and β-arrestin-2–GFP average enrichment into CCSs in COS-1 cells expressing either an empty vector construct (c) or GRK2 (d) and treated with 10 μM isoproterenol (n=15 or 12 cells, respectively, from 3 independent experiments). (e) Difference in enrichment values between β-arrestin-2–GFP and β2AR from panels c and d

showing the effect of GRK2 overexpression. (f) Representative western blot showing phosphorylated ERK1/2 and total ERK1/2 signal in extracts prepared from parental or β-arrestin knockout CRISPR HEK 293 cells expressing FLAG–β1AR and exposed to 10 μM isoproterenol for the indicated time. (g) Quantification of ERK1/2 activation from the western blots in panel a (n=5 independent experiments, p=0.004 using a one-way ANOVA). (h) Representative western blot showing phosphorylated ERK1/2 and total ERK1/2 signal in extracts prepared from parental or β-arrestin knockout CRISPR HEK 293 cells expressing FLAG–β2AR and exposed to 10 μM isoproterenol for the indicated time. (i) Quantification of ERK1/2 activation from the western blots in panel c (n=5 independent experiments). (f) and (h) show representative Western blots from 5 independent experiments. Data shown as mean ± s.e.m. For gel source data, see Supplementary Figure 2.1. Error bars represent s.e.m. ** $p < 0.01$

Table 2.1 Summary and description of β-arrestin mutations

Mutation name	Mutations*	Description	Phenotype
CCS mutant	L373A, I374A, F376A, E375K, E377K, R393A, R395A	Clathrin & AP-2 binding deficient from mutation in C-terminus	Recruits to plasma membrane but not to CCSs
Lipid mutant	K233Q R237Q, K251Q (K232Q, R236Q, K250Q in β-arrestin-1)	Lipid binding deficient from mutation in C-lobe. Residues not well conserved in visual arrestin.	Not recruited to plasma membrane nor to CCSs
Lipid & CCS mutant	K233Q, R237Q, K251Q, L373A, I374A, F376A, E375K, E377K, R393A, R395A	Lipid, clathrin, & AP-2 binding deficient from mutations in C-lobe and C-terminus	Not recruited to plasma membrane nor to CCSs
Finger loop proximal mutant	R77A, K78A, D79A (R76A, K77A, D78A in β-arrestin-1]	Triple alanine mutations in the region proximal to the finger loop	Constitutively activating – association with CCSs without GPCR activation
K78E	K78E [K77E in β-arrestin-1)	Charge swap mutation of single residue from cluster of finger loop proximal mutations	Constitutively activating – association with CCSs without GPCR activation
E314K	E314K [E313Kin β-arrestin-1)	Charge swap mutation of residue in C lobe	Constitutively activating – association with CCSs without GPCR activation
K78E E314K	K78E E314K [K77E E313K in β-arrestin-1)	Double charge swap mutations restoring putative salt bridge	Abrogates constitutively activating phenotype produced by single charge swap mutants

*Mutations are in β-arrestin-2 unless otherwise indicated

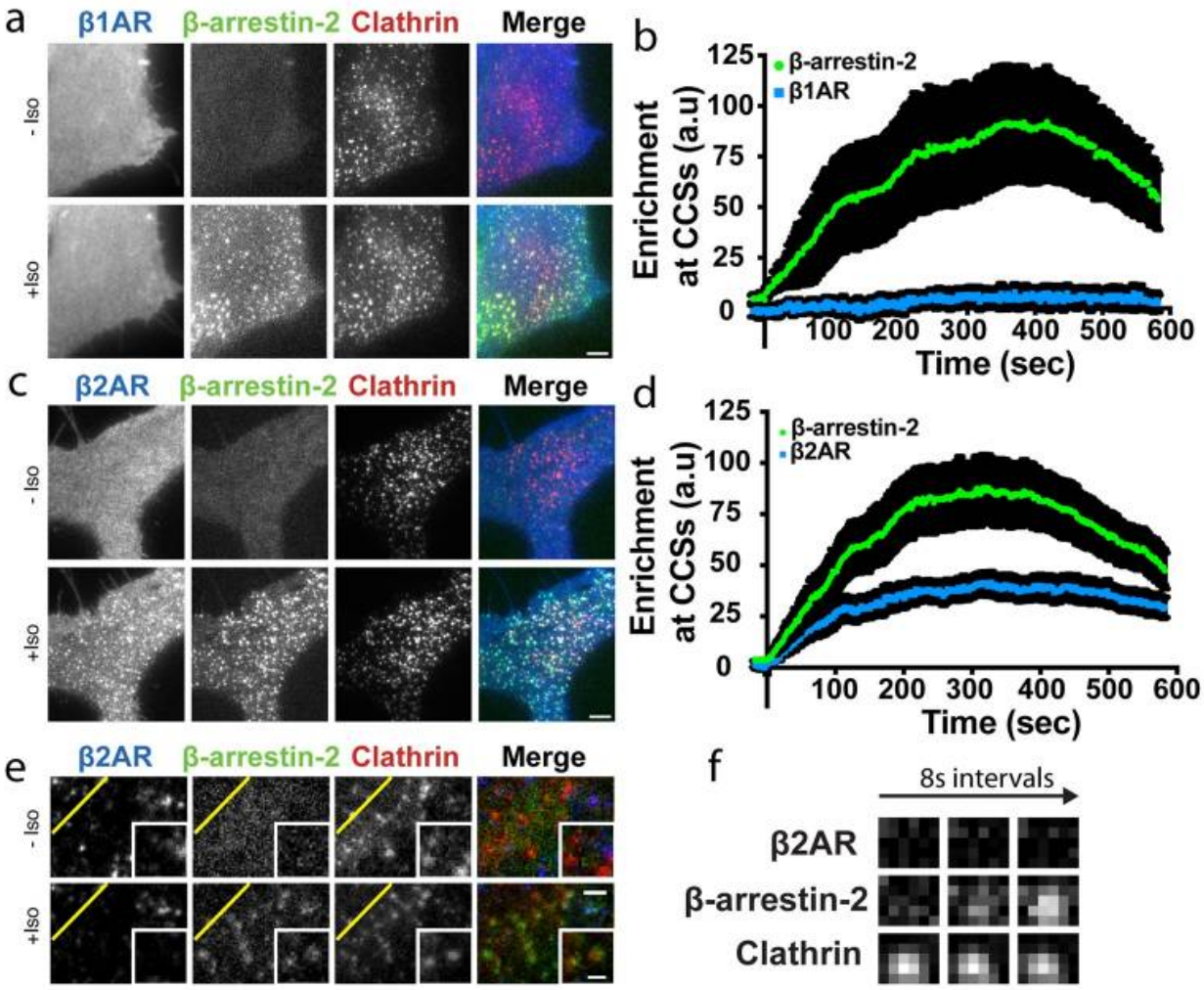

Figure 2.1 Discrete mode of GPCR-activated cellular β-arrestin trafficking is broadly conserved

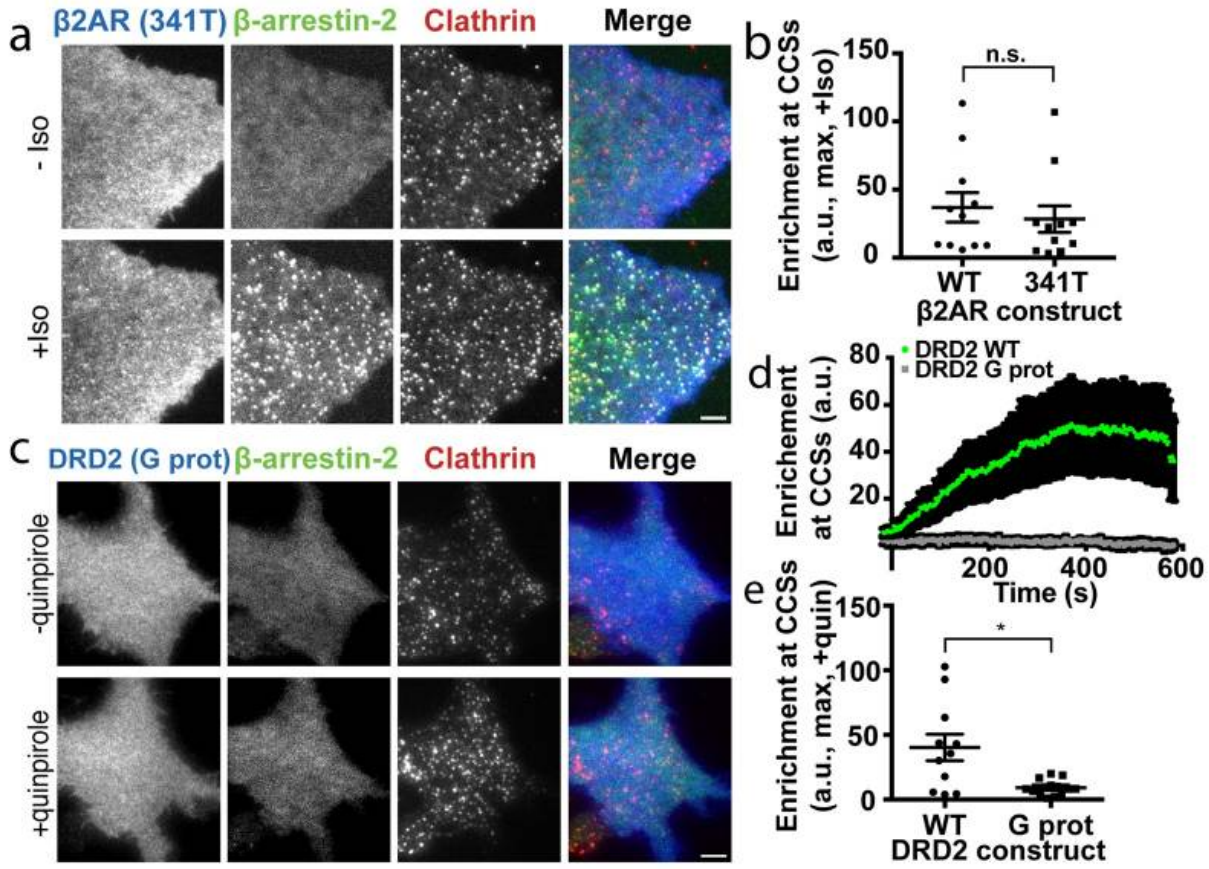

Figure 2.2 β-arrestin trafficking activation requires the GPCR core but not the GPCR cytoplasmic tail

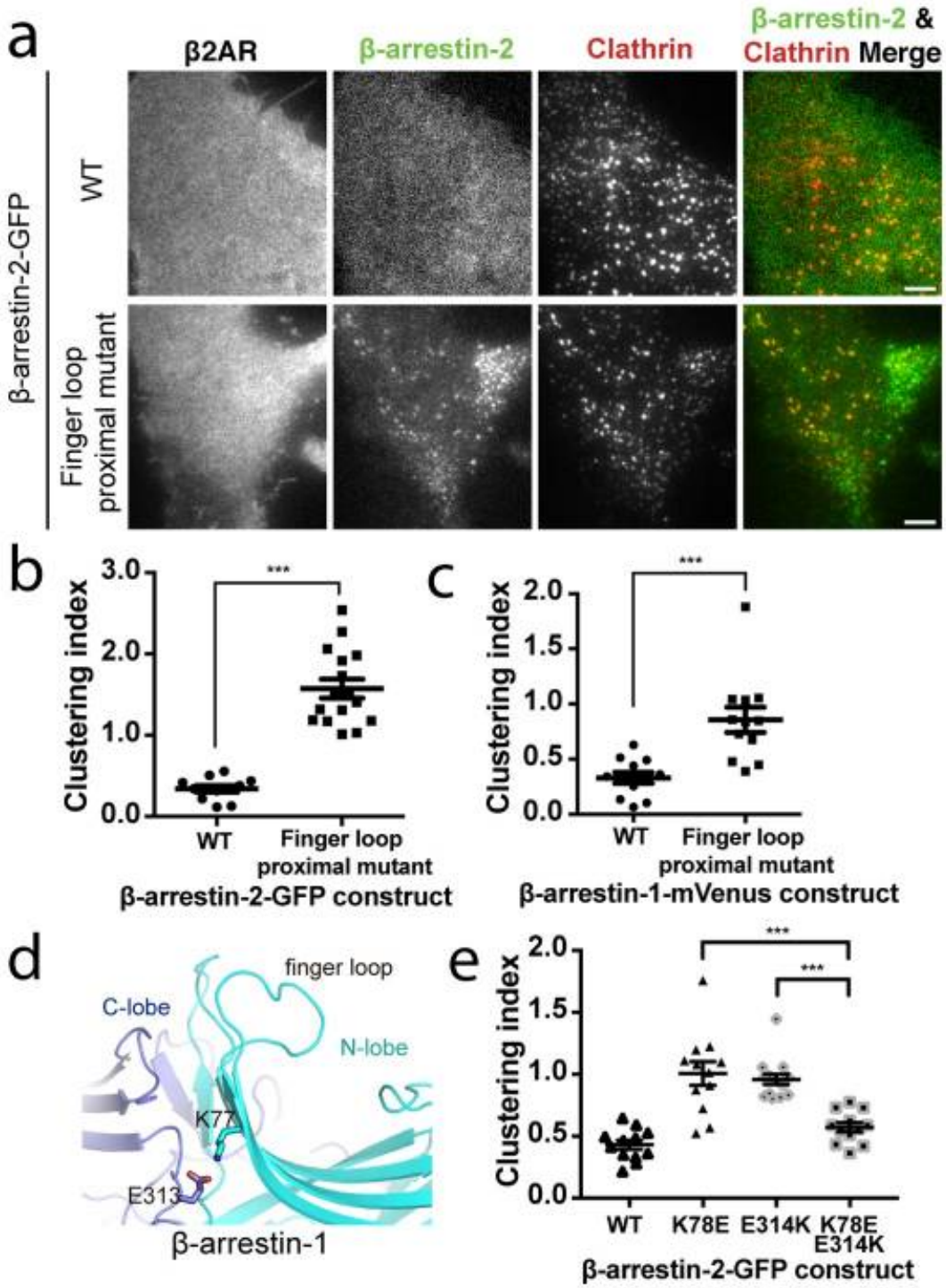

Figure 2.3 β-arrestin activation is inhibited by a polar network in a region proximal to the β-arrestin finger loop

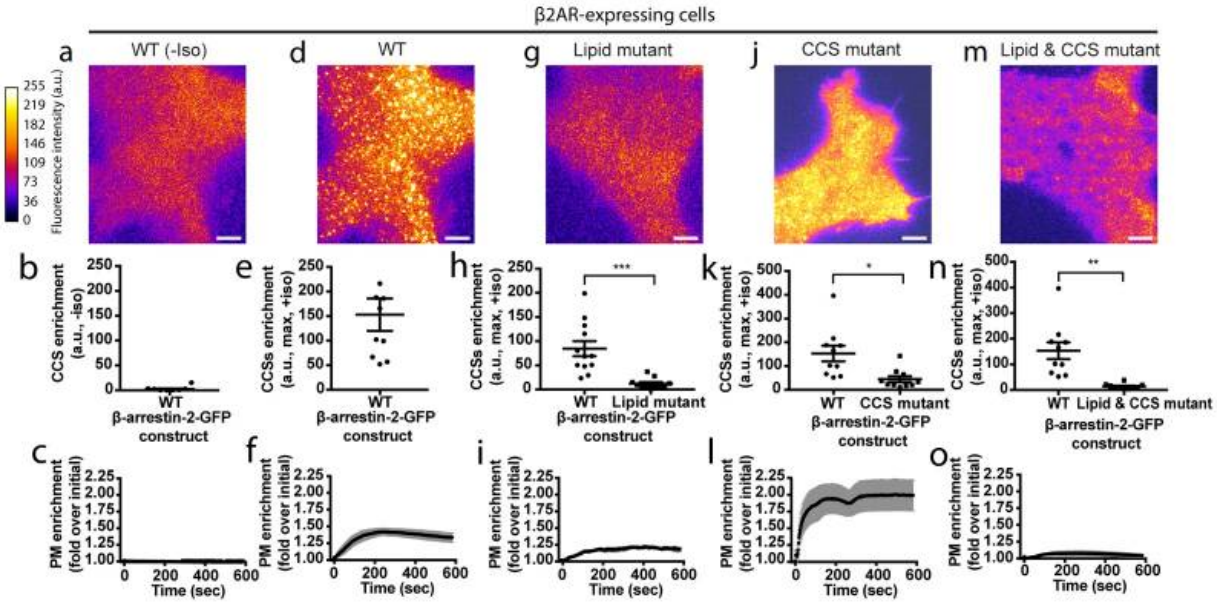

Figure 2.4 Phosphoinositide binding is required to capture β-arrestin at the plasma membrane after GPCR dissociation

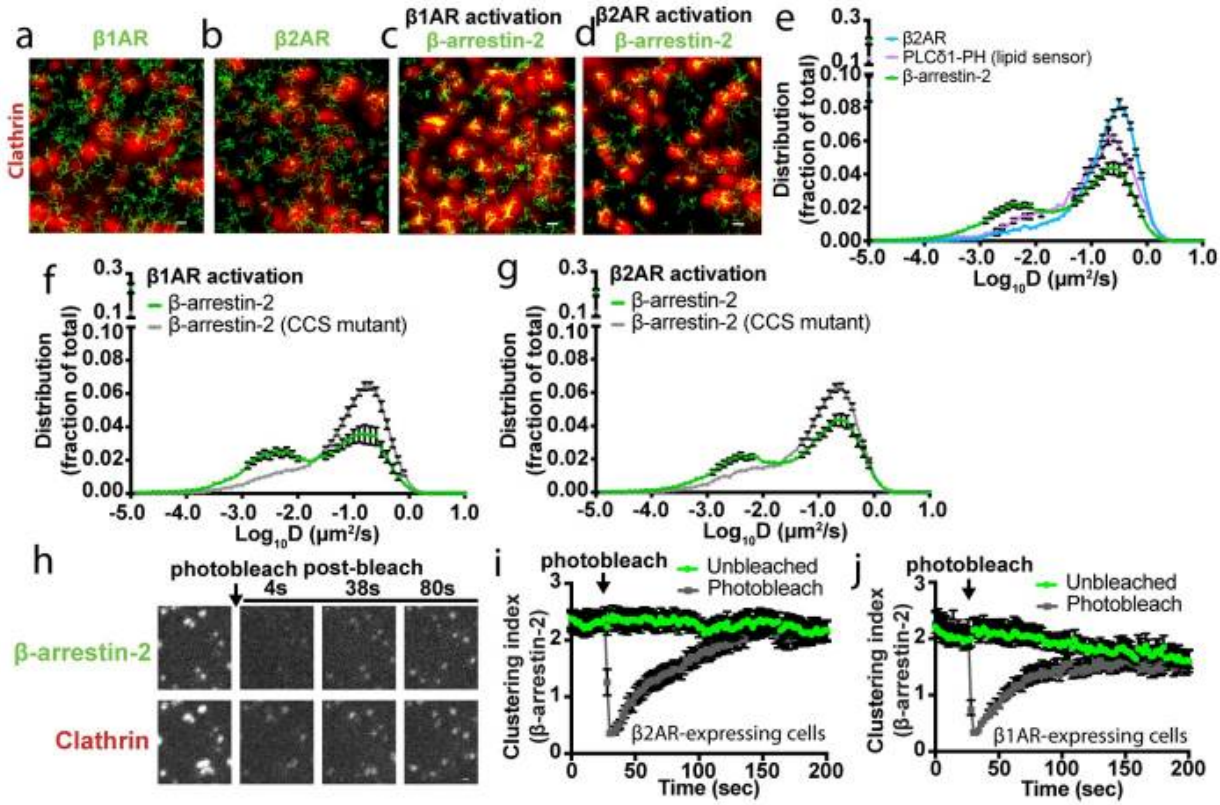

Figure 2.5 Single particle tracking-photoactivated localization microscopy (sptPALM) analysis of GPCR and β-arrestin dynamics and stable β-arrestin binding at CCSs

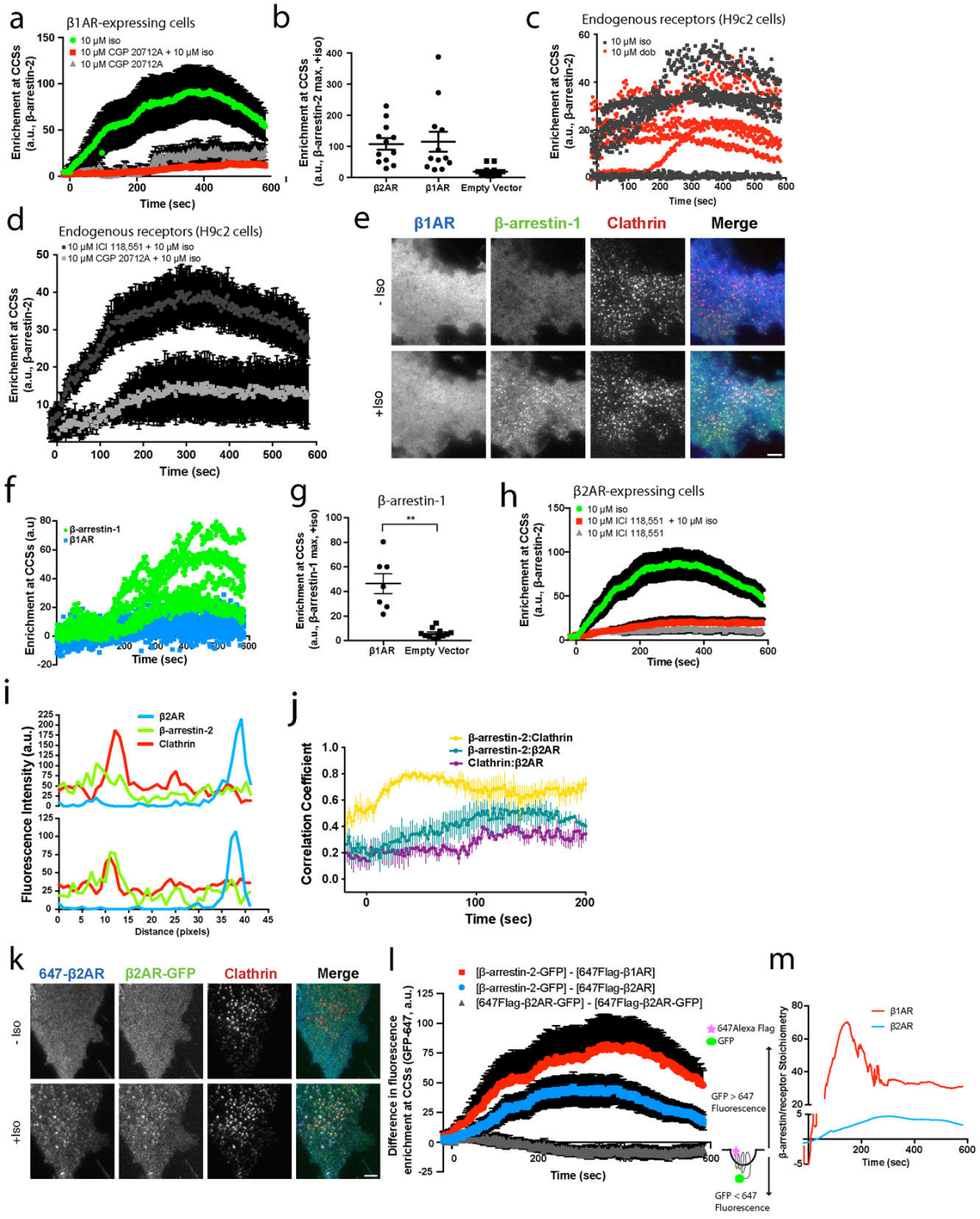

Extended Data Figure 2.1 Verification of GPCR-specificity of the discrete β-arrestin trafficking mechanism, demonstration that this mechanism produces super-stoichiometric β-arrestin accumulation in CCSs and that its activation does not require the GPCR tail

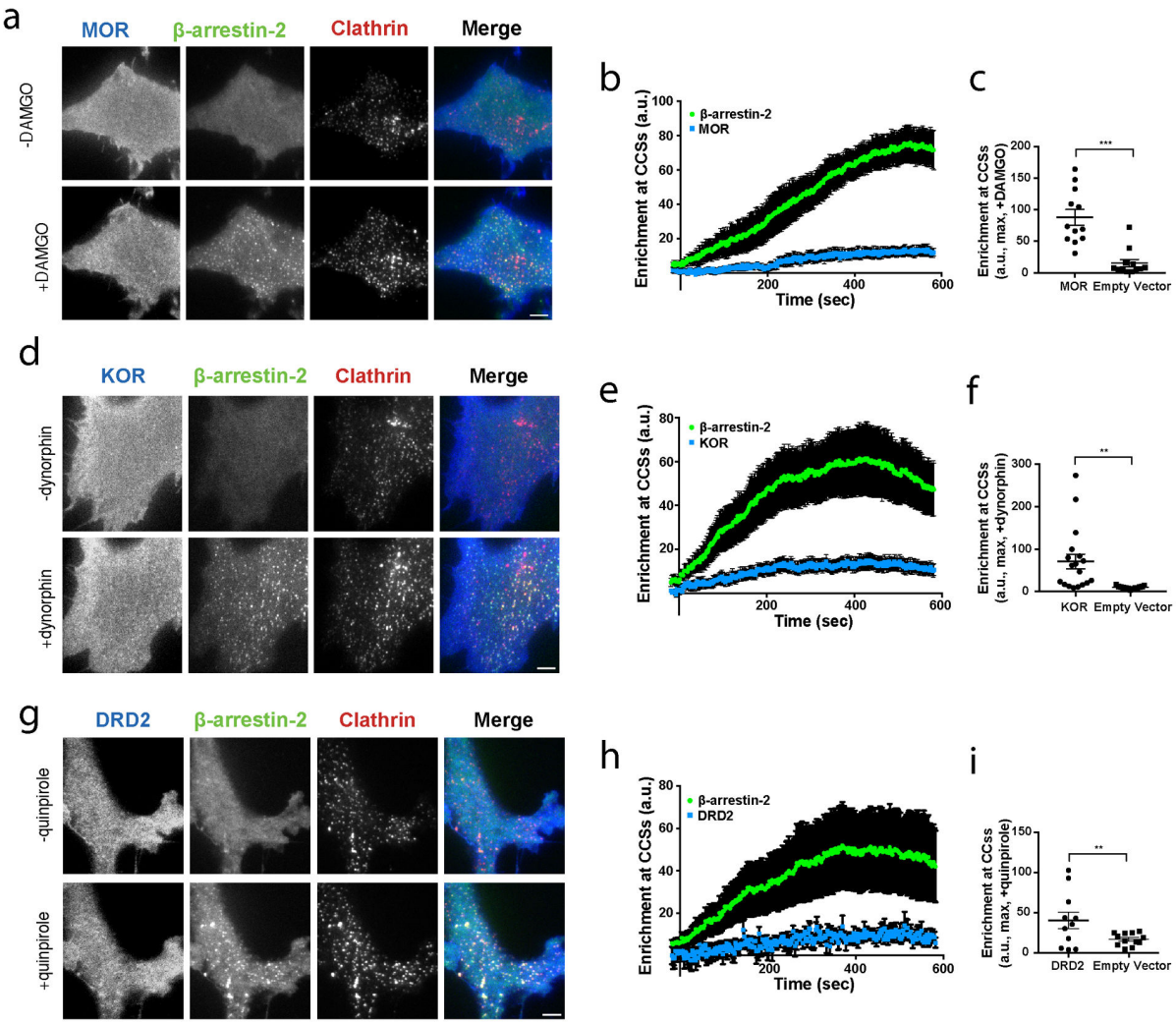

Extended Data Figure 2.2 Additional demonstration that multiple GPCRs can activate the discrete β-arrestin trafficking mechanism

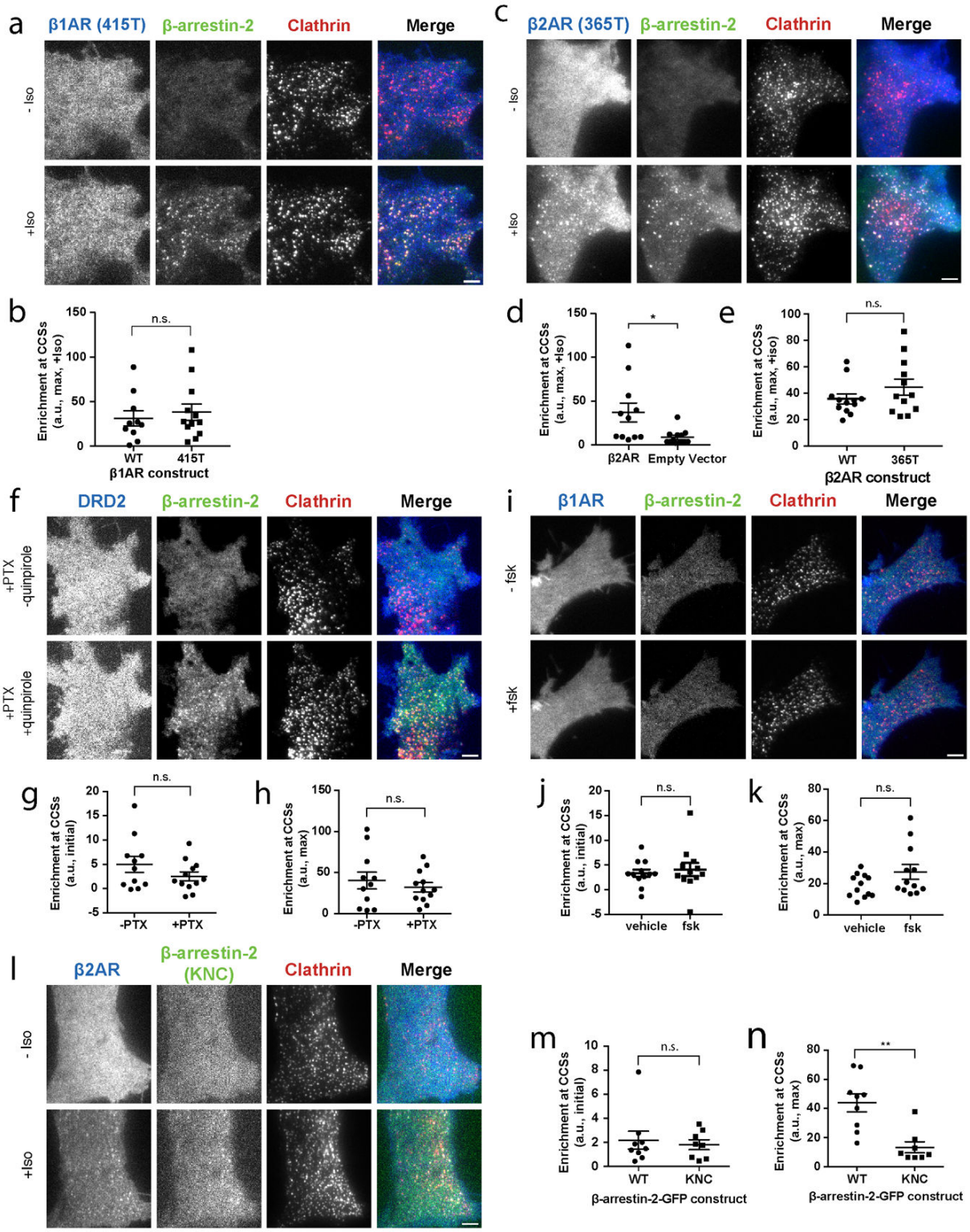

Extended Data Figure 2.3 Direct interaction with the GPCR, but not the GPCR cytoplasmic tail, is required for β-arrestin trafficking activation

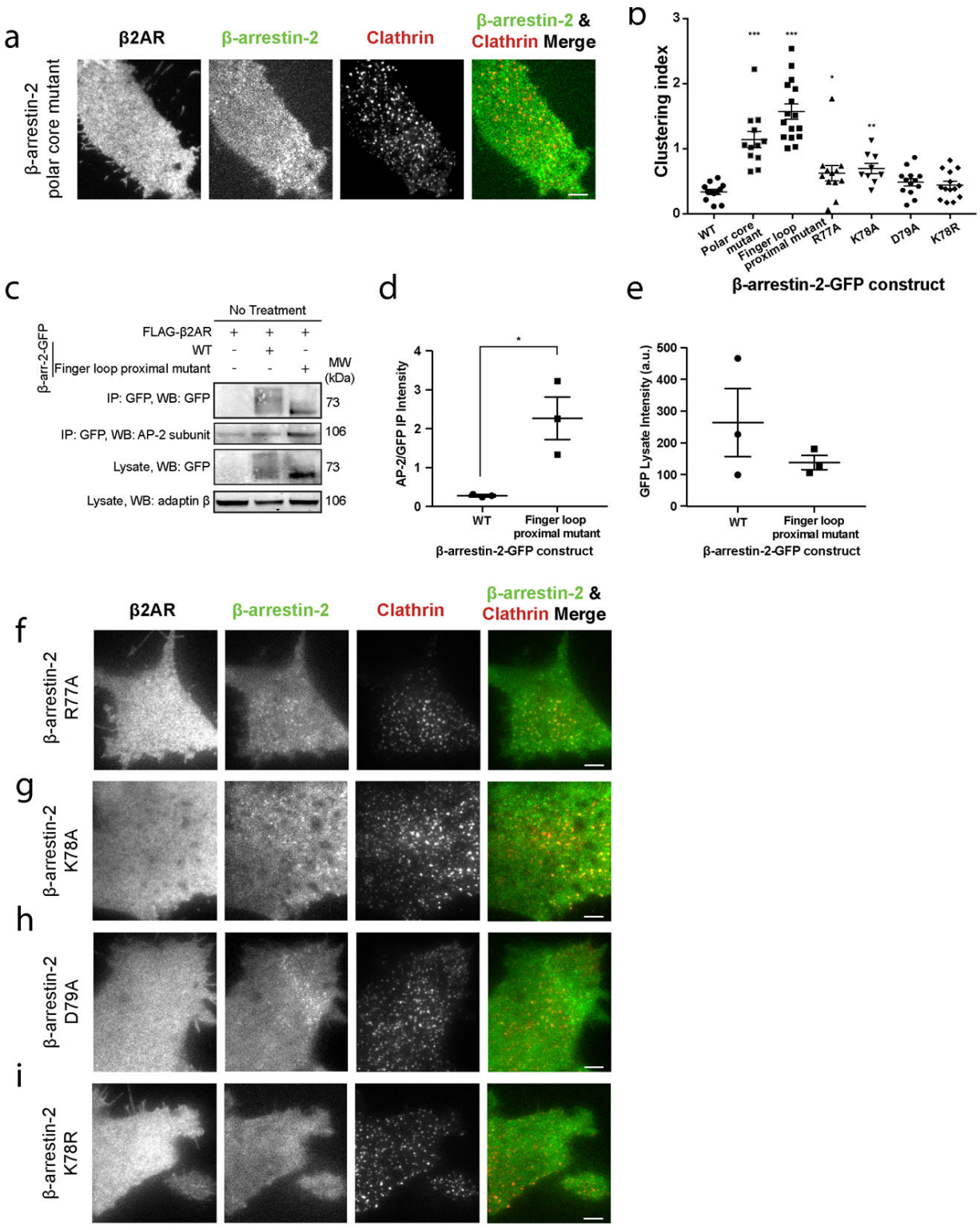

Extended Data Figure 2.4 Additional verification that charge mutations in the finger loop-proximal region of β-arrestin finger loop produce a constitutive activation phenotype

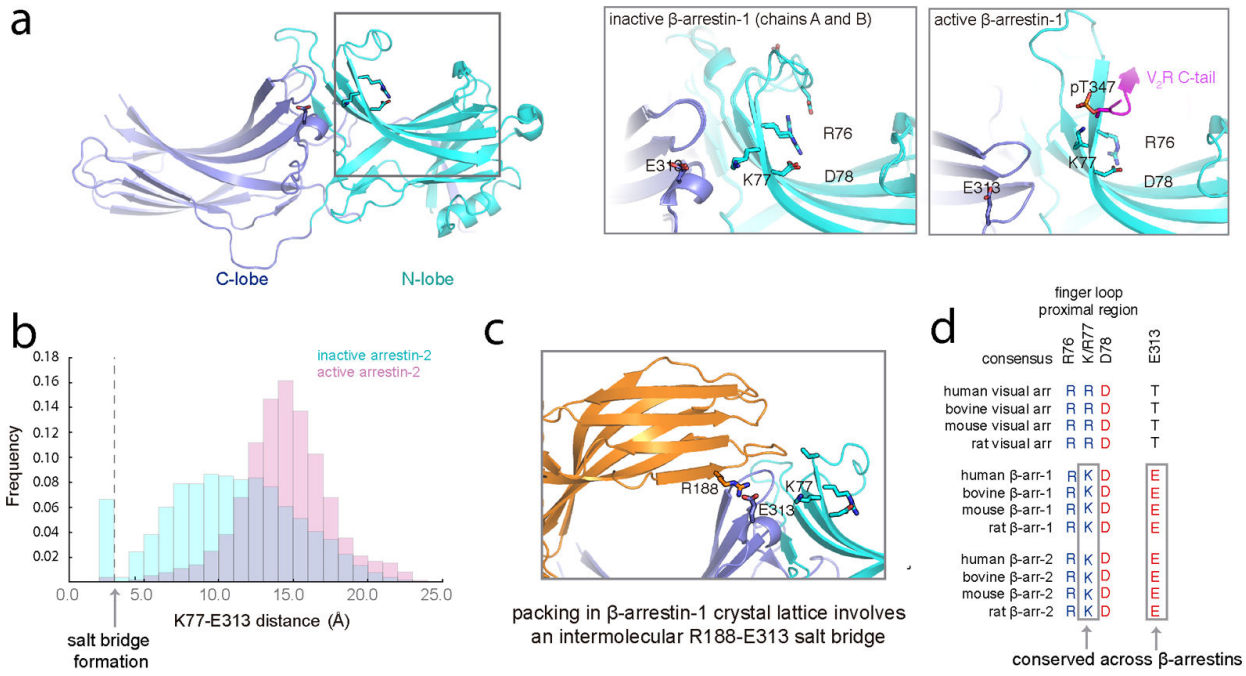

Extended Data Figure 2.5 Molecular dynamics simulations suggest that finger loop-proximal charged residues stabilize β-arrestin in an inactive state

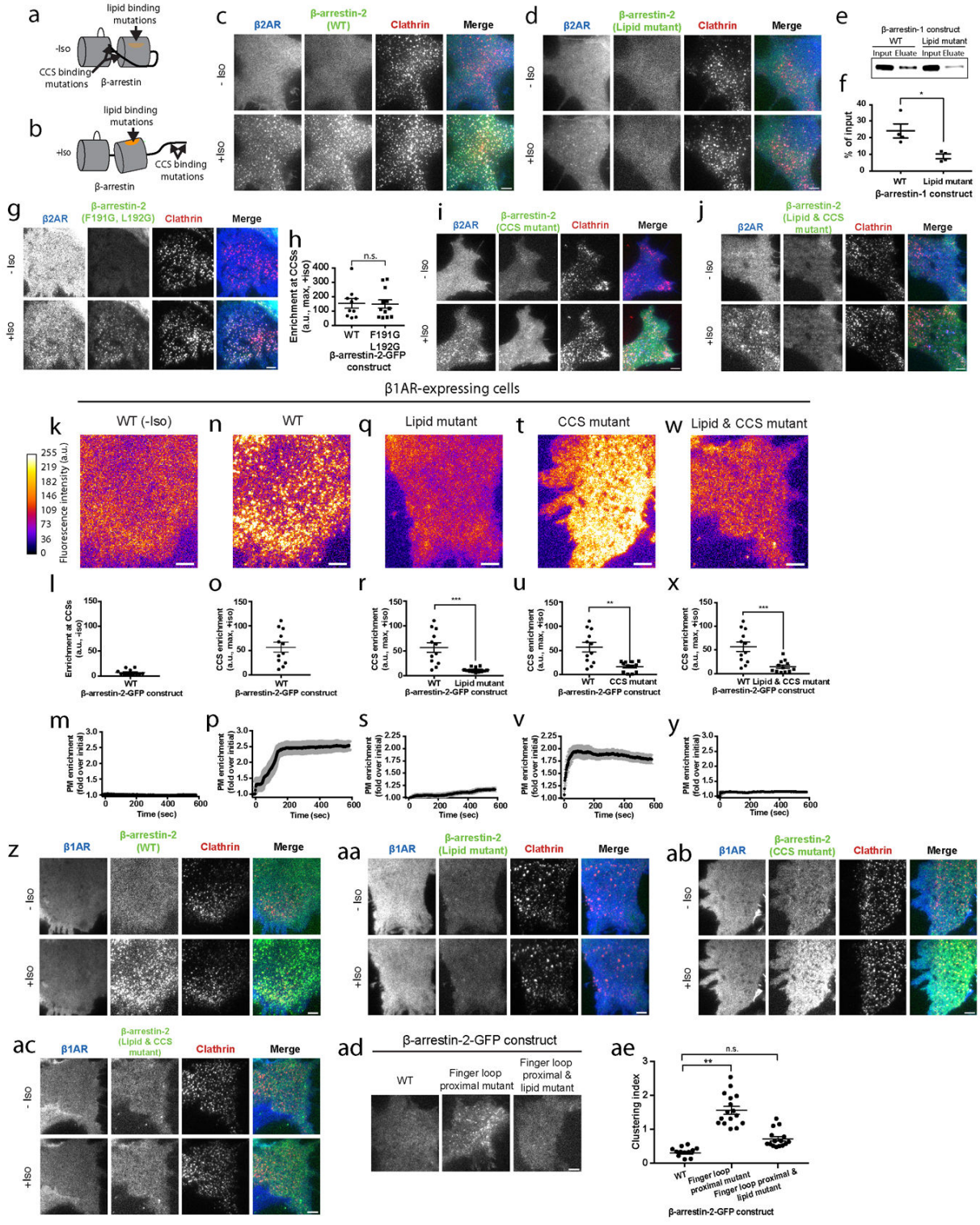

Extended Data Figure 2.6 Verification that the conserved phosphoinositide binding determinant in the β-arrestin C-domain is specifically required for the catalytic trafficking mechanism and operates upstream of clathrin and AP-2 binding interactions

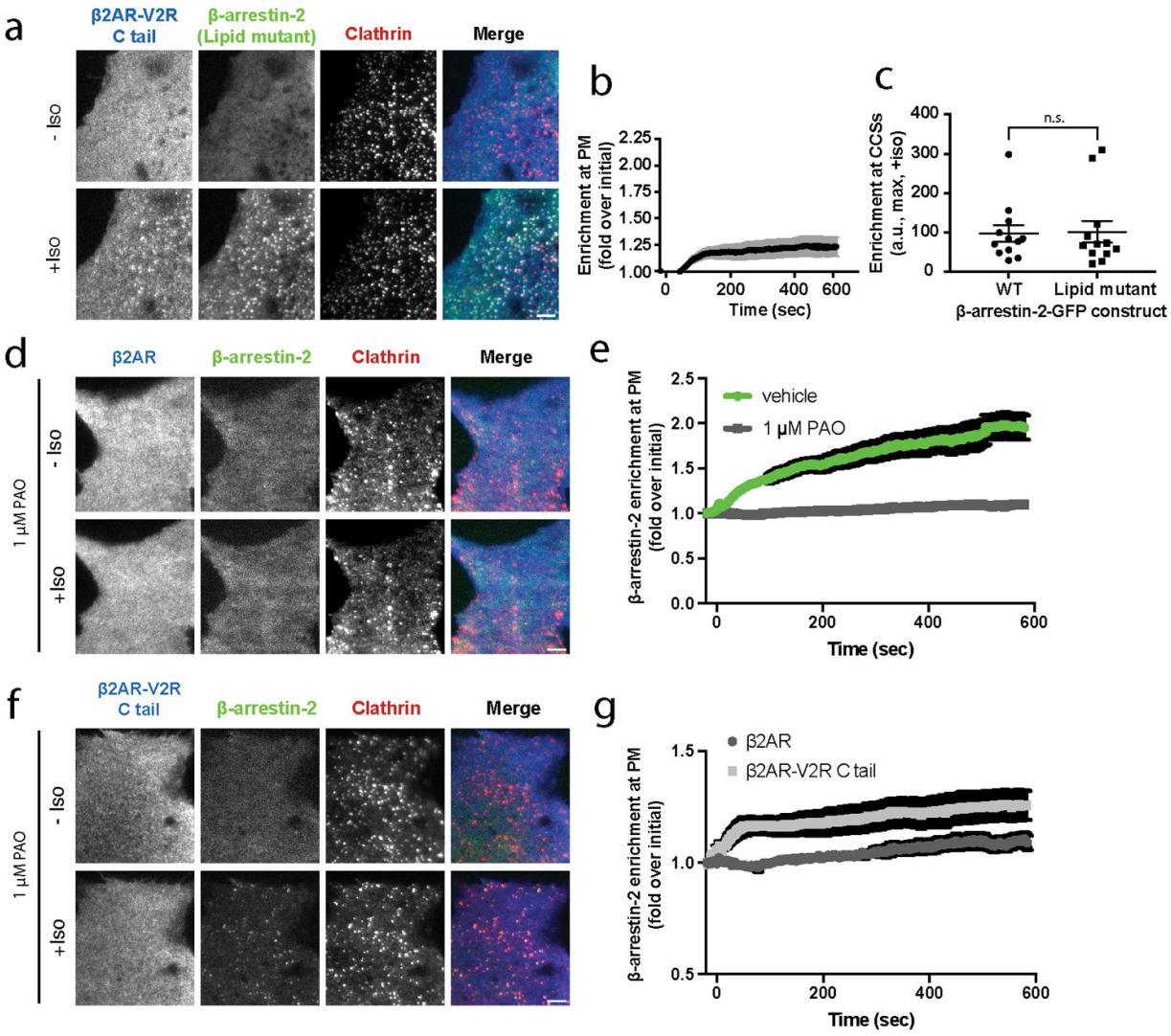

Extended Data Figure 2.7 Phosphoinositide binding is essential for catalytic activation of β-arrestin trafficking but is dispensable for trafficking mediated by the scaffold mechanism

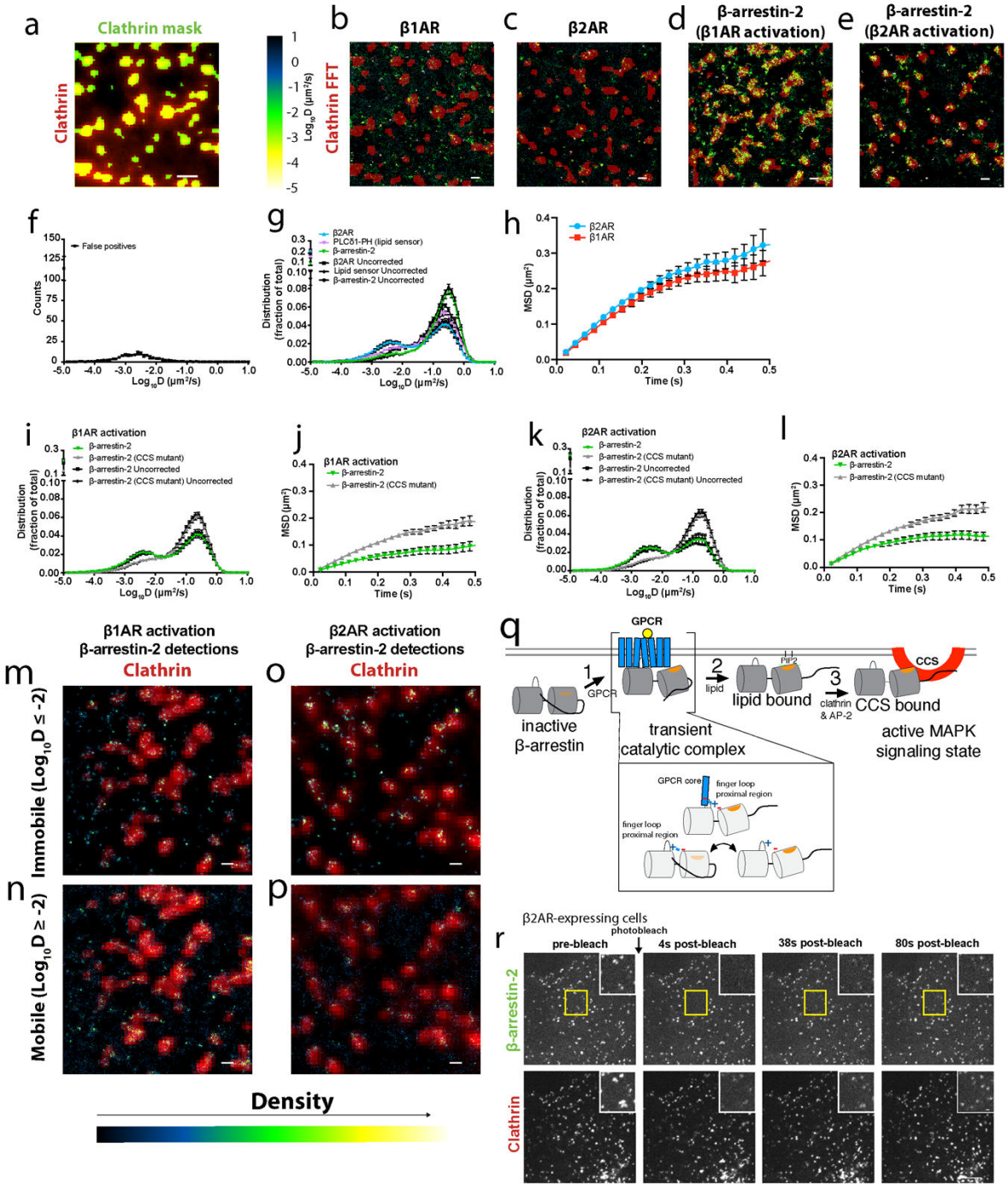

Extended Data Figure 2.8 sptPALM controls and mean square displacement (MSD) plots and cellular model

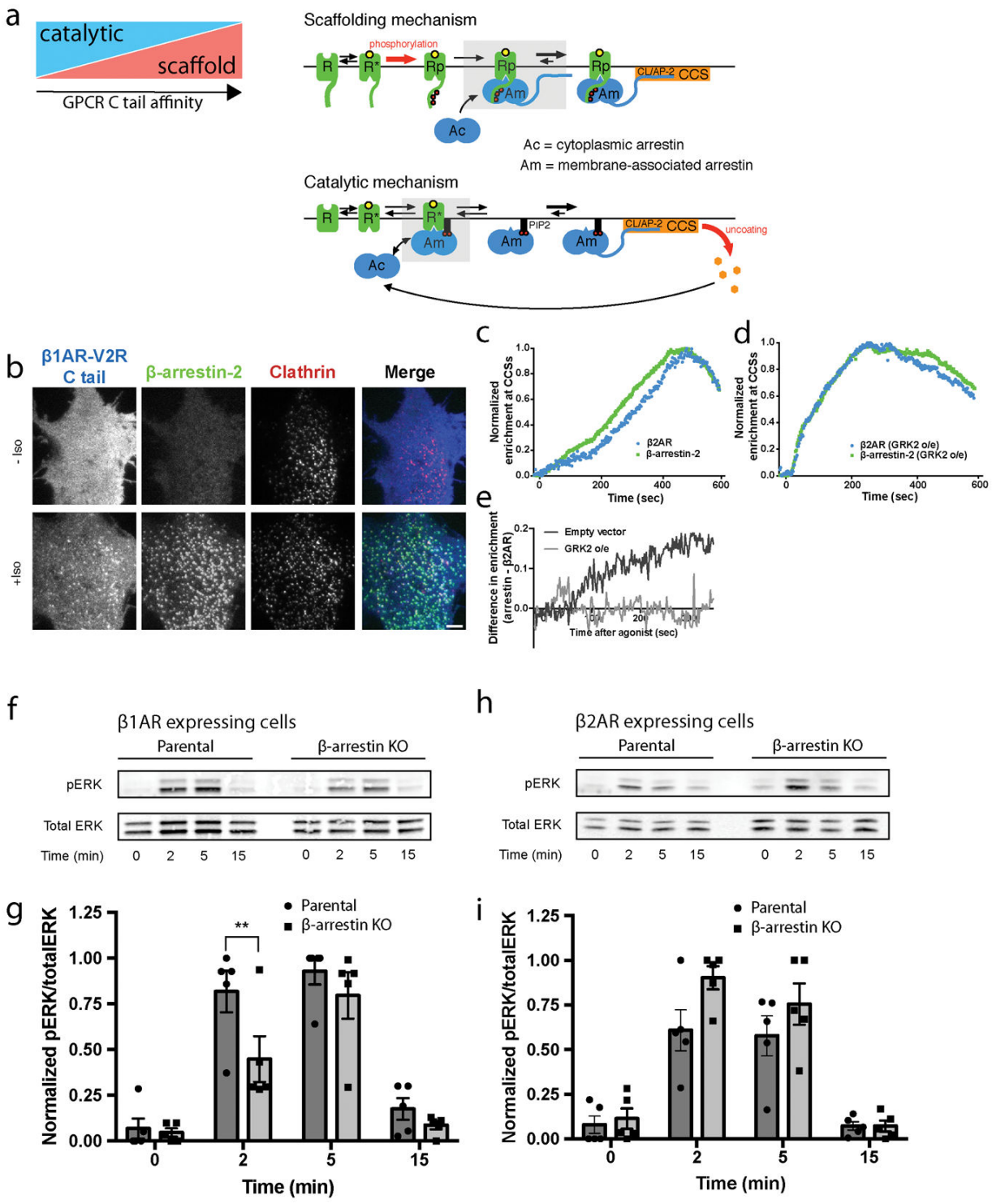

Extended Data Figure 2.9 Differences in the bioenergetics of catalytic versus scaffold mechanisms of regulated β-arrestin trafficking and β-arrestin-dependent activation of ERK1/2 promoted by catalytic activation

Chapter 3: Membrane phosphoinositides stabilize GPCR-arrestin complexes and provide temporal control of complex assembly and dynamics

Benjamin Barsi-Rhyne, in the laboratory of Mark von Zastrow (UCSF), contributed to Figs. 3.5 and S3.7 and provided consultation during experimental design and paper writing process. Most of the experiments were conceived and executed by John Janetzko (Stanford) in the laboratory of Brian Kobilka (Stanford). Additional contributions were made by Ryoji Kise (Tohoku University, Japan) in the laboratory of Asuka Inoue (Tohoku University, Japan), Dirk H. Siepe (Stanford University) in the laboratory of Christopher Garcia (Stanford University), Franziska M. Heydenreich (Stanford University) also in the laboratory of Brian Kobilka (Stanford University), Mathieu Masureel (Stanford University) also in the laboratory of Brian Kobilka (Stanford University), Kouki Kawakami (Tohoku University, Japan) also in the laboratory of Asuka Inoue (Tohoku University, Japan).

3.1 Abstract

Binding of arrestin to phosphorylated G protein-coupled receptors (GPCRs) is crucial for modulating signaling. Once internalized some GPCRs may complex with arrestin, while others interact transiently; this difference affects receptor signaling and recycling. Cell-based and in vitro biophysical assays reveal the role of membrane phosphoinositides (PIPs) in arrestin recruitment and GPCR-arrestin complex dynamics. We find that GPCRs broadly stratify into two groups, one requiring PIP-binding for arrestin recruitment and one that does not. Plasma membrane PIPs potentiate an active conformation of arrestin and stabilize GPCR-arrestin complexes by promoting a receptor core-engaged state of the complex. As allosteric modulators of GPCR-arrestin complex dynamics, membrane PIPs allow for additional conformational diversity beyond that imposed by GPCR phosphorylation alone. The dependance on membrane PIPs provides a mechanism for arrestin release from transiently associated GPCRs, allowing their rapid recycling, while explaining how stably associated GPCRs can engage G proteins at endosomes.

3.2 Introduction

G protein-coupled receptor (GPCR) activation and deactivation are tightly regulated, allowing them to achieve robust signaling. GPCR deactivation is a complex multi-step process often divided into an acute and a prolonged phase (Rajagopal and Shenoy 2018). In addition to promoting G protein engagement, agonist stimulation leads to the recruitment of GPCR kinases(GRKs), which phosphorylate the receptor and trigger recruitment of arrestins (Komolov and Benovic 2018). Arrestin first blocks further G protein engagement, resulting in an acute phase of desensitization, but also mediates the trafficking of activated receptors to clathrin-coated structures (CCSs) and their internalization. Once internalized, receptors can experience markedly different fates, with some being rapidly recycled to the plasma membrane, while others are retained in intracellular compartments, or directed to lysosomes and degraded (Hanyaloglu and von Zastrow 2008). In recent years, the discovery that GPCRs can signal from intracellular compartments has led to a re-framing of GPCR signaling to include not only temporal regulation, but also differences that result from spatially distinct receptor populations (Irannejad, Tomshine et al. 2013, Irannejad, Tsvetanova et al. 2015, Lobingier and von Zastrow 2019).

There are four human arrestins; arrestins 1 and 4 are dedicated to the visual system, and arrestins2 and 3, also known as β-arrestin 1 (βarr1) and β-arrestin 2 (βarr2), respectively, are ubiquitously expressed throughout the other tissues. Remarkably, these two β-arrestins are responsible for recognition and desensitization of hundreds of GPCRs. Though most GPCRs recruit arrestin, the nature and duration of this interaction can differ between receptors. Historically GPCRs have been classified as either a “class A” receptor, which interacts transiently with arrestin, or “class B” receptors, which interact more stably with arrestin and co-

localize with arrestin in endosomes (Zhang, Barak et al. 1999, Oakley, Laporte et al. 2000, Oakley, Laporte et al. 2001). This distinction is importantly different from that of family A (rhodopsin-like) and family B (secretin-like) GPCRs. Whether a GPCR interacted transiently or stably with arrestin appears to correlate with rates of re-sensitization, with class A receptors re-sensitizing more rapidly than class B receptors (Oakley, Laporte et al. 1999). Stable association of arrestin to “class B” GPCRs correlates with the presence of particular phosphorylation site clusters (Oakley, Laporte et al. 2001); however, it has remained unknown what event precipitates the dissociation of β-arrestins from “class A” receptors to allow their dephosphorylation and recycling.

Early structural studies into GPCR-arrestin complexes suggested that arrestin binds to a GPCR either through only the phosphorylated C-terminus (called tail-engaged), or through both the phosphorylated C-terminus and the transmembrane core of the GPCR (called core-engaged) (Shukla, Westfield et al. 2014, Latorraca, Wang et al. 2018, Staus, Wingler et al. 2018). However, it remains unclear what determines the equilibrium between these states. While core-engagement is necessary for receptor desensitization (Kumari et al., 2017), it is not required for internalization (Cahill, Thomsen et al. 2017). If, however, complexes can shift from core-engaged to tail-engaged in endosomes it would allow for G proteins to access the receptor core while remaining bound to arrestin. These so-called “megaplex” assemblies (Thomsen, Plouffe et al. 2016, Nguyen, Thomsen et al. 2019) have been implicated in the sustained cAMP signaling produced by endosomal populations of V2R and PTH1R (Ferrandon, Feinstein et al. 2009, Feinstein, Yui et al. 2013), both of which stably associate with β-arrestins.

At a molecular level, the prevailing model for arrestin activation, and thus recruitment to an active and phosphorylated GPCR, involves displacement of the auto-inhibitory C-terminus of arrestin by the GPCR phosphorylated C-terminus (or in some cases an intracellular loop). Once the arrestin C-terminus is displaced, additional structural rearrangements occur that allow for arrestin to engage a GPCR (Sente, Peer et al. 2018), including insertion of the arrestin finger loop into a cavity formed by the cytoplasmic ends of transmembrane segments. However, arrestin activation functions for more than just GPCR engagement. In its active form, arrestin is able to engage multiple signaling proteins, including JNK3, ERK1/2, p38 (Song, Coffa et al. 2009) and Src (Pakharukova, Masoudi et al. 2020). It has been suggested that distinct arrestin conformations, which can arise from different inputs (i.e., receptor phosphorylation pattern) may favor interaction with a subset of these signaling partners and affect signaling outcomes downstream of arrestin (Chen, Iverson et al. 2018, Latorraca, Wang et al. 2018). Recently the model for arrestin activation, which suggests a1:1 interaction, has been challenged by the finding that some “class A” receptors cause the accumulation of super-stoichiometric quantities of arrestin in clathrin-coated structures (CCSs), suggesting an ability to persist at the membrane without an associated GPCR (Eichel, Jullié et al. 2016, Nuber, Zabel et al. 2016). It was speculated that an association with PIP2 was responsible for retainingβ-arrestins in clathrin coated structures (Eichel, Jullié et al. 2018); however, based on the established mechanism for arrestin activation it is unclear how this would be possible, or how arrestin absent an associated GPCR promoted MAPK signaling from CCSs (Eichel, Jullié et al. 2016)

Components of the endocytic machinery such as AP2 (Kadlecova, Spielman et al. 2017), and β-arrestins (Gaidarov, Krupnick et al. 1999) have been shown to bind to PIPs. These signaling lipids serve critical functions defining the identity of lipid compartments and acting as

coincidence markers for protein-protein recognition and trafficking to occur only in the appropriate subcellular context (De Matteis and Godi 2004, Di Paolo and De Camilli 2006).While several studies have investigated the interactions of soluble inositol phosphates with both visual and non-visual arrestins (Milano, Kim et al. 2006, Zhuang, Vishnivetskiy et al. 2010, Chen, Perry et al. 2017, Chen, Zhuo et al. 2021), there has been only one where the role of membrane PIPs was explored (Gaidarov, Krupnick et al. 1999). Importantly, this work suggested that plasma membrane PIPs, such as PI(4,5)P2 and PI(3,4,5)P3, hereafter PIP2 andPIP3, respectively, may function to stabilize GPCR-β-arrestin complexes as they traffic to CCSs.

Recent structural studies showing PIP2 bound at the interface between the neurotensin type I receptor (NTSR1) and βarr1 (Huang, Masureel et al. 2020) prompted us to ask the question: what role do PIPs serve in mediating GPCR-β-arrestin complex assembly? Here we show that some GPCRs require PIP binding for β-arrestin recruitment, provided they engage β-arrestins transiently. Furthermore, we show that the requirement of PIPs depends on specific receptor phosphorylation sites. Using in vitro biochemical and biophysical assays, we demonstrate that phosphoinositide binding contributes to the stability of the GPCR-β-arrestin complex, where it promotes the core-engaged state. We also find that PIPs alone promote a partially activated state of arrestin, providing an explanation for how arrestin can persist in CCSs once dissociated from a GPCR. Together, these results explain a) how receptors that transiently associate with β-arrestin recruit and dissociate β-arrestin in a spatiotemporally resolved manner, and b) how strongly coupled receptors maintain a stable association with arrestin in subcellular compartments yet allow for further G protein engagement from subcellular structures.

3.3 Results and Discussion

Arrestin PIP-binding is important for desensitization of endogenous β2AR

The PIP-binding-deficient mutant of βarr2 (K233Q/R237Q/K251Q, henceforth 3Q, also used to denote mutation of the homologous residues in K232Q/R236Q/K250Q in βarr1) was previously found to be impaired for internalization of β2AR (Gaidarov, Krupnick et al. 1999), with βarr2 (3Q) failing to traffic to CCSs, though still being recruited from the cytoplasm to the plasma membrane, albeit toa lesser extent than wild-type (WT) (Eichel, Jullié et al. 2018). As such, we wondered how this behavior affects β2AR signaling and specifically whether βarr2 (3Q) is capable of desensitizing β2AR at the plasma membrane. Using a FRET-based cAMP sensor (Tewson, Martinka et al. 2016), we monitored cAMP production in real-time in HEK293 cells lacking both β-arrestins, and endogenously expressing the β2AR (O'Hayre, Eichel et al. 2017). In the absence of exogenously expressed βarr2, isoproterenol (iso) stimulation, via endogenous β2AR, led to a sustained cAMP response, while expression of βarr2 led to desensitization. However, expression of the 3Q βarr2 mutant resulted in significantly less desensitization over 30 minutes (Figure S3.1A); furthermore, this difference was observed in two independent β-arrestin-deficient cell lines (O'Hayre, Eichel et al. 2017, Luttrell, Wang et al. 2018). This suggests that the PIP-binding function of β-arrestins plays an important functional 150 role, in not only internalization (Gaidarov, Krupnick et al. 1999), but also receptor desensitization, and does so under conditions of endogenous GPCR expression.

GPCRs stratify into two groups in their dependence on PIP-binding for arrestin recruitment

That the βarr2 3Q mutant is impaired for recruitment to β2AR, but seemingly not for the chimeric receptor β2AR-V2C, which bears the C-terminus of the vasopressin V2 receptor (Eichel, Jullié et al. 2018), suggested that GPCRs may differ in their dependence on β-arrestin PIP-binding for recruitment. To investigate a wide range of GPCRs we used a cell-based NanoBiT assay (Dixon, Schwinn et al. 2016), wherein a plasma membrane localization sequence (CAAX) is fused to the large subunit of a modified NanoLuc luciferase (LgBiT). Recruitment of either βarr1 or βarr2, which bear an N-terminal complementary small subunit of NanoLuc (SmBiT), can be monitored by luminescence changes (Figure 3.1A). We selected a set of 22 representative GPCRs (Supplementary Data Table 1), co-expressed the sensors with each receptor of interest inHEK293 cells, and compared the recruitment of WT β-arrestin to that of the corresponding 3Q β-arrestin mutant upon agonist stimulation (Figure 3.1B, top, Supplementary Data Table 1). We used luminescence fold-change measured over the range of 10-15 minutes post-agonist stimulation for our end-point values and fit the resulting data to generate concentration response curves and extract a recruitment amplitude for each receptor-arrestin pair (see methods) (Figure 3.1B, bottom, Supplementary Data Figure 3.1A-B). We then compared the recruitment of WT and 3Q arrestin using a metric that represented the relative sensitivity of the receptor to loss of arrestin-PIP binding capacity, we termed the loss of function (LOF) index (see methods). Receptors with a low LOF value recruit WT and 3Q β-arrestins to the plasma membrane similarly, and are deemed PIP-independent, while receptors with a high LOF value show greatly diminished recruitment of 3Q β-arrestin and are deemed PIP-dependent (Figure 3.1C). Both WT and 3Q forms of βarr1 and βarr2 express similarly (Figure S3.1B, Supplementary Data Figure 3.2).

Though receptors spanned a continuum of LOF values, they seemed to cluster into two groups near the ends of the scale. To examine this, we performed k means clustering of plasma membrane recruitment data for all GPCR-β-arrestin pairs (Supplementary Data Figures 3.1 and 3, n = 55 pairs), which suggested that the data is best divided into two clusters (see methods, clusters marked by dotted ellipses in Figure 3.1C). We found only a weak inverse correlation between the amplitude of WT arrestin recruitment and the degree of LOF observed (Pearson correlation = -0.51; -0.4 when TACR1 and B2R are excluded) (Figure S3.1C), suggesting that differences in LOF were not due to lower levels of WT recruitment. Cluster 1 was defined by receptors that exhibited a high degree of LOF (center LOF = 0.73) and included GPCRs previously classified as “class A” (Oakley, Laporte et al. 2000): β2AR, μOR, ETAR, D1R, 1BR. Cluster 2, defined by receptors with a low degree of LOF (center LOF = 0.06), included GPCRs classified as “class B” (Oakley, Laporte et al. 2000): AT1R, NTSR1, V2R, TRHR, and TACR1. We also tested two chimeric receptors, β2AR-V2C and μOR-V2C (Eichel, Jullié et al. 2018), both of which showed reduced reliance on β-arrestin PIP-binding capability for plasma membrane recruitment compared to the respective parent receptor. The V1AR, which was previously shown to undergo labile phosphorylation and rapid recycling (Innamorati, Sadeghi et al. 1998, Innamorati, Sadeghi et al. 1998) clusters with the class A receptors in cluster 1, while the V1BR, bearing a closer similarity in its proximal C-terminus toV2R clusters with class B receptors in cluster 2, even though it has been found to only associate transiently with arrestin (Perkovska, Méjean et al. 2018). In addition, β1AR, S1PR1, and OR, all three of which have been shown to either recycle rapidly or interact transiently with arrestin (Trapaidze, Gomes et al. 2000, Nakagawa and Asahi 2013, Martínez-Morales, Romero-Ávila et al. 2018), were assigned to cluster1. Other receptors known to co-localize with arrestin at endosomes,

including PAR2 (Dery, Thoma et al. 1999, DeFea, Zalevsky et al. 2000, Oakley, Laporte et al. 2000), B2R (Khoury, Nikolajev et al. 2014), and PTH1R (Feinstein, Wehbi et al. 2011) were also classified into cluster 2. Two receptors, OXTR and HTR2C displayed unexpected behavior where βarr1 recruitment was dramatically more sensitive to loss of PIP-binding than βarr2, resulting in these GPCR-β-arrestin pairs being divided between the two clusters. OXTR was previously classified as a "class B" receptor (Oakley, Laporte et al. 2001); however, these studies only examined βarr2 recruitment. For the serotonin 2C receptor (HTR2C), previous studies showed PIP2-depletion did not block recruitment of βarr2 (Tóth, Tóth et al. 2012), and we observed an intermediate LOF value for βarr2 plasma membrane recruitment with HTR2C.Together, these data show that recruitment of β-arrestins is dependent on the PIP-binding capacity of arrestin for some GPCRs, but not others, and that this distinction is consistent with the previous class A/B categorization based on microscopy co-localization studies.

While our use of a plasma membrane localized LgBiT avoids modifying the receptor of interest, we wanted to confirm that plasma membrane recruitment is indeed a reliable proxy for arrestin recruitment to a GPCR of interest. For this, we used a direct NanoBiT assay in which the SmBiT component is fused to the C-terminus of each GPCR of interest, and the N-terminus of arrestin is modified with the LgBiT fragment (Figure S3.1D, left). We found that recruitment measured by direct complementation largely paralleled recruitment measured using the plasma membrane bystander, with minor exceptions (Supplementary Data Figure 3.4-5). Further, directly comparing LOF as measured by the plasma membrane bystander to that of the direct complementation showed a strong positive correlation (Pearson correlation = 0.88), suggesting that β-arrestin recruitment measured through the plasma membrane bystander was indeed a

faithful metric (Figure S3.1D, right). The most extreme outlier, HTR2C, showed βarr2 recruitment is PIP-binding independent as measured by the direct recruitment assay, as compared to being partially PIP-binding-dependent when measured using the plasma membrane bystander. As the direct recruitment assay seemed to better match prior findings for the HTR2C (Toth et al., 2012), we wondered why this might be. In addition to HTR2C, α1BR and β1AR also exhibit reduced PIP-binding sensitivity in the direct recruitment assay for βarr2. Curiously, all three of these receptors exhibit some level of Gq coupling (Inoue, Raimondi et al. 2019). We speculate that for cluster 1 receptors, such as HTR2C, which are Gq-coupled, that their dependence on PIP-binding for arrestin recruitment to the plasma membrane may be amplified by local PIP2-depletion via phospholipase C upon stimulation.

Given that “class B” receptors co-localize with β-arrestins in endosomes, we wondered whether PIP binding affected this process. We used the FYVE domain of endofin as an endosome bystander (Endo) (Namkung, Le Gouill et al. 2016), which we fused to LgBiT (termed endo-Lg) to monitor recruitment of arrestin bearing an N-terminal SmBiT (Figure S3.1E), as was done for plasma membrane recruitment. Since both βarr1 and βarr2 displayed largely similar behavior in our plasma membrane recruitment assay, we focused on βarr1 for these experiments (Supplementary Data Figure 3.6A); however, βarr2 recruitment was also examined for a subset of receptors (Supplementary Data Figure 3.6B). This assay robustly detected endosomal translocation as all receptors known to co-localize with β-arrestin in endosomes did so (Figure S3.1E). Consistent with the stark difference between βarr1 and βarr2 observed for OXTR (Figure 3.1C), we observed measurable endosomal association of βarr2, but weak and barely measurable βarr1 endosome recruitment (Supplementary Data Figure 3.6C). Our results were consistent with prior microscopy-based approaches (Oakley, Laporte et al. 2000),

thereby validating our NanoBiT assay. In contrast, HTR2C showed more robust recruitment of βarr1 than βarr2 (Supplementary Data Figure 3.6D). As expected, while cluster 1 receptors whose ability to co-localize with β-arrestins at endosomes had not yet been described displayed little signal for endosomal translocation for WT and 3Q β-arrestins, the cluster 2 receptors showed robust signal for recruitment of both WT and 3Q β-arrestins.

Though end-point recruitment of βarr1 to NTSR1 and other cluster 2 GPCRs was largely unaffected by loss of the PIP-binding site, prior NTSR1 experiments had found that loss of PIP binding slowed the kinetics of β-arrestin recruitment (Huang, Masureel et al. 2020), suggesting PIP2 may play a role in the complexes formed with cluster 2 receptors, even when end-point recruitment is unchanged. We fit the rate of β-arrestin translocation to the plasma membrane in response to stimulation for all GPCRs in cluster 2 using our CAAX bystander NanoBiT assay (Figure 3.1B, top). As was seen for NTSR1, other cluster 2 GPCRs showed a slower association for 3Q than WT (Figure S3.2A). Though the magnitude of the effect varied across receptors (Figure S3.2B), these results clearly show that even recruitment to cluster 2 GPCRs is impacted by loss of PIP-binding in β-arrestins.

Together, these results provide several major findings. First, though the tested GPCRs can be divided into two groups, the reliance on PIP-binding for arrestin recruitment is very much a continuum. Generally, GPCRs that co-localize with β-arrestins at endosomes do not require the PIP-binding capacity of β-arrestins for plasma membrane recruitment and are henceforth referred to as PIP-independent GPCRs. Secondly, though PIP-independent GPCRs retained the ability to recruit β-arrestins, the kinetics of recruitment is impaired by loss of PIP binding, suggesting that PIP-mediated interactions likely function to stabilize GPCR-arrestin complexes

across all receptors. Finally, while βarr1 and βarr2 behave similarly for most GPCRs, there were exceptions; in much the same way that a continuum of LOF values was observed, this suggests that GPCR-arrestin complexes are incredibly diverse both in their sensitivity to allosteric inputs and possibly their conformational landscape.

Receptor phosphorylation patterns determine the dependence on PIP-binding by arrestin

The distinction between class A and class B receptors was previously attributed to the presence of suitably positioned clusters of phosphosites in the receptor C-terminus (Oakley, Laporte et al. 2001).We reasoned that there must be a degree of phosphorylation required to overcome the dependence on arrestin-PIP binding for recruitment to class A receptors. We chose the NTSR1as a model receptor since WT NTSR1 stably associated with arrestins and the major phosphorylation cluster responsible for this phenomenon was previously established for the rat ortholog (Oakley, Laporte et al. 2001). Using human NTSR1, we designed a set of phosphorylation-deficient mutants, including both the C-terminus and the third intracellular loop (ICL3) (Figure 3.2A).In the recent NTSR1-βarr1 structure (Huang, Masureel et al. 2020), ICL3 was found to be phosphorylated and appeared to make contacts to arrestin, though the role of ICL3 phosphorylation in arrestin recruitment had not been explored. NTSR1 contains four S/T residues in ICL3, three of which are clustered, and 9 S/T residues in its C-terminus, 6 of which are divided into two clusters. To compare the PIP-dependence of NTSR1 phosphorylation mutants (Figure 3.2A) for their ability to recruit βarr1 to the plasma membrane, we used the CAAX bystander NanoBiT assay (Figure 3.1A). We first measured cell-surface expression of the NTSR1 constructs and found similar levels (Figure S3.3A), except for ICL3-4A, which showed slightly reduced expression. Regardless, in this range of receptor expression recruitment signal is saturated with respect to NTSR1 and these minor differences

in expression are unlikely to affect the assay response (Figure S3.3B-C). Though WT NTSR1 is classified as a PIP-independent receptor, NTSR1 phosphorylation mutants could either be classified into cluster 1 or cluster 2 (Figure 3.2A, Supplementary Data Figure 3.3), suggesting that particular phosphorylation mutants rendered arrestin recruitment to NTSR1 PIP-dependent. Removal of the two C-terminal phosphorylation site clusters (NTSR1-6A, NTSR1-298 10A) resulted in a dramatic reduction in arrestin recruitment (Supplementary Data Figure 3.3), with remaining arrestin recruitment being largely PIP-dependent (Figure 3.2A). Removal of the ICL3phosphorylation sites did not affect PIP-dependence (NTSR1-ICL3-4A); neither did removal of the proximal phosphorylation cluster (NTSR1-A401VAA), nor removal of any one residue in the distal cluster (NTSR1-TLSA, NTSR1-ALSS, NTSR1-TLAS). However, removal of the distal phosphorylation cluster (NTSR1-A407LAA) led to a dramatic reduction in recruitment, and an increase in PIP-dependence, consistent with findings that the distal cluster in the rat ortholog is necessary for stable arrestin association (Oakley, Laporte et al. 2001). NTSR1-5A, bearing a single C-terminal phosphorylation site in the distal cluster, showed PIP sensitivity comparable to NTSR-ALAA, while NTSR1-4A with two distal cluster phosphorylation sites showing much less PIP-dependence, suggesting that two phosphorylation sites are sufficient to overcome the need for PIP binding. Similarly, NTSR1-TLAA, which differs from NTSR1-5A only in the addition of the proximal cluster of phosphosites exhibits sensitivity between the NTSR1-5A and NTSR1-4Aconstructs, suggesting that a phosphorylation site from the proximal cluster may offer a partial rescue for the absence of one in the distal cluster.

As the plasma membrane bystander recruitment assay suggested that two phosphorylation sites were necessary to overcome the PIP-dependence on arrestin recruitment, we wondered whether this behavior coincided with the ability of arrestin to be recruited to endosomes. We

monitored translocation of arrestin to endosomes using the endosome bystander NanoBiT assay (Figure S3.1E). As expected, NTSR1-ALAA (Oakley, Laporte et al. 2001) as well as NTSR1-6A and NTSR1-10A failed to recruit arrestin to endosomes (Figure 3.2B, Supplementary Data Figure 3.7). A single C-terminal phosphorylation site (NTSR1-5A) was insufficient to promote arrestin traffic to endosomes; however, two phosphorylation sites in the distal cluster (NTSR1-4A) were sufficient to promote endosomal translocation. There was a further increase in recruitment when the proximal sites were returned (NTSR1-TLSA), suggesting an additional contribution from this region strengthens the interaction between NTSR1 and arrestin. Further support for a contribution from the proximal cluster stems from the difference between NTSR1-5A and NTSR1-TLAA, which differ in the presence of the proximal phosphorylation cluster and show a marked difference in both targeting of arrestin to endosomes, as well as PIP-dependence (Figure 3.2B). Within the distal cluster, any two phosphorylation sites were sufficient, and having the third present appeared to offer no additional benefit (NTSR1-AVAA compared to NTSR1-ALSS, NTSR1-TLAS and NTSR1-TLSA) (Figure 3.2B).

Given that two phosphorylation sites in the distal cluster were sufficient for both PIP-insensitivity for plasma membrane recruitment, and recruitment of arrestin to endosomes, we asked whether two phosphorylation sites were also sufficient for receptor internalization. We measured internalization of the NTSR1 constructs in β-arrestin-deficient HEK293 cells where either WT or3Q βarr1 was reintroduced. WT NTSR1 was robustly internalized by both WT and 3Q βarr1. In contrast, NTSR1-5A showed a significant difference in internalization between WT and 3Q βarr1, while NTSR1-4A showed no difference in internalization between WT and 3Q βarr1. The trend between NTSR1-5A and NTSR1-4A parallels that seen for β2AR and β2AR-

V2C (Figure 3.2C), supporting our finding that two phosphorylation sites are sufficient for robust internalization that is PIP-independent. In addition, the internalization observed for NTSR1-5A by WT βarr1 suggests that the lack of endosome recruitment observed for this construct (Figure 3.2B) is due to weakened GPCR-βarr interaction and not simply a lack of internalization for this receptor (Figure 3.2C).

Together, these data show that two suitably positioned phosphorylation sites are sufficient to render β-arrestin recruitment PIP-independent and allow for robust arrestin-dependent internalization as well as support arrestin translocation to endosomes. Furthermore, they show that NTSR1, a receptor that recruits β-arrestin in a PIP-independent manner, can become PIP-dependent by changes in receptor phosphorylation. Given that GPCRs, such as the μOR, have different phosphorylation patterns depending on the stimulating agonist (Just, Illing et al. 2013), we speculate that the resulting β-arrestin complexes may have drastically different behavior in cells.

PIP2 binding affects complex stability and tail-core equilibrium in vitro

As PIP-binding was previously suggested to stabilize the interaction between a GPCR and arrestin (Gaidarov, Krupnick et al. 1999), based on experiments in cells, we wanted to explicitly test this invitro. Using NTSR1 as our model receptor, where PIP-binding was not strictly necessary for recruitment in cells, we compared the ability of GRK5 phosphorylated NTSR1 to form a complex with βarr1 (WT or 3Q mutant) in the presence of a soluble PIP2 derivative, diC8-PI(4,5)P2 (henceforth PIP2), by size-exclusion chromatography (Figure 3.3A-B) (Huang, Masureel et al. 2020). While complexing with full-length WT βarr1 led to about 25% complex formation, use of 3Q βarr1resulted in <5% complex formation (Figure 3.3C). Use of a C-

terminally truncated βarr1 (1-382) led to a more than 2-fold enhancement in complex formation, which was only slightly reduced with the corresponding 3Q arrestin. Using the LOF metric developed to evaluate the impact of PIP-binding on arrestin recruitment in cells, we found that full-length arrestin showed a greater degree of LOF than C-terminally truncated arrestin, suggesting that removal of the arrestin C-terminus is largely able to overcome the impairment in complexing that results from the 3Q mutation (Figure S3.4A). PIP2 affinity in vitro was reduced 20x for 3Q βarr1 compared to WT (Figure S3.4B). Since arrestin activation is understood to proceed via release of its auto-inhibitory C-terminus (Shukla, Manglik et al. 2013, Sente, Peer et al. 2018), we wanted to rule-out the possibility that 3Q βarr1 complexing efficiency is simply reduced due to a lack of arrestin C-terminus release. We designed a Förster Resonance Energy Transfer (FRET) sensor to report on arrestin C-terminus release (Figure S3.4C): using a cysteine-free βarr1 construct, we introduced two new cysteine residues at positions 12and 387 – βarr1 (12-387) – to allow for selective labeling of these positions with a suitable dye pair. Given that the expected change in distance between the bound and unbound C-terminus was ~40 Å (Kim, Vishnivetskiy et al. 2012, Zhuo, Vishnivetskiy et al. 2014, Chen, Perry et al. 2017), we used an Alexa Fluor 488/Atto647N FRET pair, which offers a relatively short Förster radius (R0 ~50 Å). GRK5-phosphorylatedNTSR1 robustly displaced the C-terminus of both WT and 3Q βarr1 (12-387) (Figure S3.4D). Displacement was comparable to that seen for a saturating concentration of a peptide corresponding to the phosphorylated C-terminus of the vasopressin 2 receptor (henceforth V2Rpp) known to completely displace the arrestin C-terminus (Shukla, Manglik et al. 2013). GRK5-phosphorylated NTSR1 fully displaced the βarr1 C-terminus with 10x greater potency thanV2Rpp, suggesting an enhanced affinity for an intact receptor compared to a phosphopeptide alone. These data show that not only does in vitro phosphorylated NTSR1 fully displace the arrestin C-terminus, but with higher efficacy

than an equimolar concentration of phosphopeptide (even in the presence of unphosphorylated NTSR1), and this is independent of the PIP-binding ability of arrestin.

We reasoned that the reduced complexing efficiency of 3Q βarr1 may be due to differences in the proportion of core-engaged complex being formed (Figure 3.3D). To test this hypothesis, we used an environmentally sensitive bimane fluorophore (bim) site-specifically installed at L68 (L68bim) on the arrestin finger loop, a region that upon formation of a core-engaged complex with an active GPCR becomes buried within the receptor TM core. Such a sensor had previously been used to report on core-engagement for rhodopsin/arrestin-1 (Sommer, Smith et al. 2005, Sommer, Smith et al. 2006), whereupon receptor core-engagement a blue-shift and an increase in fluorescence emission occurs, owing to the bimane probe moving into a lower polarity environment within the receptor TM core.398 While addition of V2Rpp to βarr1 L68bim leads to C-terminus release and a ~50% increase in bimane fluorescence as seen previously (Latorraca, Masureel et al. 2020), we speculated that the addition of receptor may further increase this signal (Sommer, Smith et al. 2006). We compared the fluorescence changes of βarr1 L68bim (WT or 3Q) upon addition of NTSR1 that was either dephosphorylated or phosphorylated by GRK5 (Figure 3.3E). In the absence of NTSR1 phosphorylation, there was no increase in fluorescence; however, phosphorylated NTSR1 led to a ~2-fold enhancement in fluorescence intensity for WT, but a smaller 1.5-fold enhancement for 3Q. The addition of V2Rppat a saturating concentration to the unphosphorylated NTSR1 did not result in a significant increase over phosphopeptide alone, consistent with the behavior observed for C-terminus release (Figure S3.4D). Importantly, for the 3Q βarr1, GRK5 phosphorylated NTSR1 did not elicit a response different from V2Rpp alone.

Given that the complex exists as a dynamic equilibrium between three states (Figure 3.3D): dissociated, tail-bound and core-engaged. We reason that if PIP-binding serves to stabilize the core-engaged state then loss of PIP binding would bias the equilibrium towards a tail-engaged state (Figure 3.3F), which should have a similar spectroscopic signature to V2Rpp alone. Taken together, these data suggest a model of complex assembly where release of the arrestin C-terminus by the phosphorylated GPCR C-terminus is rapid, and reversible. The resulting tail-bound state is in equilibrium with a core-engaged state, where arrestin-PIP binding stabilized this state and thereby slows dissociation. In the context of full-length arrestin, destabilization of core-engaged state in the 3Q mutant leads to a reduction in complex stability, presumably due to arrestin C-tail-mediated dissociation from the tail-bound state. Consistent with these findings when the arrestin C-terminus is removed the reduced core-engagement of the 3Q mutant does not impact complexing efficiency due to an increased stability of the tail-bound state (as seen in Figure 3.3C, S4A).

PIP2, in the absence of a GPCR, triggers conformational changes in arrestin

The finding that β-arrestins in CCSs, even in the absence of an associated GPCR, signal through MAPK (Eichel, Jullié et al. 2016) suggested that arrestin can adopt an active-like conformation without a GPCR C-terminus to displace its own C-terminus. While PIP2 was proposed to maintain the membrane association of β-arrestins (Eichel, Jullié et al. 2018), the impact of this association on the conformational landscape of β-arrestins, and thus their ability to engage downstream signaling partners was unknown (Ranjan, Dwivedi et al. 2017). Having shown that PIP-binding affects the dynamics of NTSR1-βarr1 complexes in vitro, we wondered whether PIPs in the absence of an associated GPCR could also affect the conformation of βarr1. We compared the effect of PIP2 to the V2Rppfor promoting conformational changes in

arrestin using FRET and fluorescence reporters on the finger loop, gate loop, and C-terminus (Figure 3.4A).

Both the finger loop (Figure 3.4B, Figure S3.5A-B) and the gate loop (Figure 3.4C, Figure S3.5C-D) showed saturable conformational changes upon addition of PIP2 which were smaller than those seen for V2Rpp. Further, the corresponding 3Q mutants did not show PIP2-inducedconformational changes, though they responded to V2Rpp similarly to WT protein. These data suggest that binding of PIP2 to the arrestin C-lobe allosterically promotes conformational changes in key arrestin regions involved in GPCR recognition and activation. As the accepted mechanism for arrestin activation begins with release of its autoinhibitory C-terminus (Sente, Peer et al. 2018), we wondered whether these conformational changes were the result of allosterically promoted C-terminus release. Using our βarr1 C-terminus FRET sensor (Figure S3.4C) we found that PIP2 promoted a small movement of the arrestin C-terminus (Figure 3.4D), but only at concentrations higher than those needed to saturate the responses seen for either the finger or gate loop sensors (Figure 3.4B-C). As was the case for the other sensors, this FRET change in response to PIP2 is absent in the corresponding 3Q mutant (Figure S3.5E-F). This finding is consistent with recent DEER experiments that found little or no C-terminal displacement for βarr1 with IP6 (Chen, Zhuo et al. 2021). We reason that the conformational changes in the finger and gate loops observed together with the small FRET change in response to PIP2 could either be due to a change in the equilibrium of active-inactive βarr1, or a population of an intermediate state of arrestin bearing a change in position or orientation of the arrestin C-terminus within the arrestin N-lobe. As different membrane PIPs serve as markers for different subcellular locations, we measured the ability of other PIPs (Figure S3.6A) to promote conformational changes in the βarr1 finger loop. Like PI(4,5)P2,

PI(3,4)P2, PI(3,5)P2 and PI(3,4,5)P3 all elicited an increase in bimane fluorescence (Figure S3.6B-F). In contrast, PI(4)P showed a weaker response and PI(3)P and PG did not increase fluorescence of the bimane reporter (Figure S3.6G-I). Interestingly, these results showed that plasma membrane resident PIPs (Di Paolo and De Camilli 2006), PI(4,5)P2, PI(3,4)P2,PI(3,4,5)P3 and to a lesser extent PI(4)P were able to promote this conformational change in βarr1, but the early endosomal marker PI(3)P was unable to do so (Figure S3.6J). PI(3,5)P2 showed a similar effect to other PIP2s, but is understood to be rare within cells (Hasegawa, Strunk et al. 2017).Based on contacts observed in the NTSR1-βarr1 structure (Huang, Masureel et al. 2020), we speculate that PIPs bearing adjacent phosphates on the inositol ring may be necessary for chelation of K232and R236/K250 (Figure S3.6K); however, a phosphate at the 4-position is sufficient to coordinate K250 and R236, explaining the small effect seen for PI(4)P. Together, these data show that different PIP2 derivatives are capable of promoting conformation changes in βarr1, while PIPs bearing a single phosphate do not, raising the possibility of compartment-specific differences in the behavior of GPCR-arrestin complexes.

PIP2 increases the population of active arrestin

While our fluorescence experiments support PIP2-promoted conformational changes consistent with arrestin activation, the lack of C-terminus release raised questions of whether these conformational changes truly reflected an increase in the population of active arrestin, as would be detected by arrestin binding partners. While the active form of arrestin is understood to mediate signaling via interactions with a number of protein partners, including MAPK, ERK, SRC (Reiter, Ahn et al. 2012, Ranjan, Dwivedi et al. 2017), there has been speculation that the binding of a particular partner might be mediated by a distinct arrestin conformation. We

reasoned that the global activation state of arrestin could be probed using an engineered Fab (Fab30), which has a high-affinity for the active (V2Rpp-bound) state of βarr1 (Shukla, Manglik et al. 2013). Fab30 has found utility in a number of structural studies (Shukla, Manglik et al. 2013, Shukla, Westfield et al. 2014, Lee, Appleton et al. 2016, Nguyen, Thomsen et al. 2019, Staus, Hu et al. 2020), functional studies (Kumari, Srivastava et al. 2016, Thomsen, Plouffe et al. 2016, Cahill, Thomsen et al. 2017, Ghosh, Dwivedi et al. 2019, Latorraca, Masureel et al. 2020) and more recently it has been adapted as a single-chain intrabody (IB30) for the detection of active βarr1 in cells (Baidya, Kumari et al. 2020, Baidya, Kumari et al. 2020).

We used Surface Plasmon Resonance (SPR) to measure binding of Fab30 to immobilized βarr1(Figure 3.5A). To confirm the immobilized arrestins behave as expected, we tested binding of V2Rpp and Fab30+V2Rpp (Figure 3.5B, Figure S3.8, Supplementary Data Tables 2-3). Though selected for binding to the V2Rpp-bound state of βarr1, Fab30 bound to βarr1 weakly in the absence of V2Rpp, presumably due to a small equilibrium population of active-like arrestin (Latorraca, Wang et al. 2018). Interestingly, binding was enhanced when Fab30 was co-injected with PIP2 (Figure 3.5B). This suggested that PIP2 increased the proportion of arrestin in an active-like state which can be recognized by Fab30, consistent with our fluorescence experiments that support PIP2 playing a role in arrestin activation. We compared the effect of different additives on Fab30 binding to WT βarr1, but also a βarr1 3Q mutant, and the pre-activated C-terminally truncated βarr1(1-382) (Kim, Hofmann et al. 2013). At 1 μM, Fab30 showed 10.2 ± 0.9% (of maximal) binding to WT βarr1, compared to 56.8 ± 2.0% binding for βarr1 (1-382) (Figure 3.5C). This suggests that Fab30 binding is favored by a conformation accessible to WT βarr1, but greatly enhanced by removal of the arrestin C-terminus. When Fab30 is co-injected with a saturating concentration ofPIP2 (40 μM), binding to

WT βarr1 increased more than 3-fold, to 33.9 ± 1.8%, compared to Fab30alone. PIP2 had a smaller effect on the pre-activated βarr1(1-382), but still increased binding from 56.8% to 65.9 ± 0.8%. Titration experiments showed that specific enhancement of Fab30 binding in the presence of PIP2 was most pronounced for WT βarr1 (Figure S3.7G-L). While all three arrestin constructs showed an increase in Fab30 binding in the presence of PIP2, the degree of binding enhancement drastically shifted for WT βarr1 above the Kd for Fab30, but not for either 3Q or (1-382) βarr1 (Supplementary Data Figure 3.8). This suggests that while PIP2 enhanced the population of active-like βarr1, Fab30 binding remains rate-limiting. Since removal of the βarr1 C-terminus abrogates the PIP2-enhancement of Fab30 binding, we reason that PIP2 acts in cis with C-terminal displacement, consistent with our FRET experiments that showed a PIP2-induced movement of the βarr1 C-terminus. To determine whether this effect was specific for PIP2, we compared the ability of PG and PI(3)P to enhance binding of Fab30. Both showed a small enhancement inFab30 binding, but significantly less than that seen with PIP2 (Figure 3.5C). Further, βarr1 3Qshowed no difference between PG, PI(3)P and PIP2, suggesting that while anionic lipids weakly increase Fab30 binding to βarr1, PIP2 was unique in affecting a specific increase in Fab30 binding. Both PG and PI(3)P did not enhance Fab30 binding to βarr1 (1-382).

Based on these data we propose that spontaneous activation of arrestin to an active-like state capable of binding Fab30 is possible but rare in the absence of arrestin inputs (Figure 3.5D). V2Rpp dramatically shifts the equilibrium towards the active-state by displacement of the arrestin C-terminus, and removal of the arrestin C-terminus alone is sufficient to greatly enhance the active-population, even in the absence of V2Rpp or PIP2. Unlike V2Rpp, which displaces the arrestin C-terminus, PIP2 is unable to displace the arrestin C-terminus directly,

but able to allosterically move it. While PIP2 may stabilize the same active state of arrestin achieved with V2Rpp, albeit to a lesser extent, it may also act to stabilize an active-like state of arrestin that is on-pathway towards activation and capable of binding Fab30, though to a lesser extent than V2Rpp-bound βarr1.Further studies will be necessary to distinguish these possibilities.

3.4 Conclusions

Our results reveal new molecular details underpinning the regulation of arrestin recruitment to GPCRs, and how spatial and temporal control of GPCR-β-arrestin complexes may occur within a cell.

Our findings offer a molecular basis for understanding the phenotypic classification of GPCRs into “class A” or “class B” for arrestin recruitment. In our model (Figure 3.6), we refer to “class A” and “class B” GPCRs as “PIP-dependent” and “PIP-independent”, respectively. “PIP-dependent” GPCRs (Figure 3.6, left) require the coincident detection of membrane PIPs for recruitment to an activated and phosphorylated GPCR. We speculate that this is due to an insufficiency in phosphorylation of these receptors, requiring either an allosteric priming of C-terminus release by plasma membrane PIPs, or the simultaneous action of both phosphate-mediated contacts and PIP-mediated contacts to form a sufficiently long-lived complex for effective receptor desensitization, sequestration, and internalization. As some PIP-dependent GPCRs can recruit arrestin in a C-terminus-independent manner, we consider that release of the arrestin C-terminus may not be necessary for arrestin function in the context of these receptors. A further trait of these PIP-dependent GPCRs is that they exhibit, to a varying degree, the “catalytic activation” phenotype (Eichel, Jullié et al. 2018) wherein arrestin, after recruitment to an active GPCR, loses association with the GPCR but remains at the plasma membrane and concentrates at CCSs. This can be explained by the increasing concentration gradient of PIP2 leading into the CCS (Sun, Carroll et al. 2007) along with our biophysical evidence that PIP2 promotes conformational transitions associated with activation. Once a GPCR cargo has been translocated into a CCS, clathrin-mediated endocytosis (CME) proceeds and PIP2 levels drop. We suggest that this may serve as the timing component for

arrestin dissociation from these PIP-dependent GPCRs (Zhang, Barak et al. 1999). Presumably, once arrestin has dissociated, the receptor is susceptible to dephosphorylation, and upon arrival at early endosomes is able to be sorted for rapid recycling (Krueger, Daaka et al. 1997). In contrast, “PIP-independent receptors” (Figure 3.6, right panel) possess phosphorylation sites which alone can promote a stable association with arrestin, without the need for membrane PIPs. Since PIP-binding is not necessary to maintain the GPCR-arrestin association, arrestin co-localizes with these receptors at endosomes. Whether this co-localization is the product of PIP-independent GPCRs being able to recruit β-arrestins when at endosomes or by forming a sufficiently stable complex to allow for co-trafficking from the plasma membrane without exchange remains to be shown.

One question this model raises is: if PIP2 promotes partial activation of β-arrestins, why is it that β-arrestins are not basally associated with the plasma membrane? Consistent with our SPR experiments, and the finding that GPCR C-terminal phosphorylation is required for arrestin accumulation at CCSs (Eichel, Jullié et al. 2018), we speculate that PIP2 binding may occur when arrestin transitions to an active-like conformation and stabilize this state. We speculate that in cells, engagement with a GPCR may be necessary to facilitate PIP2 binding. GPCRs have been shown to associate with PIP2 in the local membrane environment ((Yen, Hoi et al. 2018, Song, Yen et al. 2019), and in doing so may act to “load” PIP2 onto the arrestin, which either can remain associated with the GPCR or diffuse along the membrane.

These data suggest that while PIP-mediated contacts are not necessary to maintain association, they likely affect the equilibrium of core vs. tail-engaged states of the complex. Tail-engagement has been shown to be sufficient for MAPK signaling downstream of β-arrestin

(Kumari, Srivastava et al. 2017). We speculate that this shift in equilibrium, particularly in the context of endosomes defined by PI(3)P, may explain how PIP-independent receptors, such as V2R and PTH1R are able to engage and signal through both β-arrestin and G proteins simultaneously in a so-called “megaplex” assembly (Thomsen, Plouffe et al. 2016, Nguyen, Thomsen et al. 2019).

To-date four structures of GPCR-βarr1 complexes have been described, all of which show arrestin in a core-engaged state (Yin, Li et al. 2019, Huang, Masureel et al. 2020, Lee, Warne et al. 2020, Staus, Hu et al. 2020), but only one had PIP2 bound at the interface (Huang, Masureel et al. 2020). Interestingly, this NTSR1-βarr1complex with PIP2 bound used the native NTSR1 C-terminus and did not use Fab30 to stabilize the complex. We speculate that Fab30 plays a particularly important role in stabilizing the receptor core-engaged complex (Shukla, Westfield et al. 2014).

Overall, our data offer a parsimonious explanation for several phenotypic behaviors observed for GPCR-β-arrestin complexes and provide a biophysical framework for understanding the interplay between phosphorylation-mediated and PIP-mediated contacts in complex assembly. A reliance on PIPs for arrestin recruitment offers a robust solution for recruitment of arrestin to receptors with spatial control, and temporal precision. Given the interplay between PIP-dependent recruitment and phosphorylation, we believe that distinct signaling outcomes may not only be due to differences in phosphorylation alone (Latorraca, Masureel et al. 2020), but rather that these differences may be further fine-tuned by membrane PIPs that are present in distinct subcellular locations, adding yet another layer of complexity to our understanding of GPCR signaling.

3.5 Materials and Methods

Plasmids

For cell-based assays, we used human, full-length GPCR plasmids cloned into the pCAGGS vector or the pcDNA3.1 vector derived from a previous study (Inoue, Raimondi et al. 2019). GPCR constructs were N-terminally FLAG epitope-tagged when they were intended to compare with cell surface expression levels. Specifically, NTSR1 was fused to the N-terminal FLAG epitope tag with a linker (MDYKDDDDKGTELGS; the FLAG epitope tag is underlined) and inserted into the pcDNA3.1 vector. β2AR and μOR were fused to the N-terminal FLAG epitope tag with a preceding HA-derived signal sequence and a flexible linker (MKTIIALSYIFCLVFADYKDDDDKGGSGGGGSGGSSSGGG) and inserted into the pCAGGS vector. Unless otherwise noted, other GPCR constructs were untagged. For the bystander NanoBiT-based β-arrestin assays, human full-length β-arrestin (β-arrestin1 or 2; WT or 3Q) was N-terminally SmBiT-fused with the flexible linker (MVTGYRLFEEILGGSGGGGSGGSSSGG; the SmBiT is underlined) and inserted into the pCAGGS vector (SmBiT-β-arrestin) (Baidya et al.,2020a). For the plasma membrane-localizing tag, LgBiT was C-terminally fused to the CAAX motif derived from human KRAS (SSSGGGKKKKKKSKTKCVIM) through the same flexible linker (LgBiT-CAAX). For the endosome-localizing tag, LgBiT was N-terminally fused with the human Endofin FYVE domain (amino-acid regions Gln739-Lys806) again through the same flexible linker (Endo-LgBiT). For the direct NanoBiT-based β-arrestin assay, human full-length β-arrestin was N-terminally LgBiT-fused with the same flexible linker and inserted into the pCAGGS vector (LgBiT-β-arrestin). GPCRs were C-terminally SmBiT-fused with the flexible linker (GGSGGGGSGGSSSGGVTGYRLFEEIL; the SmBiT is underlined) and inserted into the pCAGGS vector (GPCR-SmBiT).

Peptides

The V2Rpp peptide (ARGRpTPPpSLGPQDEpSCpTpTApSpSpSLAKDTSS) was obtained by custom peptide synthesis (Tufts University Core Facility). The concentration of V2Rpp stocks were determined by reaction with Ellman's reagent as previously described (Latorraca, Masureel et al. 2020).

NanoBiT-β-arrestin recruitment assays

β-arrestin recruitment to the plasma membrane was measured by the bystander NanoBiT-β-arrestin assays using the SmBiT-β-arrestin and the LgBiT-CAAX constructs. HEK293A cells (Thermo Fisher Scientific) were seeded in a 6-cm culture dish (Greiner Bio-One) at a concentration of 2 x 105 cells per ml (4 ml per dish hereafter) in DMEM (Nissui Pharmaceutical) supplemented with 10% FBS (Gibco), glutamine, penicillin, and streptomycin, one day before transfection. The transfection solution was prepared by combining 5 µl of polyethylenimine solution (1 mg/ml) and a plasmid mixture consisting of 100 ng SmBiT-β-arrestin, 500 ng LgBiT-CAAX and 200 ng of a test GPCR construct in 200 µl of Opti-MEM (Thermo Fisher Scientific). For the NTSR1 titration experiment, diluted volume of the FLAG-NTSR1 plasmid (13 ng to 200 ng) was transfected with 100 ng SmBiT-β-arrestin and 500 ng LgBiT-CAAX with a balanced volume of the pcDNA3.1 vector (total plasmid volume of 800 ng). After an incubation for one day, the transfected cells were harvested with 0.5 mM EDTA-containing Dulbecco's PBS, centrifuged, and suspended in 2 ml of Hank's balanced saline solution (HBSS) containing 0.01% bovine serum albumin (BSA fatty acid–free grade, SERVA) and 5 mM HEPES (pH 7.4) (assay buffer). The cell suspension was dispensed in a white 96-well plate (Greiner Bio-One) at a volume of 80 µl per well and loaded with 20 µl of 50 µM coelenterazine (Carbosynth), diluted in the assay buffer. After 2-hour incubation at room temperature, the plate was measured for

its baseline luminescence (SpectraMax L, 2PMT model, Molecular Devices). Thereafter, 20 µl of 6x ligand serially diluted in the assay buffer were manually added. The ligand used was dependent on the GPCR expressed, as described in Supplementary Data Table 1. The plate was immediately read for the second measurement as a kinetics mode and luminescence counts recorded for 15 min with an accumulation time of 0.18 sec per read and an interval of 20 sec per round. β-arrestin endosomal translocation was measured by following the same procedure as described above but using the SmBiT-β-arrestin and the Endo-LgBiT constructs. Similarly, direct recruitment was measured by the same protocol as described above but using LgBiT-β-arrestin (500 ng) and C-terminally fused-SmBiT GPCR (500 ng) constructs. For every well, the recorded kinetics data were first normalized to the baseline luminescence counts.

Analysis of cell-based recruitment data

NanoBiT data were analyzed by converting kinetic data into concentration-response data by determining an average fold-change (relative to signal pre-stimulation) from 10-15 minutes post-agonist addition. At least three independent experiments were performed for each receptor-sensor combination. Concentration-dependent data from two technical replicates for each independent experiment were collectively fit to a four-parameter log logistic function (LL2.4) provided in the drc package (v 3.0-1) of the statistical environment R. This equation, of the form: $f(x) = c + d{-}c$ provides pre- and post-transition values, c and d, respectively, that $1{+}e(b(\log(x){-}\log(e)))$ define the amplitude response for that assay. Cutoffs for bystander NanoBiT experiments were determined as based on a limit of detection of 3s over the response of mock-transfected cells. Amplitude values were defined as amplitude = top – bottom of fit, and amplitude error was calculated as $\delta(amplitude) = \sqrt{}(\delta top)2 + (\delta bottom)2$. Converting amplitude to LOF for each assay was based on the formula: $1 - amplitude(3Q)/amplitude(WT)$.

Errors for LOF were$\delta amplitude$(3Q) 2 $\delta amplitude$(WT) 2calculated as: $\delta(LOF) = LOF\sqrt{}$ ($amplitude$ (3Q)) + ($amplitude$(WT)). In cases where a fit failed to converge due to weak recruitment, these amplitudes and errors were set to zero. Recruitment ofβarr1 (3Q) to D1R in both plasma membrane bystander (CAAX) and direct recruitment which was set to zero. The error amplitude for βarr1 (3Q) endosome translocation assay with D1R was also set to zero. The error amplitude for βarr1 (3Q) endosome translocation assay with S1PR1 was set to zero, and the "top" value of the fit was set to 1.2 based on manual inspection. K-means clustering was performed using pre-built functions in the tidyverse package (v 1.3.1) of R. The number of clusters was varied from 1 to 10 and an elbow plot of within cluster sum of squares vsk suggested 2 clusters fit the data well.

For recruitment kinetics, luminescence fold-change was plotted against time, and the values from$L$zero to five minutes (initial rate) were fit to a logistic function of the form: $f(x) = 1+e-k(x-x0)$, where L is the curve's maximum value, x0 is the value of the sigmoid midpoint and k is the logistic growth rate. Fitting was done using the self-starting SSlogis four parameter nls function in the tidyverse package (v 1.3.1) of R.

GPCR internalization assay

GPCR internalization assays was performed as described previously with minor modifications (Grundmann, Merten et al. 2018). Δβarr1/2 double knockout (DKO) cells, previously described (O'Hayre, Eichel et al. 2017), were seeded in 6-cm dishes at concentration of 2 x 105 cells/ml (4 mL per dish) and cultured for 1 day before transfection. The cells were transfected with 1 μg of the N-terminally FLAG-tagged NTSR1 or the β2AR construct, along with 200 ng of the WT or 3Q βarr1 or empty plasmid, using PEI transfection reagent as described above. After 1-day

culture, the transfected cells were harvested by EDTA-PBS and HEPES-HBSS and, following centrifugation, the cells were suspended in 500 □L of 0.01% BSA-containing HEPES-HBSS. The cell suspension was dispensed in a 96-well V-bottom plate (100 µL per well) and mixed with 100 µL of 2× GPCR solution ligand (2 µM neurotensin for FLAG-NTSR1 or 20 µM Isoproterenol (Sigma-Aldrich) for FLAG-β2AR). After 30-min incubation in a CO2 incubator, the plate was centrifuged at 1,500 g for 5 min and the cells were washed twice with D-PBS. The cell pellets were suspended in 2% goat serum and 2 mM EDTA-containing D-PBS (blocking buffer; 100 µL per well) and incubated for 30 min on ice. After centrifugation, the cells were stained with anti-FLAG-epitope tag monoclonal antibody (Clone 1E6, FujiFilm Wako Pure Chemicals; 10 µg mL-1 in the blocking buffer; 25 µL per well) for 30 min on ice. After washing with D-PBS, the cells were labeled with a goat anti-mouse IgG secondary antibody conjugated with Alexa Fluor 647 (Thermo Fisher Scientific; 10 µgmL-1 dilution in the blocking buffer; 25 µL per well) for 15 min on ice. The cells were washed once with D-PBS, resuspended in 100 µL of 2 mM EDTA-containing-D-PBS and filtered through a 40 µm filter. The fluorescently labeled cells (approximately 20,000 cells per sample) were analyzed by the EC800 flow cytometer (Sony). Fluorescent signal derived from Alexa Fluor 647 was recorded in the FL3 channel. Mean fluorescence intensity (MFI) from all the recorded events was analyzed by a FlowJo software (FlowJo) and used for statistical analysis.

Cell surface expression analysis by flow cytometry

HEK293A cells were seeded in a 6-well culture plate at concentration of 2 x 105 cells/ml (2 mL per dish) and cultured for 1 day before transfection. The cells were transfected with 1 µg of N-terminally FLAG-tagged GPCR construct using PEI transfection reagent as described above and cultured for 1 day. The cells were collected by adding 200 µl of 0.53 mM EDTA-containing

Dulbecco's PBS (D-PBS), followed by 200 µl of 5 mM HEPES (pH 7.4)-containing Hank's Balanced Salt Solution (HBSS). The cell suspension was transferred to a 96-well V-bottom plate in duplicate and fluorescently labeled with the anti-FLAG epitope tag antibody and a goat anti-mouse IgG secondary antibody conjugated with Alexa Fluor 488 (Thermo Fisher Scientific, 10 µg per ml diluted in the blocking buffer) as described above. Live cells were gated with a forward scatter (FS-Peak-Lin) cutoff at the 390 setting, with a gain value of 1.7 and fluorescent signal derived from Alexa Fluor 488 was recorded in the FL1 channel. For each experiment, the MFI value of mutants was normalized to that of WT performed in parallel.

cAMP desensitization

HEK293 Δβarr1/2 (DKO) cells that endogenously express β2AR were seeded into 6-well plates and transiently transfected after 24 hours with mApple, βarr2-mApple, or βarr2(3Q)-mApple. Twenty-four hours after transfection, cells were transduced with CMV cADDis Green Upward cAMP sensor according to manufacturer instructions without addition of sodium butyrate (Montana Molecular #U0200G) and seeded in triplicate in a black clear-bottom 96-well plate (Corning cat# 3340). Twenty-four hours after transduction, the cells were washed once with 37°C assay buffer [135 mM NaCl, 5 mM KCl, 0.4 mM Mg2Cl, 1.8 mM CaCl2, 5 mM glucose, 20 mM HEPES pH 7.4], loaded into the pre-warmed 37°C plate reader (Biotek Synergy H4), and equilibrated for five minutes. Prior to beginning the kinetic assay, mApple was read using monochromators set to Ex:568/9.0 and Em:592/13.5. Then cADDis was read using monochromators set to Ex:500/9.0 and Em:530/20.0. Three cADDis timepoints were collected to establish baseline, the plate was ejected, isoproterenol in 37°C assay buffer was added to a final concentration of 100 nM, and the plate was returned to continue collection. Thirty minutes after isoproterenol addition, 3-isobutyl-1-methylxanthine (IBMX) and forskolin (Fsk) in 37°C

assay buffer were added to a final concentrations of 300 μM and 10 μM respectively. Responses were averaged across technical replicates, normalized to the maximum Fsk/IBMX response, and then averaged across independent experiments. Expression levels for cADDis and βarr2 were normalized based on fluorescence.

Western blotting

HEK293A cells were transfected with the SmBiT-β-arrestin and the LgBiT-CAAX constructs by following the procedure described in the NanoBiT-based β-arrestin assay. After 1-day culture, the transfected cells were lysed by SDS-PAGE sample buffer (62.5 mM Tris-HCl (pH 6.8), 50 mM dithiothreitol, 2% SDS, 10% glycerol and 4 M urea) containing 1 mM EDTA and 1 mM phenylmethylsulfonyl fluoride. Lysates derived from an equal number of cells were separated by 8% SDS-polyacrylamide gel electrophoresis. Subsequently, the proteins were transferred to PVDF membrane. The blotted membrane was blocked with 5% skim milk-containing blotting buffer (10 mM Tris-HCl (pH 7.4), 190 mM NaCl and 0.05% Tween 20), immunoblot with primary (1 μg per mL, unless otherwise indicated) and secondary antibodies conjugated with horseradish peroxidase (1:2000 dilution). Primary antibodies used in this study were: anti-β-arrestin1 (rabbit monoclonal; CST, #12697, D8O3J), anti-β-arrestin2 antibody (rabbit monoclonal; CST, #3857, C16D9) and anti-α-tubulin antibody (mouse monoclonal, clone DM1A; Santa Cruz Biotechnologies, sc-32293; 1:2000 dilution). Secondary antibodies were anti-rabbit IgG (GE Healthcare, NA9340) and anti-mouse IgG (GE Healthcare, NA9310). Membrane was soaked with an ImmunoStar Zeta reagent (FujiFilm Wako Pure Chemical). Chemiluminescence image of the membrane was acquired, and band intensity was analyzed with Amersham Imager 680 (Cytiva).

NTSR1 expression and purification

Full length human NTSR1 was modified with an N-terminal FLAG tag followed by an octa-histidine tag and cloned into pFastBac1 vector. NTSR1 was expressed in Sf9 insect cells (Expression Systems) using a FastBac-derived baculovirus. Cells were infected at a density of 4x106 cells/mL and harvested 60 hours post infection. Cells were lysed in hypotonic buffer (10 mM HEPES, pH 7.4, and protease inhibitors) and solubilized at 4 °C for 2 hours in a buffer containing 1% lauryl maltose neopentyl glycol (LMNG, Anatrace), 0.1% cholesteryl hemisuccinate tris salt (CHS, Steraloids), 0.3% sodium cholate (Sigma), 20 mM HEPES 7.4, 500 mM NaCl, 25% glycerol, iodoacetamide (to cap cysteine residues) and protease inhibitors. Insoluble debris was removed by centrifugation and the supernatant was incubated with Ni-NTA (Qiagen) resin for 1 hour at 4 °C. The resin was washed in batch with buffer containing 0.01% LMNG, 0.001% CHS, 0.003% sodium cholate, 20 mM HEPES pH 7.4, 500 mM NaCl, 10 mM imidazole and eluted with the same buffer supplemented with 200 mM imidazole, 2 mM CaCl2 and 10 μM NTS8-13 (Acetate salt, Sigma). The eluate was loaded onto M1 FLAG immunoaffinity resin and washed with buffer containing 0.01% LMNG, 0.001% CHS, 0.003% sodium cholate, 20 mM HEPES pH 7.4, 500 mM NaCl, 10 mM imidazole, 0.1 μM NTS8-13 and 2 mM CaCl2. The receptor was eluted with buffer containing 100 mM NaCl, 20 mM HEPES pH 7.4, 0.005% LMNG, 0.005% CHS, 1 μM NTS8-13, 0.2 mg/mL FLAG peptide (DYKDDDDK) and 5 mM EDTA. Elution fractions containing receptor were pooled and subjected to polishing by SEC on a Superdex 200 Increase 10/300 GL column (GE Healthcare) in 20 mM HEPES, pH 7.4, 100 mM NaCl, 0.0025% LMNG, 0.00025% CHS, and 0.1 μM NTS8-13. Peak fractions were pooled and concentrated to 200 μM and aliquots were flash-frozen and stored at -80 °C until use.

GRK5 expression and purification

Full length human GRK5 was modified with a C-terminal hexa-histidine tag and cloned into pVL1392 vector for baculovirus production. GRK5 was expressed and purified as previously published (Beyett, Fraley et al. 2019). Briefly, Sf9 insect cells (Expression Systems) were infected with a BestBac-derived baculovirus at a density of 3.5 x 106 cells/mL and harvested 48 hours post infection. Cells were resuspended, lysed by sonication and the supernatant was applied to Ni-NTA resin. The resin was washed with lysis buffer and GRK5 eluted with lysis buffer supplemented with 200 mM imidazole. The combined eluate was then subjected to cation-exchange chromatography using a MonoS 10/100 column (GE healthcare) and eluted with a linear gradient of NaCl. Fractions containing GRK5 were combined and run on a Superdex 200 10/300 GL column (GE healthcare). GRK5 was aliquoted, flash frozen, and stored at -80 ˚C until use.

Arrestin expression and purification

The parent construct for β-arrestin 1 (βarr1) is the long splice variant of human, cysteine-free (C59V, C125S, C140L, C150V, C242V, C251V, C269S) β-arrestin 1. This construct is modified with an N-terminal 6x Histidine tag, followed by a 3C protease site, a GG linker, AviTag and GGSGGS linker. The sequence was codon-optimized for expression in E. coli and cloned into a pET-15b vector. Point mutations were prepared using site-directed mutagenesis. β-arrestin 1 (1-382) was prepared by truncating β-arrestin 1 at residue 382. All arrestin constructs used were prepared as follows: NiCo21(DE3) competent E. coli (NEB) were transformed, and large-scale cultures were grown in TB + ampicillin at 37°C until an OD600 of 1.0. Cells were then transferred to room temperature and induced with 25 μM IPTG when the OD600 reached 2.0. Cells were harvested 20 h post induction and resuspended in lysis buffer [50 mM Hepes pH

7.4, 500 mM NaCl, 15% glycerol, 7.13 mM β-mercaptoethanol (BME)] to a final volume of 40 mL/L of cells. Cells were lysed by sonication and the clarified lysate applied to nickel sepharose and batch incubated for 1.5h at 4 °C. The resin was washed with 10 column volumes of wash buffer (20 mM HEPES pH 7.4, 500 mM NaCl, 10% glycerol, 7.13 mM BME) + 20 mM imidazole, followed by 10 column volumes of wash buffer + 40 mM imidazole. The protein was then eluted with 5 column volumes of wash buffer + 200mM imidazole and dialyzed overnight in 100x volume of dialysis buffer (20 mM Hepes 7.4, 200 mM NaCl, 2 mM BME, 10% glycerol) in the presence of 1:10 (w:w) of 3C protease. The digested protein was then subjected to reverse-Nickel purification and diluted with dialysis buffer containing no NaCl to bring the NaCl concentration to 75mM. The protein was then purified by ion exchange chromatography (mono Q 10/100 GL, GE Healthcare), followed by SEC using a Superdex 200 increase 10/300 GL column (GE Healthcare) with SEC buffer (20 mM HEPES pH 7.4, 300 mM NaCl, 10% glycerol). Purified protein was concentrated to between 100-300 μM using a 30 kDa spin concentrator and aliquots were flash-frozen in liquid nitrogen and stored at -80 °C until use.

Arrestin labeling and biotinylation

Following SEC, elution peak fractions were pooled to a concentration of 10-20 μM and labeled with fluorophore(s): monobromobimane (mBBr), Thermo Fisher Scientific M1378; N,N'-Dimethyl-N-(Iodoacetyl)-N'-(7-Nitrobenz-2-Oxa-1,3-Diazol-4-yl) Ethylenediamine (IANBD amide), Thermo Fisher Scientific D2004; or a 1:3 mixture of Alexa Fluor 488 C5 Maleimide, Thermo Fisher Scientific A10254, and Atto647N Maleimide, ATTO TEC AD647N-41, respectively. Fluorophores were dissolved to in DMSO and added at 10x molar excess over protein, then allowed to react for 1 h at room temperature prior to quenching with cysteine (10x

molar excess over fluorophore). The labeling reaction was further incubated for 10 minutes after cysteine addition, after which samples were spin filtered and subjected to a second round of size-exclusion chromatography, as detailed above, to remove free dye. The purified, was concentrated to between 100-300 μM using a 30 kDa spin concentrator and aliquots were flash-frozen in liquid nitrogen and stored at -80 °C until use. Arrestins (SEC-pure) were biotinylated using recombinant BirA enzyme, according to commercial protocols (Avidity), with exception that biotinylation was carried out for 12 h at 4 °C, rather than 30 °C. After biotinylation was complete, the reaction was flowed over 100 μL (packed) of nickel Sepharose, equilibrated in arrestin SEC buffer and supplemented with 10 mM imidazole, then washed with 200 μL of the equilibration buffer. The combined flow-through and wash fractions were then purified by size-exclusion as described above.

NTSR1 phosphorylation

NTSR1 (2.5 μM) was equilibrated in phosphorylation buffer (20 mM bis-tris propane (BTP) pH 7.5, 35 mM NaCl, 5 mM MgCl2, 20 μM NTS8-13, 20 μM C8-PI(4,5)P2, 0.05 mM TCEP, 0.002% MNG, 0.0002% CHS) at 25 °C with gentle mixing for 1 h. GRK5 was added to the reaction to a final concentration of 200 nM, and briefly incubated while the reaction was warmed from 25 °C to 30 °C. ATP was added to a final concentration of 1 mM. Upon completion, the reaction was supplemented with CaCl2 to a final concentration of 2 mM and applied to an equilibrated M1 FLAG immunoaffinity resin and washed with buffer containing 0.004% LMNG, 0.004% CHS, 20 mM HEPES pH 7.4, 100 mM NaCl, 0.2 μM NTS8-13, 2 mM CaCl2. The receptor was eluted with buffer containing 100 mM NaCl, 20 mM HEPES pH 7.4, 0.004% LMNG, 0.004% CHS, 0.2 μM NTS8-13, 0.2 mg/mL 1x FLAG peptide (DYKDDDDK), 5 mM EDTA), followed by SEC using

a Superdex 200 increase 10/300 GL column (GE Healthcare) with SEC buffer (20 mM HEPES pH 7.4, 100 mM NaCl, 0.004% LMNG, 0.0004% CHS).

Analytical fluorescence-detection size-exclusion chromatography

In a final volume of 20 µL, NTSR1 (4.5 µM), the respective arrestin construct (9 µM), NTS8-13 peptide (50 µM) and diC8-PI(4,5)P2 (5 µM) were incubated in buffer containing 20 mM HEPES pH 7.4, 100 mM NaCl, 0.004% LMNG, 0.0004% CHS and 0.2 µM NTS8-13. Using a Prominence-i LC autosampler (Shimadzu), 10 µL was injected onto a ENrich size-exclusion chromatography 650 10 × 300 column (Bio-rad) pre-equilibrated in 20 mM HEPES pH 7.4 100 mM NaCl, 0.004 % LMNG, 0.004% CHS and 0.2 µM NTS8-13, and run at a flow rate of 0.8 ml/min. Tryptophan fluorescence was monitored at λ(EX) of 280 nm and λ(EM) of 340 nm. Peaks in the obtained size-exclusion chromatograms were modeled as gaussians, deconvolved and quantified (AUC) using Magic Plot 3 (Magic Plot).

Surface plasmon resonance measurements

SPR experiments were performed using a GE Biacore T100 instrument. Approximately 300-400 resonance units (RU) of FPLC-purified biotinylated arrestin in HBS-P+ Buffer (GE Healthcare) were captured on an SA-chip (GE Healthcare), including a reference channel for online background subtraction of bulk solution refractive index and for evaluation of non-specific binding of analyte to the chip surface (Biacore T100 Control Software; GE Healthcare). All measurements were performed with 2-fold serial dilutions using 60 s association followed by a dissociation time of more than 240 s at 25 °C with a flow rate of at 30 µl min−1. Measurement of titrations at equilibrium were used to determine Kd values using Biacore Analysis Software (v.2.0.4, GE Healthcare) and fits to a total binding model were performed in GraphPad Prism 9.

Regeneration was performed by 2 injections of 2 M MgCl2 for 10 s at 50 µl min−1 flow rate. In all cases regeneration resulted in a complete return to baseline. Single cycle measurements were performed as described above. All single cycle measurements were performed as triplicates and quantifications calculated to the RUmax of the individual immobilized ligands (arrestin proteins).

Fluorescence anisotropy measurements

BODIPY-TMR phosphatidylinositol 4,5-bisphosphate (Echelon Biosciences) was dissolved to a stock concentration of 1 mM in 50 mM Hepes pH 7.4 and used at a final concentration of 4 nM in the assay. For the arrestin measurements, a two-fold dilution series of was made from a stock of βarr1 (1-382), yielding fourteen samples with final concentrations ranging from 150 µM to 0.02 µM. A control sample containing buffer only was included to measure the free anisotropy of BODIPY-PIP2. After mixing the BODIPY-PIP2 with arrestin or buffer, samples were incubated for 1h at room temperature prior to measurements. Samples were measured in five 20 µL replicates in a 384-well plate on a Tecan Infinite M1000 (Tecan Life Sciences), using an excitation wavelength of 530 nm, an emission wavelength of 573 nm and bandwidths of 5 nm. The obtained data was fit using to a one-site total binding model $Y = Bottom + (top - bottom)/1 + 10^{HS*log(EC50-X)}$ where HS denotes the hill-slope.

Bulk fluorescence measurements

Bulk fluorescence measurements were performed on either a Fluorolog instrument (Horiba) using FluorEssence v3.8 software and operating in photon-counting mode, or a Tecan Infinite M1000 PRO multimodal microplate reader (Tecan). Fluorolog measurements of bimane-labeled βarr1 constructs (NTSR1 experiments) were performed at final concentration of 0.4 µM

[arrestin] in buffer containing 20 mM HEPES pH 7.4, 100 mM NaCl and 0.004% LMNG (w/v)/0.0004% CHS (w/v) supplemented with 4 μM NTS (8-13). For NTSR1 experiments the following concentrations were used: 4 μM NTSR1, 4.1 μM diC8-PI(4,5)P2, 50 μM V2Rpp (depending on condition). Samples were incubated for 1 h in the dark before measurement. Fluorescence data were collected in a quartz cuvette with 135 mL of sample. Bimane fluorescence was measured by excitation at 370 nm with excitation and emission bandwidth passes of 3 nm, and emission spectra were recorded from 400 to 550 nm in 2 nm increments with 0.1 s integration time. Care was taken to extensively rinse and argon-dry the cuvette between individual measurements. To remove background fluorescence, buffer spectra were collected using the same settings, and subtracted from each sample spectrum.

FRET measurements of AF488-AT647N-labeled βarr1 constructs were performed as described for bimane measurements, with the following differences: samples were excited at 476 nm with 3 nm excitation and 4 nm emission slit widths. Spectra were collected from 485 nm to 750 nm in 1 nm increments with 0.1 s integration time. FRET measurements in the absence of NTSR1 were performed in buffer containing 20 mM HEPES pH 7.4, 100 mM NaCl and 0.004% LMNG (w/v)/0.0004% CHS (no NTS). FRET measurements with NTSR1 were done with 0.5 μM NTSR1 and 0.5 μM diC8-PI(4,5)P2.

NBD spectra measured on the Tecan Infinite M1000 PRO were collected using 384- or 96-well (1/2 area) flat black Greiner plates with 50 or 100 μL of sample, respectively, at a final concentration of 0.5 μM βarr1 in buffer containing 20 mM HEPES pH 7.4, 100 mM NaCl and 0.004% LMNG (w/v)/0.0004% CHS. For NBD the following instrument settings were used: excitation: 490 nm, emission 510-580 nm (1 nm steps) with 20 s read time and 400 Hz flash

mode. Gain and z-position were optimized prior to reading. Bimane spectra were collected in white plates using the following instrument settings: excitation: 370 nm, emission 420-500 nm (1 nm steps) with 20 s read time and 400 Hz flash mode. Efret values for FRET experiments were calculated as $Efret = A$ and normalized to donor (D+A) intensity within a given experiment. Scaled FRET values (apo = 100, min (FRET) = 0) were fit to a single exponential decay function $Y = (Y0 - NS) * e{-}K{*}x + NS$ using the nls function in R for EC50 values (obtained as t1/2 for decay). NS denotes concentration-dependent non-specific signal. L167W-293NBD was fit using the same function. L68bim data was fit to a total binding model $Y = Bmax * X + NS * X + background$, where background is a constant value. Fitting was (Kd+X) independently performed both in R and with GraphPad Prism 9 for corroboration, values reported are from Prism 9.

3.6 References

Baidya, M., et al. (2020). Key phosphorylation sites in GPCRs orchestrate the contribution of β-Arrestin 1 in ERK1/2 activation. *EMBO Rep. 21*(9): e49886. 10.15252/embr.201949886

Baidya, M., et al. (2020). Genetically encoded intrabody sensors report the interaction and trafficking of β-arrestin 1 upon activation of G-protein–coupled receptors. *J. Biol. Chem. 295*(30): 10153-10167. 10.1074/jbc.RA120.013470

Beyett, T. S., et al. (2019). Perturbation of the interactions of calmodulin with GRK5 using a natural product chemical probe. *Proc. Natl. Acad. Sci. U. S. A. 116*(32): 15895-15900. 10.1073/pnas.1818547116

Cahill, T. J., et al. (2017). Distinct conformations of GPCR–β-arrestin complexes mediate desensitization, signaling, and endocytosis. *Proc. Natl. Acad. Sci. U. S. A. 114*(10): 2562-2567. 10.1073/pnas.1701529114

Chen, Q., et al. (2018). Structural Basis of Arrestin-Dependent Signal Transduction. *Trends Biochem. Sci. 43*(6): 412-423. 10.1016/j.tibs.2018.03.005

Chen, Q., et al. (2017). Structural basis of arrestin-3 activation and signaling. *Nat. Commun. 8*(1): 1427. 10.1038/s41467-017-01218-8

Chen, Q., et al. (2021). An Eight Amino Acid Segment Controls Oligomerization and Preferred Conformation of the two Non-visual Arrestins. *J. Mol. Biol. 433*(4): 166790. 10.1016/j.jmb.2020.166790

De Matteis, M. A. and A. Godi (2004). PI-loting membrane traffic. *Nat. Cell Biol. 6*(6): 487-492. 10.1038/ncb0604-487

DeFea, K. A., et al. (2000). β-Arrestin–Dependent Endocytosis of Proteinase-Activated Receptor 2 Is Required for Intracellular Targeting of Activated Erk1/2. *J. Cell Biol. 148*(6): 1267-1282. 10.1083/jcb.148.6.1267

Dery, O., et al. (1999). Trafficking of proteinase-activated receptor-2 and β-arrestin-1 tagged with green fluorescent protein: β-arrestin-dependent endocytosis of a proteinase receptor. *J. Biol. Chem. 274*(26): 18524-18535.

Di Paolo, G. and P. De Camilli (2006). Phosphoinositides in cell regulation and membrane dynamics. *Nature 443*(7112): 651-657. 10.1038/nature05185

Dixon, A. S., et al. (2016). NanoLuc Complementation Reporter Optimized for Accurate Measurement of Protein Interactions in Cells. *ACS Chem. Biol. 11*(2): 400-408. 10.1021/acschembio.5b00753

Eichel, K., et al. (2018). Catalytic activation of β-arrestin by GPCRs. *Nature 557*(7705): 381-386. 10.1038/s41586-018-0079-1

Eichel, K., et al. (2016). β-Arrestin drives MAP kinase signalling from clathrin-coated structures after GPCR dissociation. *Nat. Cell Biol. 18*(3): 303-310. 10.1038/ncb3307

Feinstein, T. N., et al. (2011). Retromer terminates the generation of cAMP by internalized PTH receptors. *Nat. Chem. Biol. 7*(5): 278-284. 10.1038/nchembio.545

Feinstein, T. N., et al. (2013). Noncanonical control of vasopressin receptor type 2 signaling by retromer and arrestin. *J. Biol. Chem. 288*(39): 27849-27860. 10.1074/jbc.M112.445098

Ferrandon, S., et al. (2009). Sustained cyclic AMP production by parathyroid hormone receptor endocytosis. *Nat. Chem. Biol. 5*(10): 734-742. 10.1038/nchembio.206

Gaidarov, I., et al. (1999). Arrestin function in G protein-coupled receptor endocytosis requires phosphoinositide binding. *EMBO J. 18*(4): 871-881. 10.1093/emboj/18.4.871

Ghosh, E., et al. (2019). Conformational Sensors and Domain Swapping Reveal Structural and Functional Differences between β-Arrestin Isoforms. *Cell Rep. 28*(13): 3287-3299.e3286. 10.1016/j.celrep.2019.08.053

Grundmann, M., et al. (2018). Lack of beta-arrestin signaling in the absence of active G proteins. *Nat. Commun. 9*(1): 341. 10.1038/s41467-017-02661-3

Hanyaloglu, A. C. and M. von Zastrow (2008). Regulation of GPCRs by endocytic membrane trafficking and its potential implications. *Annu. Rev. Pharmacol. Toxicol. 48*: 537-568. 10.1146/annurev.pharmtox.48.113006.094830

Hasegawa, J., et al. (2017). PI5P and PI(3,5)P2: Minor, but essential phosphoinositides. *Cell Struct. Funct. 42*(1): 49-60. 10.1247/csf.17003

Huang, W., et al. (2020). Structure of the neurotensin receptor 1 in complex with β-arrestin 1. *Nature 579*(7798): 303-308. 10.1038/s41586-020-1953-1

Innamorati, G., et al. (1998). Transient phosphorylation of the V1a vasopressin receptor. *J. Biol. Chem. 273*(12): 7155-7161. 10.1074/jbc.273.12.7155

Innamorati, G., et al. (1998). A serine cluster prevents recycling of the V2 vasopressin receptor. *Proc. Natl. Acad. Sci. U. S. A. 95*(5): 2222-2226. 10.1073/pnas.95.5.2222

Inoue, A., et al. (2019). Illuminating G-Protein-Coupling Selectivity of GPCRs. *Cell 177*(7): 1933-1947.e1925. 10.1016/j.cell.2019.04.044

Irannejad, R., et al. (2013). Conformational biosensors reveal GPCR signalling from endosomes. *Nature 495*(7442): 534-538. 10.1038/nature12000

Irannejad, R., et al. (2015). Effects of endocytosis on receptor-mediated signaling. *Curr. Opin. Cell Biol. 35*: 137-143. 10.1016/j.ceb.2015.05.005

Just, S., et al. (2013). Differentiation of opioid drug effects by hierarchical multi-site phosphorylation. *Mol. Pharmacol. 83*(3): 633-639. 10.1124/mol.112.082875

Kadlecova, Z., et al. (2017). Regulation of clathrin-mediated endocytosis by hierarchical allosteric activation of AP2. *J. Cell Biol. 216*(1): 167-179. 10.1083/jcb.201608071

Khoury, E., et al. (2014). Differential regulation of endosomal GPCR/β-arrestin complexes and trafficking by MAPK. *J. Biol. Chem. 289*(34): 23302-23317. 10.1074/jbc.M114.568147

Kim, M., et al. (2012). Conformation of receptor-bound visual arrestin. *Proc. Natl. Acad. Sci. U. S. A. 109*(45): 18407-18412. 10.1073/pnas.1216304109

Kim, Y. J., et al. (2013). Crystal structure of pre-activated arrestin p44. *Nature 497*(7447): 142-146. 10.1038/nature12133

Komolov, K. E. and J. L. Benovic (2018). G protein-coupled receptor kinases: Past, present and future. *Cell. Signal. 41*: 17-24. 10.1016/j.cellsig.2017.07.004

Krueger, K. M., et al. (1997). The role of sequestration in G protein-coupled receptor resensitization: regulation of β2-adrenergic receptor dephosphorylation by vesicular acidification. *J. Biol. Chem. 272*(1): 5-8.

Kumari, P., et al. (2016). Functional competence of a partially engaged GPCR–β-arrestin complex. *Nat. Commun. 7*(1): 1-16. 10.1038/ncomms13416

Kumari, P., et al. (2017). Core engagement with β-arrestin is dispensable for agonist-induced vasopressin receptor endocytosis and ERK activation. *Mol. Biol. Cell 28*(8): 1003-1010. 10.1091/mbc.E16-12-0818

Latorraca, N. R., et al. (2020). How GPCR Phosphorylation Patterns Orchestrate Arrestin-Mediated Signaling. *Cell 183*(7): 1813-1825.e1818. 10.1016/j.cell.2020.11.014

Latorraca, N. R., et al. (2018). Molecular mechanism of GPCR-mediated arrestin activation. *Nature 557*(7705): 452-456. 10.1038/s41586-018-0077-3

Lee, M.-H., et al. (2016). The conformational signature of β-arrestin2 predicts its trafficking and signalling functions. *Nature 531*(7596): 665-668. 10.1038/nature17154

Lee, Y., et al. (2020). Molecular basis of β-arrestin coupling to formoterol-bound β1-adrenoceptor. *Nature 583*(7818): 862-866. 10.1038/s41586-020-2419-1

Lobingier, B. T. and M. von Zastrow (2019). When trafficking and signaling mix: How subcellular location shapes G protein-coupled receptor activation of heterotrimeric G proteins. *Traffic 20*(2): 130-136. 10.1111/tra.12634

Luttrell, L. M., et al. (2018). Manifold roles of β-arrestins in GPCR signaling elucidated with siRNA and CRISPR/Cas9. *Sci. Signal. 11*(549). 10.1126/scisignal.aat7650

Martínez-Morales, J. C., et al. (2018). S1P1 receptor phosphorylation, internalization, and interaction with Rab proteins: effects of sphingosine 1-phosphate, FTY720-P, phorbol esters, and paroxetine. *Biosci. Rep. 38*(6). 10.1042/BSR20181612

Milano, S. K., et al. (2006). Nonvisual arrestin oligomerization and cellular localization are regulated by inositol hexakisphosphate binding. *J. Biol. Chem. 281*(14): 9812-9823. 10.1074/jbc.M512703200

Nakagawa, T. and M. Asahi (2013). β1-adrenergic receptor recycles via a membranous organelle, recycling endosome, by binding with sorting nexin27. *J. Membr. Biol. 246*(7): 571-579. 10.1007/s00232-013-9571-6

Namkung, Y., et al. (2016). Monitoring G protein-coupled receptor and β-arrestin trafficking in live cells using enhanced bystander BRET. *Nat. Commun. 7*: 12178. 10.1038/ncomms12178

Nguyen, A. H., et al. (2019). Structure of an endosomal signaling GPCR–G protein–β-arrestin megacomplex. *Nat. Struct. Mol. Biol. 26*(12): 1123-1131. 10.1038/s41594-019-0330-y

Nuber, S., et al. (2016). β-Arrestin biosensors reveal a rapid, receptor-dependent activation/deactivation cycle. *Nature 531*(7596): 661-664. 10.1038/nature17198

O'Hayre, M., et al. (2017). Genetic evidence that β-arrestins are dispensable for the initiation of β2-adrenergic receptor signaling to ERK. *Sci. Signal. 10*(484). 10.1126/scisignal.aal3395

Oakley, R. H., et al. (1999). Association of β-arrestin with G protein-coupled receptors during clathrin-mediated endocytosis dictates the profile of receptor resensitization. *J. Biol. Chem. 274*(45): 32248-32257.

Oakley, R. H., et al. (2001). Molecular determinants underlying the formation of stable intracellular G protein-coupled receptor-β-arrestin complexes after receptor endocytosis. *J. Biol. Chem. 276*(22): 19452-19460.

Oakley, R. H., et al. (2000). Differential affinities of visual arrestin, βarrestin1, and βarrestin2 for G protein-coupled receptors delineate two major classes of receptors. *J. Biol. Chem. 275*(22): 17201-17210.

Pakharukova, N., et al. (2020). Allosteric activation of proto-oncogene kinase Src by GPCR-beta-arrestin complexes. *J. Biol. Chem. 295*(49): 16773-16784. 10.1074/jbc.RA120.015400

Perkovska, S., et al. (2018). V1b vasopressin receptor trafficking and signaling: Role of arrestins, G proteins and Src kinase. *Traffic 19*(1): 58-82. 10.1111/tra.12535

Rajagopal, S. and S. K. Shenoy (2018). GPCR desensitization: Acute and prolonged phases. *Cell. Signal. 41*: 9-16. 10.1016/j.cellsig.2017.01.024

Ranjan, R., et al. (2017). Novel Structural Insights into GPCR–β-Arrestin Interaction and Signaling. *Trends Cell Biol. 27*(11): 851-862. 10.1016/j.tcb.2017.05.008

Reiter, E., et al. (2012). Molecular mechanism of β-arrestin-biased agonism at seven-transmembrane receptors. *Annu. Rev. Pharmacol. Toxicol. 52*: 179-197. 10.1146/annurev.pharmtox.010909.105800

Sente, A., et al. (2018). Molecular mechanism of modulating arrestin conformation by GPCR phosphorylation. *Nat. Struct. Mol. Biol. 25*(6): 538-545. 10.1038/s41594-018-0071-3

Shukla, A. K., et al. (2013). Structure of active β-arrestin-1 bound to a G-protein-coupled receptor phosphopeptide. *Nature 497*(7447): 137-141. 10.1038/nature12120

Shukla, A. K., et al. (2014). Visualization of arrestin recruitment by a G-protein-coupled receptor. *Nature 512*(7513): 218-222. 10.1038/nature13430

Sommer, M. E., et al. (2005). Dynamics of arrestin-rhodopsin interactions: arrestin and retinal release are directly linked events. *J. Biol. Chem. 280*(8): 6861-6871. 10.1074/jbc.M411341200

Sommer, M. E., et al. (2006). Dynamics of arrestin-rhodopsin interactions: acidic phospholipids enable binding of arrestin to purified rhodopsin in detergent. *J. Biol. Chem. 281*(14): 9407-9417. 10.1074/jbc.M510037200

Song, W., et al. (2019). State-dependent Lipid Interactions with the A2a Receptor Revealed by MD Simulations Using In Vivo-Mimetic Membranes. *Structure 27*(2): 392-403.e393. 10.1016/j.str.2018.10.024

Song, X., et al. (2009). How does arrestin assemble MAPKs into a signaling complex? *J. Biol. Chem. 284*(1): 685-695. 10.1074/jbc.M806124200

Staus, D. P., et al. (2020). Structure of the M2 muscarinic receptor–β-arrestin complex in a lipid nanodisc. *Nature 579*(7798): 297-302. 10.1038/s41586-020-1954-0

Staus, D. P., et al. (2018). Sortase ligation enables homogeneous GPCR phosphorylation to reveal diversity in β-arrestin coupling. *Proc. Natl. Acad. Sci. U. S. A. 115*(15): 3834-3839. 10.1073/pnas.1722336115

Sun, Y., et al. (2007). PtdIns(4,5)P2 turnover is required for multiple stages during clathrin- and actin-dependent endocytic internalization. *J. Cell Biol. 177*(2): 355-367. 10.1083/jcb.200611011

Tewson, P. H., et al. (2016). New DAG and cAMP Sensors Optimized for Live-Cell Assays in Automated Laboratories. *J. Biomol. Screen. 21*(3): 298-305. 10.1177/1087057115618608

Thomsen, A. R. B., et al. (2016). GPCR-G Protein-β-Arrestin Super-Complex Mediates Sustained G Protein Signaling. *Cell 166*(4): 907-919. 10.1016/j.cell.2016.07.004

Tóth, D. J., et al. (2012). Acute depletion of plasma membrane phosphatidylinositol 4,5-bisphosphate impairs specific steps in endocytosis of the G-protein-coupled receptor. *J. Cell Sci. 125*(Pt 9): 2185-2197. 10.1242/jcs.097279

Trapaidze, N., et al. (2000). Recycling and resensitization of delta opioid receptors. *DNA Cell Biol. 19*(4): 195-204. 10.1089/104454900314465

Yen, H.-Y., et al. (2018). PtdIns(4,5)P2 stabilizes active states of GPCRs and enhances selectivity of G-protein coupling. *Nature 559*(7714): 423-427. 10.1038/s41586-018-0325-6

Yin, W., et al. (2019). A complex structure of arrestin-2 bound to a G protein-coupled receptor. *Cell Res. 29*(12): 971-983. 10.1038/s41422-019-0256-2

Zhang, J., et al. (1999). Cellular trafficking of G protein-coupled receptor/β-arrestin endocytic complexes. *J. Biol. Chem. 274*(16): 10999-11006.

Zhuang, T., et al. (2010). Elucidation of inositol hexaphosphate and heparin interaction sites and conformational changes in arrestin-1 by solution nuclear magnetic resonance. *Biochemistry 49*(49): 10473-10485. 10.1021/bi101596g

Zhuo, Y., et al. (2014). Identification of receptor binding-induced conformational changes in non-visual arrestins. *J. Biol. Chem. 289*(30): 20991-21002. 10.1074/jbc.M114.560680

3.7 Figures

Figure 3.1 Arrestin phosphoinositide binding is required for recruitment to some GPCRs

A) Cartoon depicting NanoBiT assay for measuring arrestin plasma membrane recruitment upon agonist stimulation. Upon complementation SmBiT and LgBiT form a functional NanoLuc luciferase. In key, “phosphate” denotes phosphorylated Ser/Thr residues and “X” denotes KRK to 3Q mutant of β-arrestin. B) Two representative GPCRs, β1AR and NTSR1 illustrate data obtained for β-arrestin recruitment by NanoBiT assay shown in panel A. Data were collected over time after agonist addition (t=0 min), and values are shown as luminescence fold-change (over vehicle treatment) ± standard deviation (measured as 2 technical replicates for each of n=3 independent experiments). Colors denote concentrations of agonist used for stimulation. Agonists used were isoproterenol for β1AR and neurotensin for NTSR1. Grey boxes mark the time region (10-15 minutes post agonist addition) over which luminescence is integrated, for each concentration of agonist, to produce concentration response curves (bottom). WT and 3Q amplitudes were determined as the difference of fitted pre- and post-transition plateaus. C) Plot of LOF values for panel of tested GPCRs. Points represent LOF value obtained as ratio of WT and 3Q recruitment, and error bars reflect error in LOF derived from standard errors of fits (see methods). Dashed ellipses denote clusters obtained from k means clustering of data (see methods); AT1R is in cluster 2 for both βarr1/2, while β2AR-V2C is split with βarr1 (cluster2) and βarr2 (cluster 1). Vertical gray lines denote LOF=0 and LOF=1; vertical purple and orange lines reflect the centers of the respective cluster from k means and correspond to LOF =0.06 and LOF = 0.73, respectively.

Figure 3.2 Receptor phosphorylation patterns govern PIP-dependence for arrestin recruitment.

A) Left, schematic of human NTSR1 showing motifs in receptor ICL3 and C-terminus that are subject to phosphorylation. Phosphorylation sites examined in this study are shown in red and numbered 1-10 (above). Residue numbers corresponding to the region of human NTSR1 are listed at the start and end of the shown sequences. Construct key shows possible phosphosites as empty boxes, which when mutated to alanine are filled with an "X". Plasma membrane recruitment of arrestin upon stimulation of cells expressing different NTSR1 constructs, measured using the NanoBiT assay described in Figure 3.1. Right, points represent LOF value obtained as ratio of WT and 3Q recruitment, and error bars represent standard error of fits (see methods). Points are colored based on cluster designation obtained from k means clustering of all receptor-arrestin recruitment data. B) Translocation of βarr1 to endosomes upon stimulation of cells expressing different NTSR1 constructs, measured using an endosome bystander NanoBiT assay, as described in Figure S3.1. Points represent recruitment (fold chance over basal upon stimulation) for WT and 3Q recruitment, denoted by circles and triangles, respectively. Points are based on data from n=3 biological experiments. Error bars represent standard error of fit used to determine recruitment. Points are colored based on the cluster assignment of that mutant. C) Internalization, measured by loss of cell-surface receptors upon agonist stimulation, for Δβarr1/2 cells expressing NTSR1 or β2AR constructs and transfected with arrestin constructs indicated. Values represent independent experiments (n = 5-10). Internalization by 3Q βarr1 and mock were compared to WT using a two-tailed paired t-test. ns: $p > 0.05$; *: $p \leq 0.05$; **: $p \leq 0.01$; ***: $p \leq 0.001$; ****: $p \leq 0.0001$

Figure 3.3 Lipid binding stabilizes core-engaged arrestin complexes.

A) cartoon of complexing efficiency assay. Size-exclusion chromatography (SEC) resolves complex from components. B) Representative experiment showing SEC chromatograms with vertical dashed lines indicating free NTSR1, complex, and free arrestins. C) Complexing efficiency, for NTSR1 with indicated arrestins. Boxplots: center line, median; box range, 25–75th percentiles; whiskers denote minimum–maximum values. Individual points are shown (n=6 independent experiments). Two-tailed unpaired t-test used to compare conditions. ns: $p > 0.05$; ****: $p \leq 0.0001$. D) Cartoon showing equilibrium of NTSR1-arrestin complex. Pink star denotes L68bim probe used for experiment shown in panel E. E) Bimane spectra for L68bim labeled βarr1 in complex with NTSR1. All NTSR1 samples contained diC8-PI(4,5)P2 (4.1μM) Boxplots: center line, median; box range, 25–75th percentiles; whiskers denote minimum–maximum values. Individual points are shown (n=3 independent experiments). V2Rpp-NTSR1 (GRK5p) and V2Rpp-NTSR1 (unphos) + V2Rpp were compared by two-tailed unpaired t-test. ns: $p > 0.05$; *: $p \leq 0.05$. Apo indicates free arrestin; unphos indicates unphosphorylated receptor and GRK5p indicates GRK5-in vitro phosphorylated receptor. Spectra are normalized to apo (100%) within each experiment and the fluorescence intensity at lambda max was used as the value. F) Free energy diagram illustrating how PIP-binding, by stabilizing the core-engaged state of the NTSR1-arrestin complex slows arrestin dissociation. Loss of the PIP-binding element of arrestin destabilizes the core-engaged state, shifting equilibrium towards the tail-engaged state leading to a higher degree of complex disassembly. Removal of the arrestin C-terminus stabilizes the complex in the tail-engaged state and reduces disassembly even when core-engaged complex is destabilized by lack of PIP-binding.

Figure 3.4 PIP_2 alone promotes conformational changes in arrestin, including C-movement, but not release.

A) overlay of inactive (PDB: 1G4M) [grey] and active (PDB: 4JQI) [black] βarr1. The N and C lobes of βarr1 are indicated. Activation leads to reorganization of several loops, and the gate loop and finger loop are highlighted. Re-orientation of these loops from inactive (yellow) to active (green) can be monitored by site-specific fluorescence spectroscopy. In finger loop inset the sphere denotes Ca L68C which is labeled with bim. In gate loop inset, the sphere denotes Ca L293C which is labeled with NBD. An installed W residue replacing L167 dynamically quenches 293NBD. B) Spectra of bimane labeled (L68C) βarr1 in response to V2Rpp andPIP2. Arrow indicates direction of spectral shift with increasing concentration. Values are mean ± SD (n=3 independent experiments). Spectra were normalized to the apo condition within a given experiment. C) Spectra of NBD labeled (L167W-L293C) βarr1 in response to V2Rpp andPIP2. Arrow indicates direction of spectral shift with increasing concentration. Values are mean ± SD (n=3 independent experiments). Spectra were normalized to the apo condition within a given experiment. D) Left, cartoon showing how FRET change is release. Right, spectra of AF488/AT647N labeled (A12C-V387C) βarr1 in linked to C-terminus response to V2Rpp andPIP2. Arrow indicates direction of spectral shift with increasing concentration. Spectra were normalized via donor intensity within a given experiment. Data shown are for a representative experiment (n=3 independent experiments).

Figure 3.5 PIP_2 enhances Fab30 binding to βarr1.

A) Cartoon of surface plasmon resonance (SPR) experiments, where βarr1 is immobilized via N-terminal biotinylation and a Fab30 binder is injected in the presence of absence ofPIP2 or V2Rpp. B) Representative sensogram for SPR binding experiment. With WT βarr1 immobilized, Fab30 (1 μM) was injected alone or together with V2Rpp (40 μM) or diC8-PI(4,5)P2 (40 μM). The shown sensogram is representative of the outcome seen for independent experiments (n=3). Dissociation/regeneration phase not shown. C) Binding of Fab30 to immobilized arrestin constructs in the presence of different additives. Maximum binding is defined based on normalization of the observed response to the amount of arrestin immobilized for each construct. Additives: diC8-PG (40M), diC8-PI(3)P (40M), diC8-PI(4,5)P2 (40 μM) and V2Rpp (40 μM) were mixed with Fab30 (1 μM) and injected together. Points reflect independent measurements; open points represent the binding observed for the additive in the absence of Fab30. Fab30 binding was compared using a two-tailed unpaired t-test. ns: $p > 0.05$; *: $p \leq 0.05$; **: $p \leq 0.01$; ***: $p \leq 0.001$. D) The proportion of active-like βarr1 increases in the presence of PIP2.

Figure 3.6 Model for phosphoinositide regulation of GPCR-β-arrestin complex assembly and disassembly.

GPCRs stratify into two groups with respect to the strength of their interaction with β-arrestins: one group requires an interaction between β-arrestin and PIP2 at the plasma membrane for recruitment (PIP-dependent), while the other does not (PIP-independent). In the case of PIP-dependent GPCRs, arrestin engagement is unstable and can result in dissociation of arrestin from the receptor, while maintaining an association with the plasma membrane (left panel). PIP2 is enriched at CCSs and in both cases complex assembly can occur. During endocytosis, PIP2 is depleted and for PIP-dependent GPCRs, the loss of this PIP2 contact may facilitate dissociation of arrestin thereby allowing for receptor recycling. In contrast, a PIP independent GPCR will retain the interaction with arrestin even onceis depleted owing to the strong phosphorylation-dependent interactions; however, the fully-engaged state of the complex is less stable in endosomes than at the plasma membrane, thereby allowing further G protein engagement to occur.

Supplementary Figure 3.1 Arrestin phosphoinositide binding is required for plasma membrane recruitment to some GPCRs.

A) cAMP response in HEK293 cells devoid of β-arrestins upon stimulation of endogenous β2AR with 100 nM isoproterenol (iso). Clone 1 (CL1) and Clone 2 (CL2) are independent βarr1/2 knock-out cell lines (O'Hayre et al.). Data are normalized to response with Forskolin (Fsk)/3-isobutyl-1-methylxanthine (IBMX) and show mean with 95% confidence intervals (n=3 independent experiments). Two-way analysis of variance (ANOVA), Tukey's multiple comparison test. For CL2 * denotes $p < 0.05$ for WT vs. mApple over the interval of 17-32 minutes, while 3Q vs. mApple was not significant. For CL1 * denotes $p < 0.05$ for WT vs. mApple over the interval of 19-29 minutes, while 3Q vs. mApple was not significant. B) Quantification of expression for βarr1 and βarr2 (both WT and 3Q) NanoBiT constructs, as determined by western blot (Supplementary data figure 3.2). Mean values of 3-4 independent experiments were compared by a two-tailed unpaired t-test, where ns denotes $p > 0.05$, * $P \leq 0.05$. Boxplots: center line, median; box range, 25–75th percentiles; whiskers denote minimum– maximum values. Individual points are shown. C) LOF is only weakly correlated with recruitment of WT β-arrestins. Data are mean LOF and mean WT βarr1/2 recruitment. βarr1 recruitment is shown as circles and βarr2 recruitment is shown as triangles. Data are colored based on assigned cluster. Dashed line shows expected linear relationship and R is the Pearson coefficient, with -0.51 reflecting a weak negative correlation. D) Plot of LOF data for plasma membrane bystander (CAAX) vs. LOF for direct recruitment. βarr1 recruitment is shown as circles and βarr2 recruitment is shown as triangles. Data are colored based on assigned cluster. Dashed line shows expected linear relationship and R is the Pearson coefficient, with 0.88 reflecting a very strong positive correlation. E) NanoBiT assay for measuring endosome translocation of βarr1. Cartoon of endosome bystander assay (left). βarr1 endosome

recruitment data (right) with dashed ellipses to indicate clusters based on CAAX data. β-arrestin endosome recruitment determined by span of luminescence fold change. Data are mean SEM (n=3 independent experiments). Dashed line indicates three times the maximum signal measured in mock (receptor) transfected cells.

Supplementary Figure 3.2 Loss of PIP binding slows β-arrestin recruitment to cluster 2 GPCRs.

A) initial rate (0-5 minutes post-agonist stimulation) expressed as luminescence fold-change (FC)/min. Data from n=3 independent experiments fit independently (see methods). Boxplots: center line, median; box range, 25–75th percentiles; whiskers denote minimum–maximum values. For each receptor, and for each βarr1 and βarr2 WT and 3Q were compared by a two-tailed unpaired t-test, where ns denotes $p > 0.05$, * $P \leq 0.05$, ** $P \leq 0.01$, **** $P \leq 0.0001$. B) Data from A) expressed as a difference in rate shows that except for βarr1-TACR1 all cluster 2 receptors show faster recruitment of WT β-arrestin1/2 than corresponding 3Q mutant. Data are mean SEM (n=3 independent experiments).

Supplementary Figure 3.3 Arrestin recruitment to NTSR1 mutants can be measured by NanoBiT recruitment assay.

A) Expression of NTSR1 constructs in HEK293A cells used for NanoBiT assays. Boxplots: center line, median; box range, 25–75th percentiles; whiskers denote minimum–maximum values. Individual points are shown. Values are mean, relative to NTSR1-WT (n=4 independent experiments). For each construct, a comparison to NTSR1-WT by a two-tailed unpaired Wilcoxon test was performed, where ns denotes $p > 0.05$, * $P \leq 0.05$. B) Direct complementation NanoBiT assay Emax for Sm-βarr1 interaction with Lg-CAAX for cells expressing NTSR1-WT as a function of mean fluorescence intensity (MFI), as determined by cell-surface staining. Amount of NTSR1- WT DNA transfected is written; blue arrow denotes 200 ng, the amount used in recruitment assays in Figure 3.2C) As B, except the pEC50 of recruitment response upon NTS stimulation is plotted vs. MFI, instead of Emax. In both B and C, points represent mean values and error bars indicate 95% CI (n=3 independent experiments).

Supplementary Figure 3.4 PIP binding stabilizes core-engaged arrestin complexes.

A) LOF in complexing efficiency as determined by SEC. A) LOF = 1 corresponds to complete loss of complex formation, while LOF = 0 corresponds to no difference in complexing efficiency between WT and 3Q βarr1 (n=5 independent experiments). Boxplots: center line, median; box range, 25–75th percentiles; whiskers denote minimum–maximum values. Individual points are shown. compared by a two- tailed unpaired t-test, where **** $P \leq 0.0001$. B) Binding of BODIPY-TMR PI(4,5)P2 to βarr1 (1- 382) protein (WT or 3Q). Points are mean and error bars reflect 95% CI (n=5 independent experiments). Data were fit to a logistical function as described in methods and best fit values for Bmax and Kd are provided with 95% CI in parentheses. C) Structure of transition from inactive (PDB: 1G4M) to active (PDB: 4JQI) βarr1 involves displacement of the βarr1 C-terminus (dark grey) by V2Rpp (blue). Two cysteine residues were added to a cys-less βarr1 background at positions A12 and V387 (pink spheres). These positions were labeled with fluorophores that, through FRET, allow for monitoring the position of the C-terminus. D) When labeled with a FRET pair, βarr1-12C/387C shows a high-FRET state in the absence of V2Rpp, and a low-FRET state when the βarr1 C-terminus is displaced by V2Rpp. FRET measured when βarr1 (WT or 3Q)- 12C/387C-AF488-AT647N is bound to V2Rpp (0.5 μM), NTSR1 (GRK5p, 0.5 μM), or NTSR1 (unphosphorylated, 0.5 μM) +V2Rpp (0.5 μM). All samples containing NTSR1 were supplemented with diC8-PI(4,5)P2 (0.5 μM). Apo βarr1 (WT or 3Q)-12C/387C-AF488-AT647N was normalized to 1.0 and βarr1 (WT or 3Q)-12C/387C-AF488-AT647N + V2Rpp (10 μM) was normalized 0.0 for each experiment (n=3 independent measurements) (right). Boxplots: center line, median; box range, 25–75th percentiles; whiskers denote minimum–maximum values. Individual points are shown.

Supplementary Figure 3.5 PIP2 allosterically triggers movement of the arrestin C-tail, but not release.

A-B) Finger loop (L68C-bim) responses. % apo is scaled such that the fluorescence intensity (at Bmax) for apo arrestin is 100% and each condition is scaled as a factor of apo. ND denotes not determined values. Values for Bmax (max response) and Kd (based on single-site binding fitting) are provided and ranges in parentheses correspond to 95% CI. Points are mean and error bars reflect 95% CI (n=3 independent experiments). C-D) Gate loop (L167W-293C-NBD) responses. % apo is scaled such that the fluorescence intensity (at Bmax) for apo arrestin is 100% and each condition is scaled as a factor of apo. Values for EC50 (half maximal response) and k (rate constant based on single exponential decay) are provided and ranges in parentheses correspond to 95% CI. Points are mean and error bars reflect 95% CI (n=3 independent experiments). E-F) C-terminus release (A12C-V387C-AF488-AT647N) responses. %FRET is scaled such that apo arrestin is 100% and the highest concentration of V2Rpp (100 μM) is 0%. INF denotes infinite upper bound. ND denotes not determined values. Range of EC50 values is indicated in parentheses and represents 95% CI. Points represent mean and error bars reflect 95% CI (n=3 independent experiments).

Supplementary Figure 3.6 Plasma membrane PIPs promote conformational changes in arrestin.

A) Structure of soluble lipid derivatives examined in this work. B-I) Concentration response curves for L68bim βarr1. Values for Bmax (max response) and EC50 (based on single-site binding fitting) are provided and ranges in parentheses correspond to 95% CI. Points are mean and error bars reflect 95% CI (n=3 independent experiments). ND denotes not determined values. J) Summary of effect size (Bmax) for different lipids with L68bim βarr1. Values represent Bmax obtained from fitting independent experiments. ND is used for PG and PI(3)P as data could not be fit. Bars represent mean Bmax and error bars denote standard deviation across the fits. K) A PI(4,5)P2 derivative bound in the C-terminal domain of βarr1 (PDB: 6UP7). The side chain of K232 was modeled based on PDB: 4JQI as it was not ordered in PDB: 6UP7.

Supplementary Figure 3.7 Titration of interactions with immobilized βarr1 by SPR.

Immobilized βarr1 construct (ligand) is listed as column heading. Rows represent analyte flowed during titration. Kd and Bmax values obtained as described in methods are listed with 95% CI range in parentheses. ND denotes value not determined. PIP2 binding was not fit (D-F), whereas Bmax for Fab30+V2Rpp (M-O) failed to converge. In all cases the darkest blue curve corresponds to the highest concentration and the darkest red curve corresponds to the lowest concentration. Titrations, as described in methods, for V2Rpp and PIP2 (A-F) ranged from 40 μM to 78.1 nM. Titrations of Fab30 ranged from nM to 3.9 nM with fixed concentration of V2Rpp (40 μM) or PIP2 (40 μM), as indicated. Vertical axes are raw RU, and not corrected for channel loading.

Supplementary Data Figure 3.1 Recruitment amplitude for arrestins to a CAAX plasma membrane bystander using NanoBiT assay. Points reflect best fit values from three biological replicates and error bars show standard error of fits. Vertical axis is scaled such that Luminescence fold-change refers to the span of the fit (top – bottom) A) βarr1 data. Dashed horizontal line corresponds to three times the max signal measured with receptor mock-transfected cells y = 0.43; B) βarr2 data. Dashed horizontal line corresponds to three times the max signal measured with receptor mock-transfected cells y = 0.096.

Supplementary Data Figure 3.2 Full western blots of βarr1/2-SmBiT both WT and 3Q for measuring expression levels. Representative protein marker labeled top left.

Supplementary Data Figure 3.3 Direct recruitment assay for recruitment of LgBiT labeled arrestins to SmBiT containing GPCRs. Points reflect best fit values from three biological replicates and error bars show standard error of fits. Vertical axis is scaled such that luminescence fold-change refers to the span of the fit (top – bottom) A) βarr1 data; B) βarr2 data.

Supplementary Data Figure 3.4 A) Loss of function (LOF) measured by direct recruitment NanoBiT assay. Data are mean ± SEM (n=3 biological replicates). Dashed shapes group cluster 1 and cluster 2 receptors. V1AR (βarr1 and βarr2 points overlap) belongs to cluster 1, while β2AR- V2C and OXTR βarr1 recruitment belong to cluster 2.

Supplementary Data Figure 3.5 Recruitment amplitude for arrestins to endosomes as measured by an endosome bystander NanoBiT assay. Points reflect best fit values from three biological replicates and error bars show standard error of fits. Vertical axis is scaled such that Luminescence fold-change refers to the span of the fit (top – bottom) A) βarr1 data: dashed horizontal line corresponds to three times the max signal measured with receptor mock-transfected cells y = 0.20; B) βarr2 data, for selected receptors: dashed horizontal line corresponds to three times the max signal measured with receptor mock-transfected cells y = 0.14. C-D) Zooms of arrestin translocation to endosomes measured by endosome bystander NanoBiT assay for cells expressing OXTR and HTR2C, respectively. Dashed horizontal lines corresponds to three times the max signal measured with receptor mock-transfected cells, as stated in B) and C).

Supplementary Data Figure 3.6 A) NanoBiT recruitment amplitudes for βarr1 recruitment to a CAAX plasma membrane bystander. Points reflect best fit values from three biological replicates and error bars show standard error of fits. Vertical axis is scaled such that Luminescence fold- change refers to the span of the fit (top – bottom). Dashed horizontal line corresponds to three times the max signal measured with receptor mock-transfected cells y = 0.43; B) NanoBiT recruitment amplitudes for βarr1 recruitment to endosomes. Points reflect best fit values from three biological replicates and error bars show standard error of fits. Vertical axis is scaled such that Luminescence fold-change refers to the span of the fit (top – bottom). Dashed horizontal line corresponds to three times the max signal measured with receptor mock-transfected cells y = 0.20.

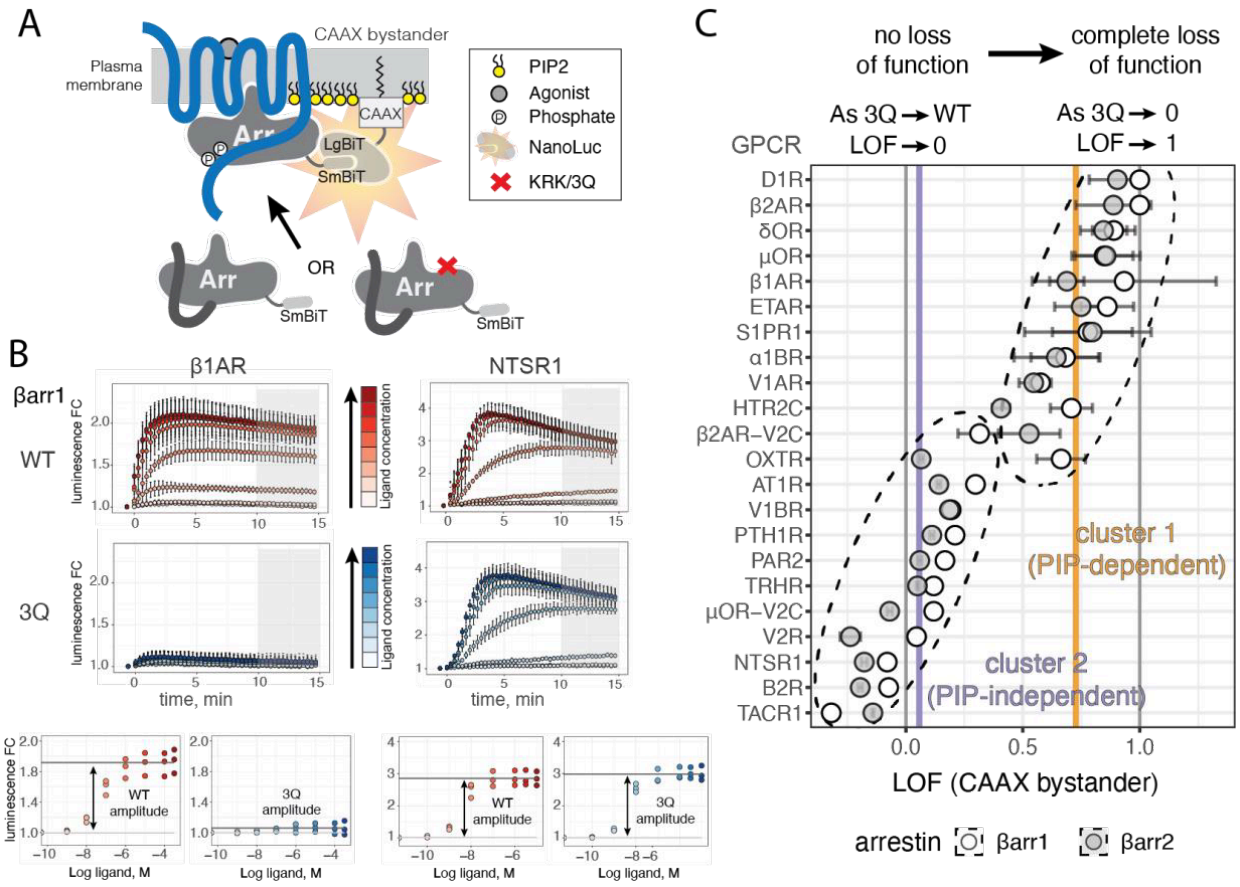

Figure 3.1 β-arrestin phosphoinositide binding is required for recruitment to some GPCRs

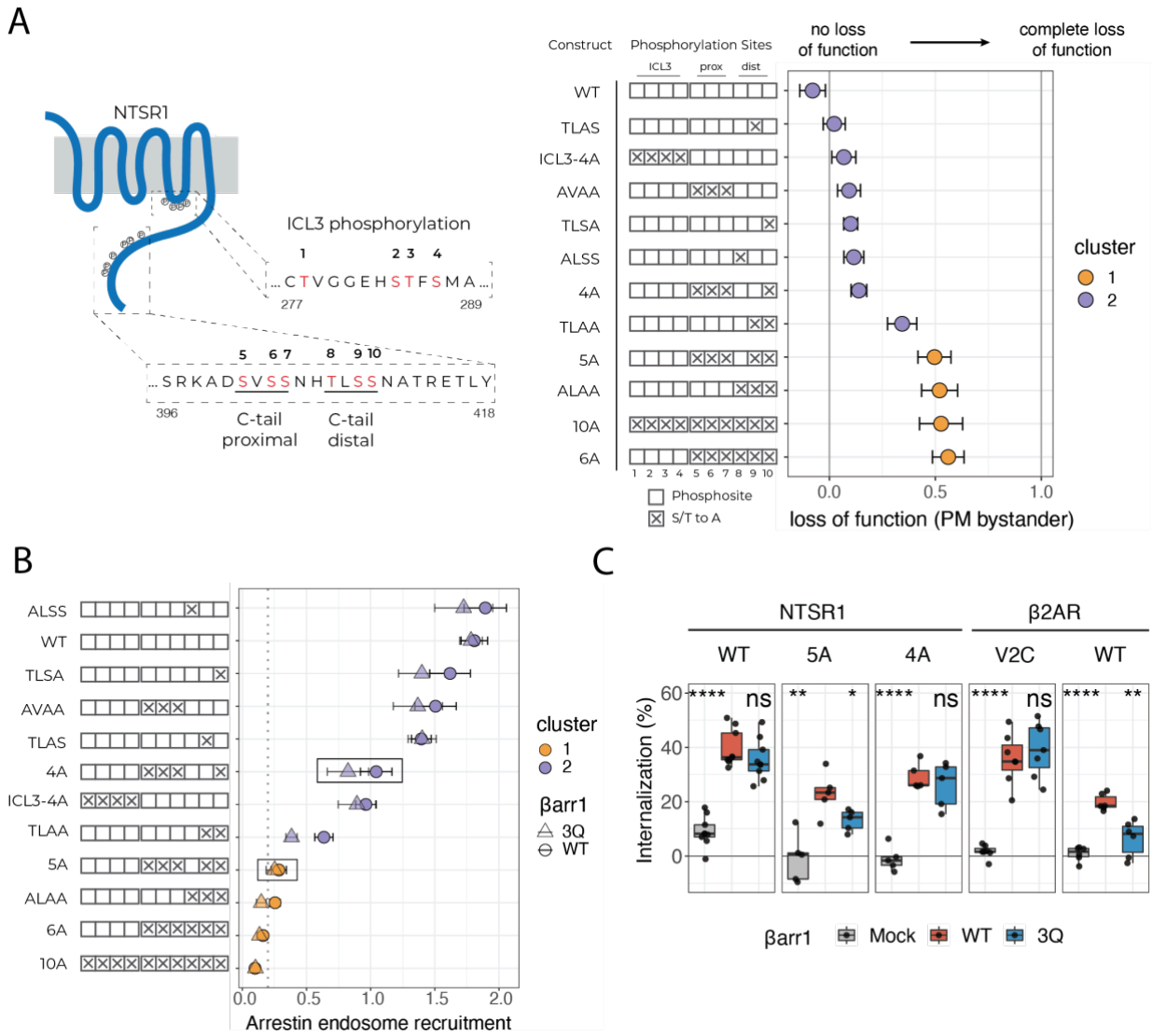

Figure 3.2 Receptor phosphorylation patterns govern PIP-dependence for arrestin recruitment

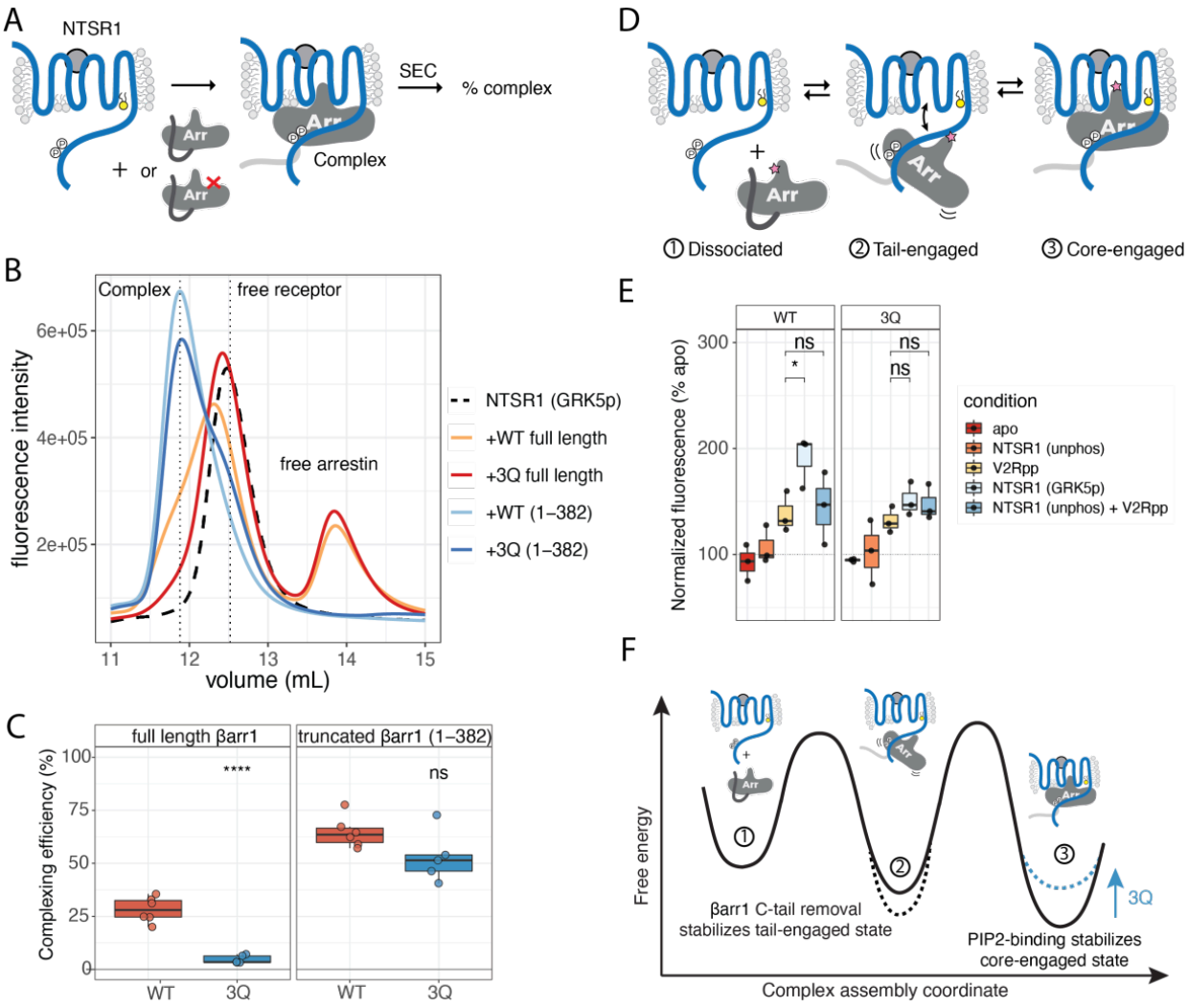

Figure 3.3 Lipid binding stabilizes core-engaged arrestin complexes

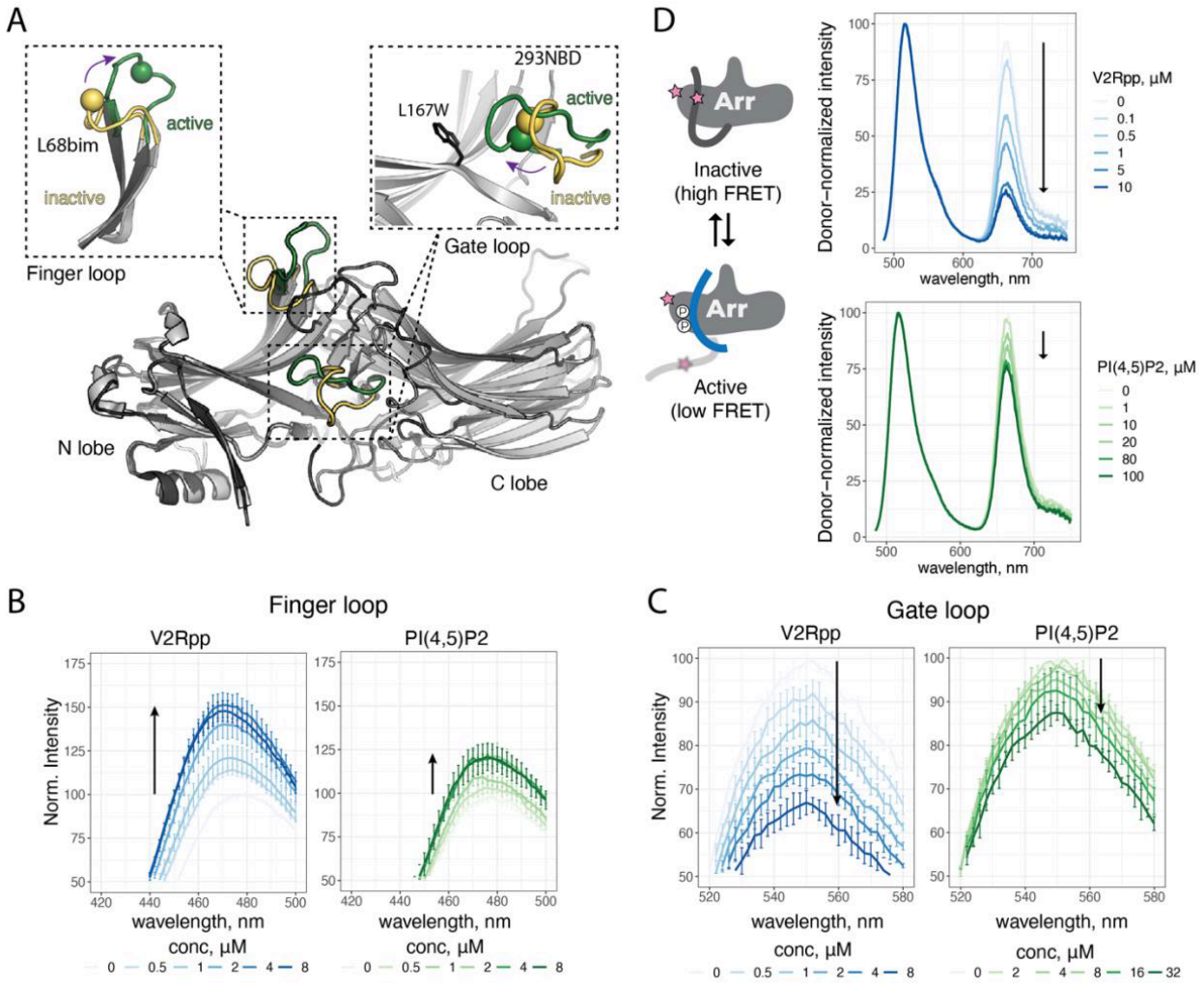

Figure 3.4 PIP2 alone promotes conformational changes in arrestin, including C-terminus movement, but not release

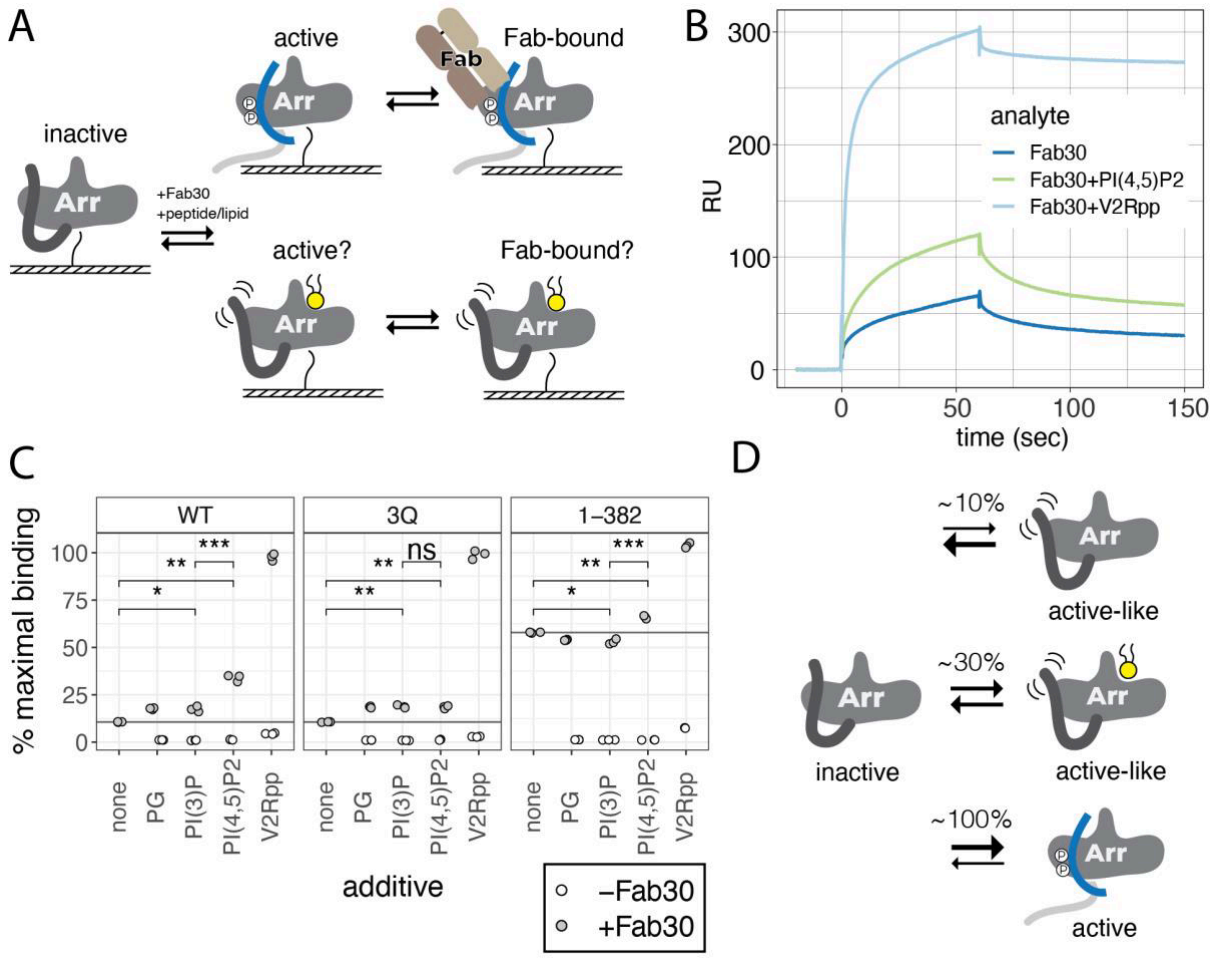

Figure 3.5 PIP2 enhances Fab30 binding to βarr1

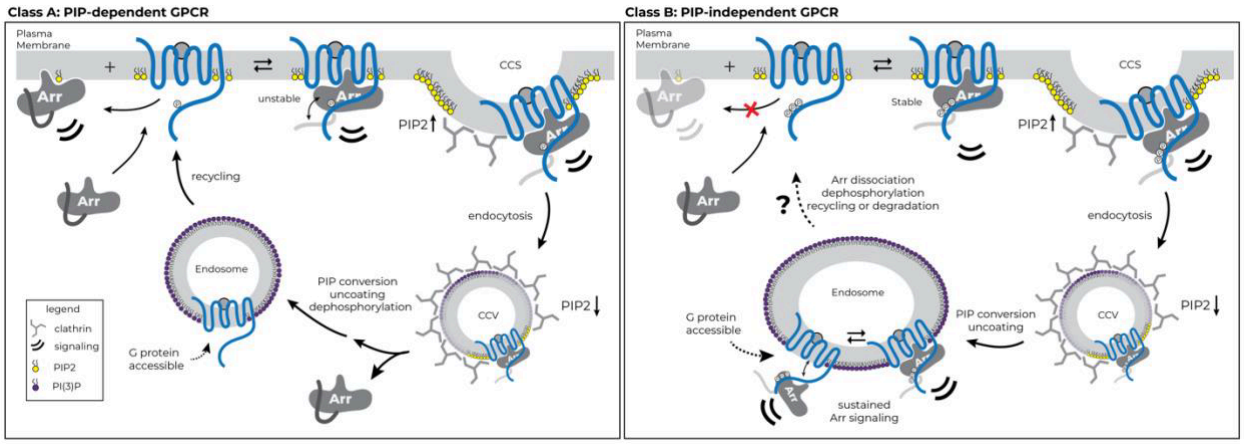

Figure 3.6 Model for phosphoinositide regulation of GPCR-β-arrestin complex assembly and disassembly

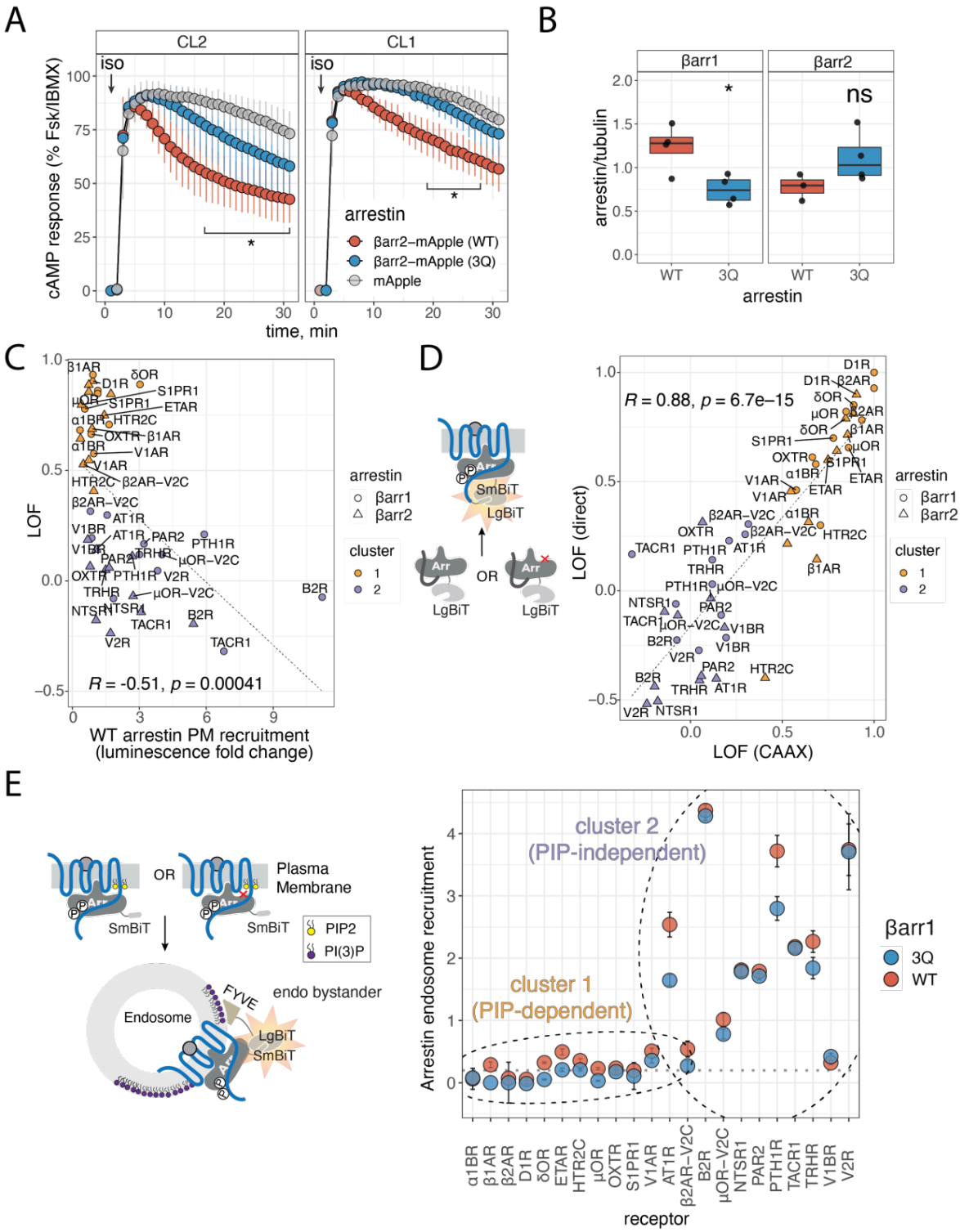

Supplementary Figure 3.1 β-arrestin phosphoinositide binding is required for plasma membrane recruitment to some GPCRs.

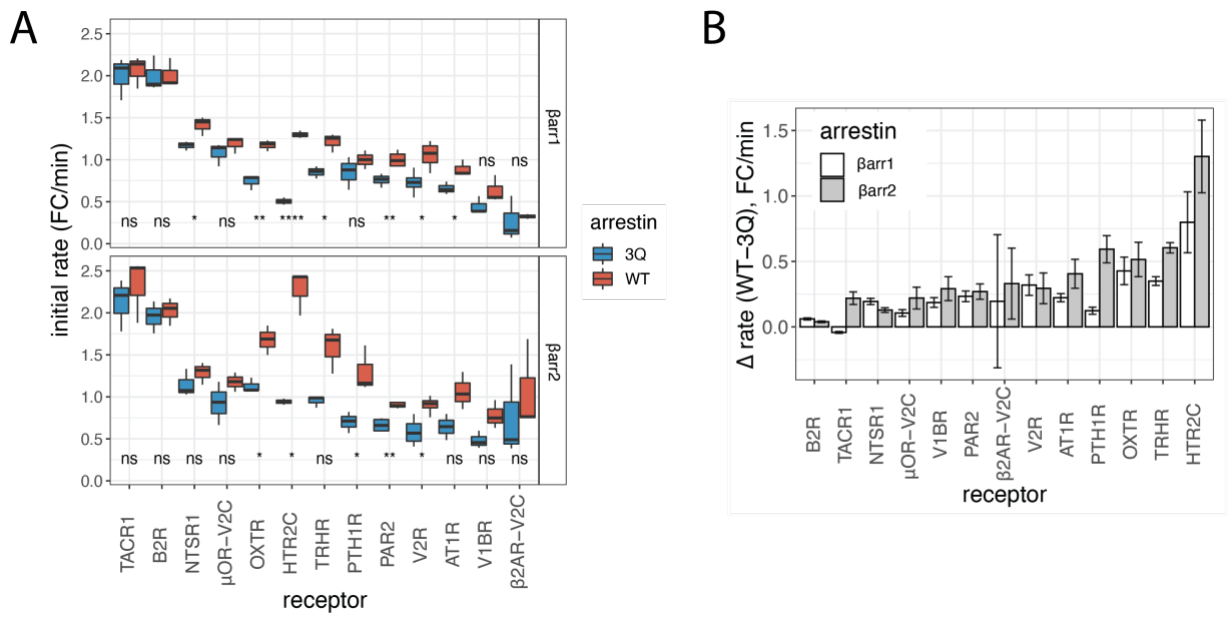

Supplementary Figure 3.2 Loss of PIP binding slows β-arrestin recruitment to cluster 2 GPCRs.

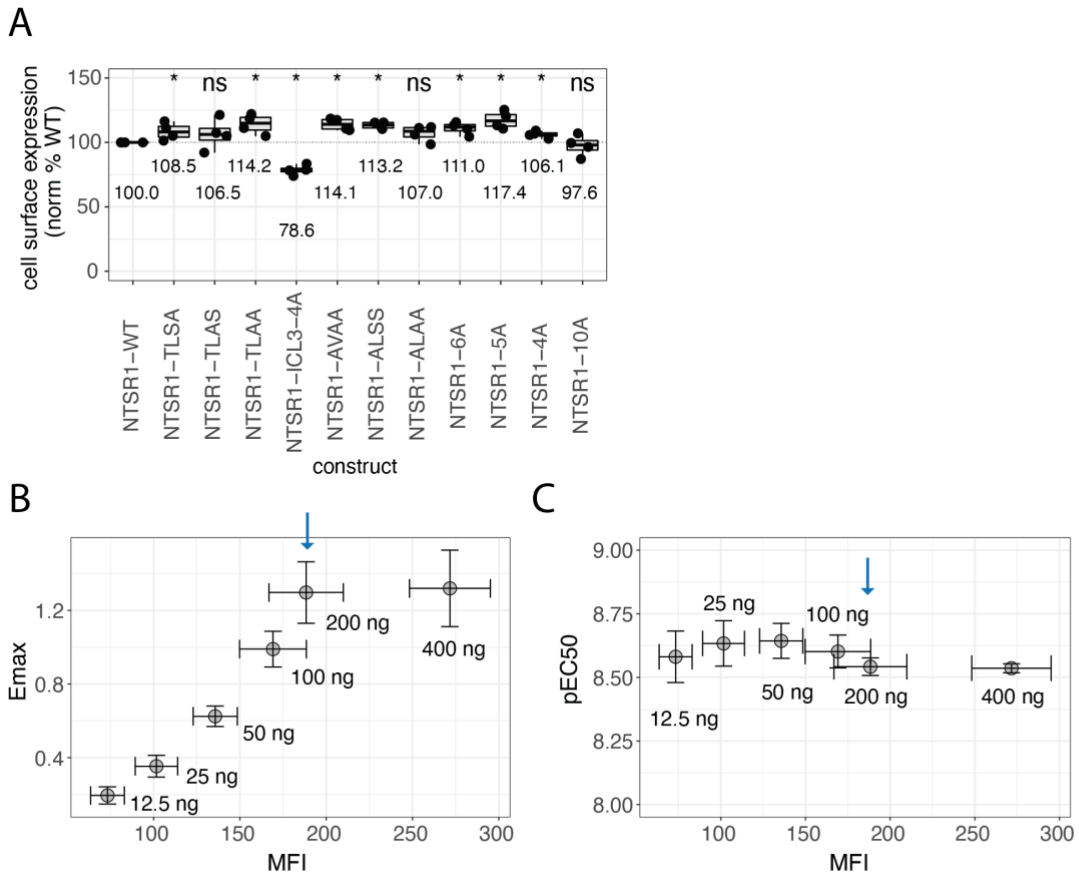

Supplementary Figure 3.3 β-arrestin recruitment to NTSR1 mutants can be measured by NanoBiT recruitment assay

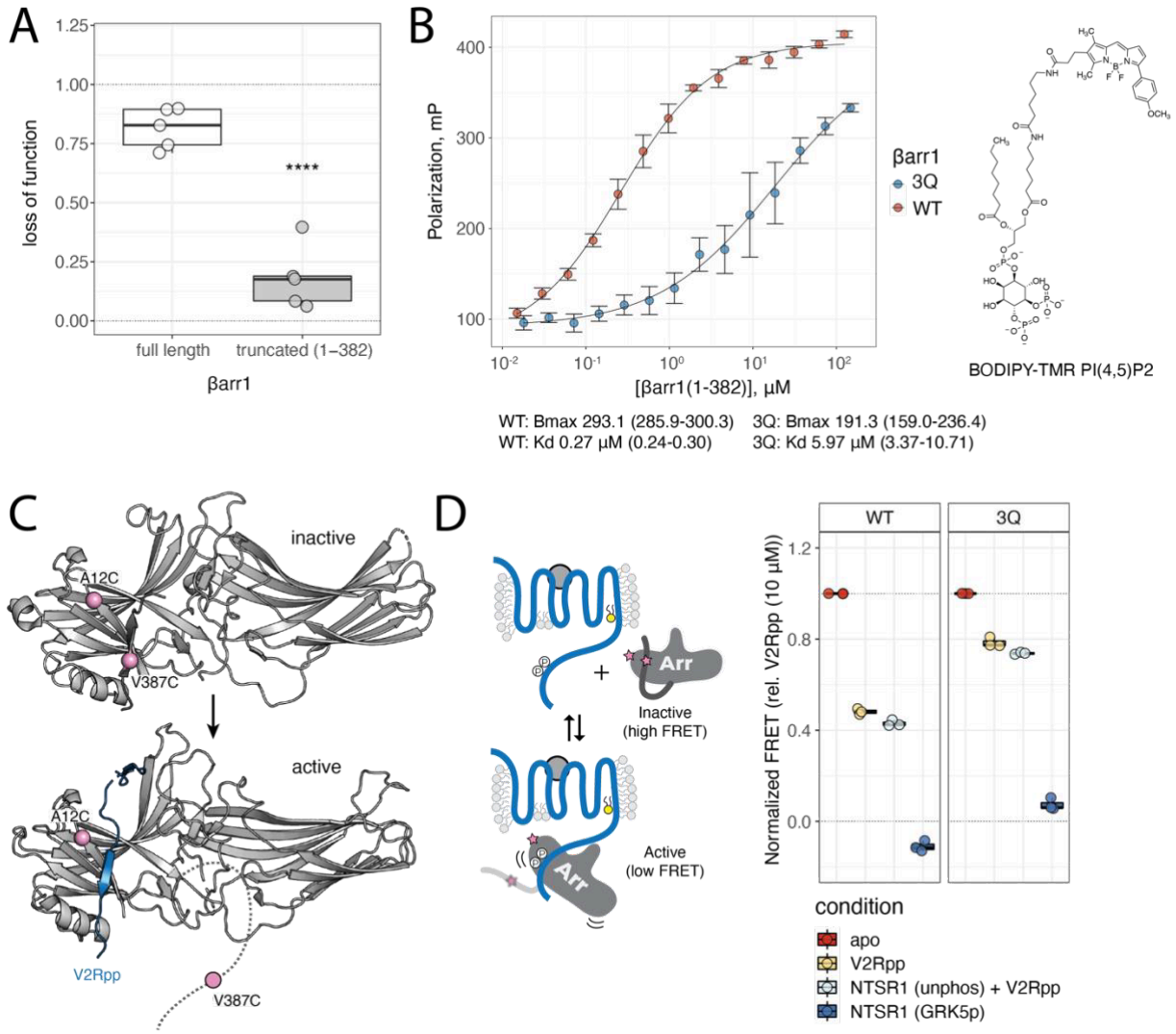

Supplementary Figure 3.4 PIP binding stabilizes core-engaged arrestin complexes.

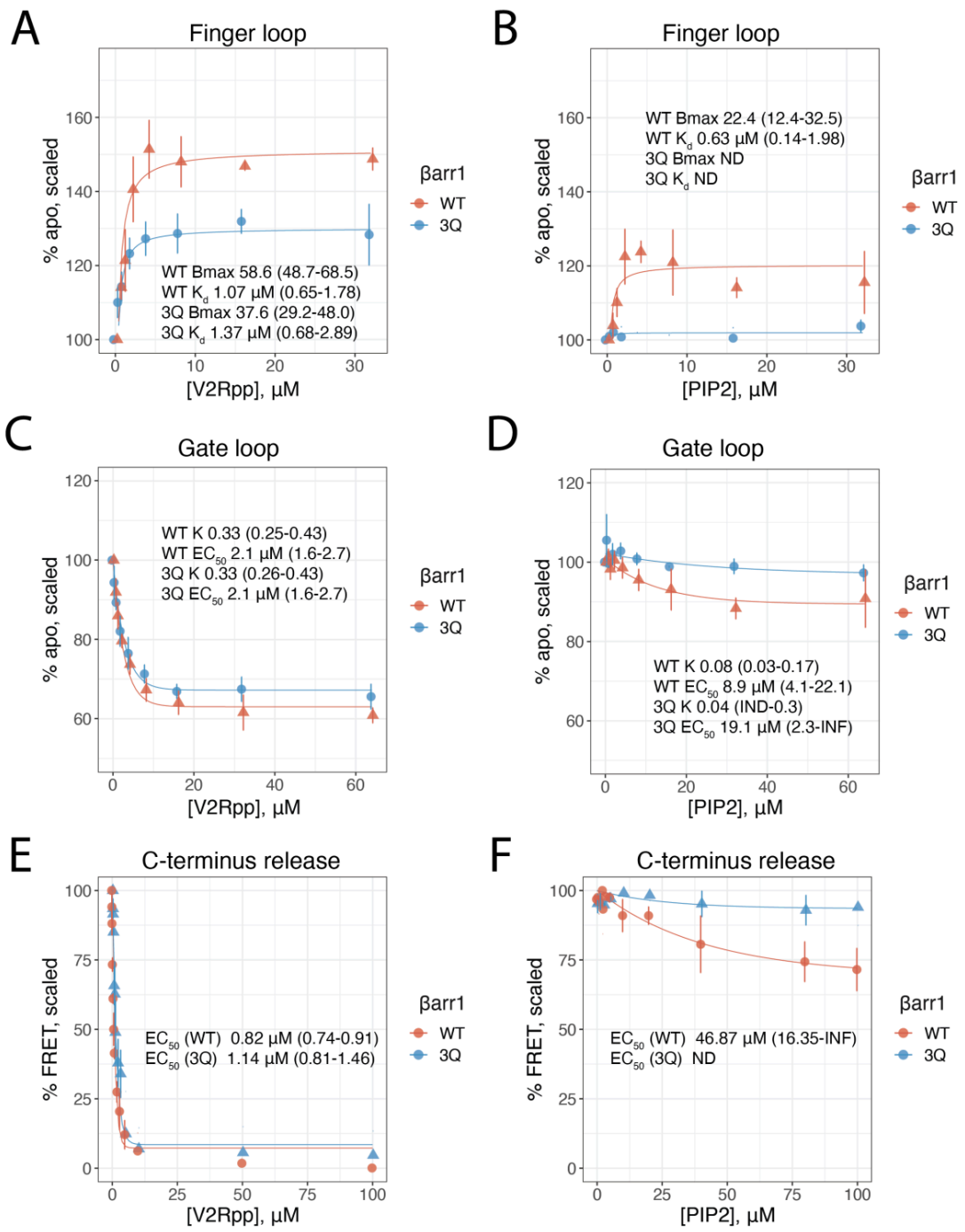

Supplementary Figure 3.5 PIP2 allosterically triggers movement of the arrestin C-tail but not release.

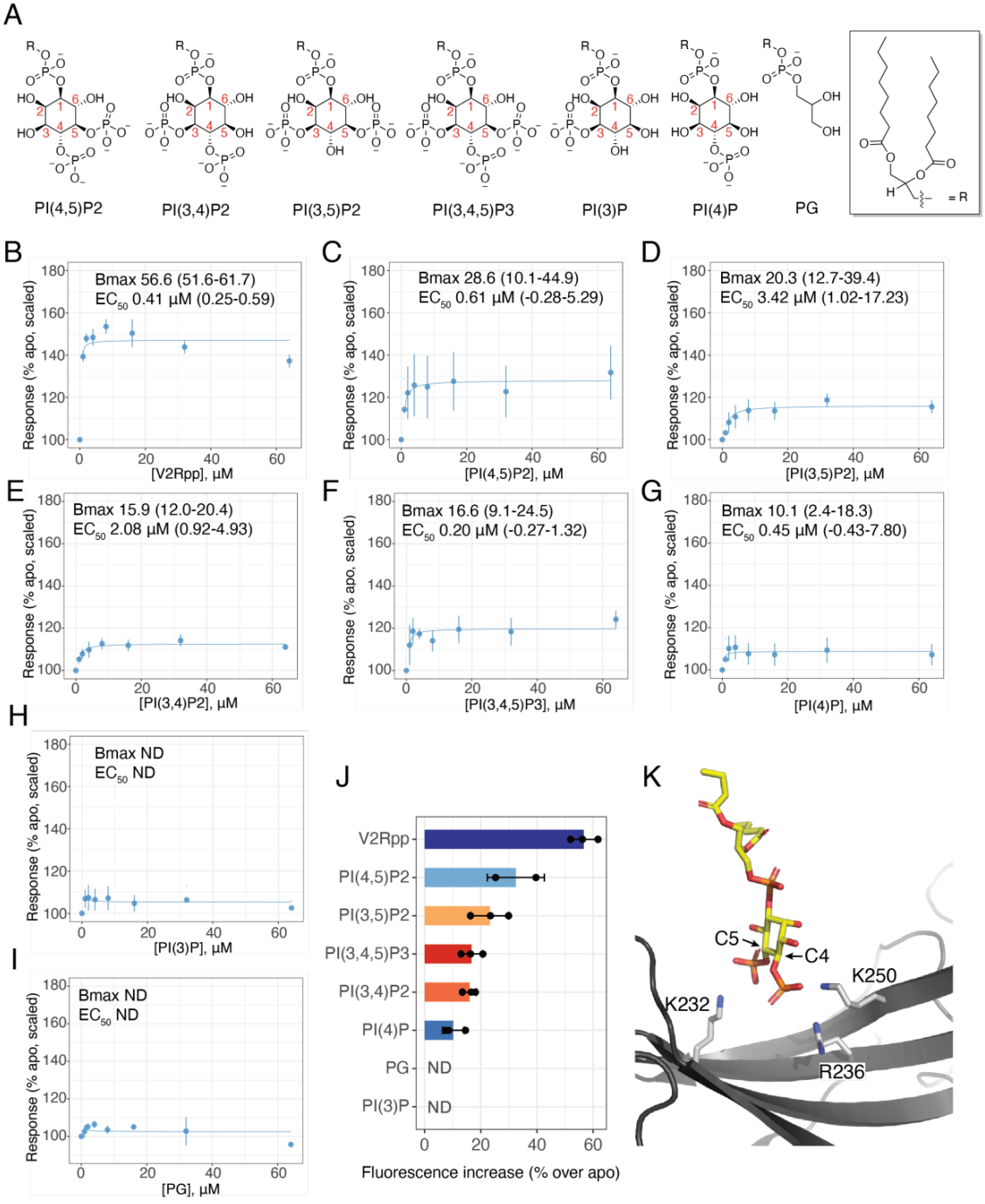

Supplementary Figure 3.6 Plasma membrane PIPs promote conformational changes in arrestin

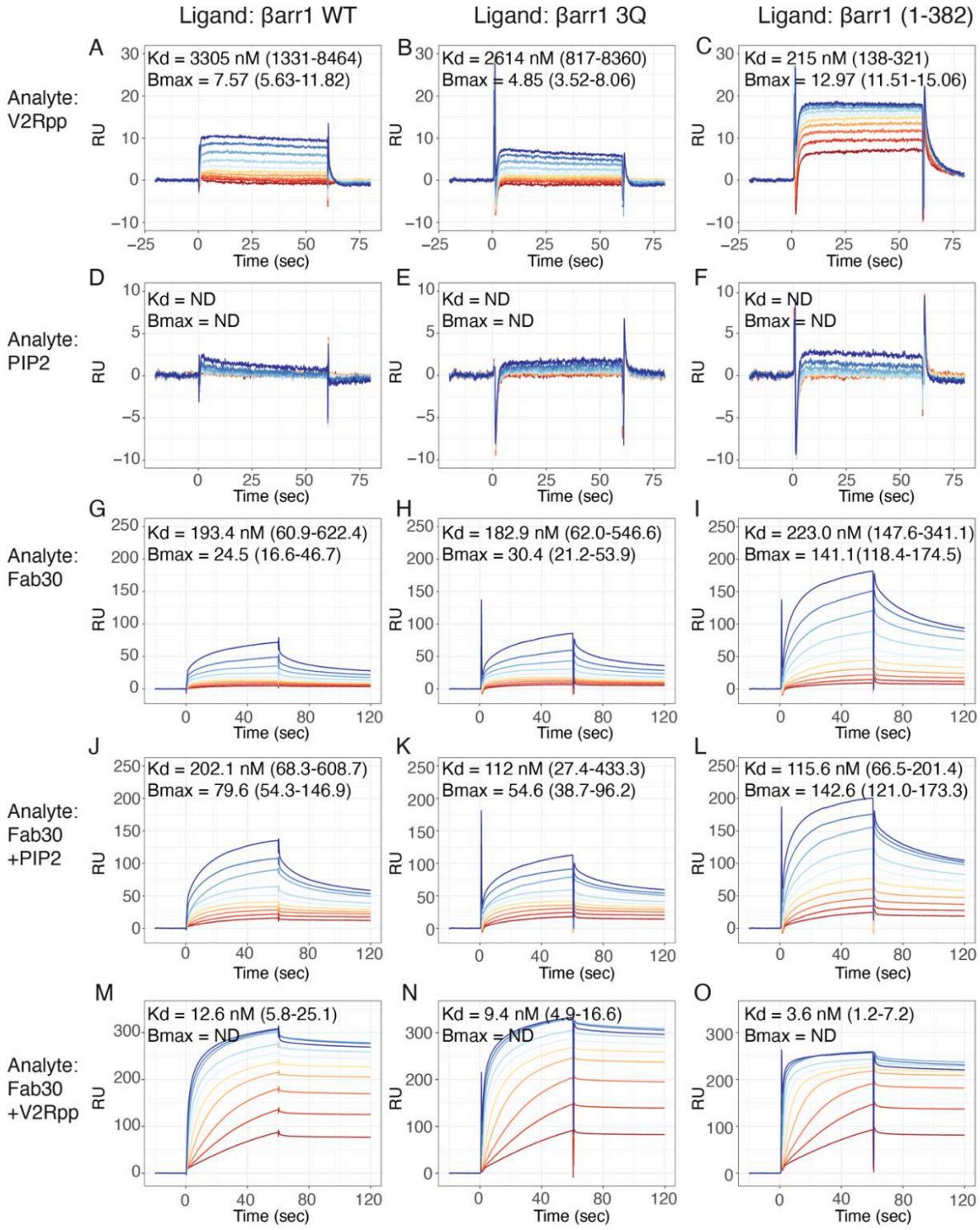

Supplementary Figure 3.7 Titration of interactions with immobilized βarr1 by SPR

Table 3.1 GPCR ligands and concentrations used in cell experiments.

GPCR	Abbreviation	Ligand	Log concentrations tested
Tachykinin Receptor 1	TACR1	Substance P	-15, -11, -10, -9, -8, -7, -6, -5
B2 bradykinin receptor	B2R	Bradykinin	-15, -11, -10, -9, -8, -7, -6, -5
Neurotensin receptor type 1	NTSR1	Neurotensin	-15, -10, -9, -8, -7, -6, -5.5, -5
Vasopressin V2 receptor	V2R	AVP	-15, -9, -8.5, -8, -7.5, -7, -6.5, -6
Proteinase-activated receptor 2	PAR2	PAR2 peptide	-15, -7.5, -7, -6.5, -6, -5.5, -5, -4.5
Mu-type opioid receptor V2R CT chimera	μOR-V2C	DAMGO	-15, -9, -8, -7, -6, -5, -4.5, -4
Thyrotropin-releasing hormone receptor	TRHR	TRH	-15, -10, -9, -8, -7, -6, -5, -4
Parathyroid hormone/parathyroid hormone-related peptide receptor	PTH1R	PTH	-15, -10, -9, -8, -7, -6.5, -6, -5.5
Vasopressin V1b receptor	V1BR	AVP	-15, -9, -8.5, -8, -7.5, -7, -6.5, -6
Type-1 angiotensin II receptor	AT1R	AngII	-15, -11, -10, -9, -8, -7, -6, -5
Oxytocin receptor	OXTR	Oxytocin	-15, -10, -9, -8, -7, -6, -5.5, -5
Beta-2 adrenergic receptor V2R CT chimera	β2AR-V2C	Isoproterenol	-15, -9, -8, -7, -6, -5, -4, -3.5
5-hydroxytryptamine receptor 2C	HTR2C	Serotonin	-15, -9, -8, -7, -6, -5, -4, -3.5
Vasopressin V1a receptor	V1AR	AVP	-15, -9, -8.5, -8, -7.5, -7, -6.5, -6
Alpha-1 adrenergic receptor	α1BR	Norepinephrine	-15, -9, -8, -7, -6, -5, -4.5, -4
Beta-1 adrenergic receptor	β1AR	Isoproterenol	-15, -9, -8, -7, -6, -5, -4, -3.5
Endothelin receptor type A	ETAR	Endothelin	-15, -11, -10, -9, -8, -7, -6.5, -6
Sphingosine 1-phosphate receptor 1	S1PR1	S1P	-15, -10, -9, -8, -7, -6.5, -6, -5.5
Mu-type opioid receptor	μOR	DAMGO	-15, -9, -8, -7, -6, -5, -4.5, -4
Delta-type opioid receptor	δOR	Met-Enk	-15, -10, -9, -8, -7, -6, -5.5, -5
Beta-2 adrenergic receptor	β2AR	Isoproterenol	-15, -9, -8, -7, -6, -5, -4, -3.5
D(1A) dopamine receptor	D1R	Dopamine	-15, -7, -6, -5.5, -5, -4.5, -4, -3.5

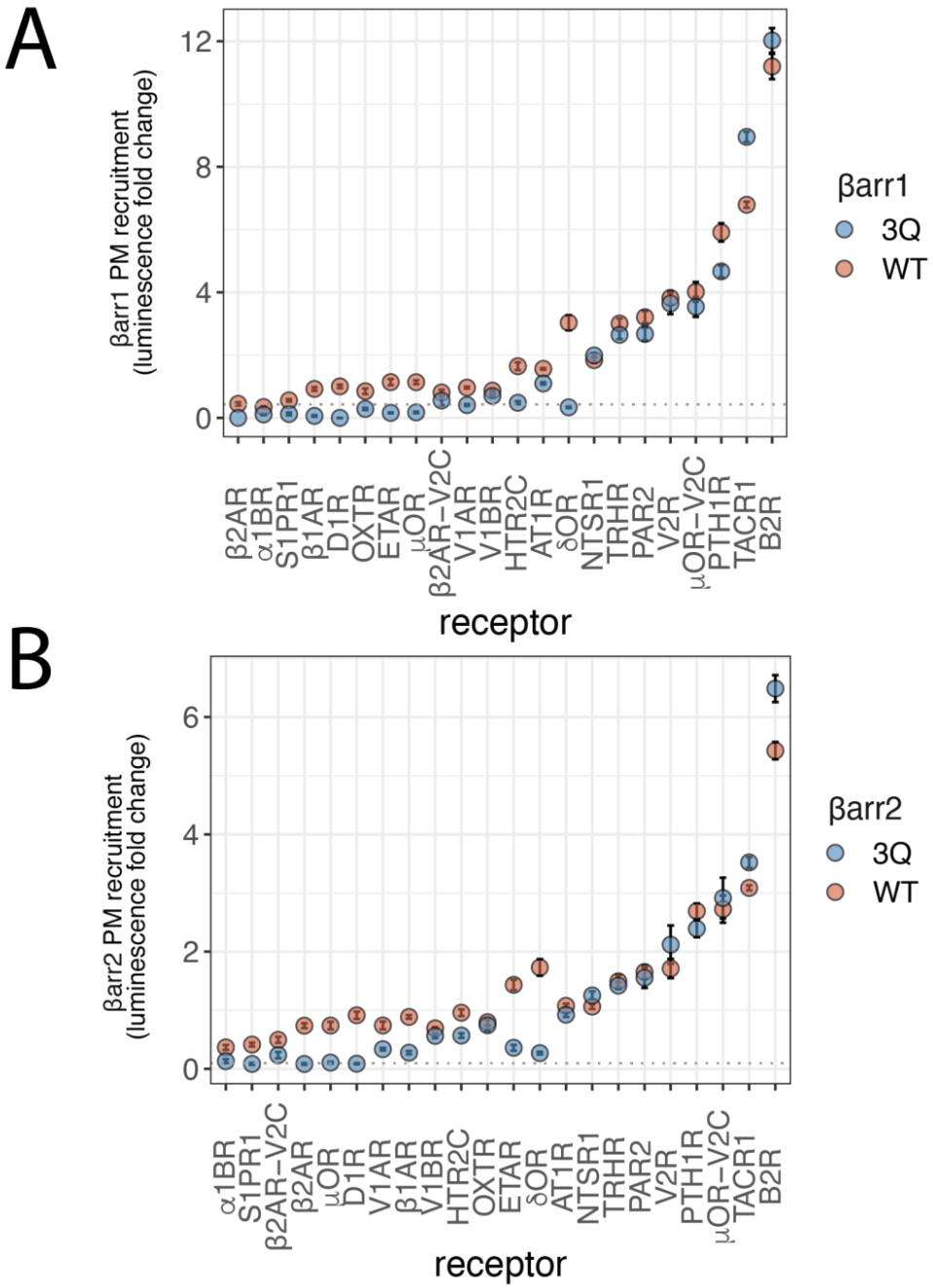

Supplementary Data Figure 3.1 Recruitment amplitude for arrestins to a CAAX plasma membrane bystander using NanoBiT assay.

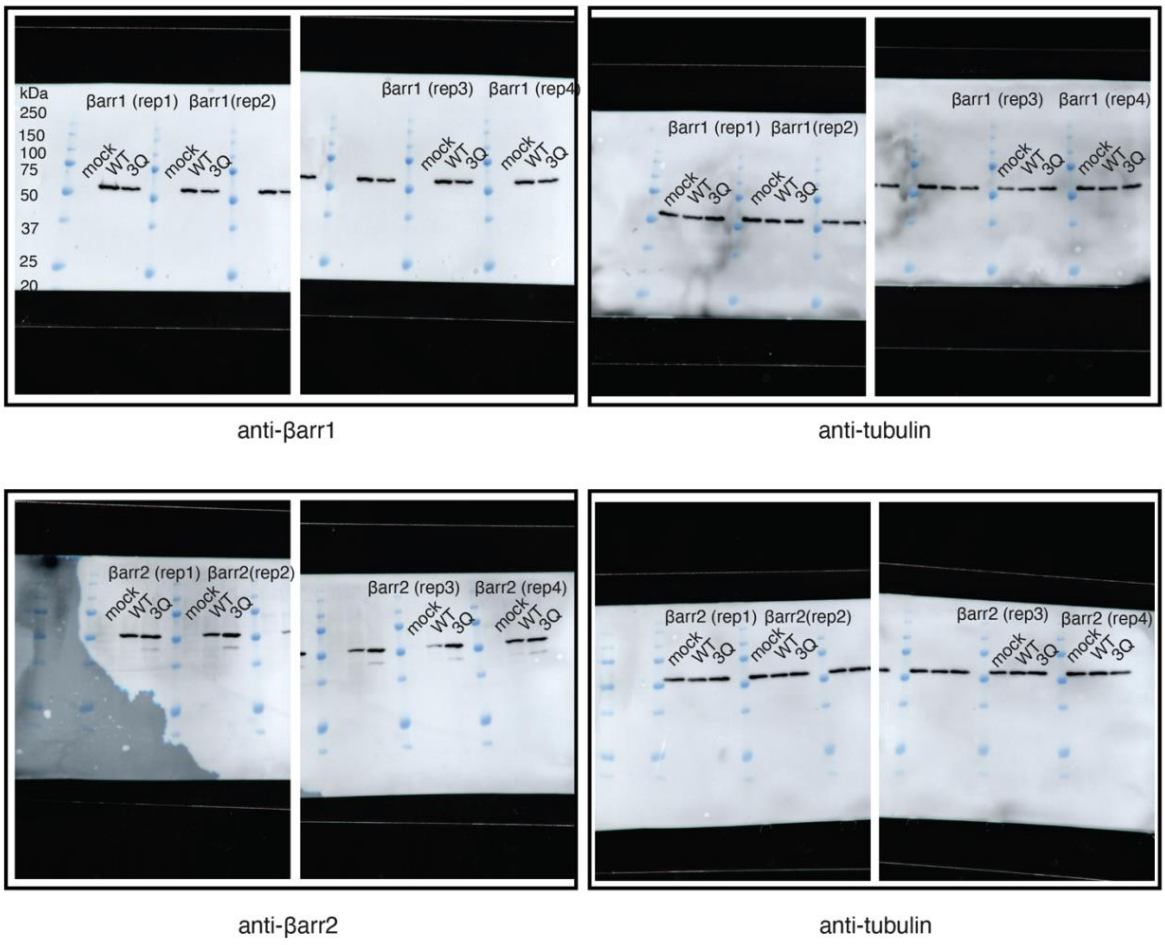

Supplementary Data Figure 3.2 Full western blots of βarr1/2-SmBiT both WT and 3Q for measuring expression levels. Representative protein marker labeled top left.

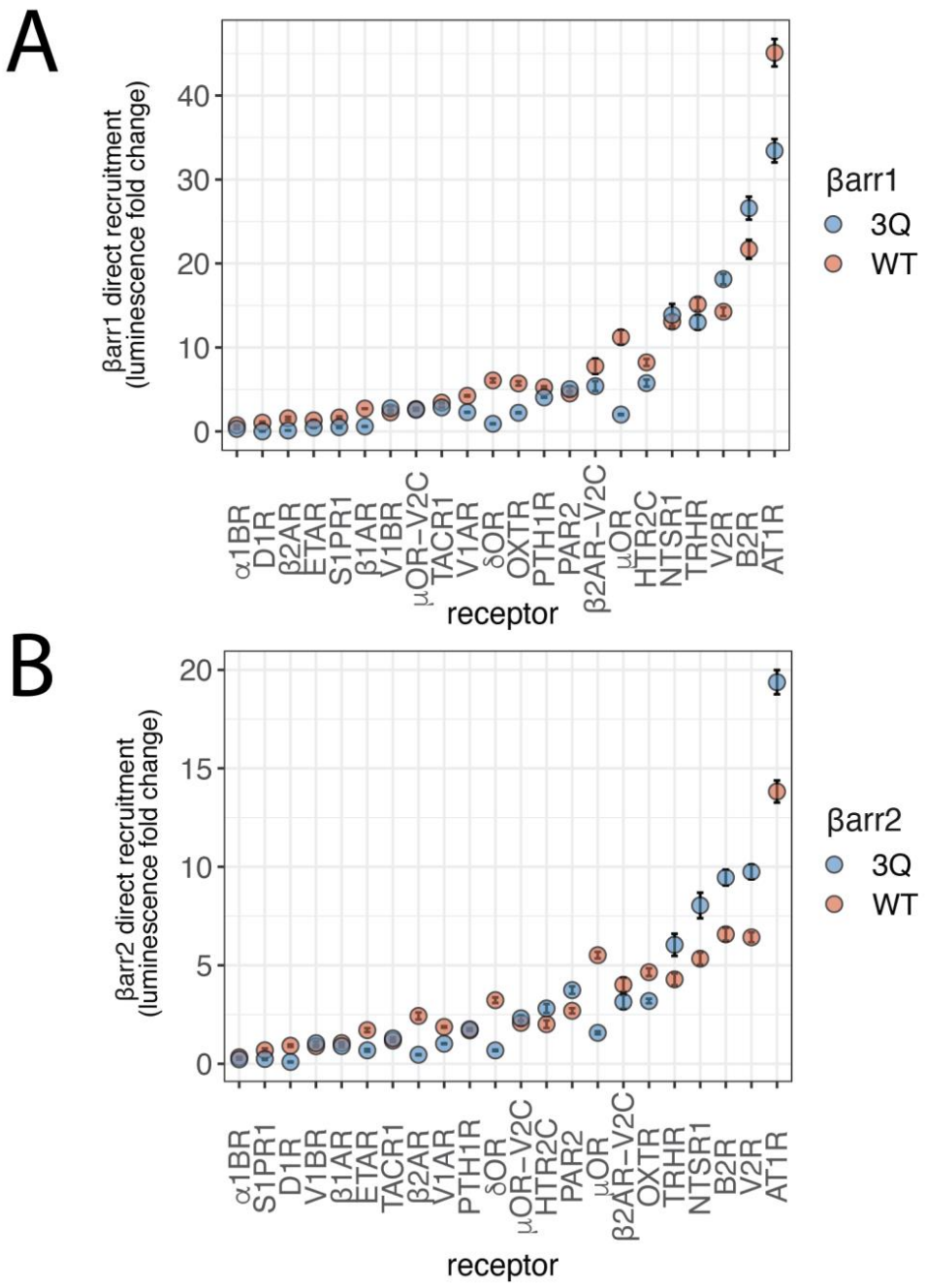

Supplementary Data Figure 3.3 Direct recruitment assay for recruitment of LgBiT labeled arrestins to SmBiT containing GPCRs.

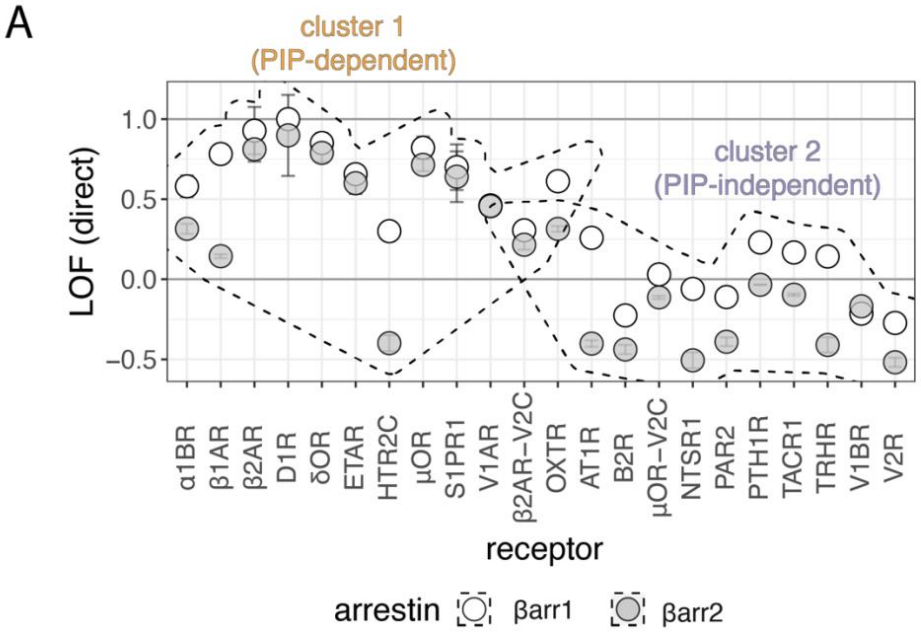

Supplementary Data Figure 3.4

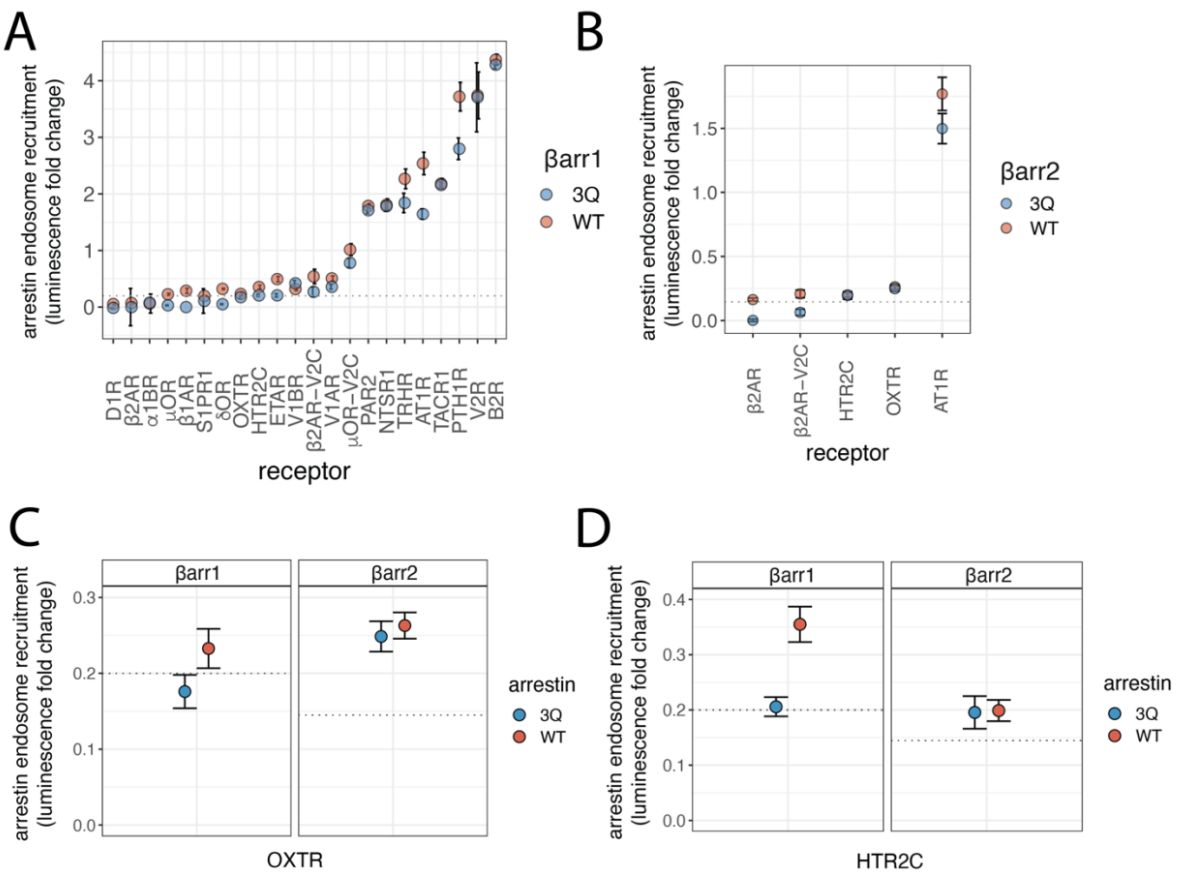

Supplementary Data Figure 3.5 Recruitment amplitude for arrestins to endosomes as measured by an endosome bystander NanoBiT assay.

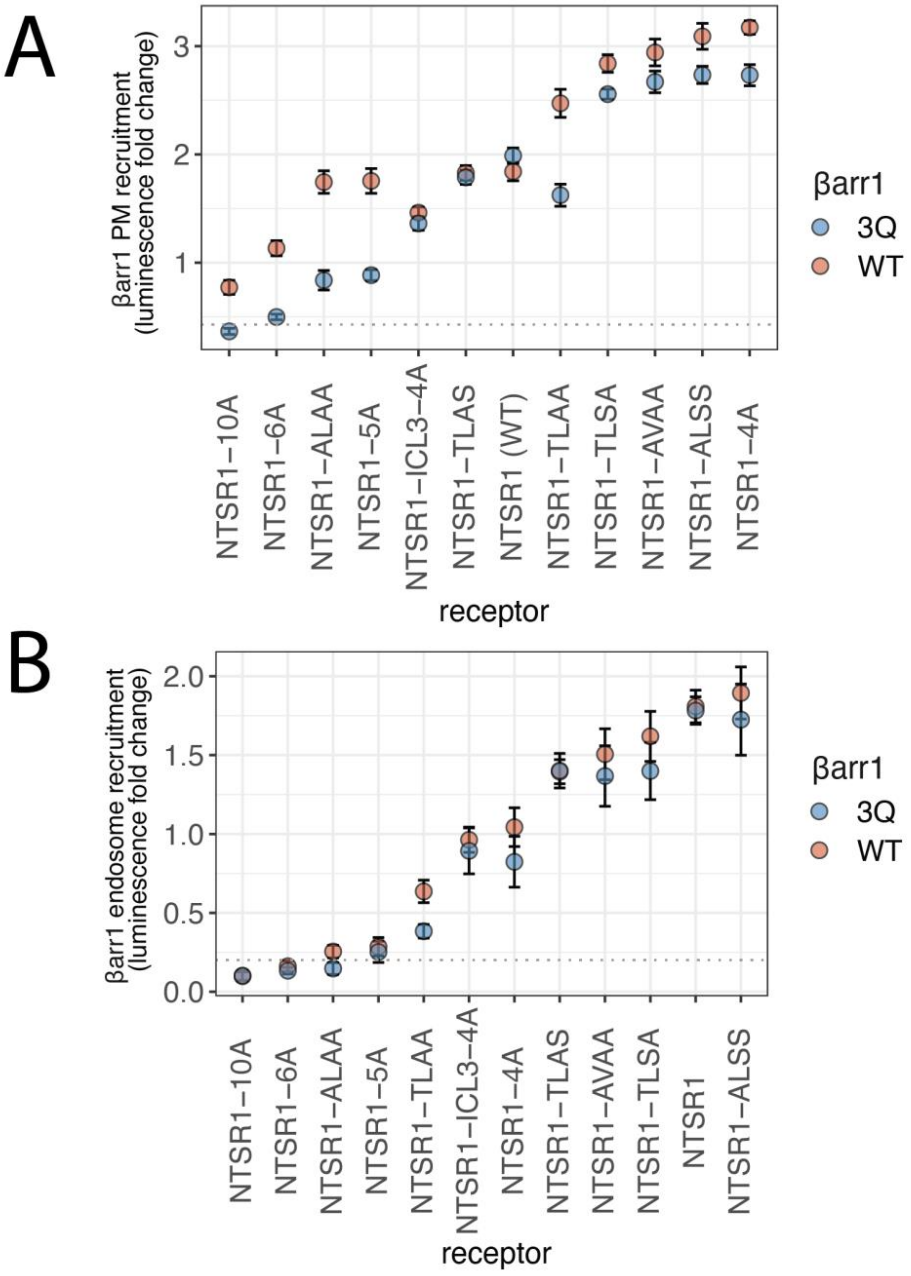

Supplementary Data Figure 3.6

Chapter 4: Developing β-arrestin conformational biosensors

Benjamin Barsi-Rhyne, in the laboratories of Aashish Manglik and Mark von Zastrow (UCSF), conceived and executed all the experiments and wrote the following chapter.

4.1 Abstract

β-arrestins are transducers and regulators of GPCR signaling and trafficking. By binding directly to GPCRs, the β-arrestins can influence the type, duration, and location of cellular signaling and do so in a highly receptor specific manner (Shukla, Xiao et al. 2011, Gurevich and Gurevich 2018, Rajagopal and Shenoy 2018). How β-arrestins accomplish such flexible control has been proposed to be due to their ability to form conformationally distinct and receptor-specific GPCR/β-arrestin complexes (Nobles 2011) (Lee, Appleton et al. 2016). However, recent studies have shown that β-arrestins remain active after GPCR dissociation and that this 'action at a distance' mechanism produces previously unrecognized method of signaling (Eichel, Jullié et al. 2016, Nuber, Zabel et al. 2016, Eichel, Jullié et al. 2018). However, observing the conformational state of receptor-dissociated active β-arrestin has been challenging in live cells. Here we show preliminary studies aimed at developing two new classes of β-arrestin conformational biosensors. First, we show that an existing single chain fragment variable (scFv) derived from Fab30, a stabilizer of a β-arrestin-1 active state (Shukla, Manglik et al. 2013), may function as β-arrestin conformational biosensor in living cells. Next, we show strategies aimed at producing nanobodies that bind specifically to activated β-arrestins. Finally, we present preliminary data for two circularly permuted GFP-based β-arrestin conformational biosensors. Taken together, these data may provide an entry point into detection of β-arrestin conformation in living cells.

4.2 Introduction

GPCRs regulate nearly every aspect of physiology and are important drug targets (Lohse, Benovic et al. 1990, Pierce, Premont et al. 2002, Rosenbaum, Rasmussen et al. 2009, Kang, Tian et al. 2014). Their cellular signals are generated and modulated by heterotrimer G proteins and β-arrestins. β-arrestins, discovered as proteins that "arrest" G protein signaling, are now understood to undergo conformational changes that allow them to operate as flexible signal transducers and inducible endocytic adaptors. These functions were traditionally thought to cease upon GPCR/β-arrestin dissociation but this view has recently been challenged by observations of β-arrestin that remained active after dissociation from its activating GPCR, a mechanism termed catalytic activation. When activated in this way, β-arrestin can stall clathrin-coated pits to generate a plasma membrane delimited MAPK signal (Eichel, Jullié et al. 2016, Eichel, Jullié et al. 2018). However, how these signals are produced remains unclear. One possibility is that β-arrestin adopts a distinct active conformation after GPCR dissociation that facilitates this signal. To test this hypothesis, we sought to generate new tools to detect conformational activation.

4.3 Results

scFv30 may function as a biosensor for βarr1 activation

Fab30 (fragment antigen binding 30) was previously identified by phage display against V2Rpp bound β-arrestin-1 and subsequently used to stabilize a truncated β-arrestin-1-V2Rpp (vasopressin type II receptor tail phosphopeptide) complex in its active conformation (Shukla 2013). As Fabs are nonfunctional in the reducing environment of the cytosol, Fab30 was converted into scFv30 (single chain fragment variable 30), also known as Ib30 (Ghosh, Dwivedi et al. 2019). Recent work has shown that scFv30 can recognize β-arrestin-1 when activated by 'Class B' GPCRs (Oakley, Laporte et al. 2000), a subgroup that stably associates with β-arrestins and includes V2R (Baidya, Kumari et al. 2020). However, whether scFv30 functions as a β-arrestin conformational biosensor upon β-arrestin activation by less stably associated receptors such as 'Class A' or the purely catalytic β1AR, to my knowledge, has not been show.

To test this, we used TIRF microscopy to assess plasma membrane recruitment of scFv30 and βarr1 in response to isoproterenol stimulation of cells co-expressing GPCRs known to differ substantially in the duration of their association with β-arrestins. We confirmed that the β2V2R promoted strong recruitment of β-arrestin-1 and scFv30 to the plasma membrane, an observation in line with previous findings (Baidya, Kumari et al. 2020) (Figure 4.1A). To our surprise, plasma membrane co-recruitment and co-clustering, presumably to clathrin-coated pits, of scFv30 with βarr1 was observed for the medium affinity receptor, β2AR, and the low-affinity receptor, β1AR (Figure 4.1B-C). Plasma membrane recruitment of both scFv30 and β-arrestin-1 were apparent visually and recruitment was quantified by fluorescence intensity (see methods) (Figure 1D, E).

As basal association of β-arrestin-1 and scFv30 prior to receptor activation would lead to similar results, we set out to verify our TIRF microscopy biochemically and by receptor independent β-arrestin recruitment to endosomes. When examined by co-immunoprecipitation, our biochemical readout, we found that scFv30 bound βarr1 in an agonist-dependent manner for the β2V2R, but similar results were not detectable for β1AR (Figure 4.1H). When β-arrestin-1 was recruited to a membrane independently from receptor through endosome targeted FKBP, fusion of FRB to the β-arrestin-1 C-terminus, and treatment with rapamycin, we observed co-recruitment of scFv30 (Figure 4.1F, G). This may suggest that β-arrestin-1 can be activated by membrane proximity, an idea that is discussed in chapter 3 of this thesis. Taken together, these results suggests scFv30 functions as a biosensor for β2V2R-mediated activation of β-arrestin-1 but do not firmly establish a similar function for β2AR and β1AR. However, the degree of basal association between scFv30 and β-arrestin-1 in living cells remains to be determined.

Towards developing β-arrestin-1 active state-specific nanobodies

Conformationally specific nanobodies have revolutionized our understanding of GPCR active states structurally, biophysically, and as biosensors in living cells. We wondered if the ability of biosensor nanobodies to read out both the subcellular location and conformational state of their interaction partners could be applied to β-arrestins.

We set out to identify conformationally specific β-arrestin-1 nanobodies by conducting multiple rounds of positive and negative selection on a previously described yeast display nanobody library containing $2x10^8$ unique nanobodies (McMahon, Baier et al. 2018). As V2Rpp-bound β-arrestin-1 was used to isolate the active state specific β-arrestin-1 binding protein, Fab30, we

reasoned that a similar approach would yield similarly specific nanobodies. We carried out our positive selections by incubating purified βarr1-V2Rpp and our negative selection was done with purified apo-βarr (Figure 4.2A). In addition, the tags on β-arrestin-1 and the probes used to bind those tags were swapped at different rounds of the selection process (see methods). Upon completing four rounds of selection, we extracted DNA from each round, PCR amplified the nanobody coding region, and submitted the resulting DNA library for deep sequencing (see methods). This yielded the complete coding sequences for >130,000 nanobodies, which we further analyzed and ranked using two metrics – fold-enrichment of each unique nanobody sequence between rounds three and four as well as abundance of each unique nanobody after the final selection (Figure 4.2B). We then chose five unique nanobody sequences from each ranked list for further characterization in vitro and as biosensors in living cells.

Of the eight nanobodies that expressed in bacteria and were crudely purified, none were observed to co-immunoprecipitate with β-arrestin-1 either in the presence or absence of V2Rpp (Figure 4.2E). In contrast, our positive control, MBP-scFv30, co-immunoprecipitated with β-arrestin-1 in a V2Rpp dependent manner (Figure 4.2D). As an additional validation step, we cloned all eight nanobodies into a mApple mammalian expression plasmid and co-expressed them with β2V2R in HEK293s. As β2V2R and β-arrestin redistribute from the plasma membrane to endosomes in response to agonist addition, we reasoned nanobodies that bound β-arrestin-1 would be similarly recruited to endosomes. When all eight nanobodies were imaging in living cells using spinning disk microscopy, we found that one nanobody, Nb9, weakly colocalized with β2V2R/βarr1 at some endosomes (Figure 4.2C). However, as Nb9 did not co-immunoprecipitate with βarr1 and its colocalization was hard to detect, we chose not to pursue this nanobody any further. Taken together, these results suggest that nanobodies that

bind well to β-arrestin-1 were not isolated from the yeast display library with described strategy.

We then asked why our nanobody selections were unsuccessful. One possibility we considered was that β-arrestin-1/V2Rpp complexes were dissociating during the time consuming FACS-based selections. To test this, we conducted a biolayer interferometry experiment where β-arrestin-1/V2Rpp association and dissociation could be assessed directly. Upon probe exposure to V2Rpp, we observed a small, saturable, and concentration dependent wavelength shift that was absent in our unloaded probe, indicating specific binding between β-arrestin-1 and V2Rpp. We further noted that the wavelength shifted rapid upward during association phase and at a similar velocity during the dissociation phase (t1/2on ~ 5 seconds and t1/2off ~5 seconds, respectively (Figure 4.2A). These data suggest that V2Rpp underwent rapid dissociation from βarr1 during our yeast selections, allowing βarr1 to relax back to its inactive state and likely preventing efficient selection of conformationally specific nanobodies.

To get around this, we engineered a cysteine into the V2Rpp binding site in the β-arrestin-1 N-lobe (βarr1(12C) mutant) that we thought may form a disulfide with a naturally occurring cysteine in the V2Rpp. After incubating βarr1(12C) with the V2Rpp in an oxidizing environment, we observed that its apparent molecular weight shifted by roughly the molecular weight of V2Rpp that was reversed by subsequent reduction (Figure 4.3B), indicating formation of a disulfide linked β-arrestin-1/V2Rpp complex. We then validated that this complex was correctly folded by performing a co-immunoprecipitation of the complex, βarr1(12C)-Btn-V2Rpp, and MBP-scFv30, which binds a non-continuous epitope in βarr1. We also verified biotin (btn) conjugated to V2Rpp in the complex was accessible to streptavidin (SAv) by observation of a

gel shift corresponding to the size of the complex plus streptavidin (Figure 4.3C). After these validation steps, we restarted our nanobody selection from the naïve library and used our disulfide complex, βarr1(12C)-Btn-V2Rpp, for three rounds of positive selection. We assessed the resulting yeast library for specific binding to V2Rpp bound, but not disulfide linked, βarr1 or apo β-arrestin-1 by performing pseudo-binding directly on yeast and read out by flow cytometry. We found that the yeast library was enriched for βarr1 binders overall but observed no additional enrichment for V2Rpp bound samples (Figure 4.3D). In summary, these data suggest that βarr1 active state-specific nanobodies are in principle achievable but will require additional troubleshooting steps.

Initial experiments towards developing a cpGFP based βarr1 conformational sensor

An alternative strategy for assessing β-arrestin conformational activation was inspired by development of the GCaMP family of circularly permuted calcium sensors (Nakai, Ohkura et al. 2001). All circularly permuted sensors rely on the coupling a conformational change in the protein of interest to solvent exposure of the fluorochrome in a fluorescent protein. We reasoned that fusion of β-arrestin to cpGFP could couple the conformational twist between the N- and C-lobes of β-arrestin to changes in cpGFP fluorescence (Figure 4.4A). Examination of β-arrestin structures led us to target cpGFP insertion to either the back loop (BL) or the interdomain hinge (IDH), both of which transit the N- and C-lobes (Figure 4.4B). Expression and crude purification of both cpGFP fusions yielded samples whose fluorescence could be detected by eye on a blue light box with yellow filter. To check that both of our cpGFP/β-arrestin-1 fusions were properly folded, we performed fluorescence size exclusion chromatography (FSEC) with each protein alone as well as in the presence of the activating V2Rpp and the stabilizing scFv30. When run alone both cpGFP/β-arrestin fusions produced a

monodisperse fluorescence peak (Figure 4.4C) and subsequent SDS/page showed that they were the expected molecular weight (not shown). Samples where V2Rpp and scFv30 were preincubated with cpGFP/β-arrestin-1 fusions eluted at a lower volume, indicating that these proteins could be recognized by scFv30 (Figure 4.4C). Together, these results suggest that cpGFP insertions into β-arrestin-1 back loop or interdomain hinge are well tolerated and produce fluorescence.

We next assessed if the fluorescence observed in our previous experiments could be altered upon β-arrestin-1 activation. To test this, we collected excitation and emission spectra (excitation not shown) of our back loop fusion alone, βarr1-cpGFP BL, or preincubated with Fab30, V2Rpp, or both Fab30 and V2Rpp. To our surprise, the peak emission intensity was significantly reduced in response to V2Rpp addition and further reduced upon addition of both Fab30 and V2Rpp (Figure 4.4D). As there are many possible reasons for a decrease in fluorescence intensity, we aimed to further assess changes in fluorescence intensity of βarr1-cpGFP BL by preincubating with V2Rpp and Fab30 and then outcompeting their binding to our cpGFP fusion by adding a large concentration of non-fluorescent βarr1. We found that the fluorescence intensity was indeed increased, but surprisingly, did not reach plateau even one hour after βarr1 addition. We also noted that the magnitude of the increase in intensity did not match the decrease from the previous experiment, suggesting that either kinetics of dissociation are very slow or that some fraction of the decrease in fluorescence intensity was due to other factors (Figure 4.4E). Together, these results show that our cpGFP insertions were well tolerated and that the fluorescence of one of them, our back loop construct, may be decreased upon β-arrestin activation.

We next determined if our cpGFP fusions could recruit the plasma membrane, co-cluster with β2V2Rs, and promote β2V2R internalization. First, we performed internalization assays with β2V2R co-expressed with either wild type βarr1, βarr1-cpGFP BL, or βarr1-cpGFP IDH in βarr1/2 DKO cells. We found that while wild type βarr1 produced robust internalization neither of our cpGFP constructs produced significant internalization (Figure 4.5A). A possible explanation for this is that these constructs could not be efficiently recruited to the β2V2R or facilitate their clustering into CCPs. To assess this, we turned to TIRF microscopy. As expected, prior to stimulation with isoproterenol wild type βarr1 and β2V2R were diffusely localized in the cytosol and plasma membrane, respectively. Upon agonist addition, wild type β-arrestin-2 underwent rapid recruitment to the plasma membrane and co-clustered with β2V2R (Figure 4.5B). While agonist-induced recruitment to the plasma membrane was also observed in cells expressing our β-arrestin-1-cpGFP back loop construct, its clustering was markedly reduced, and it failed to promote significant β2V2R clustering (Figure 4.5C). Similar plasma membrane recruitment was observed for the IDH construct, although it neither detectably clustered itself nor promoted β2V2R clustering (Figure 4.5G). These results were verified by quantifying changes in fluorescence intensity (PM recruitment) of βarr1 cpGFP proteins and by measuring clustering of βarr1 and β2V2R (Figure 4.5D-F, H-J). Taken together, these results indicate that insertion of cpGFP into either the back loop or interdomain hinge of β-arrestin-1 results in fusion proteins that undergo agonist-promoted association with β2V2R but fail to promote subsequent clustering and internalization.

A significant caveat of this approach is that it cannot distinguish between βarr1-cpGFP recruitment to the plasma membrane and an increase in fluorescence from βarr1-cpGFP

molecules. However, the latter interpretation is less likely, at least for our back loop construct, as the fluorescence intensity increased in cells and decreased in our in vitro experiments.

4.4 Discussion

Together, our preliminary experiments propose multiple routes towards development of novel β-arrestin biosensors. We show that scFv30, an established biosensor for some class B GPCRs, may detect conformational activation of β-arrestin-1 by class A GPCRs. In addition, our attempts at developing conformational specific nanobodies and initial our experiments into cpGFP-based conformational may be useful to those considering similar strategies.

Since performing these experiments, significant advances in the development of β-arrestin conformational biosensors have been made. Of these developments, two are particularly relevant to the work presented in this chapter. First, Montana Molecular, a private company that specializes in the development of biosensors, has demonstrated a β-arrestin conformational sensor based on cpGFP. In contrast to our approach, they placed portions of cpGFP at the N- and C- termini of β-arrestin, a location that is likely to couple release of the C-terminus to changes in cpGFP (Figure 4.6). The second development is adaptation of the NanoBiT split luciferase complementation system to report on association of scFv30 with β-arrestin-1 (Baidya, Chaturvedi et al. 2022). Compared to fluorescence microscopy where coordinated changes in localization of β-arrestin-1 and scFv30 are inferred to represent association, this system should report only on an increase in the number of scFv30/β-arrestin-1 complexes and is likely to be compatible with high throughput methods. Finally, while these technologies represent major technological developments that allow for new measures β-arrestin conformational activation in living cells, they have yet to be applied to catalytic activation of β-arrestins.

4.5 Materials and Methods

Cell culture

Plasmids

N-terminally FLAG-tagged versions of the human β1AR and β2AR were previously described (Cao, Deacon et al. 1999, Temkin, Lauffer et al. 2011). N-terminally FLAG-tagged β2V2R (Oakley, Laporte et al. 2000) was a gift from Marc Caron.

Clathrin light chain-dsRed was previously described (Merrifield, Feldman et al. 2002).

Mammalian expression plasmids of 2xFYVE-2xFKBP, βarr1-cpGFP back loop, and βarr1-cpGFP interdomain hinge were generated by PCR and InFusion HD cloning (Takara Bio) into the pcDNA3.1 vector. βarr1-mApple and βarr1-FRB-mApple were generated by PCR and InFusion HD cloning (Takara Bio) into the mApple-N1 vector, which was a gift from Michael Davidson (Shaner, Lin et al. 2008).

6xHis-3C-Protein C-βarr1, a plasmid engineered to be cysteine free, was a gift from Brian Kobilka (Huang, Masureel et al. 2020). This parent plasmid was then modified by PCR and InFusion HD cloning (Takara Bio) to generate 6H-3C-Protein C-βarr1, 6H-3C-Protein C-βarr1(12C), 6H-3C-Protein C-βarr1-cpGFP back loop, and 6H-3C-Protein C-βarr1-cpGFP interdomain hinge.

Fab30 was a gift from Arun Shukla (Shukla 2013). Maltose binding protein-tagged scFv30 (MBP-scFv30) was generated by PCR and Gibson assembly. scFv30-HA was generated by PCR and InFusion HD cloning (Takara Bio) into pcDNA3.0.

Nanobody sequences were synthesized (Twist Biosciences) and subcloned into either pET26-b(+) bacterial expression vector by Gibson assembly or mApple-N1 mammalian expression vector by InFusion HD cloning (Takara Bio).

Peptides

V2R phosphopeptides (ARGRpTPPpSLGPQDEpSCpTpTApSpSpSLAKDTSS), untagged or N-terminally labeled with either FITC or biotin, were obtained by custom peptide synthesis (Tufts University Core Facility).

Live cell total internal reflection fluorescence (TIRF) microscopy

TIRF microscopy was performed at 37 °C using a Nikon Ti-E inverted microscope equipped for through-the-objective TIRF microscopy and outfitted with a temperature-, humidity- and CO2-controlled chamber (Okolab). Images were obtained with an Apo TIRF 100X, 1.49 numerical aperture objective (Nikon) with solid-state 405, 488, 561 and 647 nm lasers (Keysight Technologies). An Andor iXon DU897 EMCCD camera controlled by NIS-Elements 4.1 software was used to acquire image sequences every 2 s for 10 min. Unless indicated otherwise, live-cell microscopy assays were performed using HEK 293 cells. Cells were transfected as indicated according to the manufacturer's protocol 48 h before imaging and then plated on poly-l-lysine (0.0001%, Sigma) coated 35-mm glass-bottomed culture dishes (MatTekCorporation) 24h before imaging. Cells were labelled with monoclonal FLAG antibody (M1) (1:1000, Sigma F-3040) conjugated to Alexa Fluor 647 dye (Life Technologies) for 10 min at 37 °C before imaging, washed, and imaged live in DMEM without phenol red (UCSF Cell Culture Facility) supplemented with 30 mM HEPES, pH 7.4 (UCSF Cell Culture Facility). Cells

were treated with bath application of the indicated agonist for experiments shown as time courses.

TIRF microscopy image analysis

Quantitative image analysis was performed on unprocessed images using ImageJ and Fiji software (Schindelin, Arganda-Carreras et al. 2012, Schneider, Rasband et al. 2012). To quantify change in β-arrestin fluorescence over time in TIRF microscopy images, which was reported as plasma membrane recruitment, fluorescence values were measured over the entire time course in a region of interest (ROI) corresponding to the cell. Fluorescence values of the ROI were normalized to initial fluorescence values before agonist addition. Minimal bleed-through and photobleaching was verified using single-labeled and untreated samples, respectively. Line scan analysis of receptor, β-arrestin, or clathrin fluorescence from the shown line were carried out using the Fiji plot profile function to measure pixel values from this line. Clustering index was determined using the skew statistical measurement applied to fluorescence intensity values of β-arrestin–GFP or labeled receptor pixels in a ROI corresponding to the cell.

Spinning disk microscopy

Spinning disk images were acquired at 37°C on a Andor Borealis CSW-W1 spinning disk confocal Nikon Ti Microscope with Andor 4-line laser launch and a temperature-, humidity- and CO2-controlled chamber (Okolab). HEK293 cells transiently expressing constructs were imaged using a 100X 1.40 NA Plan APO VC objective (Nikon) and an Andor Zyla 4.2 sCMOS camera controlled by MicroManager software (Edelstein, Amodaj et al. 2010).

Nanobody selections

To identify nanobodies against the activated βarr1, we used a yeast surface displayed library of synthetic nanobody sequences that was previously described (McMahon, Baier et al. 2018).

Our first approach relied on a cysteine free βarr1 that was bound to unlabeled V2Rpp for selections. For the first round of selection, 5e9 yeast induced in YPG (Yeast Extract-Peptone-Galactose) were washed repeatedly in selection buffer (20 mM HEPES, pH 7.5, 150 mM sodium chloride, 0.1% (w/v) low biotin bovine serum albumin, 5mM calcium chloride, and 5 mM maltose) and finally resuspended in 10 mL of selection buffer. Purified 6H-3C-Protein C-βarr1 and untagged V2Rpp that had been preincubated together for 30 minutes at room temperature were then added to the resuspended yeast at a final concentration of 1 μM and mixed by slow rotation for 30 minutes at room temperature. Yeast were then washed once with selection buffer and an Alexa647 conjugated antibody against the Protein C tag on βarr1 was added and mixed by rotation for 15 minutes at 4°C. Yeast were then washed twice with selection buffer at 4°C followed by addition of 200 uL of anti-Alexa 647 magnetic beads and further incubation at 4°C for minutes. Yeast were again washed with selection buffer and applied to a pre-equilibrated Miltenyi MACS LS column and recovered in YPD. For round 2, 2.5e7 induced yeast from Round 1 were incubated with 1 μM of Biotinylated 6H-3C-AviTag-βarr1 that was prebound to V2Rpp for 10 minutes at room temperature. Yeast were then washed with selection buffer, labeled with Streptavidin conjugated FITC (Thermo Fisher) for 15 minutes at 4°C, washed twice with selection buffer, incubated with anti-FITC magnetic beads (Miltenyl), captured on a Miltenyil LS column, and recovered in YPD. For round 3, a similar approach was taken except that yeast preincubated were selected by fluorescence activated

cell sorting on a Sony SH800. For round 4, induced yeast were precleared by addition of Miltenyi magnetic beads, incubated for 30 minutes at room temperature, washed twice, and applied to a Miltenyi LD column. Recovered yeast were then incubated with biotinylated βarr1 pre-bound to V2Rpp and streptavidin FITC and rotated by mixing for 1 hour at 4°C. These yeast were washed once and then incubated with anti-FITC Miltenyi magnetic beads for 20 minutes at 4°C, washed twice, applied to a Miltenyi LS column, and recovered in YPD.

For our second approach, we induced yeast obtained after the two rounds of selection described above and performed a similar selection by FACS with βarr1 disulfide linked to biotinylated V2Rpp (ProC-βarr1-Btn-V2Rpp).

Deep sequencing library preparation and analysis

To assess nanobody sequence diversity across multiple rounds of selection with cysteine free βarr1 activated by V2Rpp, we extracted DNA using a Yeast Plasmid Miniprep Kit (Zymo Research). We then performed two rounds of PCR to produce nanobody DNA flanked on the 5' end by P5, read one primer, barcode, and phase shifting sequences; and phase shifting, read two primer, i7 indices, and P7 sequences on the 3' end. Four unique i7 indexes corresponded to each round of the nanobody selection. PCR products were then purified by gel extraction and concentration was determined by QuBiT dsDNA assay (Thermo Fisher). DNA from each round was then pooled and submitted for PE250 deep sequencing (Admera).

Sequencing results were assessed for quality and assembled into complete nanobody sequences by joining based on 80 base pairs of overlap between the first and second sequencing reads using the Galaxy platform (Afgan, Baker et al. 2016). Further analysis of the

>130,000 unique nanobody sequences was performed using biopython (Cock, Antao et al. 2009) to determine the diversity of the library at each round, the abundance of individual nanobody sequences in the round 4 library, and the fold enrichment of individual sequences from round 3 to round 4. The latter two metrics were assembled into ranked lists of nanobody sequences from which nanobodies 1-5 and 6-10 were selected, respectively.

Expression and purification of MBP-scFv30

The pMAL-scFv30 plasmid was transformed into BL21(DE3) E. coli, grown in Terrific broth at 37 °C until OD500 0.7-0.8, and induced with 500 μM IPTG for 18-22 hours at 20 °C. Coli were harvested and resuspended in SET Buffer (200 mM Tris, pH 8.0, 500 mM sucrose, 0.5 mM EDTA, 1X cOmplete protease inhibitor (Roche), and a small amount of lysozyme), for 30 minutes at 25 °C before a 45-minute osmotic shock with a two-fold volume addition of water. Lysate was then clarified by centrifugation at 16,000xg for 30 minutes and loaded onto a column containing 3 mL of settled amylose resin. Resin was washed with 20 bed volumes of 20 mM HEPES, pH 7.4, 100 mM NaCl and eluted with 20 mM HEPES, pH 7.4, 100 mM NaCl, and 10 mM maltose. Eluate was concentrated using a 50k MWCO centrifugal filter unit and loaded on 10/300 Superdex 200 GL column. Fractions corresponding to the correct molecular weight were pooled, concentrated in 20 mM HEPES, pH 7, 100 mM NaCl, 20% glycerol buffer, and flash frozen with liquid nitrogen.

Expression and purification of Fab30

Fab30 was expressed and purified as describe previously (Shukla 2013)

Expression and purification of β-arrestin-1

All β-arrestin-1 purifications were initiated by transformation into BL21(DE3) E. coli, grown in terrific broth at 37°C until OD500 was 1.0-2.0, induced with 50-100 μM IPTG for 20-24 hours at 20 °C. E. coli were harvested and then resuspended in cold lysis buffer (20 mM HEPES, pH 7.5, 500 mM NaCl, 15% glycerol, 7.13 mM βME, 25 U/μl benzonase, 2 μg/ml leupeptin, with 1-2 mg of lysozyme), passed through a microfluidizer, and centrifuged at 16,000xg for 30 minutes. Clarified lysate was applied to a column of pre-equilibrated HisPur Ni-NTA resin (Thermo Scientific) which was then washed with 20 column volumes of wash buffer 1 (20 mM HEPES pH 7.0, 500 mM NaCl, 20 mM Imidazole, 10% glycerol, 7.13 mM βME), 20 column volumes of wash buffer 2 (20 mM HEPES, pH 7.0, 500 mM NaCl, 40 mM Imidazole, 10% glycerol, 7.13 mM βME), eluted with 3 bed volumes of 20 mM HEPES, pH 7.0, 500 mM NaCl, 200 mM Imidazole, 10% glycerol, 7.13 mM BME. Eluate was then transferred to 10k MWCO Snakeskin dialysis tubing (Thermo Scientific) and incubated overnight in 20 mM HEPES, 7.0, 100 mM NaCl, 7.13 mM BME. The sample was then diluted to 20 mM HEPES, pH 7.0, 80 mM NaCl by addition of ice cold 20 mM HEPES, pH 7.0 buffer, applied to a MonoQ column, washed with 10 column volumes with 20 mM HEPES, pH 7.0, 80 mM NaCl, and eluted at 20 mM HEPES, pH 7.0, 180-250 mM NaCl. Fractions corresponding to the correct molecular weight were pooled, concentrated using a 10k MWCO centrifugal filter, and loaded onto a 10/300 Superdex S200. Fractions corresponding to the correct molecular weight were again pooled, glycerol was added to 20%, concentrated, and flash frozen in liquid nitrogen.

This protocol was altered for each of the following β-arrestin-1 constructs. βME was excluded for the cysteine free constructs, 6H-3C-ProC-βarr1 and 6H-3C-AviTag-βarr1. Size exclusion chromatography was omitted for βarr1-cpGFP back loop. Finally, AviTag βarr1 was

biotinylated with BirA according to the manufacturers protocol (Avidity). Near complete biotinylation of βarr1 was verified by observing a molecular weight shift on an SDS/PAGE gel that corresponded to the size of neutravidin.

Formation and verification of a disulfide linked βarr1(12C)-Btn-V2Rpp complex

Purified 6H-3C-Protein C-βarr1(12C) at 5 μM was mixed with 1 μM V2Rpp and incubated for 20 minutes at room temperature, and then transferred to a 2k MWCO Slide-a-lyzer (Thermo Scientific). Dialysis was carried out in 2L 20 mM HEPES, pH 7.0, 150 mM NaCl for at room temperature for three days. Nearly all βarr1(12C) had formed a disulfide linked complex with V2Rpp complex formation based on molecular weight shifts corresponding to the molecular weight of V2Rpp on an SDS/PAGE gel.

Expression and purification of Nanobodies

Nanobody sequences were cloned into the pET26-b(+) expression vector using In-Fusion HD cloning (Takara Bio), transformed into BL21(DE3) E. coli, grown in Terrific Broth at 37 °C until OD 0.7-0.8, followed by gene induction using 1 mM IPTG for 18-22 hours at 25°C. E. Coli were harvested and resuspended in SET Buffer (200 mM Tris, pH 8.0, 500 mM sucrose, 0.5 mM EDTA, 1X cOmplete protease inhibitor (Roche)) for 30 minutes at 25 °C before a 45 minute osmotic shock with a two-fold volume addition of water. NaCl, MgCl2, and imidazole were added to the lysate to 150 mM, 2 mM, and 40 mM respectively before centrifugation at 20,000xg for 15 minutes to separate cell debris from the periplasmic fraction. For every liter of bacterial culture, the periplasmic fraction was then slowly applied to a column containing 2 mL of packed HisPur Ni-NTA resin (Thermo Scientific) which had been equilibrated in Nickel Wash Buffer (20 mM HEPES, pH 7.5, 150 mM NaCl, 40 mM imidazole). The resin was then washed

with at least 50 bed volumes of Nickel Wash buffer. Bound proteins were then eluted using four bed volumes of Elution Buffer (20 mM HEPES, pH 7.5, 150 mM NaCl, 500 mM imidazole). Nanobodies were then transferred to 3.5 MWCO Snakeskin dialysis tubing (Thermo Scientific), sealed, and dialyzed overnight in 20 mM HEPES, pH 7.5, 150 mM NaCl at 4°C. Nanobodies were concentrated again using a 3.5k MWCO centrifugal filter unit, and flash frozen in liquid nitrogen.

Anti-Protein C tag co-immunoprecipitations

Co-immunoprecipitation experiments were performed by coincubation of purified Protein-C tagged β-arrestin-1 with the indicated peptides or proteins (concentrations in the figure legends) and anti-Protein C tag Sepharose in binding buffer (20 mM HEPES, 150 mM NaCl, 2 mM $CaCl_2$) for at least 30 minutes at room temperature with gentle agitation. Sepharose was then washed at least three times with 500 ul of cold binding buffer. Binding buffer was then removed and Sepharose was incubated with 50-100 uL of elution buffer (20 mM HEPES, pH 7.5, 150 mM NaCl, 5 mM EDTA, 0.5 mg/ml Protein C peptide) at room temperature for at least 30 minutes. Eluate was then removed and Laemelli sample buffer supplemented with 7.13 mM βME was added. Samples were either run SDS/PAGE gels immediately or after storage at -20°C.

Biolayer interferometry (BLI)

BLI studies were carried out on an Octet RED384 instrument at 24°C with shaking at 1000 RPM. BLI assay buffer consists of 2% BSA in 20 mM HEPES, pH7.5, 150 mM NaCl, which was 0.22-μm filtered. Before use, (anti-biotin) streptavidin (SA) biosensors were loaded into the columns of a biosensor holding plate and pre-hydrated in BLI assay buffer for 10 min. Flat

bottom 384-well microplates were loaded with 45 µL per well. The assay plate was prepared with one well containing BLI assay buffer alone (reference) and seven wells of containing 20 nM βarr1 in assay buffer. Loading took place over 5 minutes, wash took place over 2 minutes, association over one minute, and dissociation over 140 seconds. Traces during association and dissociation phases from each well are shown.

Pseudo binding to nanobodies displayed on yeast surface by flow cytometry

After three rounds of positive selection with βarr1(12C)-Btn-V2Rpp, yeast were induced with YPG (Yeast Extract-Peptone-Galactose) for 24 hours, washed repeatedly in selection buffer (20 mM HEPES, pH 7.5, 150 mM sodium chloride, 0.1% (w/v) low biotin bovine serum albumin, 5mM calcium chloride, and 5 mM maltose) and finally resuspended in selection buffer with no additions, Btn-βarr1, or Btn-βarr1 and V2Rpp. Yeast were then incubated for 30 minutes, washed once with selection buffer, and labeled by addition of APC- or FITC-labeled streptavidin for 10 minutes, washed once, and run on the flow cytometer.

Flow cytometry-based internalization assay

Internalization assays were performed with βarr1/2 DKO HEK 293A cells. Cells were transfected according to the manufacturer's protocol 24 hours before beginning the assay. The next morning cells were lifted using TrypLE express (Thermo Fisher), resuspended in complete media, transferred to 12-well plates in triplicate, and incubated under standard culture conditions for three hours to allow them to adhere. Cells were then treated with agonist for the indicated time and placed on ice to stop trafficking. Cells were washed once with ice cold PBS and FLAG-tagged surface receptors were labeled with M1 conjugated to Alexa Fluor 647 for 30 minutes at 4°C while shaking. Surface staining was measured using a CytoFlex (Beckman

Coulter) and gated for single cells expressing EGFP. Mean M1-647 fluorescence measured in the APC channel. Percent internalization was calculated by dividing agonist treated by untreated conditions, subtracting the result from one, and multiplying by 100.

Fluorescence size exclusion chromatography (FSEC)

Binding of cpGFP containing β-arrestin-1 proteins to scFv30 was tested by preincubation of crudely purified 6H-3C-ProC-βarr1-cpGFP back loop and interdomain hinge proteins with 1 μM scFv30 and 5 μM V2Rpp in binding buffer (20 mM HEPES, pH 7.5, 150 mM NaCl) at room temperature for 30 minutes. Samples, including indicated controls, were sequentially loaded onto a Superdex S200 Increase 10/300 GL column (GE Healthcare) and fluorescence of cpGFP was measured.

β-arrestin-1-cpGFP back loop fluorescence measurements

Fluorescence properties of βarr1-cpGFP back loop, including excitation (not shown) and emission spectra (excited at 470 nm), were measured on a Horiba Jobin Yvon FluoroMax spectrofluorometer. Fluorescence emission spectra were measured after 1 hour room temperature preincubation of 200 nM βarr1-cpGFP back loop alone, or with 5 μM V2Rpp or 1 μM Fab30, or both Fab30 and V2Rpp. Quantification of fluorescence changes was done by normalizing all conditions the maximum fluorescence of βarr1-cpGFP back loop.

Changes in fluorescence intensity over time were measured after one-hour preincubation of 200 nM βarr1-cpGFP backloop with 5 μM V2Rpp and1 μM Fab30. BSA (0.13% final concentration) or dark βarr1 (5 μM final concentration) were added immediately before starting the time course and fluorescence measurements were made every 30 seconds for one hour.

4.6 References

Afgan, E., et al. (2016). The Galaxy platform for accessible, reproducible and collaborative biomedical analyses: 2016 update. *Nucleic Acids Res 44*(W1): W3-W10. 10.1093/nar/gkw343

Baidya, M., et al. (2022). Allosteric modulation of GPCR-induced β-arrestin trafficking and signaling by a synthetic intrabody. *bioRxiv*: 2022.2001.2011.475811. 10.1101/2022.01.11.475811

Baidya, M., et al. (2020). Genetically encoded intrabody sensors report the interaction and trafficking of β-arrestin 1 upon activation of G-protein–coupled receptors. *J. Biol. Chem. 295*(30): 10153-10167. 10.1074/jbc.RA120.013470

Cao, T. T., et al. (1999). A kinase-regulated PDZ-domain interaction controls endocytic sorting of the beta2-adrenergic receptor. *Nature 401*(6750): 286-290. 10.1038/45816

Cock, P. J., et al. (2009). Biopython: freely available Python tools for computational molecular biology and bioinformatics. *Bioinformatics 25*(11): 1422-1423. 10.1093/bioinformatics/btp163

Edelstein, A., et al. (2010). Computer control of microscopes using microManager. *Curr Protoc Mol Biol Chapter 14*: Unit14 20. 10.1002/0471142727.mb1420s92

Eichel, K., et al. (2018). Catalytic activation of β-arrestin by GPCRs. *Nature 557*(7705): 381-386. 10.1038/s41586-018-0079-1

Eichel, K., et al. (2016). β-Arrestin drives MAP kinase signalling from clathrin-coated structures after GPCR dissociation. *Nat. Cell Biol. 18*(3): 303-310. 10.1038/ncb3307

Ghosh, E., et al. (2019). Conformational Sensors and Domain Swapping Reveal Structural and Functional Differences between β-Arrestin Isoforms. *Cell Rep. 28*(13): 3287-3299.e3286. 10.1016/j.celrep.2019.08.053

Gurevich, V. V. and E. V. Gurevich (2018). Arrestin-mediated signaling: Is there a controversy? *World J Biol Chem 9*(3): 25-35. 10.4331/wjbc.v9.i3.25

Huang, W., et al. (2020). Structure of the neurotensin receptor 1 in complex with β-arrestin 1. *Nature 579*(7798): 303-308. 10.1038/s41586-020-1953-1

Kang, D. S., et al. (2014). Role of β-arrestins and arrestin domain-containing proteins in G protein-coupled receptor trafficking. *Curr. Opin. Cell Biol. 27*: 63-71. 10.1016/j.ceb.2013.11.005

Lee, M.-H., et al. (2016). The conformational signature of β-arrestin2 predicts its trafficking and signalling functions. *Nature 531*(7596): 665-668. 10.1038/nature17154

Lohse, M. J., et al. (1990). beta-Arrestin: a protein that regulates beta-adrenergic receptor function. *Science 248*(4962): 1547-1550. 10.1126/science.2163110

McMahon, C., et al. (2018). Yeast surface display platform for rapid discovery of conformationally selective nanobodies. *Nat Struct Mol Biol 25*(3): 289-296. 10.1038/s41594-018-0028-6

Merrifield, C. J., et al. (2002). Imaging actin and dynamin recruitment during invagination of single clathrin-coated pits. *Nat. Cell Biol. 4*(9): 691-698. 10.1038/ncb837

Nakai, J., et al. (2001). A high signal-to-noise Ca(2+) probe composed of a single green fluorescent protein. *Nat Biotechnol 19*(2): 137-141. 10.1038/84397

Nobles, K. N. (2011). Distinct phosphorylation sites on the β(2)-adrenergic receptor establish a barcode that encodes differential functions of β-arrestin. *Sci. Signal. 4*. 10.1126/scisignal.2001707

Nuber, S., et al. (2016). β-Arrestin biosensors reveal a rapid, receptor-dependent activation/deactivation cycle. *Nature 531*(7596): 661-664. 10.1038/nature17198

Oakley, R. H., et al. (2000). Differential affinities of visual arrestin, βarrestin1, and βarrestin2 for G protein-coupled receptors delineate two major classes of receptors. *J. Biol. Chem. 275*(22): 17201-17210.

Pierce, K. L., et al. (2002). Seven-transmembrane receptors. *Nat. Rev. Mol. Cell Biol. 3*(9): 639-650. 10.1038/nrm908

Rajagopal, S. and S. K. Shenoy (2018). GPCR desensitization: Acute and prolonged phases. *Cell. Signal. 41*: 9-16. 10.1016/j.cellsig.2017.01.024

Rosenbaum, D. M., et al. (2009). The structure and function of G-protein-coupled receptors. *Nature 459*(7245): 356-363. 10.1038/nature08144

Schindelin, J., et al. (2012). Fiji: an open-source platform for biological-image analysis. *Nat. Methods 9*(7): 676-682. 10.1038/nmeth.2019

Schneider, C. A., et al. (2012). NIH Image to ImageJ: 25 years of image analysis. *Nat. Methods 9*(7): 671-675. 10.1038/nmeth.2089

Shaner, N. C., et al. (2008). Improving the photostability of bright monomeric orange and red fluorescent proteins. *Nat Methods 5*(6): 545-551. 10.1038/nmeth.1209

Shukla, A. K. (2013). Structure of active β-arrestin-1 bound to a G-protein-coupled receptor phosphopeptide. *Nature 497*. 10.1038/nature12120

Shukla, A. K., et al. (2013). Structure of active β-arrestin-1 bound to a G-protein-coupled receptor phosphopeptide. *Nature 497*(7447): 137-141. 10.1038/nature12120

Shukla, A. K., et al. (2011). Emerging paradigms of β-arrestin-dependent seven transmembrane receptor signaling. *Trends Biochem. Sci. 36*(9): 457-469. 10.1016/j.tibs.2011.06.003

Temkin, P., et al. (2011). SNX27 mediates retromer tubule entry and endosome-to-plasma membrane trafficking of signalling receptors. *Nat. Cell Biol. 13*(6): 715-721. 10.1038/ncb2252

4.6 Figures

Figure 4.1 scFv30 does not require receptor activation to be recruited to β-arrestin

A-C) TIRF microscopy images of scFv30-tYFP (green), βarr1-mApple (magenta), and either β1AR (a), β2AR (b), or β2V2R (c) (all blue) pre- and post-stimulation with 10 μM of the adrenergic agonist isoproterenol (Iso) in HEK293. Insets correspond to roughly the center of each cell. **D, E**) Quantification of plasma membrane recruitment (see methods) of scFv30-tYFP and βarr1-mApple, respectively. **F**) Rapamycin induced recruitment of βarr1-mApple-FRB to 2xFYVE-2xFKBP at endosomes in HEK293 cells expressing scFv30-tYFP. **G**) Diagram of results observed in F. **H**) Co-immunoprecipitation of β-arrestin-1 in cells expressing scFv30 and either β1AR or β2V2R before and after stimulation with 10 μM of isoproterenol for the indicated period.

Figure 4.2 Nanobody selection with wild type βarr1 activated with V2Rpp did not yield biosensors.

A) Selection strategy from naïve nanobody yeast surface display through round four. Green indicates positive selection while red indicates negative selection (see methods). **B**) Library diversity and enrichment at each round of selection determined by deep sequencing of nanobody DNA extract from yeast and PCR amplified. Inset shows the fraction of unique nanobodies at each round of selection. **C**) Live-cell spinning disk microscopy images of Nb9-mApple or mApple co-expressed with βarr1-EGFP and FLAG-tagged β2V2R after 20 minutes of stimulation with isoproterenol showing weak Nb9 colocalization at endosomes (yellow arrows denote example endosomes). **D**) Positive control coimmunoprecipitation and Coomassie of purified Protein C-tagged β-arrestin-1 (5 μM) incubated with purified MBP-scFv30 (10 μM) showing that V2Rpp (10 μM) potentiates β-arrestin-1-scFv30 binding (see methods). **E**) Immunoprecipitation and Coomassie of purified Protein C-tagged β-arrestin-1 (5 μM) mixed with nanobodies (10 μM) obtained from selection strategy shown in a and b, showing no detectable binding irrespective of V2Rpp (10 μM).

Figure 4.3 Disulfide linked βarr1-V2Rpp complex did not yield a nanobody library enriched for βarr1 active state binders

A) Association and dissociation of multiple concentrations of V2Rpp from purified and biotinylated β-arrestin-1 measured by biolayer interferometry (BLI). **B**) SDS/PAGE and Coomassie stain after incubation of βarr1(12C) (1 μM) in the presence or absence of biotinylated (Btn) V2Rpp (10 μM) under oxidizing conditions and the subsequent reduction by β-mercaptoethanol, showing a reversible molecular weight shift corresponding to the molecular weight of V2Rpp. **C**) Immunoprecipitation of βarr1(12C)-V2Rpp disulfide complex (1 μM) in the presence of MBP-scFv30 (5 μM). **D**) Pseudo-binding of the indicated conditions on yeast measured by flow cytometry after three rounds of positive selection using βarr1(12C)-V2Rpp disulfide complex (see methods), showing a lack of enrichment for V2Rpp bound Btn-β-arrestin-1.

Figure 4.4 Strategy and in vitro characterization of two β-arrestin-1-cpGFP conformation sensors.

A) Diagram of a β-arrestin conformational transition from inactive to active (C-lobe rotated ~20°) states and its desired effect on circularly permuted GFP (cpGFP) fluorescence. **B**) cpGFP insertion sites in either the back loop or interdomain hinge regions of β-arrestin, both of which span the N- and C-lobes. **C**) Fluorescence size exclusion chromatography runs of βarr1-cpGFP back loop (BL, blue), βarr1-cpGFP interdomain hinge (IDH, green), scFv30 (red), BL pre-incubated with scFv30 and V2Rpp (cyan), or IDH pre-incubated with scFv30 and V2Rpp (purple). Shift to lower elution volume indicates complex formation. **D**) Emission spectra of βarr1-cpGFP BL alone (blue) or pre-incubated with either Fab30 (green), V2Rpp (orange), or both Fab30 and V2Rpp (cyan). Inset is the maximum intensity of each condition normalized to βarr1-cpGFP BL. **E**) Fluorescence of βarr1-cpGFP BL (200 nM) pre-incubated with V2Rpp (1.3 μM) and Fab30 (350 nM). Kinetic trace begins shortly after addition of BSA (2 μM) or unlabeled βarr1 (6 μM).

Figure 4.5 cpGFP incorporation into the β-arrestin back loop or interdomain hinge prevents clustering and internalization across a range of GPCRs

A) Internalization of wild-type β-arrestin-1 and β-arrestin-1 with two different cpGFP insertion sites, one in the back loop (BL) and another in the interdomain hinge (IDH). **B, C, G**) TIRF microscopy images of clathrin-light-chain-DsRed and FLAG-tagged β2V2R with either wild type β-arrestin-2 (b), β-arrestin-1-cpGFP back loop (BL) (c), or β-arrestin-1-cpGFP interdomain hinge (IDH (g) before (top) and after (bottom) stimulation with the adrenergic agonist isoproterenol (Iso). **D, E**) Quantification of TIRF microscopy measuring plasma membrane recruitment (d) and clustering (e) of wild-type β-arrestin-2 in response to β2V2R activation (purple) or β-arrestin-1-cpGFP BL in response to activation of β2V2R (green), β2AR (pink), or β1AR (black). **F**) Quantification of receptor clustering observed by TIRF microscopy. Conditions and their corresponding colors are the same as shown in d and e. **H, I**) Quantification of TIRF microscopy measuring plasma membrane recruitment (h) and clustering (i) of wild-type β-arrestin-2 in response to β2V2R activation (purple) or β-arrestin-1-cpGFP IDH in response to activation of β2V2R (green), β2AR (pink), or β1AR (black). **J**) Quantification of receptor clustering observed by TIRF microscopy. Conditions and corresponding colors are the same as shown in h and j. n=1 for all experiments.

Figure 4.6 AlphaFold2 structure of a previously characterized β-arrestin circularly permuted mNeonGreen conformation biosensor

A) AlphaFold2 generated structure showing both the N- and C-lobes of β-arrestin as well as the β-arrestin tail bound to the N-lobe. Part of mNeonGreen is fused to the β-arrestin N-terminus (light green) and the other section is fused the β-arrestin C-terminus. **B**) The same structure rotated and viewed from the C-lobe of β-arrestin, showing where mNeonGreen transitions to β-arrestin and where β-arrestin transitions to the other portion of mNeonGreen.

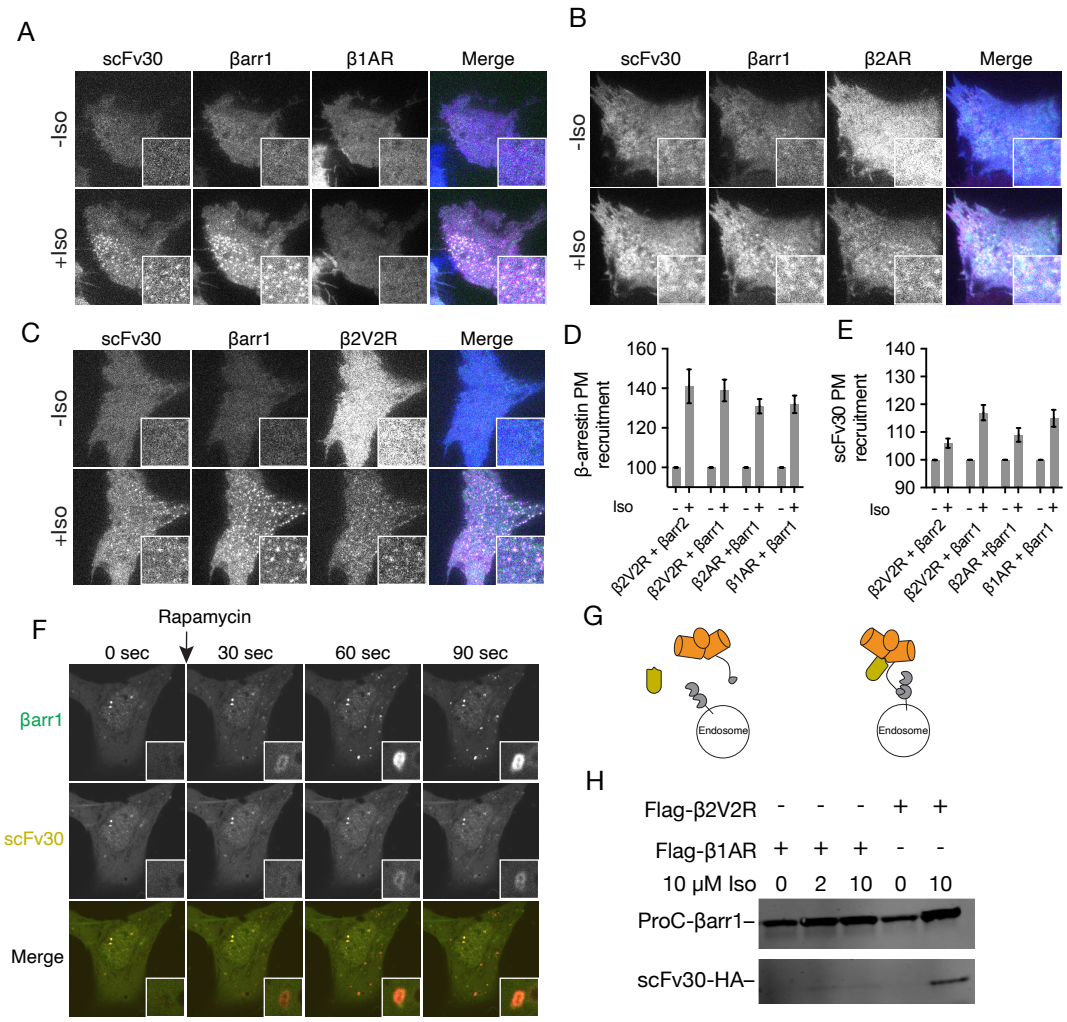

Figure 4.1 scFv30 does not require receptor activation to co-recruitment with β-arrestin

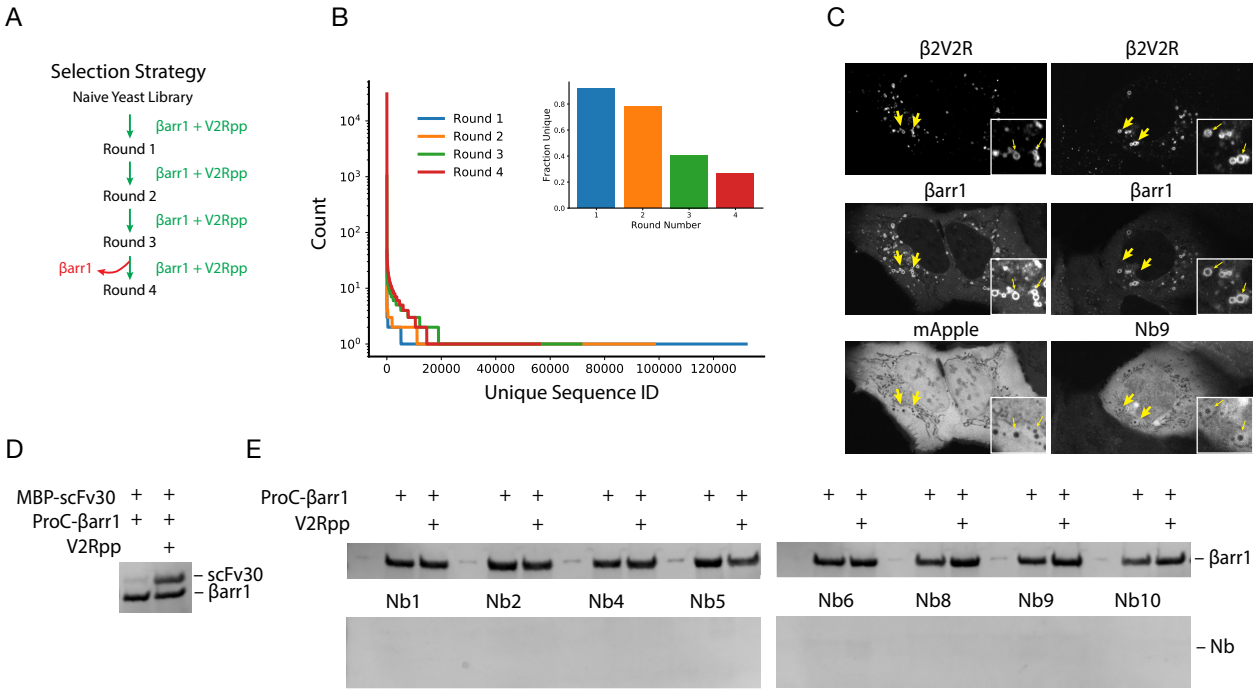

Figure 4.2 Nanobody selection with wild type βarr1 activated with V2Rpp did not yield biosensors.

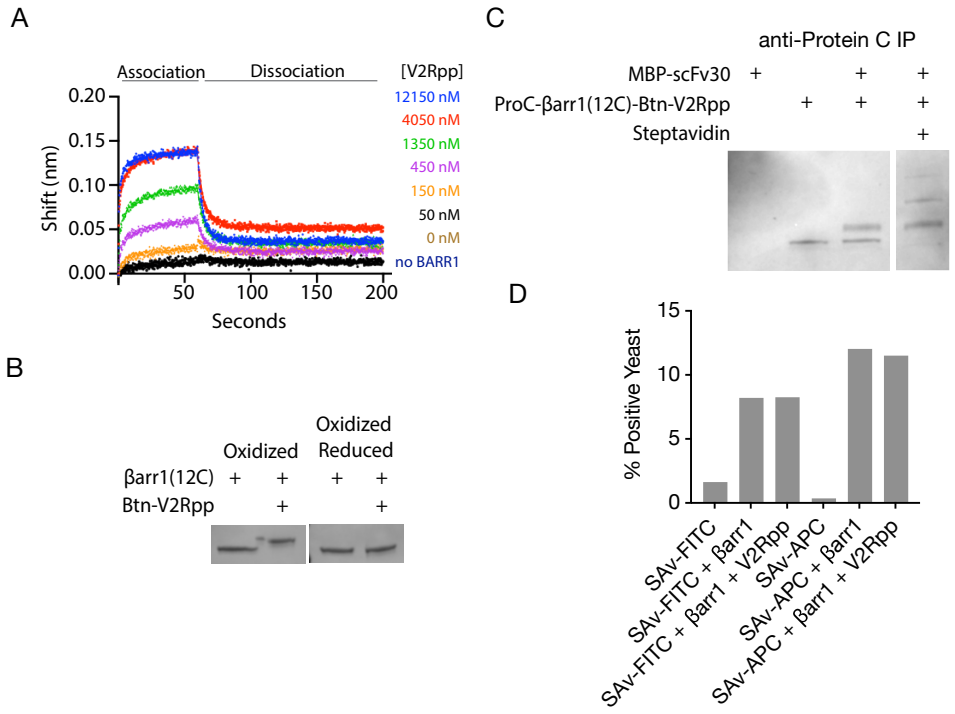

Figure 4.3 Disulfide linked βarr1-V2Rpp complex did not yield a nanobody library enriched for βarr1 active state binders

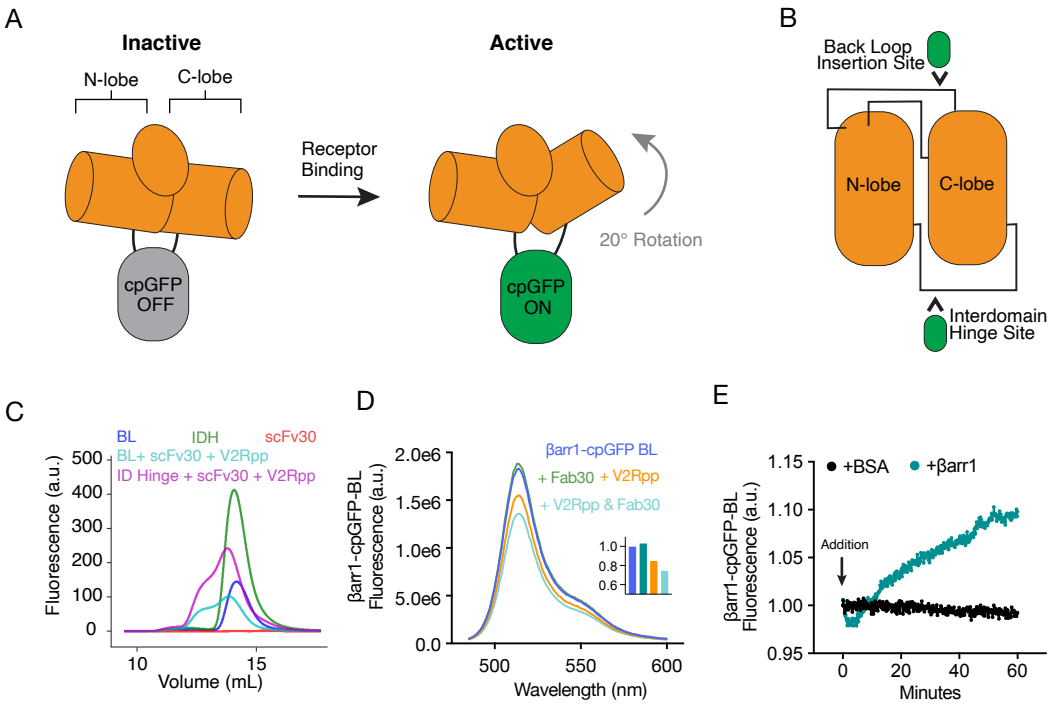

Figure 4.4 Strategy and in vitro characterization of two β-arrestin-1-cpGFP conformation sensors.

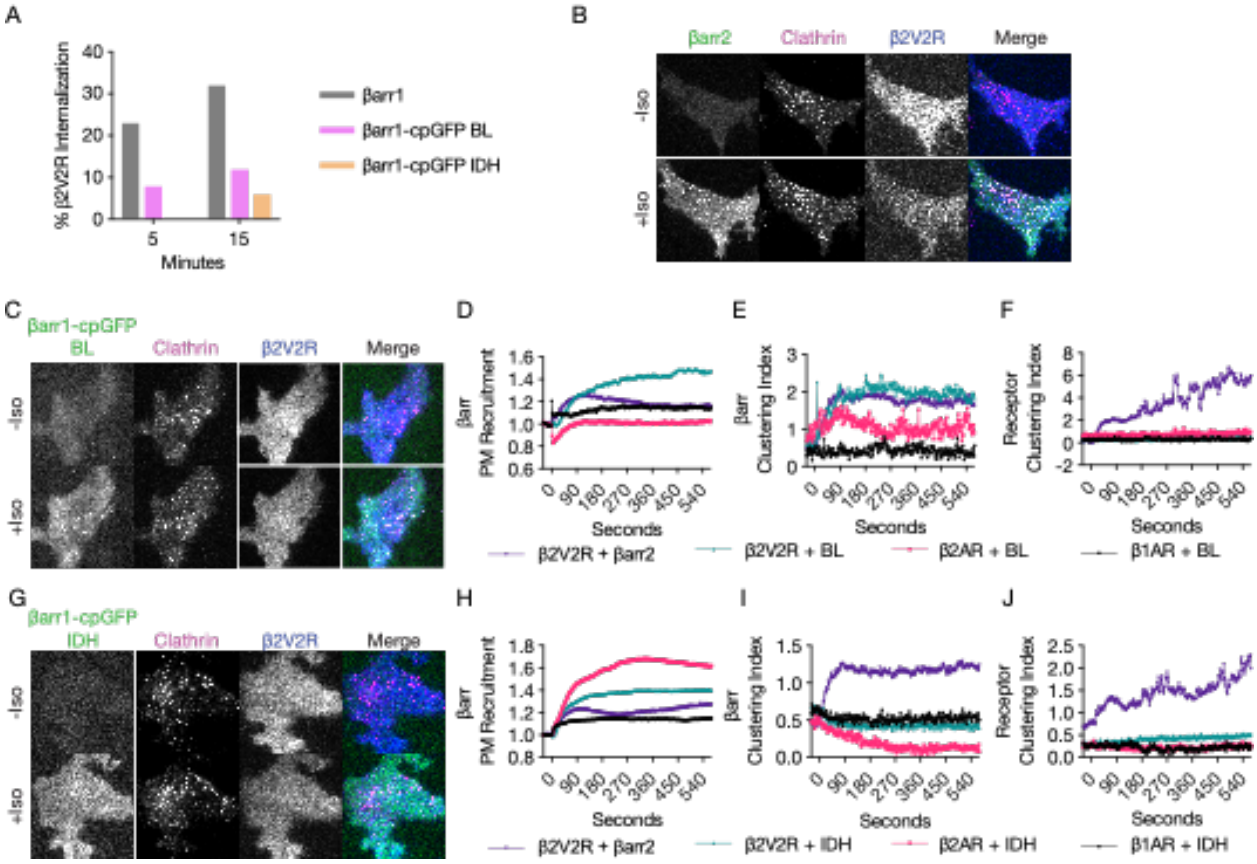

Figure 4.5 cpGFP incorporation into the β-arrestin back loop or interdomain hinge prevents GPCR clustering and internalization

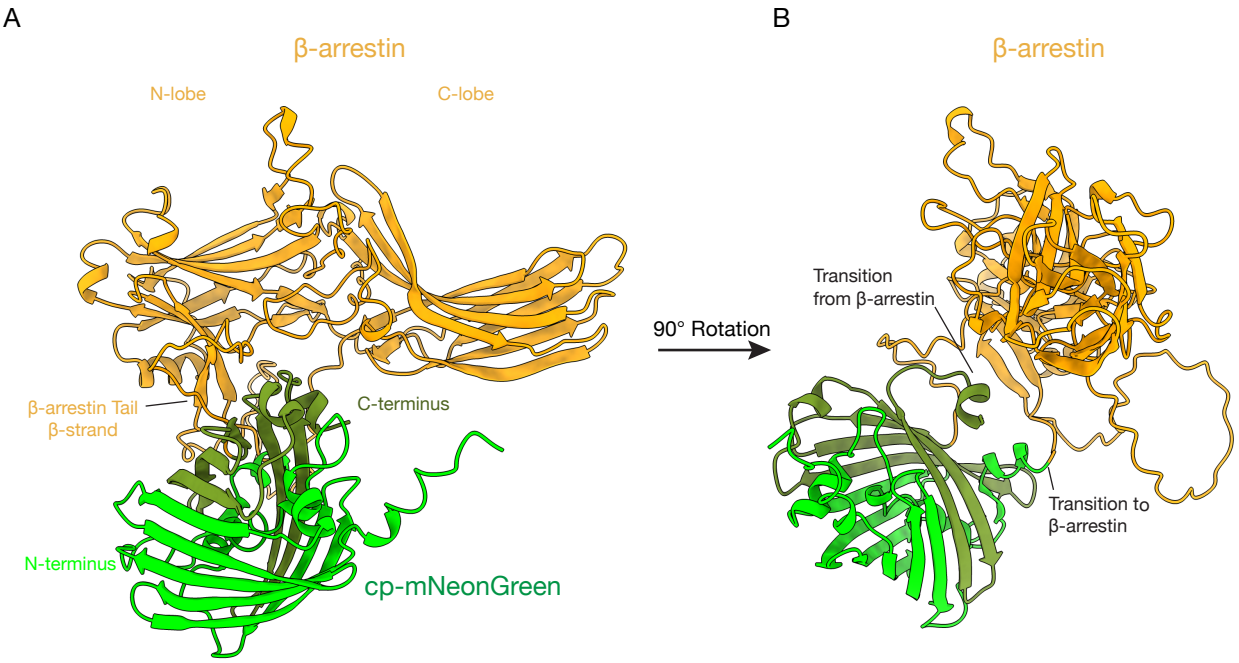

Figure 4.6 AlphaFold2 structure of a previously characterized β-arrestin circularly permuted mNeonGreen conformation sensor.

Chapter 5: A cellular basis for GPCR-biased control of the endocytic network by β-arrestin

Benjamin Barsi-Rhyne, in the laboratories of Aashish Manglik and Mark von Zastrow (UCSF), conceived the project, executed all the experiments, and wrote the following chapter. Mark von Zastrow contributed to project development, data analysis, and writing the following chapter.

5.1 Abstract

β-arrestins were named for their ability to desensitize or 'arrest' ligand-dependent GPCR signaling and are now known to be flexible regulators that also promote signaling by engaging the endocytic network through association with clathrin-coated pits (CCPs) (Lohse, Benovic et al. 1990, Irannejad and von Zastrow 2014, Eichel and von Zastrow 2018). CCP association is triggered by GPCR binding to β-arrestin, and distinct GPCR can produce different signaling effects through β-arrestins that depend on conformational differences imposed at the GPCR/β-arrestin interface (Tian, Kang et al. 2014, Gurevich and Gurevich 2019, Latorraca, Masureel et al. 2020). However, it remains unknown whether or how GPCR-specific control is communicated downstream to the endocytic network, as the current understanding holds that only a single conformation-sensitive determinant in β-arrestin – the β-arrestin C-terminus (CT) – mediates the GPCR-triggered association. We revise this view by showing that the β-arrestin CT, while sufficient to promote agonist-induced clustering of β2-adrenergic receptors in CCPs, only weakly drives endocytosis of receptors after clustering. We define a second determinant in β-arrestin, located on the cytosolic base of the β-arrestin C-lobe (CLB), which also promotes receptor clustering but – unlike the CT – strongly drives endocytosis after clustering. We further show that these discrete trafficking determinants can operate in tandem but are differentially deployed in a receptor-specific manner. Moreover, we provide evidence suggesting that deployment of each determinant is oppositely coupled to the formation of functionally distinct GPCR/β-arrestin complexes – with CLB deployment stabilizing a desensitized complex and CT deployment enabling prolonged signaling. Together, these findings revise the model of how β-arrestins function as regulated endocytic adaptors and reveal a simple allosteric 'code' explaining how β-arrestin can transduce GPCR-biased information to the endocytic network.

5.2 Introduction

β-arrestins are paralogs of visual arrestins that have the unique, additional property of engaging the endocytic network by clustering in clathrin-coated pits (CCPs) after GPCR-triggered conformational activation. The prevailing view is that this endocytic activity requires displacement of the β-arrestin C-terminus, a determinant that is exposed upon binding of phosphorylated GPCRs to the β-arrestin N-lobe and contains clathrin (CHC) and AP2 (AP2-β) -binding motifs not present in the C-terminus of visual arrestins (Extended Data Figure 5.1A) (Goodman, Krupnick et al. 1996, Laporte, Oakley et al. 2000, Moaven, Koike et al. 2013, Tian, Kang et al. 2014). This model is well supported by structural and biophysical studies, and by cell biological studies demonstrating dominant-negative effects of the β-arrestin CT on GPCR trafficking (Krupnick, Santini et al. 1997, Orsini and Benovic 1998, Schmid, Ford et al. 2006, Kang, Kern et al. 2009). However, to our knowledge, it remains unknown if the β-arrestin CT is required for triggered internalization. We tested this using a genetic rescue strategy in HEK293 cells engineered using CRISPR to lack both endogenous β-arrestins (βarr1/2 DKO) (O'Hayre, Eichel et al. 2017).

5.3 Results

β-arrestin C-terminus is dispensable for β2AR internalization

We focused on the β2-adrenergic receptor (β2AR) as a prototype for β-arrestin-dependent endocytosis via CCPs. We first examined lateral clustering of receptors into clathrin-coated pits on the plasma membrane, which is the initiating agonist-triggered step. To assess this, we used total internal reflection fluorescence microscopy (TIRFM) to image the basal plasma membrane of βarr1/2 DKO cells with a high signal-to-noise ratio. β2ARs remained diffusely distributed in the plasma membrane irrespective of agonist exposure in cells not expressing recombinant β-arrestin (Figure 5.1A), verifying functionally that these cells lack endogenous β-arrestin. In cells expressing recombinant β-arrestin (βarr2-EGFP), β2ARs were also diffusely distributed in the absence of agonist. Indicating rescue of wild type behavior, application of the β-adrenergic agonist isoproterenol (Iso) promoted robust recruitment of βarr2-EGFP to the plasma membrane and co-clustering with β2ARs in CCPs.

We were surprised to observe similarly robust co-clustering after Iso application in cells rescued with a βarr2 mutant construct in which critical CHC and AP2β binding residues present in the β-arrestin CT were disrupted by a previously described set of point mutations (βarr2(CCS) construct) (Eichel, Jullié et al. 2018). A similarly strong genetic rescue of clustering was also observed after full removal of the β-arrestin CT by truncation (βarr2(372T) construct) (Figure 5.1C-E). Consistent with the co-clustering phenotype, β-arrestin-2 devoid of its C-terminal CCP binding elements supported robust agonist-induced β2AR internalization in two different βarr1/2 DKO cell lines (Figure 5.1F), the first of which is used in all subsequent experiments unless otherwise noted. Further, β-arrestin C-terminus independent trafficking appears to be a general phenomenon as similar clustering and internalization results were

obtained across two GPCRs that differ substantially in their relative affinity for β-arrestins, the β2AR which has relatively low affinity (‘class A’) and a β2V2R receptor chimera that has higher affinity (’class B’) due to a more extensive phosphorylation (Extended Data Figure 5.1B-D) (Oakley, Laporte et al. 2000, Oakley, Laporte et al. 2001). Nevertheless, receptor internalization measured in our experiments was still dependent on receptor phosphorylation because a mutant β2AR lacking major phosphorylation sites (β2AR(3A) mutant) had significantly reduced internalization relative to wild type β2AR (Extended Data Figure 5.1E). Furthermore, the ability of β-arrestin to drive GPCR trafficking in the absence of the CT is not unique to βarr2 because a mutant β-arrestin-1 construct lacking the CT (βarr1(376T) construct) also promoted iso-induced β2AR internalization (Extended Data Figure 5.1F). Together, these observations indicate that the β-arrestin C-terminus is not essential for agonist-induced β2AR clustering and endocytosis. As β-arrestins are essential for these functions, we hypothesized that β-arrestins contain another determinant that is sufficient to promote both GPCR-triggered clustering and internalization.

Cytosolic face of βarr2 contains a discrete endocytic determinant

As an independent means to test this hypothesis, we took advantage of the observation that visual arrestin (v-arr) naturally lacks functional endocytic motifs in its C-terminus (Moaven, Koike et al. 2013). We asked if it is possible to generate a chimera between v-arr and βarr2 that contains the v-arr C-terminus but promotes GPCR clustering and endocytosis. A caveat to this strategy is that v-arr binds with high affinity to rhodopsin (light-activated GPCR) but very weakly to ligand-activated GPCRs. Accordingly, we generated a series of chimeric mutant arrestin constructs that contain sequences derived from βarr2 which were shown previously to enhance visual arrestin binding to non-rhodopsin GPCRs (Vishnivetskiy, Hosey et al. 2004),

and we included several additional βarr2-derived sequences while retaining the v-arr C-terminus (Extended Data Figure 5.2A, B). We were indeed able to generate a chimeric mutant arrestin (here called ChiA) that promoted robust agonist-induced internalization of the β2V2R despite containing the v-arr C-terminus (Figure 5.2A, Extended Data Figure 5.2). This independently verifies that the β-arrestin CT is not essential for endocytic function.

To search for sequence(s) responsible for endocytic activity apart from the β-arrestin CT, we systematically reverted small sections of β-arrestin-2 sequence in ChiA to the corresponding sequence in v-arr (ChiA.1-14) (Extended Data Figure 5.1A, B). We then expressed each chimera in βarr1/2 DKO HEK293 cells with FLAG-tagged β2V2R and measured their ability to drive agonist-induced β2V2R endocytosis. Of the 15 chimeras tested, we found that three had lost the ability to support β2V2R internalization, ChiA.9,10, and 11 (Figure 5.2A). TIRF imaging indicated that all these internalization-defective chimeras were strongly recruited to the plasma membrane in response to isoproterenol addition but localized diffusely and failed to cluster receptors. This was evident visually (Figure 5.2B, C) and quantified by measuring fluorescence intensity changes in response to agonist addition (Figure 5.2D, E). The internalization and microscopy results indicate that each of the mutations specifically interfered with β-arrestin's endocytic function, preventing accumulation in CCPs without detectably affecting receptor-triggered recruitment to the plasma membrane. We noticed that mutations unique to the three defective chimeras mapped to a similar area in the 3D structure of active β-arrestin-2, located at the cytoplasmic face of the C-lobe and opposite the receptor binding interface (Figure 5.2F, pink). As all three chimeras specifically disrupted clustering without affecting GPCR-triggered recruitment to the plasma membrane, and their unique mutations map contiguously to a face

of the β-arrestin–2 C-lobe, we hypothesized that this region of β-arrestin–2 is a discrete endocytic determinant which we call the C-lobe base (CLB).

C-lobe base is necessary for β2AR internalization

Considering that the CLB was identified through its function in an extensively modified arrestin chimera, we next asked if this region also has endocytic activity in β-arrestin-2. To do so, we replaced a small segment of the β-arrestin-2 CLB with the corresponding visual arrestin-derived sequence (D205S, L208I, L215I, N216P, N218T, and H220A). The resulting mutant construct, βarr2(CLB), was robustly recruited to the plasma membrane and clustered into CCPs with β2AR after agonist-induced activation (Figure 5.3B). This was not surprising because the β-arrestin-2 CT remained intact. However, when the βarr2 CLB was mutated in combination with the CT (βarr2(CLB,372T) mutant), iso-induced clustering was abolished, while recruitment to the plasma membrane remained intact. Closer inspection of TIR-FM images revealed that mutating either the CLB or CT produced a partial reduction in clustering, relative to wild type β-arrestin-2, and verified a loss of clustering in the double mutant (Figure 5.3E). When quantified using a previously described clustering metric (Eichel, Jullié et al. 2018), we verified that mutating either the CT or CLB reduced the degree of β2AR clustering relative to that produced by rescue with wild type βarr2, and that mutating the CT and CLB in combination abolished receptor clustering altogether (Figure 5.3F, G). The effect of these mutations was specific for βarr-mediated receptor clustering because the overall degree of βarr2 recruitment to the plasma membrane was unaffected (Figure 5.3H). These results indicate that both the CT and CLB promote β2AR clustering and do so in an additive manner. As the βarr2(CLB,372T) mutant lacks all clustering activity, despite being recruited (diffusely) to the

plasma membrane, these results further indicate that the CT and CLB fully account for the receptor clustering activity of β-arrestin-2.

Considering that mutating either the CT or CLB reduced clustering to a similar degree, we were surprised that these mutations differed in their effects on the subsequent endocytosis of β2AR. Whereas mutating the CT did not significantly impair β2AR internalization, mutating the CLB caused a pronounced reduction (Figure 5.3I). This distinction was clarified by plotting β2AR clustering relative to internalization. Mutating the CLB reduced β2AR internalization comparably to its effect on receptor clustering but mutating the CT disproportionally reduced clustering relative to its effect internalization (Figure 5.3J). These data indicate that the CLB and CT are not simply redundant. Rather, they both drive β2AR clustering into clathrin-coated pits but the β-arrestin–2 CLB is the main driver of subsequent endocytosis.

GPCRs selectively deploy the discrete endocytic determinants

Having learned that the CLB and C-terminus differ considerably in their ability to drive endocytosis of the β2AR, we wondered what advantage these two determinants might provide more generally. To investigate this, we selected a series of GPCRs that internalize in a β-arrestin-dependent manner but are known to form different GPCR/β-arrestin complexes. As the CLB and CT, together, account for all endocytic activity of βarr2, we inferred the endocytic activity of each individual determinant by selectively mutating the other. Surprisingly, the β-arrestin-2 CLB accounted for most of the endocytic activity measured for all the GPCRs tested. The amount of endocytic activity contributed by the β-arrestin-2 CT, by contrast, varied more dramatically across the receptors (Figure 5.4A). These results confirm that both the CT and

CLB operate as independent endocytic determinants and indicate that individual GPCRs functionally deploy each to different degrees.

Some insight into the underlying logic of such receptor-specific control emerged upon plotting the relative endocytic activities of the CLB and CT against each other. For most of the GPCRs tested (β2AR, κOR, μOR, M2R, NTSR1, V2R), an inverse correlation between the endocytic activities contributed by each determinant was observed, with the total contribution summing to unity (Figure 5.4B). Within this group, we also noticed a tendency for receptors to segregate according to differences in their biochemical mode of association with β-arrestin. 'Class B' GPCRs that form a more stable complex with β-arrestin relied more on the β-arrestin CT (V2R, M2R, NTSR1), whereas 'class A' GPCRs that bind β-arrestin more transiently relied more on the CLB (β2AR, κOR, μOR). These observations suggest that GPCR-specific deployment of each endocytic determinant depends on differences in the stability or conformation of the complex formed with β-arrestin.

The δOR and β2V2R provided additional insight. These examples deviated from the inverse correlation, as indicated by individual endocytic activities assessed for each determinant summing well above 100%. This suggests that these GPCRs drive strong deployment of both determinants, enabling each to promote internalization semi-redundantly. One of these receptors, the β2V2R, is engineered to selectively strengthen receptor interaction with the β-arrestin N-lobe relative to the wild type β2AR, without changing the receptor core interaction with β-arrestin (Oakley, Laporte et al. 1999, Thomsen, Plouffe et al. 2016). The β2V2R drove functional deployment of the β-arrestin C-terminus more strongly than the β2AR, while deployment of the CLB was similar between the receptors. We further noted that the δOR, a

naturally occurring GPCR, deployed both determinants with similar strength as the β2V2R, yet this GPCR is a transient-binding 'class A' GPCR. Together, these observations suggest that GPCR-specific deployment of the discrete endocytic determinants is not dictated simply by differences in overall stability of the GPCR/β-arrestin complex. Rather, it appears to be 'programmed' in a more flexible and specific manner through differences in the conformation of individual GPCR/β-arrestin complexes.

CLB couples receptor desensitization and internalization

GPCR binding to the β-arrestin N-lobe displaces the CT, allosterically coupling complex formation to deployment of the β-arrestin CT. As our data indicate that the CLB is a discrete determinant that is deployed in response to receptor engagement, we hypothesized that this determinant is also allosterically coupled to receptor binding. To test this, we returned to our prototypical receptor, the β2AR, and sought to measure how mutating each domain affects β2AR/βarr2 complex formation.

To quantify complex formation in living cells, we used direct NanoBiT luciferase complementation (Dixon, Schwinn et al. 2016) between the β2AR and βarr2. We observed robust complementation of wild type βarr2, as indicated both by concentration-response analysis and kinetic measurement of protein complementation. We also observed robust complex formation after mutating the CT and CLB determinants individually or in combination, fully consistent with the microscopy data (Figure 5.5A, B). These results indicate that neither the CT nor CLB is essential for agonist-promoted β2AR/β-arrestin complex formation.

A surprising result was obtained when β2AR/β-arrestin complex formation was assessed functionally, by desensitization of endogenous β2AR-elicited cAMP signaling. We assessed this by monitoring the cAMP response in live βarr1/2 DKO cells using a genetically encoded fluorescent cAMP biosensor (cADDis) (Tewson, Martinka et al. 2016). β-arrestin-2 rescue did not detectably affect the initial cAMP increase elicited by 10 μM isoproterenol, as indicated by the peak observed within 5 min after agonist application. However, β-arrestin-2 rescue significantly accelerated the subsequent decay of the cAMP response, indicating β-arrestin-mediated desensitization. Mutating the βarr2 C-terminus, βarr2(372T), enhanced the desensitization response. In contrast, mutating the CLB, βarr2(CLB), inhibited desensitization and resulted in a sustained cAMP elevation near to that observed in knockout cells not rescued with β-arrestin-2. Combining both mutations, βarr2(CLB,372T), resulted in a desensitization response that was comparable to that produced by rescue with wild type β-arrestin-2 (Figure 5.5C, D). These results indicate a specific and distinct role for the β-arrestin CLB in promoting formation of a desensitized β2AR/β-arrestin complex, and which is opposed by the CT.

We were surprised that mutations in the β-arrestin CT or CLB produced profound and opposing effects on functional desensitization, while having little effect on overall complex formation as assessed biochemically. Reconciling this apparent conflict, we noticed slight changes in potency (shown as logEC50 ± 95% confidence interval) for βarr2(CLB) and βarr2(372T) recruitment as measured using the NanoBiT assay; these were increased and decreased, respectively (-6.8 ± 0.2 and -7.3 ± 0.1) when compared to wild-type (-7.1 ± 0.1). In addition, the slight increase in logEC50 measured by mutation of the CLB was counteracted by removal of the C-terminus, βarr2(CLB,372T), making this mutant indistinguishable from wild-type (-7.1 ± 0.3) (Figure 5.5A). A similar trend was observed in the kinetic data, where

βarr2(CLB) had the slowest association and this was restored to the wild-type rate in the double mutant, βarr2(CLB,372T) (Figure 5.5B). Additional mutation of the CLB identified a single residue conserved in β-arrestins but not visual arrestin, N218 in β-arrestin-2, that is necessary for both β2AR internalization and desensitization (Extended Data Figure 5.5). Together, these results support the hypothesis that both the CLB and CT are allosterically coupled to β2AR/β-arrestin complex formation, with each determinant producing an opposite effect on functional signaling while cooperating to promote the productive endocytosis of GPCRs.

5.4 Discussion

It is now well-established that β-arrestin adopts distinct receptor-specific conformations that produce receptor-specific signaling outcomes through engagement with the endocytic network. Prior to this work, only one conformationally sensitive determinant in β-arrestin – its C-terminus – was known to couple β-arrestin/GPCR engagement with accumulation at the clathrin-coated pit to drive subsequent internalization. Here we redefine this view.

First, we reaffirm that the C-terminus is involved in β-arrestin-mediated endocytosis, but contrary to the current view, is not as critical as the newly identified CLB determinant. As such, our findings may require reassessment of additional factors involved in β-arrestin-mediated receptor endocytosis (Tian, Kang et al. 2014).

Second, we demonstrate that clustering and endocytosis, long-believed to be tightly coupled, are in fact separable processes for the β2AR, which is clustered by both the CT and CLB determinants, but its subsequent internalization is driven primarily by the CLB. These observations provide a molecular basis for an emerging and poorly understood β-arrestin function – cargo-mediated control of endocytosis to restrict signaling to the plasma membrane.

Third, we show that GPCRs differentially utilize the CLB and CT of β-arrestin to drive receptor endocytosis. Receptors known to recruit β-arrestins more strongly, an ability determined by the number and distribution of phosphates on the receptor cytoplasmic tail, in general, trigger greater endocytic activity of the β-arrestin CT. This observation fits knowledge gained through elegant biochemical and structural studies showing GPCRs displace the CT to enable its binding to CHC/AP2β. By contrast, receptors that recruit β-arrestins weakly, except for the

δOR, promote only a small degree of CT endocytic activity, suggesting that they are relatively poor displacers of the β-arrestin C-terminus. How two GPCRs, the chimeric β2V2R and the naturally occurring δOR, deploy both remains strongly remains unclear. However, that these receptors produce a combined CLB and CT endocytic activity ~50% greater than wild-type βarr2 suggests that a downstream step limits total receptor internalization. [need something here]

Finally, we show that the CT and CLB determinants act in opposition at the β2AR/β-arrestin interface to either promote or attenuate signaling from endogenous β2ARs. We propose that these determinants represent two distinct allosteric paths from the GPCR through β-arrestin to the clathrin-coated pit. Given that β-arrestins bind hundreds of GPCRs and that these complexes can adopt different conformations, an interesting possibility is that these two allosteric paths allow for conformationally distinct β-arrestin/GPCR complexes while ensuring their endocytosis. When viewed through this lens, enhanced GPCR/β-arrestin complex formation through the CLB may compensate for relatively poor β-arrestin N-lobe binding of some GPCRs, allowing for the formation of a desensitized complex. While speculative, such a system would allow GPCRs that vary considerably in their ability to displace the β-arrestin C-terminus to efficiently enter the endocytic network and enable flexible and receptor-specific signal control. Viewed more broadly, our findings provide a framework for understanding how β-arrestins transduce receptor-specific engagement to the endocytic network to produce exquisite control of cellular signaling.

5.5 Materials and Methods

Cell culture, expression constructs, and transfections

βarr1/2 double knockout HEK 293A lines, a gift from Asuka Inouye and Silvio Gutkind (O'Hayre, Eichel et al. 2017), were cultured in complete growth Dulbecco's modified Eagle's medium (DMEM, Gibco) supplemented with 10% fetal bovine serum (UCSF Cell Culture Facility). Cell line cultures were free of mycoplasma contamination. Transfections were carried out using Lipofectamine 2000 according to the manufacturer's protocol. Cells were transfected 24-48h before experiments.

N-terminally FLAG-tagged versions of the human β1AR, β2AR, V2R, μ-opioid receptor, κOR, and NTSR1 were previously described (Chu, Murray et al. 1997, Cao, Deacon et al. 1999, Temkin, Lauffer et al. 2011). The β2AR–V2R chimera was a gift from M. Caron (Oakley, Laporte et al. 2000). pcDNA3.1(+) zeo FLAG-M2R was previously generated in the lab by James Hislop. δOR was previously generated in the lab by Miriam Stoeber.

β-arrestin-2–GFP and β-arrestin-2–mApple were previously described (Barak, Ferguson et al. 1997, Eichel, Jullié et al. 2016). β-arrestin-1–EGFP was generated by PCR amplifying from β-arrestin-1–mVenus, which was a gift from R. Sunahara (University of California, San Diego), and subcloned into EGFP-N1. Visual arrestin–EGFP was generated by synthesis of bovine visual arrestin (Twist Biosciences) and directly subcloned into EGFP-N1 using InFusion (Takara). β-arrestin-2(CCS)–EGFP was previously described (Eichel, Jullié et al. 2018). β-arrestin-2(372T)–EGFP was generated by PCR amplifying from β-arrestin-2–EGFP and subcloning into EGFP-N1 using InFusion HD (Takara Bio).

Visual arrestin and β-arrestin-2 EGFP-tagged chimeras were generated by synthesis of the template chimera, ChiA, (Twist Bioscience) and subcloned into EGFP-N1. Subsequent chimeras, ChiA.1-14, were generated by PCR and InFusion HD (Takara Bio).

Clathrin–dsRed was previously described (Merrifield, Feldman et al. 2002).

Live cell TIRF microscopy imaging

TIRF microscopy was performed at 37°C using a Nikon Ti-E inverted microscope equipped for through-the-objective TIRF microscopy and outfitted with a temperature-, humidity- and CO2-controlled chamber (Okolab). Images were obtained with an Apo TIRF 100X, 1.49 numerical aperture objective (Nikon) with solid-state 405, 488, 561 and 647nm lasers (Keysight Technologies). An Andor iXon DU897 EMCCD camera controlled by NIS-Elements 4.1 software was used to acquire image sequences every 2s for 10min. βarr1/2 double knockout HEK293s were transfected as indicated according to the manufacturer's protocol 48h before imaging and then plated on poly-L-lysine (0.0001%, Sigma) coated 35-mm glass-bottomed culture dishes (MatTek Corporation) 24h before imaging. Cells were labelled with monoclonal FLAG antibody (M1) (1:1000, Sigma F-3040) conjugated to Alexa Fluor 647 dye (Life Technologies) for 10min at 37°C before imaging, washed, and imaged live in DMEM without phenol red (UCSF Cell Culture Facility) supplemented with 30mM HEPES, pH 7.4 (UCSF Cell Culture Facility). Cells were treated with bath application isoproterenol at the indicated time for experiments shown as time courses. At least three independent experiments were performed for all live-cell microscopy.

TIRF microscopy image analysis

Quantitative image analysis was performed on unprocessed images using ImageJ and Fiji software (Schindelin, Arganda-Carreras et al. 2012, Schneider, Rasband et al. 2012). To quantify change in β-arrestin fluorescence over time in TIRF microscopy images, which was reported as plasma membrane recruitment, fluorescence values were measured over the entire stack in a region of interest (ROI) corresponding to the cell. Fluorescence values of the ROI were normalized to initial fluorescence values before agonist addition. Minimal bleed-through and photobleaching was verified using single-labelled and untreated samples, respectively. Line scan analysis of receptor, β-arrestin, or clathrin fluorescence from the shown line were carried out using the Fiji plot profile function to measure pixel values from this line. Clustering index was determined using the skew statistical measurement applied to fluorescence intensity values of β-arrestin–GFP or M1-Alexa647 labeled receptor pixels in a ROI corresponding to the cell.

Receptor internalization assay

All internalization assays were performed with βarr1/2 DKO HEK293 cells that were transfected according to the manufacturer's protocol 24 hours before beginning the assay. The next morning cells were lifted using TrypLE express (Thermo Scientific), a dissociation reagent that leaves extracellular epitopes intact, resuspended in complete media, transferred to 12-well plates in triplicate, and incubated under standard culture conditions until. Cells were then treated with agonist for the indicated period and placed on ice to stop trafficking. Cells were washed once with ice cold PBS following by labeling of FLAG-tagged surface receptors with M1 antibody (Thermo Scientific) conjugated to Alexa Fluor 647 (Thermo Scientific) for 30 minutes at 4°C while shaking. Surface staining of receptors was measured using a CytoFlex

(Beckman Coulter) with gates set for single cells expressing EGFP. Percent internalization was calculated by taking the mean M1-647 fluorescence measured in the APC channel for the ligand stimulated cells and dividing it by the same measure for the corresponding unstimulated cells, subtracted this from one, and multiplying by 100. At least three independent experiments were performed for all internalization assays.

NanoBiT complementation assays

β-arrestin-1/2 double knockout HEK293s were plated in 6-well dishes, transfected with β2AR-LgBiT and one of the following: Nb33-EGFP-SmBiT, arr1-SmBiT, βarr2-SmBiT, βarr2(372T)-SmBiT, βarr2(CLB)-SmBiT, or βarr2(372T,CLB)-SmBiT. Twenty-four hours later, cells were lifted with TrpLE Express, resuspended in 37°C assay buffer (135 mM NaCl, 5 mM KCl, 0.4 mM $MgCl_2$,1.8 mM $CaCl_2$, 20 mM HEPES and 5 mM d-glucose, adjusted to pH 7.4), and transferred to a white flat bottom 96-well plate in triplicate with 20,000 cells per well. Coelenterazine-H (Thermo Scientific) in 37°C assay buffer was added to a final concentration of 5 μM and incubated for at least 5 minutes before data collection. For kinetic experiments, three time points were collected to establish baseline before assay buffer or 10 μM isoproterenol addition. Fold response was calculated by averaging the values across each triplicate and then dividing the isoproterenol treated samples by the corresponding buffer treated samples. For dose-response experiments, isoproterenol was added at the indicated final concentrations in 37°C assay buffer and data was collected for 20 minutes. Fold response was calculated by averaging the values across each triplicate and then dividing the maximum by the minimum responses within each dose range. Dose-response curves were generated by a three-parameter non-linear fit in Prism 9. [Expression of βarr2 and βarr2 and βarr2(CLB) was verified by western blot using an antibody against the βarr2 N-terminus (Abcam, ab167047) with anti-

GAPDH (EMD Millipore, MAB374) as a loading control.] At least three independent experiments were performed for all NanoBiT assays.

Live cell cADDis cAMP assay

β-arrestin-1/2 double knockout HEK293 cells were plated in 6-well plates, transfected with either mApple, βarr2-mApple, βarr2(372T)-mApple, βarr2(CLB)-mApple, or βarr2(CLB,372T)-mApple. The following day, cells were lifted with TrypLE, transduced with CMV cADDis Green Upward (Montana Molecular) according to manufacturer's instructions, and transferred in triplicate at 50,000 cells per well in a black clear bottom 96-well plate (Corning). On the day of the experiment, the media was removed and replaced with 37°C assay buffer (135 mM NaCl, 5 mM KCl, 0.4 mM $MgCl_2$,1.8 mM $CaCl_2$, 20 mM HEPES and 5 mM d-glucose, adjusted to pH 7.4) and incubated for five minutes in the pre-warmed plate reader (H4 Synergy BioTek). Expression of mApple tagged plasmids was determined by fluorescence with monochromators set to Ex: 568/9.0 and Em: 592/13.5. Next, cADDis fluorescence baseline was established by three time points a minute apart using monochromators set to Ex: 500/9.0 and Em: 530/20.0. Isoproterenol was then added to a final concentration of 10 μM and cADDis fluorescence was measured every minute for the indicated time. Change in fluorescence was calculated by averaging across each triplicate and then dividing by the baseline. Fluorescence bleed through nor significant photobleaching were observed in separate experiment where cells expressing only mApple or cADDis green were measured with the same optical configuration. At least three independent experiments were performed.

5.6 References

Barak, L. S., et al. (1997). A beta-arrestin/green fluorescent protein biosensor for detecting G protein-coupled receptor activation. *J Biol Chem 272*(44): 27497-27500. 10.1074/jbc.272.44.27497

Cao, T. T., et al. (1999). A kinase-regulated PDZ-domain interaction controls endocytic sorting of the beta2-adrenergic receptor. *Nature 401*(6750): 286-290. 10.1038/45816

Chu, P., et al. (1997). Delta and kappa opioid receptors are differentially regulated by dynamin-dependent endocytosis when activated by the same alkaloid agonist. *J Biol Chem 272*(43): 27124-27130. 10.1074/jbc.272.43.27124

Dixon, A. S., et al. (2016). NanoLuc Complementation Reporter Optimized for Accurate Measurement of Protein Interactions in Cells. *ACS Chem. Biol. 11*(2): 400-408. 10.1021/acschembio.5b00753

Eichel, K., et al. (2018). Catalytic activation of β-arrestin by GPCRs. *Nature 557*(7705): 381-386. 10.1038/s41586-018-0079-1

Eichel, K., et al. (2016). β-Arrestin drives MAP kinase signalling from clathrin-coated structures after GPCR dissociation. *Nat. Cell Biol. 18*(3): 303-310. 10.1038/ncb3307

Eichel, K. and M. von Zastrow (2018). Subcellular Organization of GPCR Signaling. *Trends Pharmacol Sci 39*(2): 200-208. 10.1016/j.tips.2017.11.009

Goodman, O. B., et al. (1996). β-Arrestin acts as a clathrin adaptor in endocytosis of the β2-adrenergic receptor. *Nature 383*(6599): 447-450. 10.1038/383447a0

Gurevich, V. V. and E. V. Gurevich (2019). GPCR Signaling Regulation: The Role of GRKs and Arrestins. *Front Pharmacol 10*: 125. 10.3389/fphar.2019.00125

Irannejad, R. and M. von Zastrow (2014). GPCR signaling along the endocytic pathway. *Curr Opin Cell Biol 27*: 109-116. 10.1016/j.ceb.2013.10.003

Kang, D. S., et al. (2009). Structure of an arrestin2-clathrin complex reveals a novel clathrin binding domain that modulates receptor trafficking. *J Biol Chem 284*(43): 29860-29872. 10.1074/jbc.M109.023366

Krupnick, J. G., et al. (1997). Modulation of the arrestin-clathrin interaction in cells. Characterization of beta-arrestin dominant-negative mutants. *J Biol Chem 272*(51): 32507-32512. 10.1074/jbc.272.51.32507

Laporte, S. A., et al. (2000). The interaction of β-arrestin with the AP-2 adaptor is required for the clustering of β2-adrenergic receptor into clathrin-coated pits. *J. Biol. Chem. 275*(30): 23120-23126.

Latorraca, N. R., et al. (2020). How GPCR Phosphorylation Patterns Orchestrate Arrestin-Mediated Signaling. *Cell 183*(7): 1813-1825 e1818. 10.1016/j.cell.2020.11.014

Lohse, M. J., et al. (1990). beta-Arrestin: a protein that regulates beta-adrenergic receptor function. *Science 248*(4962): 1547-1550. 10.1126/science.2163110

Merrifield, C. J., et al. (2002). Imaging actin and dynamin recruitment during invagination of single clathrin-coated pits. *Nat. Cell Biol. 4*(9): 691-698. 10.1038/ncb837

Moaven, H., et al. (2013). Visual arrestin interaction with clathrin adaptor AP-2 regulates photoreceptor survival in the vertebrate retina. *Proc Natl Acad Sci U S A 110*(23): 9463-9468. 10.1073/pnas.1301126110

O'Hayre, M., et al. (2017). Genetic evidence that β-arrestins are dispensable for the initiation of β2-adrenergic receptor signaling to ERK. *Sci. Signal. 10*(484). 10.1126/scisignal.aal3395

Oakley, R. H., et al. (1999). Association of β-arrestin with G protein-coupled receptors during clathrin-mediated endocytosis dictates the profile of receptor resensitization. *J. Biol. Chem. 274*(45): 32248-32257.

Oakley, R. H., et al. (2001). Molecular determinants underlying the formation of stable intracellular G protein-coupled receptor-β-arrestin complexes after receptor endocytosis. *J. Biol. Chem. 276*(22): 19452-19460.

Oakley, R. H., et al. (2000). Differential affinities of visual arrestin, βarrestin1, and βarrestin2 for G protein-coupled receptors delineate two major classes of receptors. *J. Biol. Chem. 275*(22): 17201-17210.

Orsini, M. J. and J. L. Benovic (1998). Characterization of dominant negative arrestins that inhibit beta2-adrenergic receptor internalization by distinct mechanisms. *J Biol Chem 273*(51): 34616-34622. 10.1074/jbc.273.51.34616

Schindelin, J., et al. (2012). Fiji: an open-source platform for biological-image analysis. *Nat. Methods 9*(7): 676-682. 10.1038/nmeth.2019

Schmid, E. M., et al. (2006). Role of the AP2 beta-appendage hub in recruiting partners for clathrin-coated vesicle assembly. *PLoS Biol 4*(9): e262. 10.1371/journal.pbio.0040262

Schneider, C. A., et al. (2012). NIH Image to ImageJ: 25 years of image analysis. *Nat. Methods 9*(7): 671-675. 10.1038/nmeth.2089

Temkin, P., et al. (2011). SNX27 mediates retromer tubule entry and endosome-to-plasma membrane trafficking of signalling receptors. *Nat. Cell Biol. 13*(6): 715-721. 10.1038/ncb2252

Tewson, P. H., et al. (2016). New DAG and cAMP Sensors Optimized for Live-Cell Assays in Automated Laboratories. *J. Biomol. Screen. 21*(3): 298-305. 10.1177/1087057115618608

Thomsen, A. R. B., et al. (2016). GPCR-G Protein-β-Arrestin Super-Complex Mediates Sustained G Protein Signaling. *Cell 166*(4): 907-919. 10.1016/j.cell.2016.07.004

Tian, X., et al. (2014). beta-arrestins and G protein-coupled receptor trafficking. *Handb Exp Pharmacol 219*: 173-186. 10.1007/978-3-642-41199-1_9

Vishnivetskiy, S. A., et al. (2004). Mapping the arrestin-receptor interface. Structural elements responsible for receptor specificity of arrestin proteins. *J Biol Chem 279*(2): 1262-1268. 10.1074/jbc.M308834200

5.7 Figures

Figure 5.1 Known βarr2 endocytic motifs are dispensable for co-clustering with β2AR subsequent internalization

A-D) Representative live-cell TIRF microscopy images of βarr1/2 double knockout HEK293s co-expressing clathrin light chain-DsRed (magenta) and FLAG-β2AR (blue) with either EGFP (a), βarr2-EGFP (b), βarr2(CCS)-EGFP (c), or βarr2(372T)-EGFP (d) (all in green) and pre- and post-stimulation with 10 μM isoproterenol (Iso). **E**) fluorescence intensity profiles from the line scans shown in insets from b-d. **F**) flow cytometry-based internalization of FLAG-β2AR co-expressed with the same βarr2 constructs from panels a-d in two different lines of βarr1/2 DKO HEK293s at five- and 30-minutes post-stimulation with 10 μM isoproterenol. Scale bars are 5 μm. All experiments were repeated at least three times.

Figure 5.2 Identification of the C-lobe base (CLB), a distributed endocytic determinant

A) Internalization of β2V2R after 30 minutes of 10 μM isoproterenol stimulation in βarr1/2 DKO HEK293s co-expressing the indicated construct. **B**, **C**) Representative TIR-FM images of cells expressing β2AR (blue) and clathrin light chain dsRed (magenta) with either wild-type βarr2-EGFP (b) or an example of one of the three internalization defective chimeras, ChiA.10-EGFP (c), pre- and post-stimulation with 10 μM isoproterenol. Scale bars are 5 μm. **D**) Quantification of plasma membrane recruitment of the indicated EGFP-tagged proteins (see methods) in response to stimulation of β2V2R with 10 μM isoproterenol. **E**, Max clustering index (see methods) of β2V2R after stimulation with 10 μM isoproterenol in DKO cells co-expressing the indicated constructs. All experiments were repeated at least three times. For image quantification each dot represents an individual cell (line = mean, error = SEM, $n \geq 9$). **F**, Location of mutations unique to ChiA.9-11 (shades of pink and purple) in an active state structure of β-arrestin-2 (5TV1, green) fit to the NTSR1/βarr1 structure (6UP7, gray) (βarr1 not shown) and the same model rotated and zoomed to the cytoplasmic face of the C-lobe.

Figure 5.3 β-arrestin C-tail is not sufficient for β2AR internalization

A-D, Representative live-cell TIR-FM images of βarr1/2 double knockout HEK293s co-expressing clathrin light chain-DsRed (magenta) and FLAG-β2AR (blue) with either βarr2-EGFP (a), βarr2(CLB)-EGFP (b), βarr2(372T)-EGFP (c), or βarr2(CLB,372T)-EGFP (d) (all in green) pre- and post-stimulation with 10 μM isoproterenol (Iso). EGFP condition not shown (see figure 5.1). **E**) Zoomed images corresponding to yellow dashed boxes in panels a-d for βarr2 and β2AR images. **F**, β2AR mean clustering index pre- and post-stimulation with 10 μM isoproterenol over ten minutes (n ≥ 9 cells, error = SEM). **G**, Max plasma membrane recruitment of the indicated EGFP-tagged proteins in response to stimulation with 10 μM isoproterenol. (line = mean, n ≥ 9 cells, error = SEM). **H**, Max clustering index of β2AR calculated from the first 300 seconds of (f) (line = mean, n ≥ 9 cells, error = SEM). **I**, Internalization of β2AR when co-expressing the indicated EGFP-tagged proteins (n = 3) in βarr1/2 DKO HEK293s. **J**, Correlation between β2AR clustering index and internalization. Solid line fit to βarr2 and βarr2(CLB,372T). (R^2 = 0.6, dashed lines = 95% CI, vertical error = SEM and horizontal error = STD). All experiments were repeated at least three times.

Figure 5.4 GPCRs selectivity deploy the CLB or C-terminus to drive endocytosis

A, Endocytic activity of each determinant within β-arrestin-2 defined by subtracting the internalization measured in the negative control, EGFP, from βarr2, βarr2(372T), βarr2(CLB) and dividing the mutant values by the wild-type value. **B**, Endocytic activity of each determinant plotted as x and y coordinates for each receptor. Additive relationship is defined as 100% endocytic activity when individual activities are summed. Clusters determined by k means are colored with blue, purple, and gold. Error bars are STD. Each experiment was repeated at least three times.

Figure 5.5 β-arrestin CLB and CT determinants represent two allosteric paths from GPCRs to the endocytic network.

A, **B**) Direct NanoBiT luciferase complementation in βarr1/2 DKO HEK293 cell co-expressing β2AR-LgBiT with SmBiT tagged: Nb33 (a μOR receptor nanobody, black), visual arrestin (pink), wild type β-arrestin-2 (green), 372T mutant (dark purple), CLB mutant (light purple), or double mutant (cyan) measured as an end point across a range of isoproterenol (Iso) concentrations (a) and kinetically pre- and post-stimulation with 10 μM Iso for 15 minutes (b). **C**) Endogenous β2AR cAMP response to 10 μM Iso stimulation measured by a genetically encoded fluorescent biosensor, cADDis, and normalized to response elicited by simultaneous treatment with 10 μM forskolin (fsk) and 300 μM IBMX. **D**) Area of the curve calculated from panel c. Error bars represent STD for all experiments shown. Experiments were repeated at least three times. **E**) Diagram of two differentially deployed allosteric paths from GPCRs through β-arrestins to the to promote endocytosis. Blue receptors, exemplified by the β2AR, primarily deploy the CLB to drive endocytosis, while pink and orange receptors, exemplified by V2R and δOR respectively, deploy both determinants. The latter group of receptors (orange) are distinguished by strong and redundant deployment of both the CT and CLB. Solid arrows are the CLB and dashed represent the CT. Interestingly, these two groups produce weak (gray) and strong (light blue) endosomal signals respectively.

Extended Data Figure 5.1 β-arrestin-2 C-terminus is dispensable for clustering and internalization for β2V2R, the β-arrestin-1 C-terminus is not strictly necessary for β2AR internalization, and β2AR phosphorylation sites are necessary for efficient internalization. a-e, Representative live-cell TIRF microscopy images of βarr1/2 DKO HEK293s pre- and post-stimulation with 10 μM isoproterenol (Iso) with insets corresponding the central area of each cell. Images show clathrin-light chain-DsRed (magenta), as well as the indicated EGFP-tagged proteins (green) and GPCRs (blue). a, FLAG-β2AR and EGFP. b-c, FLAG-β1AR with (a) βArr2 or (c) βarr2(372T). d-e, FLAG-β2V2R with (d) βArr2 or (e) βarr2(372T). f-g, Normalized fluorescence intensity from line scans shown in insets b-e with colors corresponding to the image labels. f, Left and right columns correspond to insets in b and c, respectively. g, Left and right columns correspond to insets in d and e, respectively. h, Percent internalization of FLAG-β2V2R in DKO cells co-expressing either EGFP, βarr2-EGFP, or βarr2(372T)-EGFP after five- or 30-minutes treatment with 10 μM isoproterenol (Iso). i, Percent internalization of FLAG-β2AR after 30 minutes of stimulation with 10 μM isoproterenol in DKO cells expressing either EGFP, βarr1-EGFP, or βarr1(376T)-EGFP. j, Normalized internalization of FLAG-β2AR or its phosphorylation site mutant, β2AR(3A), after five- or 30-minute treatments with isoproterenol in DKO cells co-expressing βArr2-EGFP. All experiments were repeated at least three times. Scale bar represents 5 μM. Error bars represent STD.

Extended Data Figure 5.2 Diagram and sequence maps of visual arrestin—βarr2 chimeras

a, Diagram of βarr2 (gray) and visual arrestin (black) sequences as rectangles. Visual arrestin sequences swapped into ChiA are gold to make ChiA.1-14. Major landmarks are shown for βarr2. b, Multiple sequence alignment of visual arrestin (v-arr), βarr2, and ChiA. Gold boxes in the v-arr sequence replace gold boxes in the ChiA sequence to make the indicated chimera.

Extended Data Figure 5.3 Internalization of β2AR with β-arrestin-1 and its CLB mutant

Internalization of β2AR in βarr1/2 DKO HEK293s when co-expressed with EGFP or EGFP-tagged wild-type or CLB mutant (D204S, S215P, N217T, and H219A) of βarr1.

Extended Data Figure 5.4 Internalization of various receptors when co-expressed with either EGFP, wild type, the CLB mutant, or the 372T.

Internalization of β2AR in βarr1/2 DKO HEK293s when co-expressed with EGFP or EGFP-tagged wild-type or CLB mutant (D204S, S215P, N217T, and H219A) of βarr1.

Extended Figure 5.5 N218 in the β-arrestin-2 CLB is required for β2AR internalization and desensitization.

A, Endogenous β2AR cAMP response measured by changes in cADDis fluorescence after 10 μM isoproterenol addition in βarr1/2 DKO HEK293s expressing either: mApple, wild type arrestin, CLB mutant, or N218T mutant (other mutants aren't shown for clarity). B, Area under the curve calculated from cAMP experiments with conditions omitted from panel a shown. C, Conservation measured by % identity of each amino acid in the β-arrestins (green) and visual arrestin (black). Y-axis is the wild-type sequence in β-arrestin-2 corresponding to the area that was swapped with visual arrestin sequence to create the βarr2(CLB) mutant. D, Percent internalization of β2AR for all point mutants. Three independent experiments were conducted for all experiments shown. Error bars represent STD.

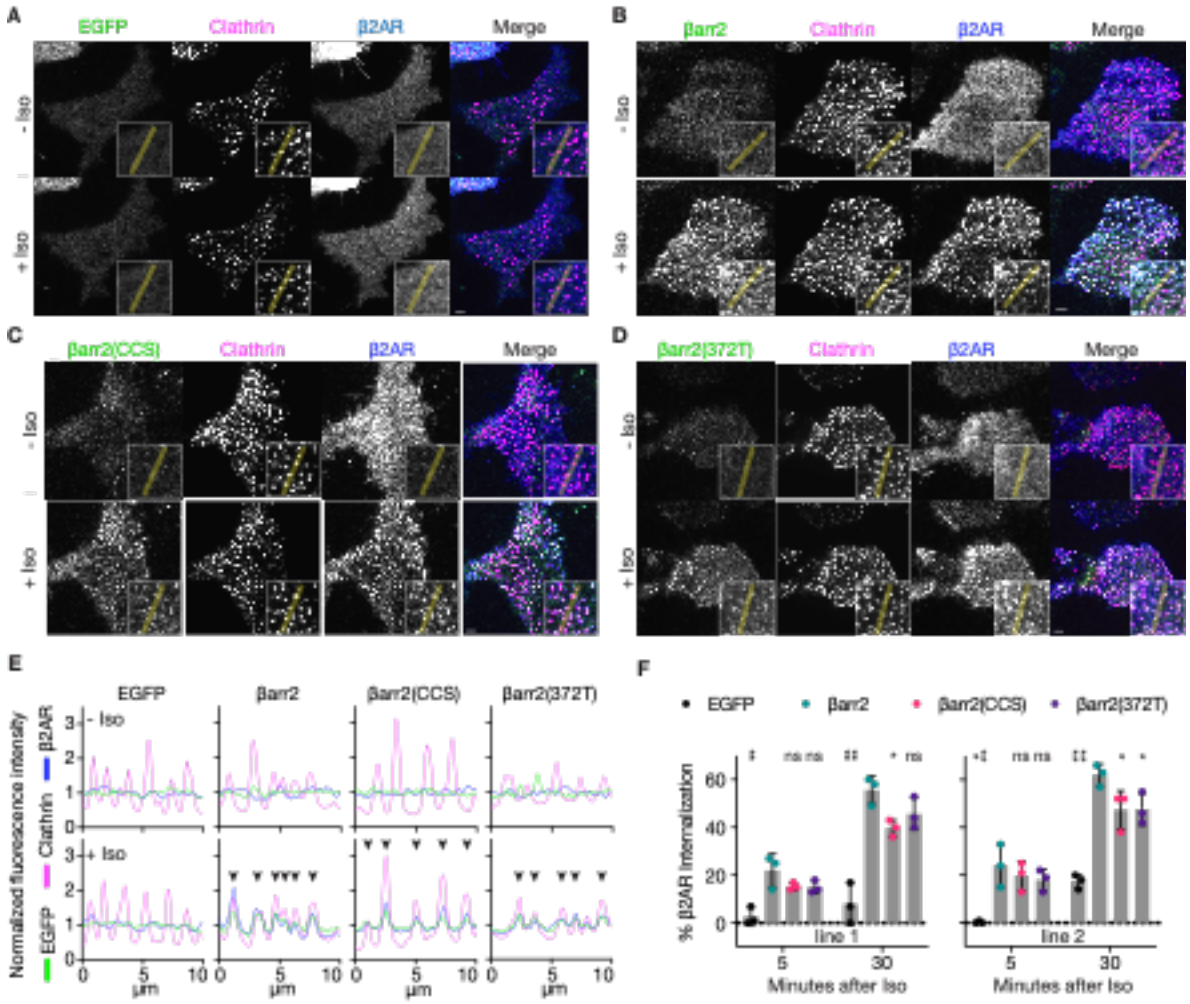

Figure 5.1 Known β-arrestin-2 endocytic motifs are dispensable for co-clustering with β2AR and subsequent internalization

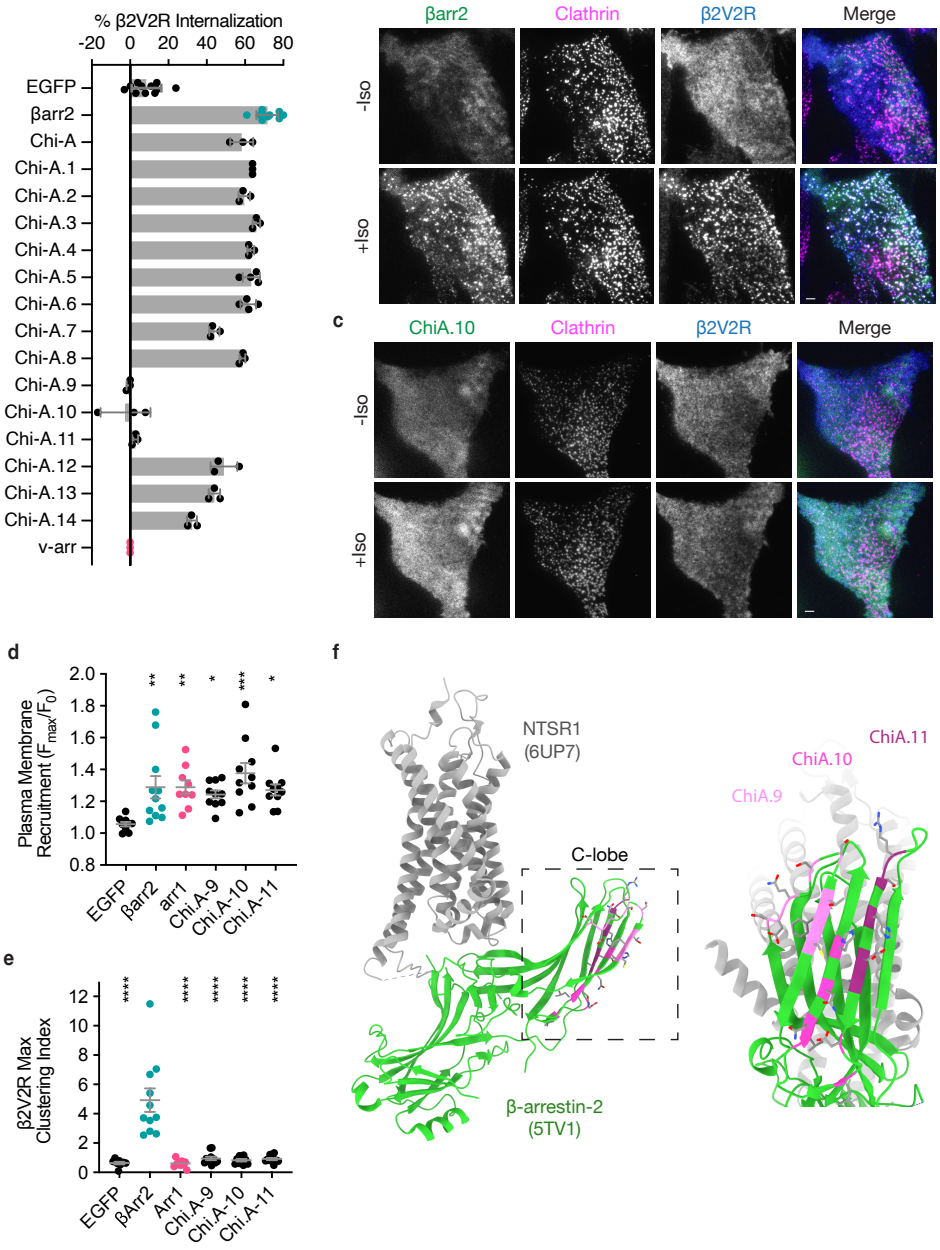

Figure 5.2 Identification of the C-lobe base as the location of a distributed endocytic determinant

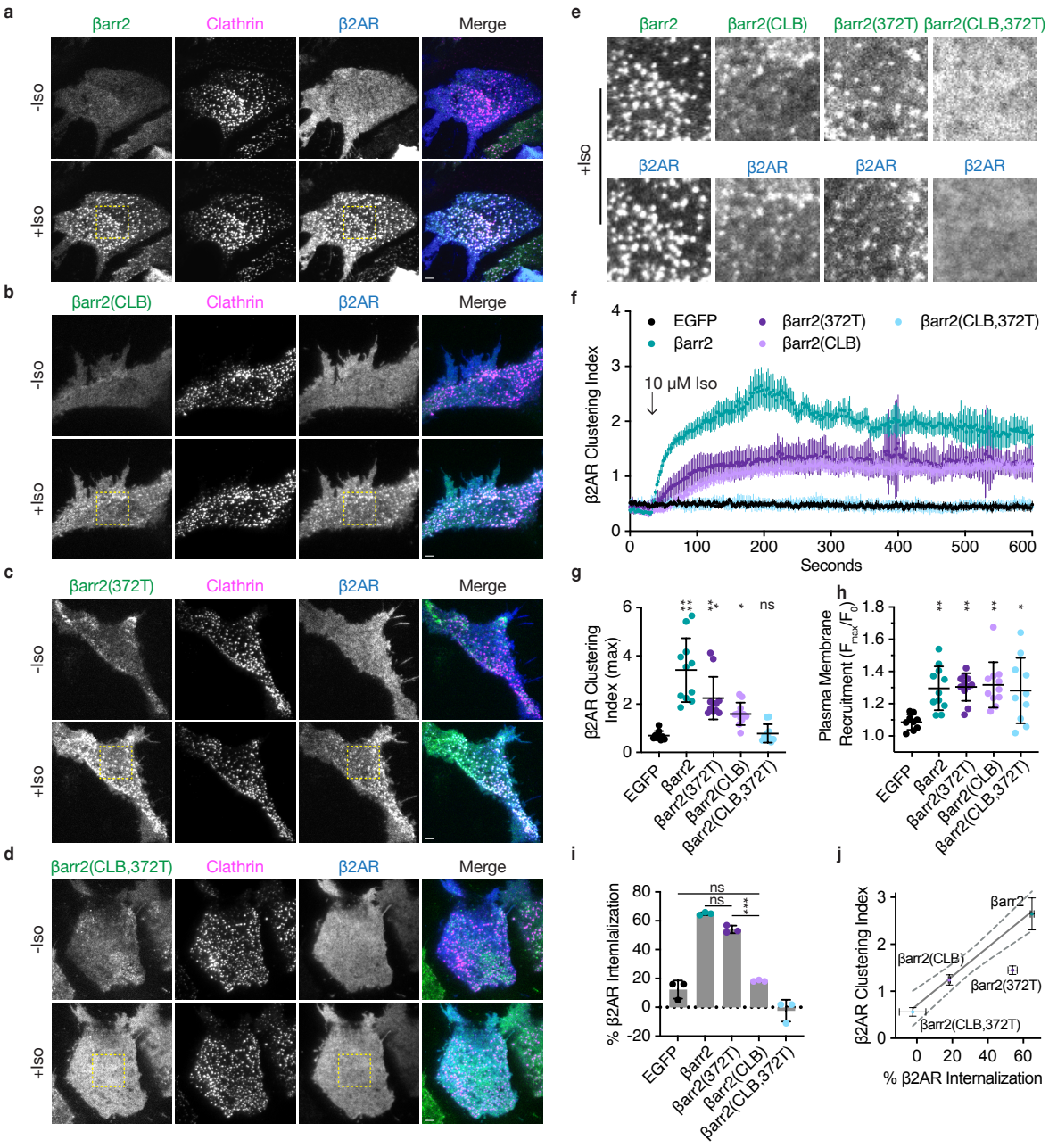

Figure 5.3 β-arrestin C-terminus is not sufficient for β2AR internalization

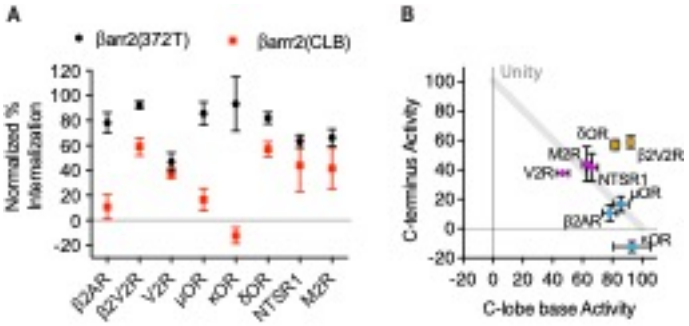

Figure 5.4 GPCRs selectivity utilize the CLB or C-terminus to drive endocytosis

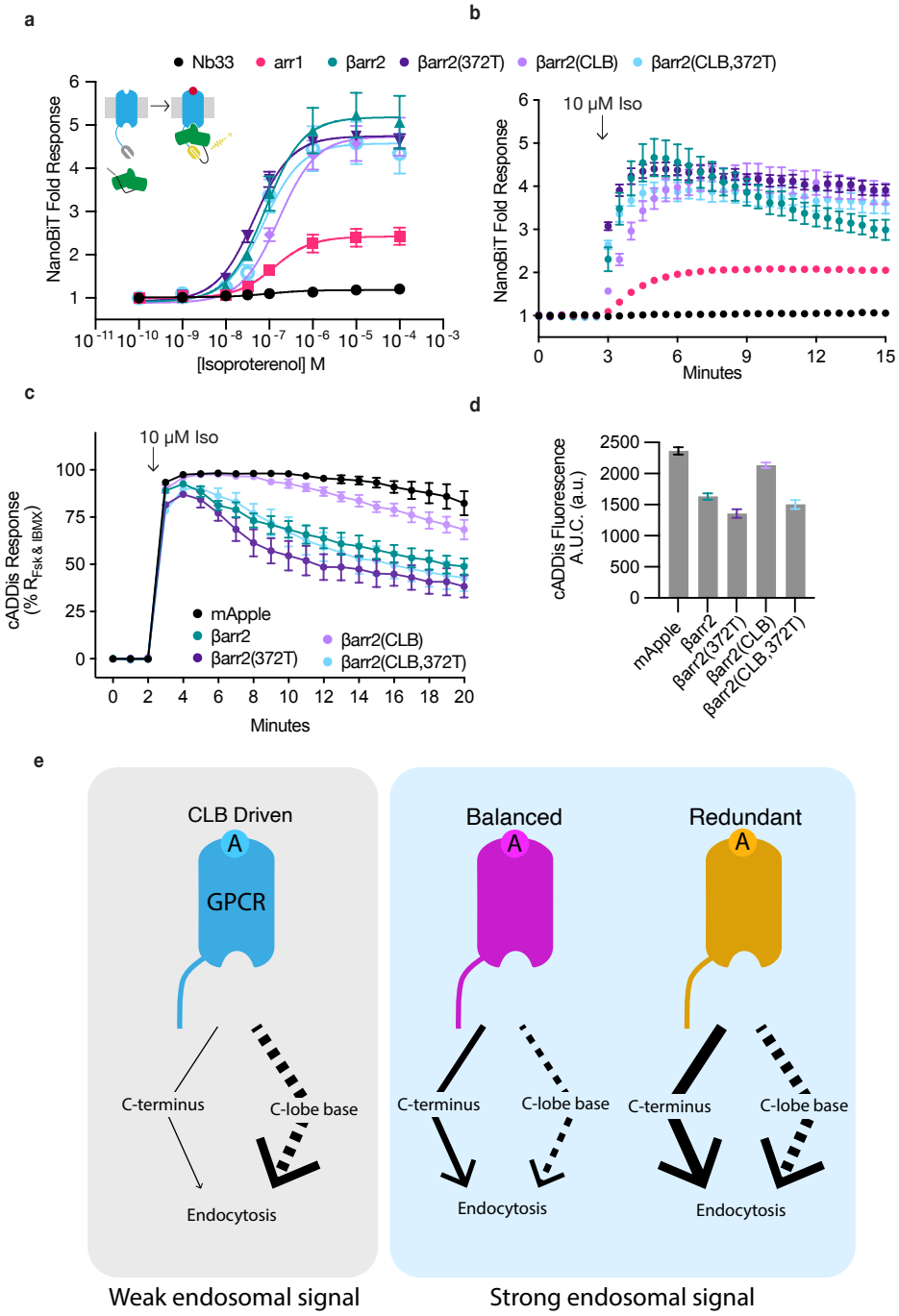

Figure 5.5 β-arrestin CLB and CT determinants represent two allosteric paths from GPCRs to the endocytic network.

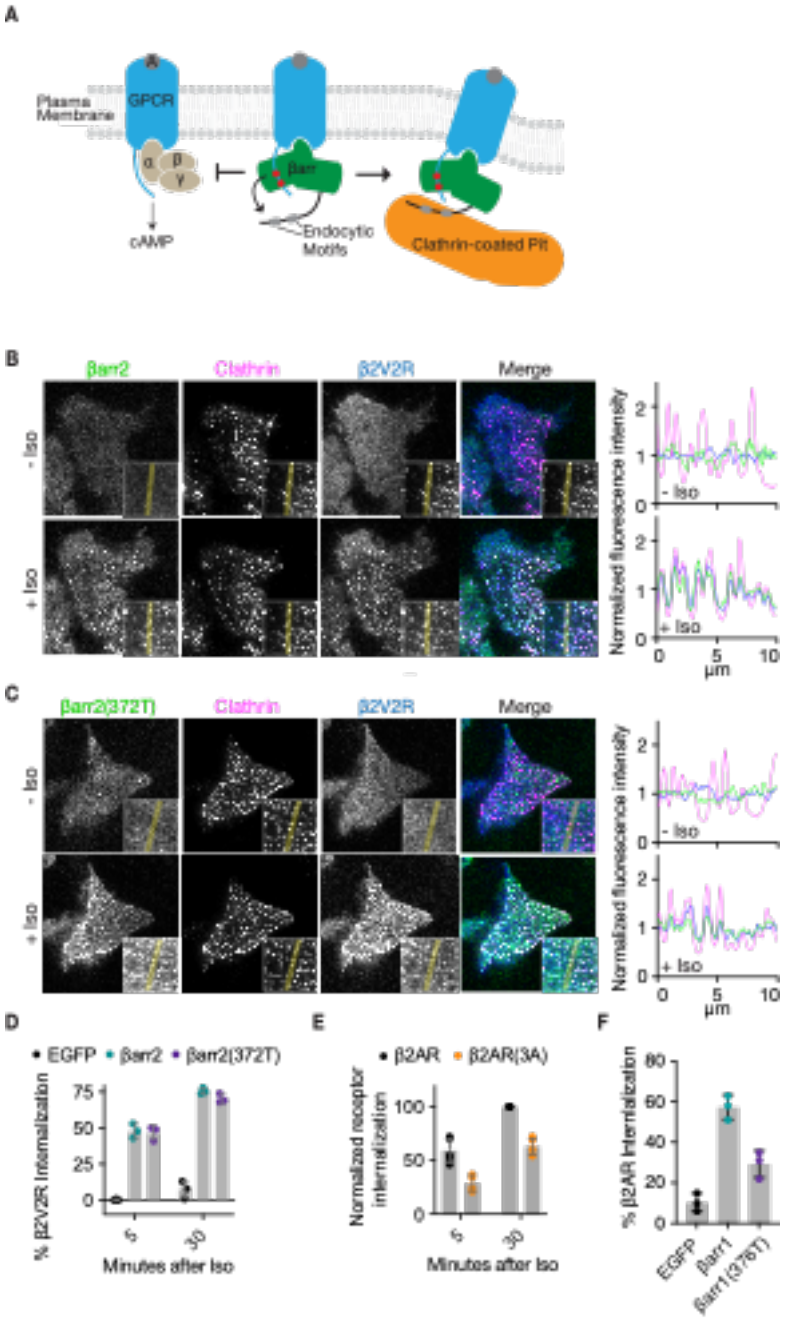

Extended Data Figure 5.1 β-arrestin-2 C-terminus is dispensable for clustering and internalization for β2V2R, the β-arrestin-1 C-terminus is not strictly necessary for β2AR internalization, and β2AR phosphorylation sites are necessary for efficient internalization.

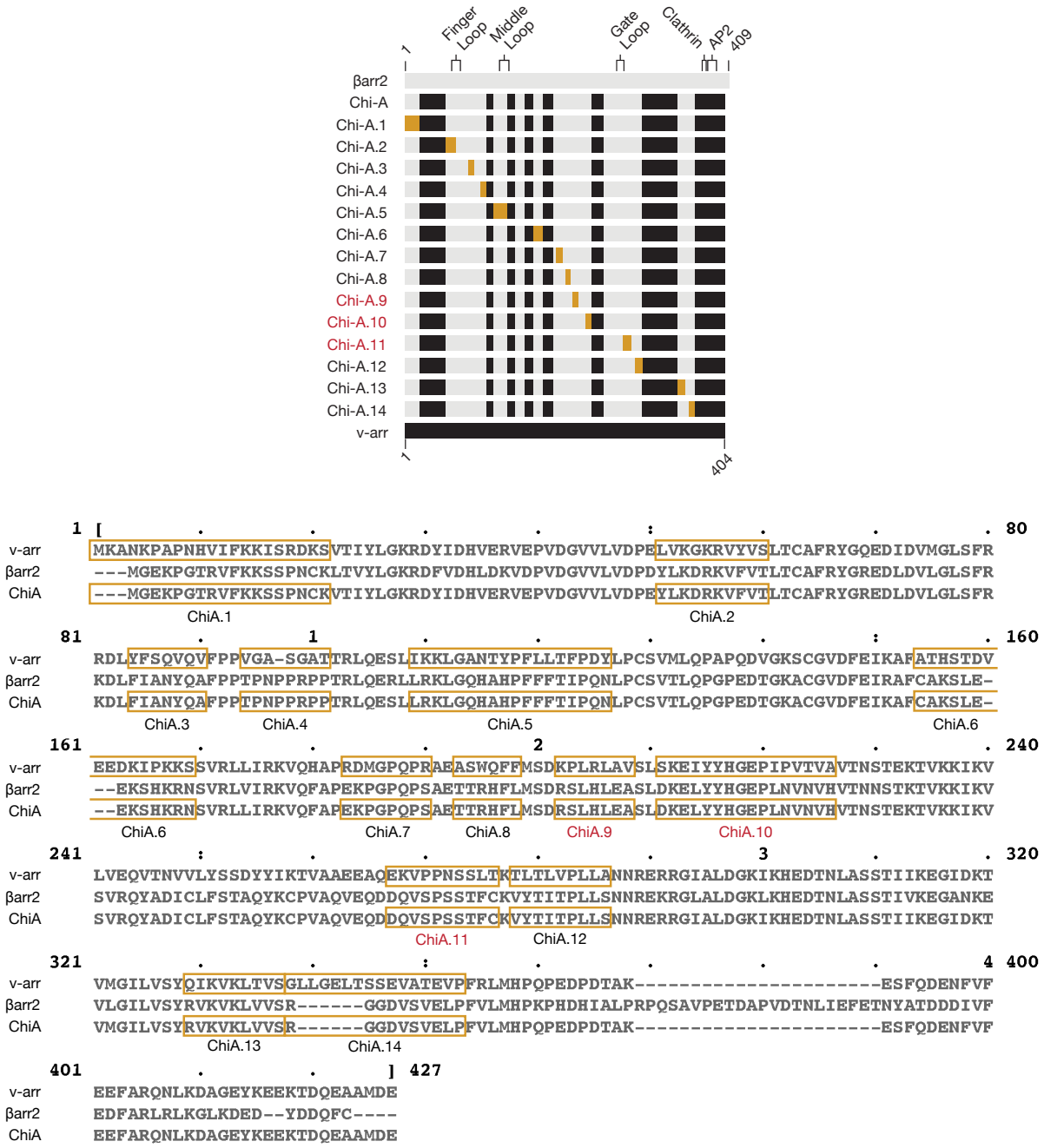

Extended Data Figure 5.2 Diagram and sequence maps of visual arrestin—β-arrestin-2 chimeras

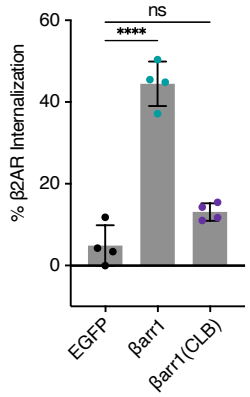

Extended Data Figure 5.3 Internalization of β2AR with β-arrestin-1 and the CLB mutant

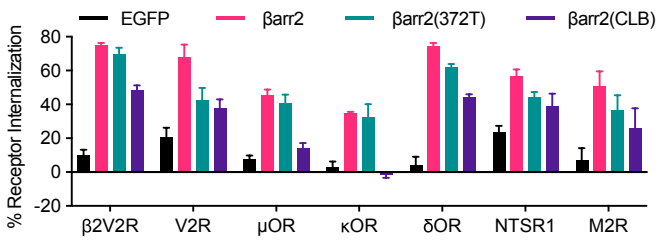

Extended Data Figure 5.4 Internalization of various receptors when co-expressed with either EGFP, wild type β-arrestin-2, the CLB mutant, or the 372T.

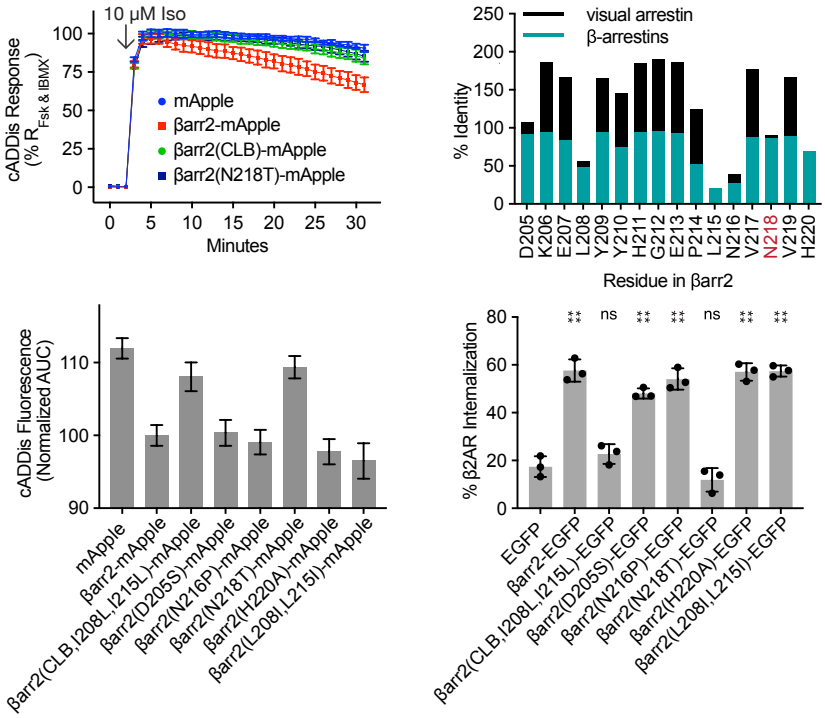

Extended Data Figure 5.5 N218 in the β-arrestin-2 CLB is required for β2AR internalization and desensitization.

Chapter 6: Discussion

Benjamin Barsi-Rhyne, in the laboratories of Aashish Manglik and Mark von Zastrow (UCSF), conceived the project, executed most of the experiments, and wrote the following chapter. Ruth Huttenhain, Qiongyu Li, and Jiewei Xu (UCSF) performed AP-MS and analyzed the results. Mark von Zastrow and Aashish Manglik contributed to project development, data analysis, and writing the following chapter.

6.1 Questions about GPCR-biased control of the endocytic network by β-arrestin

Why aren't clustered β2ARs internalized?

One of the more interesting observations made during this study was that β2ARs were clustered but not internalized in β-arrestin double knockout cells expressing the β-arrestin-2 C-lobe base mutant. This suggests that β2ARs clustered to clathrin-coated pits are not necessarily internalized and that the C-lobe base is specifically responsible for producing subsequent internalization. A caveat to these experiments is that the metric we used to measure β2AR clustering describes the histogram of the TIRF images and does not directly assess the degree of clustering in clathrin-coated structures. Despite not knowing the precise degree of receptor clustering into clathrin-coated structures, the CLB mutant of β-arrestin can promote β2AR clustering without undergoing subsequent internalization.

A possible explanation of clustering without internalization in the CLB mutant expressing cells is that the remaining endocytic determinant, the β-arrestin C-terminus, acts as a brake on endocytosis when in a particular conformation at the clathrin-coated pit. We sought to test this by lengthening and shorting the C-terminus and measuring internalization of the β2AR. This set of experiments showed that neither lengthening nor shorting the β-arrestin C-terminus significantly impacted β2AR internalization. We also tested if the lack of internalization seen in the CLB mutant could be relieved by altering the c-terminus length. These mutants showed no significant enhancement of internalization. Together, these data suggest that the length and presumably position of the β-arrestin C-terminus is unlikely to be a significant factor in controlling GPCR endocytosis.

Do GPCRs displace the β-arrestin C-terminus?

An area of β-arrestin that is poorly understood is how β-arrestin-mediated endocytosis occurs across receptors known to interact differently with the β-arrestins. An interpretation of our data is that some receptors (specifically β2AR, μOR, and κOR) displace the β-arrestin C-terminus weakly by comparison with other receptors (specifically δOR, β2V2R, M2R, V2R, NTSR1). Determining whether this is indeed the case is yet to be determined. To do so would require extending some existing biophysical tools, in vitro FRET to assess β-arrestin C-terminus release, from studies of phosphopeptides to phosphorylated receptors. With such a system, one could determine the relative propensity of distinct GPCRs to displace the β-arrestin C-terminus and confirm our hypothesis.

Is the CLB an interaction interface?

Perhaps the most important question raised by this study is how the β-arrestin CLB promotes internalization and desensitization of β2ARs. Our leading hypothesis is that the β-arrestin CLB acts as docking site for a yet to be identified protein interactor. A similar surface in an arrestin-like protein, VPS26, that is part of the retromer complex functions as a binding site for SNX3 and VPS35 (Lucas, Gershlick et al. 2016). We sought to identify this hypothesized binding partner by assessing known interactors and by unbiased proteomic analysis. The following preliminary experiments represent some attempts to identify a CLB interactor and are followed by a short discussion of other potential strategies.

To begin our candidate approach we compiled a list of proteins that were known to interact with β-arrestins (Kang, Tian et al. 2014) (Lane, Argoud-Puy et al. 2012) (Xiao, McClatchy et al.

2007), affected internalization of GPCRs (Kang, Tian et al. 2014), localized to the clathrin-coated pits, or some combination of these properties (Trexler and Taraska 2017).

Our first candidates were clathrin heavy-chain and the AP2 β-appendage, both of which are known to bind to the β-arrestin C-terminus, but haven't, as far as we know, been explicitly tested for binding to other regions of β-arrestin. To assess this, we purified GST-tagged terminal domain of clathrin heavy chain and the β-appendage (excluding the hinge region). We then incubated each protein with lysate from HEK293s that were transiently expressing β-arrestin-2-EGFP, either full length or C-terminally truncated to remove known AP2β and CTD, and then performed a pulldown on GSH resin. These experiments confirmed that binding to the terminal domain of clathrin heavy chain and the AP2β appendage relied on the β-arrestin-2 C-terminus.

We next tested other candidates by co-expressing each with β-arrestin-2-3xFLAG and performing anti-FLAG immunoprecipitations. Chief among these were the μ subunit of AP2, PIP5K1A, and select ubiquitin ligases. Our positive control, scFv30-HA, co-immunoprecipitated with β-arrestin-1 under basal conditions and was enriched in samples when cells were pretreated with the V2R agonist AVP. In contrast, none of our candidate proteins (PIP5K1A, Nedd4, Smurf2, Wwp2, and AP2μ) candidate proteins co-immunoprecipitated with wild type β-arrestin-2. An interpretation of these results is that wild type β-arrestin-2 does not bind stably to these candidate proteins. Additionally, it is unclear if stable binding to β-arrestin is necessary to fulfill the desensitization and internalization functions driven by the CLB.

We also sought to identify potential interacting proteins using affinity purification mass spectrometry (AP-MS). To do this, we co-expressed our β-arrestin-2-3xFLAG constructs (either wild type, 372T, CLB, or double mutants) with HA-tagged β2AR in β-arrestin-1/2 double knockout HEK293s with our without stimulation with 10 μM isoproterenol. Prior to sample submission, similar expression for β2AR and β-arrestin constructs were verified by western blot (CLB and double mutants not shown). AP-MS and subsequent statistical comparison of the conditions yielded ranked lists of candidate proteins (Tables 1 and 2) that were visualized as volcano plots. Comparisons between wild type and tail truncation mutants of β-arrestin were hard to make as the abundance of each protein were significantly different, likely the result of losing a NES from the β-arrestin-2 CT. Instead, we focused two proteins, PP1MG and FLNB whose abundance were altered when we compared the wild-type and CLB mutant of β-arrestin-2. Immunoprecipitation of wild type and CLB mutants of β-arrestin-2 overexpressed in these cells did not validate our AP-MS observations.

Taken together, these data suggest that identification of β-arrestin binding partners is nontrivial and may require alternative screening methods. As the β-arrestin CLB is necessary for both internalization and desensitization of β2AR, an interesting approach may be to perform sequential gene knockdown screens for these two functions. Once identified, a small number of genes required for both functions could then be tested for direct binding to β-arrestin.

What are β-arrestin(372T) clusters?

A fascinating observation made during these studies was that removal of the β-arrestin-2 CT resulted in plasma membrane associated β-arrestin-2 clusters that were distinct from clathrin structures. In addition, these clusters appeared to be dynamic as agonist addition resulted in

β-arrestin fluorescence redistribution from these clusters to clathrin structures. These results were reminiscent of pre-activated β-arrestin observed by mutation of the finger loop proximal region (Figure 2.3), but it is currently unclear if these represent distinct subcellular locations of β-arrestins. Although, it is curious that both removal of the CT and mutation of the FL are known to push β-arrestin towards an active conformation. It is possible that clusters observed upon removal of the β-arrestin CT represent a biologically relevant

Why does the CLB enhance β-arrestin/GPCR engagement?

It is well established the GPCRs differ significantly in how they bind the N-lobe of β-arrestins. It is also well established that the β-arrestin C-terminus competes with receptors for binding at this site. Therefore, it is not unreasonable to imagine that some GPCRs cannot effectively outcompete the β-arrestin C-terminus. As the N-lobe and finger loop of β-arrestins represent the key interaction surfaces that together drive the total affinity of the complex, it is possible that weak N-lobe binding would prevent a desensitization competent complex from forming. The ability of the CLB to enhance desensitization suggests a route to overcome this potential weakness.

6.2 Materials and Methods

Cell culture, expression constructs, and transfections

βarr1/2 double knockout HEK 293A lines, a gift from Aska Inouye and Silvio Gutkind (O'Hayre, Eichel et al. 2017), were cultured in complete growth Dulbecco's modified Eagle's medium (DMEM, Gibco) supplemented with 10% fetal bovine serum (UCSF Cell Culture Facility). Cell line cultures were free of mycoplasma contamination. Transfections were carried out using Lipofectamine 2000 according to the manufacturer's protocol. Cells were transfected 24-48h before experiments.

GST-CHC (clathrin heavy chain terminal domain) and GST-AP2β (appendage) were gifts from Jeffrey Benovic. Arrestin-3-EGFP (β-arrestin-2-EGFP) was previously described (Barak, Ferguson et al. 1997, Eichel, Jullié et al. 2016). Arrestin-3(372T)-EGFP (β-arrestin-2(372T)-EGFP) was generated by PCR and cloned into EGFP-N1 by InFusion HD (Takara). Arrestin-3(CLB) was generated by PCR and cloned into EGFP-N1 by InFusion HD (Takara). HA-V2R was previously described (Rochdi, Vargas et al. 2010). Arrestin-2-3xFLAG was generated by PCR and cloned by InFusion HD (Takara). HaloTag-β2AR was a gift from Justin Farlow. pcDNA3.1 was previously described (ClonTech). Myc-tagged Nedd4, Smurf2, and Wwp2 were previously generated by James Hislop. AP2μ-HA was a gift from Alexander Sorkin (Nesterov, Carter et al. 1999). Myc-tagged PIP5K1A was PCR amplified from pDONR223-PIP5K1A, a gift from William Hahn & David Root, and subcloned using InFusion HD (Takara).

Phosphopeptide

V2R phosphopeptide (ARGRpTPPpSLGPQDEpSCpTpTApSpSpSLAKDTSS) (Tufts University Core Facility).

GST Pull downs

HEK 293A β-arrestin-1/2 double knockout cells were seeded to 10-cm plates, transfected with the indicated construct 24 hour later, and harvested 48 hours post-transfection. Cells were resuspended in 500 µL lysis buffer (50 mM HEPES 7.5, 150 mM NaCl, 1% NP-40, 5% glycerol, cOmplete mini protease inhibitor), gently rotated at 4°C for 15 minutes, and then spun down at 15 ,000 x G for 15 minutes. GSH resin (Thermo Fisher) was pre-incubated with 1 mg of either GST-tagged AP2β or CHC (purified from E. coli) and washed 3 times with lysis buffer. Clarified HEK lysate was then loaded onto GSH resin ± 1 µM V2Rpp, rotated for 2 hours at 4°C, washed three times with lysis buffer and eluted (50 mM HEPES 7.5, 150 mM NaCl, 1% NP-40, 5% glycerol, 10 mM reduced glutathione). Samples were then mixed with Laemelli sample buffer, boiled for five minutes, and storage at -20°C until gel electrophoresis.

Co-immunoprecipitations

HEK 293A β-arrestin-1/2 double knockout cells were seeded onto 6-cm dishes 24 hours prior to transfection with the indicated constructs. After transfection, cells were incubated in complete media for 24-hours. Cells were treated with the indicated agonist for 5-20 minutes, washed with ice cold PBS, and 250 µL lysis buffer (50 mM HEPES 7.5, 150 mM NaCl, 1% NP-40, 5% glycerol, cOmplete mini protease inhibitor) was added. Cells were removed and placed into microfuge tubes that were gently rotated at 4°C for 15 minutes and then spun down at 15 ,000 x G for 15 minutes. Supernatant was applied to pre-equilibrated magnetic M2 dynabeads (Thermo Fisher) and rotated in the cold for at least 2 hours, washed three times with lysis buffer, and eluted (50 mM HEPES 7.5 150 mM NaCl, 1% NP-40, 5% glycerol, 500 ug/ml 3xFlag peptide). Samples were then mixed with Laemelli sample buffer, boiled for five minutes, and storage at -20°C until gel electrophoresis.

Western blots

Protein samples were loaded onto SDS/PAGE gels (Thermo Fisher), run until the dye front reach the bottom of the gel, and transferred to nitrocellulose. Nitrocellulose was blocked with TBS Odyssey blocking buffer (LI-COR) for one hour at room temperature and then incubated for one hour with primary antibodies at 1:1000: anti-EGFP (Sigma Aldrich 11814460001), anti-HA (Covance PRB-101P), anti-β-arrestin-1/2 (CST 4674S), anti-myc (CST 2276S), anti-filamen B (CST 12979S), anti-PIP5K1A (CST 9693S), and anti-PP1MG (Bethyl Laboratories A300-880A-M). Membranes were washed three times for 5 min in TBS-Tween (0.1% v/v) and incubated with a IRDye 680-labeled anti-rabbit secondary antibody (1:3,000, LI-COR 926-68073) and an IRDye 800-labeled anti-mouse secondary antibody (1:3,000, LI-COR 926-32212) for one hour at room temperature. Membranes were washed three times for 5 min in TBS-Tween (0.1% v/v), imaged using an Odyssey Infrared Imaging System (LI-COR) in the linear range.

GST-CHC and GST-AP2β purifications

N-terminally GST-tagged CHC (amino acids 1-363) or AP2β (amino acids 70–937) constructs in the pGEX4T vector were transformed into BL21-(DE3)-Rosetta2 cells. The next day, cultures were grown overnight at 30°C overnight at 160 RPM. The following day, cultures were inoculated and grown at 37 °C to an absorbance ($A_{600\ nm}$) of 0.5 in Terrific broth and then equilibrated to 20 °C. Expression was induced with 0.3 mM isopropyl 1-thio-β-d-galactopyranoside overnight at this temperature, and cells were collected by centrifugation at 6,000 x *g*. Pellets were resuspended with cold lysis buffer (50 mM TRIS pH 8.0, 500 mM NaCl, protease inhibitors, lysozyme, benzonase, 2 mM DTT). Cells were lysed by sonication and cleared by centrifugation at 16,000*g* for 30 min. The clarified supernatant was loaded onto a

column containing 1 mL of settled GSH resin (Thermo Fisher) at room temperature and recirculated once. Resin was washed on-column with 10 column volumes of wash buffer (20 mM Tris pH 8.0, 150 mM NaCl, 2 mM DTT). GST-tagged protein was eluted (20 mM Tris pH 8.0, 150 mM NaCl, 10 mM reduced glutathione). Fractions were analyzed by SDS–PAGE, fractions containing the correct molecular weight were pooled, dialyzed overnight, concentrated, flash-frozen in liquid N_2, and stored at −80 °C.

6.3 Frontiers of β-arrestin biology

β-arrestin at the clathrin-coated pit

Relatively little is currently known about β-arrestins and GPCR/β-arrestin complexes at the clathrin-coated pit and there is accumulating evidence of β-arrestins carrying out unique functions at this complex subcellular structure. First, multiple studies how shown that GPCRs can influence clathrin-coated pit lifetime and that a possible mechanism for doing so is through engagement with β-arrestins. How β-arrestins can switch from promoting endocytosis to stalling clathrin-coated pits and inhibiting endocytosis of other cargoes, is currently unclear. Interestingly, β-arrestin appears to stall clathrin coated pits when recruited to CCSs without co-clustering of its activating GPCR. As GPCRs are not known to strongly engage the endocytic machinery directly, it is interesting to speculate about possible mechanisms by which β-arrestins may specifically stall endocytosis. One possibility is that β-arrestins, when dissociated from their activating GPCR, function as a brake on endocytosis that can be release upon subsequent GPCR rebinding. β-arrestins may be capable of stalling CCPs because of their direct binding to both AP2β and clathrin, as well as a yet to be determinant CCP protein, which may bridge these interactions in a way that prevents clathrin-coat maturation. Since AP2β and clathrin move relative to each other in the nascent pit (Saffarian and Kirchhausen 2008, Loerke, Mettlen et al. 2011), tethering the two by the β-arrestin may stop this motion and thereby prevent clathrin-coat from transitioning from flat lattices to curved pits. Another intriguing and much simpler possibility is that β-arrestins control CCPs by local control of PIP2 composition of the plasma membrane (Jung, Jiang et al. 2021).

Another area that may be starting to become tractable is assembly of large molecular complexes of β-arrestin and its associated proteins. There have been several GPCR/β-arrestin

structures published recently and similarly large advances have been made in solving structures of complexes associated with the clathrin-coated pit. However, to my knowledge, no structures of GPCR/β-arrestin/CCP proteins have been described. Getting a high-resolution view of these complexes would tell us much about GPCR/β-arrestin endocytosis and might help explain β-arrestins ability to stall CCPs.

β-arrestin role in GPCR recycling

It has been inferred from multiple studies of β-arrestin trafficking effects on GPCRs that they somehow prevent recycling of GPCRs back to the plasma membrane after endocytosis. While the experimental evidence for this is quite convincing, relatively little is currently known about how β-arrestin could control such a process. A requirement for recycling of some GPCRs appears to be entry into recycling tubules on endosomes, which is facilitated by the presence of PDZ ligands on the cytoplasmic tail of some GPCRs. As β-arrestin remains associated with many GPCRs at the endosome, it is interesting to speculate that it physically prevents entry into in recycling tubule.

6.4 Final Summary

β-arrestins are critical players in signaling and trafficking of hundreds of GPCRs. The role of these receptors in nearly every aspect of physiology means that any significant advance in understand β-arrestins is likely to have far-reaching implications. Work described in this thesis has led to a reevaluation of β-arrestin function as an endocytic adaptor and revealed new mechanisms by which they are activated. I hope that the conclusions draw here will inspire further investigation into this fascinating protein.

6.5 References

Barak, L. S., et al. (1997). A beta-arrestin/green fluorescent protein biosensor for detecting G protein-coupled receptor activation. *J Biol Chem 272*(44): 27497-27500. 10.1074/jbc.272.44.27497

Eichel, K., et al. (2016). β-Arrestin drives MAP kinase signalling from clathrin-coated structures after GPCR dissociation. *Nat. Cell Biol. 18*(3): 303-310. 10.1038/ncb3307

Jung, S. R., et al. (2021). beta-arrestin-dependent PI(4,5)P2 synthesis boosts GPCR endocytosis. *Proc Natl Acad Sci U S A 118*(17). 10.1073/pnas.2011023118

Kang, D. S., et al. (2009). Structure of an arrestin2-clathrin complex reveals a novel clathrin binding domain that modulates receptor trafficking. *J Biol Chem 284*(43): 29860-29872. 10.1074/jbc.M109.023366

Kang, D. S., et al. (2014). Role of β-arrestins and arrestin domain-containing proteins in G protein-coupled receptor trafficking. *Curr. Opin. Cell Biol. 27*: 63-71. 10.1016/j.ceb.2013.11.005

Lane, L., et al. (2012). neXtProt: a knowledge platform for human proteins. *Nucleic Acids Res 40*(Database issue): D76-83. 10.1093/nar/gkr1179

Latorraca, N. R., et al. (2020). How GPCR Phosphorylation Patterns Orchestrate Arrestin-Mediated Signaling. *Cell 183*(7): 1813-1825 e1818. 10.1016/j.cell.2020.11.014

Loerke, D., et al. (2011). Measuring the hierarchy of molecular events during clathrin-mediated endocytosis. *Traffic 12*(7): 815-825. 10.1111/j.1600-0854.2011.01197.x

Lucas, M., et al. (2016). Structural Mechanism for Cargo Recognition by the Retromer Complex. *Cell 167*(6): 1623-1635 e1614. 10.1016/j.cell.2016.10.056

Maib, H., et al. (2018). Cargo regulates clathrin-coated pit invagination via clathrin light chain phosphorylation. *J Cell Biol 217*(12): 4253-4266. 10.1083/jcb.201805005

Nesterov, A., et al. (1999). Inhibition of the receptor-binding function of clathrin adaptor protein AP-2 by dominant-negative mutant mu2 subunit and its effects on endocytosis. *EMBO J 18*(9): 2489-2499. 10.1093/emboj/18.9.2489

O'Hayre, M., et al. (2017). Genetic evidence that β-arrestins are dispensable for the initiation of β2-adrenergic receptor signaling to ERK. *Sci. Signal. 10*(484). 10.1126/scisignal.aal3395

Puthenveedu, M. A. and M. von Zastrow (2006). Cargo regulates clathrin-coated pit dynamics. *Cell 127*(1): 113-124. 10.1016/j.cell.2006.08.035

Rochdi, M. D., et al. (2010). Functional characterization of vasopressin type 2 receptor substitutions (R137H/C/L) leading to nephrogenic diabetes insipidus and nephrogenic syndrome of inappropriate antidiuresis: implications for treatments. *Mol Pharmacol 77*(5): 836-845. 10.1124/mol.109.061804

Saffarian, S. and T. Kirchhausen (2008). Differential evanescence nanometry: live-cell fluorescence measurements with 10-nm axial resolution on the plasma membrane. *Biophys J 94*(6): 2333-2342. 10.1529/biophysj.107.117234

Trexler, A. J. and J. W. Taraska (2017). Two-Color Total Internal Reflection Fluorescence Microscopy of Exocytosis in Endocrine Cells. *Methods Mol Biol 1563*: 151-165. 10.1007/978-1-4939-6810-7_11

von Kleist, L., et al. (2011). Role of the clathrin terminal domain in regulating coated pit dynamics revealed by small molecule inhibition. *Cell 146*(3): 471-484. 10.1016/j.cell.2011.06.025

Xiao, K., et al. (2007). Functional specialization of beta-arrestin interactions revealed by proteomic analysis. *Proc Natl Acad Sci U S A 104*(29): 12011-12016. 10.1073/pnas.0704849104

6.6 Figures

Figure 6.1 β-arrestin C-terminus is required to bind the clathrin-terminal domain and the AP2 β-appendage

A) Diagram of the experimental workflow showing purification of the GST fusion of either clathrin terminal domain (CHC) or AP2 β-appendage (AP2β) purified from bacteria. Incubated with HEK293 lysate expressing β-arrestin-2-EGFP (Arr3-EGFP) or β-arrestin-2-EGFP C-terminus truncation (Arr3(372T)-EGFP) and then pulled-down. B) Western blot of HEK293 lysate expressing either β-arrestin-2 construct, the flow through, and eluate from GSH resin in the presence of absence of GST-AP2β. GST-AP2β is not shown and addition of V2Rpp during incubation step had no obvious impact. C) Western blot of HEK293 lysate expressing either β-arrestin-2 construct, the flow through, and eluate from GSH resin in the presence of absence of GST-CHC. GST-AP2β is not shown and addition of V2Rpp during incubation step had no obvious impact.

Figure 6.2 Immunoprecipitation of β-arrestins and candidate interacting proteins.

A) Immunoprecipitation and western blots of β-arrestin-1 with co-expressed with HA-V2R and scFv30-HA in βarr1/2 DKO HEK293s showing that scFv30 co-immunoprecipitates with βarr1 under basal conditions and which is increased after stimulation of V2R with 1 μM AVP. B) Immunoprecipitation and western blots of β-arrestin-2 with co-expressed with HA-V2R and myc-PIP5K1A in βarr1/2 DKO HEK293s showing that neither PIP5K1A nor V2R detectably co-immunoprecipitate after stimulation with 1 μM AVP. C) Immunoprecipitation and western blots of β-arrestin-2 wild type or CLB mutant with co-expressed with AP2μ-HA in βarr1/2 DKO HEK293s showing that they do not detectably co-immunoprecipitate. D) Immunoprecipitation and western blots of β-arrestin-2 co-expressed with either HaloTag-β2AR and scFv30-HA, or the E3 ligases Nedd4-myc, Smurf2-myc, or Wwp2-myc showing a lack of detectable co-immunoprecipitation.

Figure 6.3 AP-MS volcano plots from comparisons across isoproterenol treated or untreated cells expressing β2AR and either β-arrestin-2, 372T, CLB, or double mutants and immunoprecipitation to validate labeled hits.

A) Volcano plots showing p-values against log2 fold concentration comparisons across the indicated samples (gray boxes). Blue colored dots are hits enriched in the first condition (e.g., ARR3_ISO) and red colored dots are hits enriched in the second condition (e.g., ARR3_372T_CLB_ISO). B) Immunoprecipitation and western blots of β-arrestin-2 expressed in HEK293 βarr1/2 DKO showing no detectable immunoprecipitation of protein phosphatase 1 gamma (PP1MG), filamen B, and phosphoinositol 5 phosphate kinase 1 a (PP5K1A)

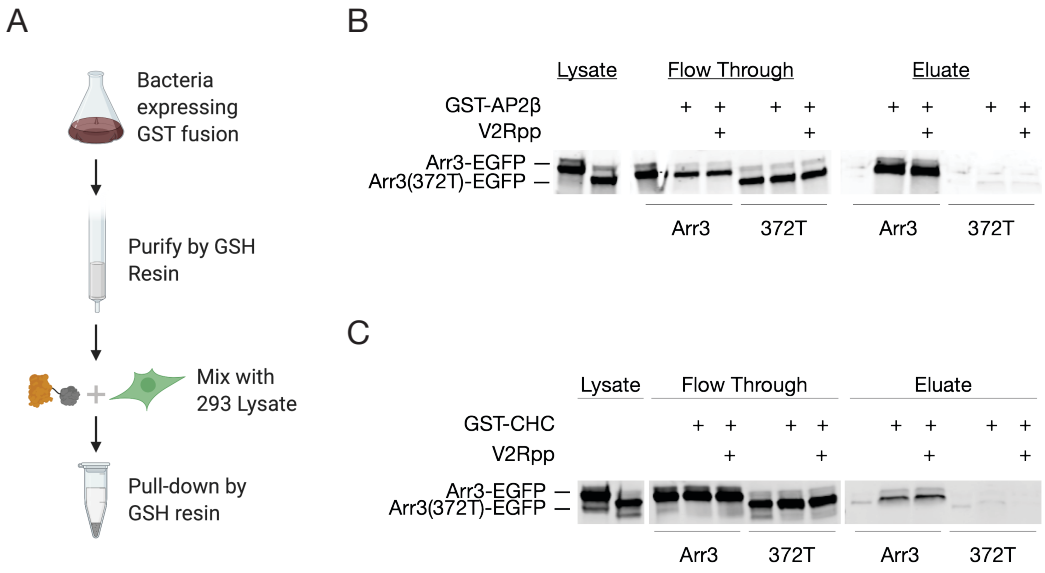

Figure 6.1 β-arrestin C-terminus is required to bind the clathrin-terminal domain and the AP2 β-appendage

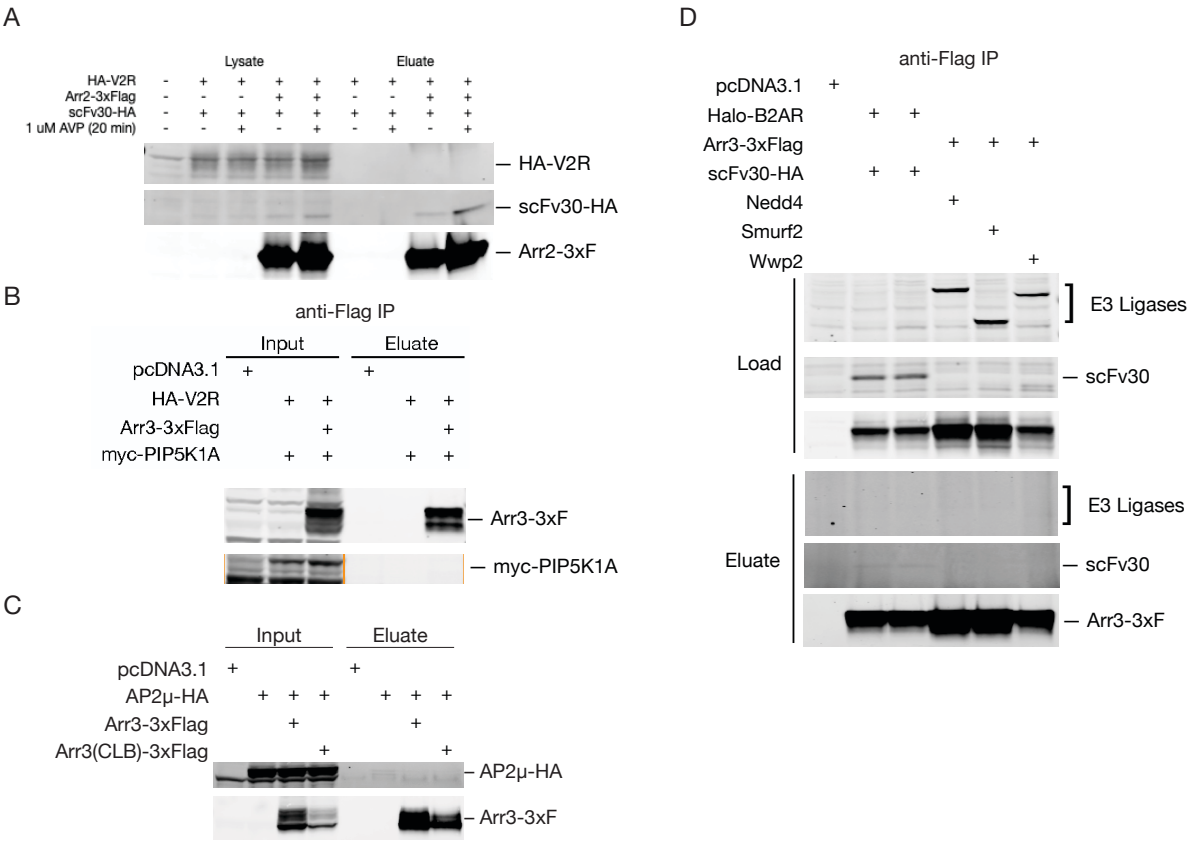

Figure 6.2 Co-immunoprecipitation of β-arrestins and candidate interacting proteins.

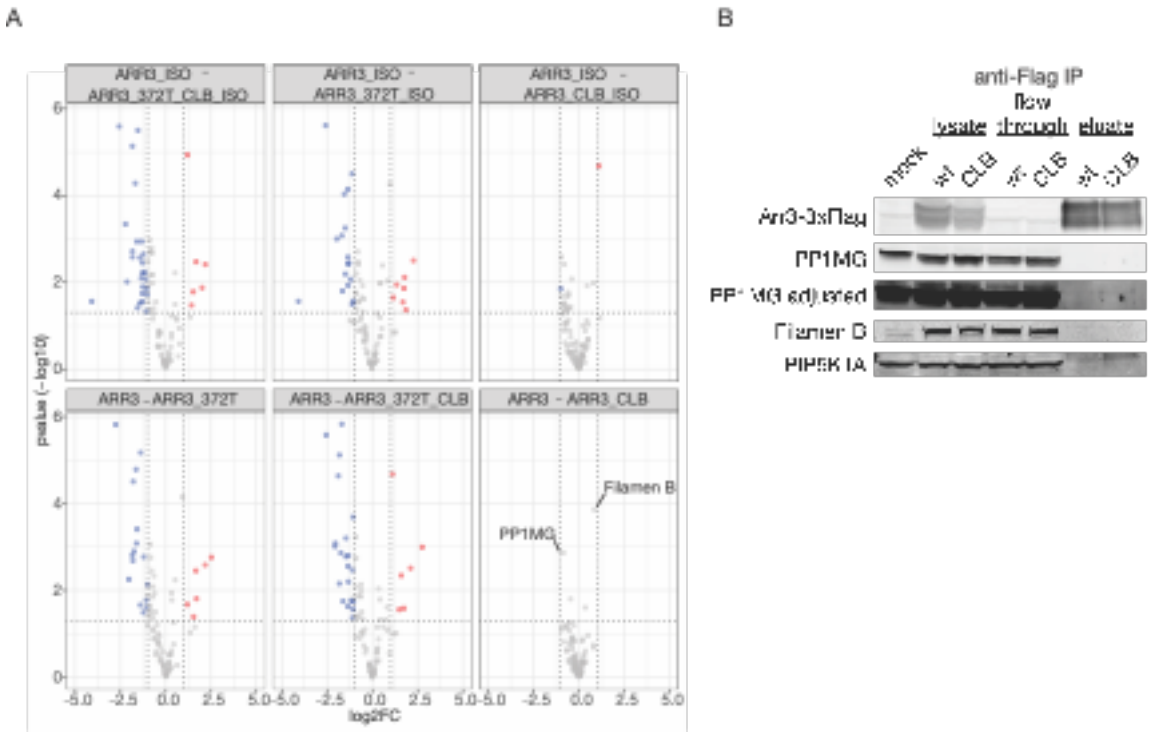

Figure 6.3 AP-MS volcano plots from comparisons across isoproterenol treated or untreated cells expressing β2AR and either β-arrestin-2, 372T, CLB, or double mutants and immunoprecipitation to validate labeled hits.

Table 6.1 AP-MS data comparing hits from βarr2, βarr2(372T), βarr2(CLB), and βarr2(CLB,372T) with and without isoproterenol stimulation

Protein	Gene	ProteinName	EntrezID	ProteinRef	ARR3-ARR3_372T		ARR3-ARR3_372T_CLB		ARR3-ARR3_CLB		ARR3_ISO-ARR3_372T_ISO		ARR3_ISO-ARR3_372T_CLB_ISO		ARR3_CLB-ARR3_CLB_ISO	
					log2FC	pvalue	log2FC	pvalue	log2FC	pvalue	log2FC	pvalue	log2FC	pvalue	log2FC	pvalue
Q96CW1	AP2M1	adaptor relat	1173	Q96CW1	-0.1465626	0.52852706	0.1882454	0.42204937	0.00105307	0.99633910	0.190770626	0.41610984	0.318822047		0.189727293	0.17032408	0.465896187
O00203	AP3B1	adaptor relat	8546	O00203	-0.439795	0.14193606	-0.3542264	0.22586543	-0.347307294	0.23424000	-0.416509396	0.16143787	-0.398429548		0.178213428	-0.6801244	0.035844099
O14617	AP3D1	adaptor relat	8943	O14617	-0.3518132	0.11552014	-0.4024725	0.07812748	-0.348680372	0.11831807	-0.56326299	0.02227988	-0.530691461		0.02868163	-0.8010227	0.003845534
Q9Y2T2	AP3M1	adaptor relat	26985	Q9Y2T2	-0.6995854	0.00825665	-0.6289341	0.01394755	-0.206331314	0.33407156	-0.687477036	0.00902306	-0.728867834		0.006674829	-0.6027931	0.016994355
Q92572	AP3S1	adaptor relat	1176	Q92572	-0.783023	0.00354856	-0.6423933	0.01015806	-0.324545367	0.12952661	-0.788042797	0.00342262	-0.869030773		0.001937384	-0.5594547	0.019499874
P23526	AHCY	adenosylhom	191	P23526	-2.0323205	0.00554464	-1.6034092	0.01796857	-0.847761882	0.15541845	-1.647807316	0.01585520	-1.423860366		0.029979272	-0.4539356	0.425394583
O43865	AHCYL1	adenosylhom	10768	O43865	-2.7478486	1.52E-06	-2.5573024	2.63E-06	-0.488989511	0.05592169	-2.582437713	2.44E-06	-2.566201243		2.56E-06	-0.5342654	0.040491103
Q96HN2	AHCYL2	adenosylhom	23382	Q96HN2	negInf	NA	negInf	NA	negInf	NA	-4.07687026	0.02714821	-4.068897349		0.027335122	Inf	NA
P07550	ADRB2	adrenoceptor	154	P07550	1.67164762	0.00353335	1.59569342	0.00457828	-0.21340923	0.61654994	1.154894301	0.02253307	1.683177472		0.003398574	-0.3573058	0.40855722
Q8N302	AGGF1	angiogenic f	55109	Q8N302	-0.8529342	0.02269381	-0.5287138	0.08926075	-0.107863784	0.71326155	negInf	NA	negInf	NA	negInf	NA	
Q12955	ANK3	ankyrin 3	288	Q12955	-0.3872721	0.16283005	-0.0121519	0.96271476	0.279533297	0.29946496	-0.419024097	0.13486429	-0.014567972		0.955310155	0.19668812	0.457482642
O75179	ANKRD17	ankyrin repe	26057	O75179	-1.760533	0.00126842	-1.7341405	0.00138234	-0.710863745	0.07440146	-1.110881126	0.03184577	-1.276575467		0.018015056	-0.2906607	0.506827515
Q9UKV3	ACIN1	apoptotic chr	22985	Q9UKV3	-0.5829993	0.03211118	-0.5830225	0.03210665	0.037399375	0.87216123	-0.365309187	0.14326318	-0.749891561		0.010361879	-0.6438553	0.021138919
P53396	ACLY	ATP citrate l	47	P53396	0.06085116	0.77265062	0.12248954	0.56408271	0.012026752	0.95434474	0.164692536	0.44196047	0.121455953		0.567305302	0.22755637	0.29614703
O75947	ATP5PD	ATP synthase	10476	O75947	0.0847459	0.77907915	0.61113888	0.06975657	0.362910021	0.24922766	-0.116951277	0.69933047	0.122593865		0.685724577	0.0615774	0.838292909
P25440	BRD2	bromodomai	6046	P25440	1.17825635	0.02136022	0.82173056	0.08175502	-0.318359426	0.46285001	1.351816651	0.01128933	0.732270547		0.114079372	-0.7132175	0.122375948
Q15059	BRD3	bromodomai	8019	Q15059	1.59804119	0.06999708	1.74354799	0.02590618	-0.151774143	0.80647856	1.848116309	0.04375317	1.352760329		0.062627386	-0.7598372	0.247217686
O60885	BRD4	bromodomai	23476	O60885	1.54510515	0.04051409	1.16595424	0.10275281	-0.321758402	0.62497261	1.682091515	0.02893110	2.006202655		0.013210728	-0.4869922	0.46382087
Q16543	CDC37	cell division c	11140	Q16543	-0.6481515	0.00466358	-0.912666	0.00059738	-0.146086957	0.40712834	-0.538625875	0.01213381	-0.780010052		0.001599643	-0.0233638	0.892179369
Q6P199	CDC73	cell division c	79577	Q6P199	0.08057284	0.65023687	0.02706995	0.8781957	0.133883544	0.45640777	0.184552064	0.31214392	0.068375071		0.699857107	0.12022202	0.502156294
Q96B23	C18orf25	chromosome	147339	Q96B23	0.03307065	0.92527036	-0.1116108	0.75229674	-0.088179673	0.80284994	-0.136434419	0.70009773	-0.714372658		0.069919706	-0.981356	0.020754201
Q12996	CSTF3	cleavage stin	1479	Q12996	0.3066026	0.20623359	-0.1557199	0.50457525	-0.144657843	0.53451486	-0.410989493	0.10242831	-0.374459787		0.131463756	-0.2613059	0.27477983
Q6PD62	CTR9	CTR9 homolc	9646	Q6PD62	-0.1102363	0.57053379	-0.0498405	0.79591083	-0.078911671	0.68315561	0.079758983	0.6799766	-0.088176342		0.64877383	-0.1792539	0.364321003
Q6UX04	CWC27	CWC27 splic	10283	Q6UX04	-0.9902788	0.01320781	-1.3295388	0.00277974	-0.666696233	0.06541215	-0.938868304	0.01694722	-1.155380591		0.006062302	-0.8034948	0.033048033
Q96S94	CCNL2	cyclin L2	81669	Q96S94	-0.5477618	0.30763492	-0.9355166	0.11678029	0.806254838	0.21071985	negInf	NA	negInf	NA	NA	NA	NA
P61962	DCAF7	DDB1 and CL	10238	P61962	0.00979377	0.97630146	0.13587677	0.68189926	0.257062832	0.44439849	-0.65906181	0.07308792	-0.224700472		0.501907839	0.04964378	0.880393974
Q9UJV9	DDX41	DEAD-box he	51428	Q9UJV9	-1.2189686	0.00170452	-1.4483361	0.00062974	-0.422863676	0.13131699	-1.687864833	0.00084402	-1.600168435		0.001149987	-0.4503291	0.180996215
Q7L014	DDX46	DEAD-box he	9879	Q7L014	-0.8219399	0.00174708	-0.6358464	0.00738614	-0.148348566	0.43013137	-0.805314087	0.00197441	-0.894667011		0.001038468	-0.0511645	0.781722869
Q13838	DDX39B	DExD-box hel	7919	Q13838	negInf	NA	negInf	NA	negInf	NA	-1.057567202	0.08251092	-2.131120632		0.009703091	Inf	NA
Q9NPA8	ENY2	ENY2 transcr	56943	Q9NPA8	-0.8411669	0.02921075	-0.9911974	0.01414667	-0.252313183	0.44945423	-1.291967813	0.00357488	-1.100593006		0.00844023	-0.7281121	0.050890615
P38919	EIF4A3	eukaryotic tr	9775	P38919	-1.8141244	0.00207198	-2.0525647	0.00097446	-0.858802301	0.06703141	-1.483428584	0.00641505	-1.833165573		0.001947227	-0.9162531	0.05374682
O75369	FLNB	filamin B	2317	O75369	0.93081822	7.16E-05	1.10230299	2.11E-05	0.848379513	0.00013721	0.966869959	5.46E-05	1.194573764		1.17E-05	1.10336501	2.10E-05
P35269	GTF2F1	general trans	2962	P35269	0.64258159	0.53596247	0.94689091	0.28434928	-0.31910553	0.70293343	Inf	NA	Inf	NA	0.506044787	0.31582768	0.70579724
Q8IXQ4	GPALPP1	GPALPP moti	55425	Q8IXQ4	-1.8357266	0.00155485	-2.0325634	0.00082587	-0.368106886	0.37418803	-1.97212187	0.0009991	-2.228928346		0.000455117	-0.1602335	0.692804233
Q6Y7W6	GIGYF2	GRB10 interi	26058	Q6Y7W6	0.30519588	0.24675625	0.28375901	0.27878443	0.174102354	0.49619505	0.830481717	0.00935485	0.267660326		0.304999571	0.8117429	0.010482511
Q7Z4V5	HDGFL2	HDGF like 2	84717	Q7Z4V5	-0.6279071	0.12315044	-0.8856004	0.04117842	-0.169233612	0.65471628	-0.379204474	0.32846023	-0.875758707		0.042950795	-0.9428588	0.032237858
Q7Z6Z7	HUWE1	HECT, UBA a	10075	Q7Z6Z7	-0.0246172	0.90903604	-0.1522521	0.48660472	-0.040312584	0.85168767	-0.310282634	0.17550085	-0.349370002		0.132751658	-0.0750612	0.728481714
Q9NX55	HYPK	huntingtin in	25764	Q9NX55	-0.94842	0.03997972	-0.1818805	0.54584317	0.272156734	0.46472649	-0.078950052	0.78991228	0.233849009		0.443037736	0.49733852	0.207890272
O60921	HUS1	interacts wit	3364	O60921	Inf	NA	Inf	NA	-0.455978866	0.01599405	Inf	NA	Inf	NA		0.06455902	0.600539052
Q96ST2	IWS1	interacts wit	55677	Q96ST2	0.18986462	0.7539031	0.11164473	0.85343817	0.153097361	0.80021129	0.289721474	0.63382501	0.285937853		0.638198331	-0.5437224	0.379968856
O00505	KPNA3	karyopherin s	3839	O00505	0.52214306	0.00586333	0.4249987	0.01634229	-0.224430579	0.14840719	0.557677059	0.00409487	0.518079198		0.006112596	0.0055463	0.969440552
Q07666	KHDRBS1	KH RNA bind	10657	Q07666	2.50657184	0.00173627	2.74023181	0.00100412	0.79223464	0.18333994	2.266551995	0.00313443	2.178994462		0.003916042	1.15460139	0.066537737
Q92945	KHSRP	KH-type splic	8570	Q92945	0.19890608	0.31543285	0.21561534	0.27914083	0.017781055	0.92608403	0.115971425	0.54974276	0.055108598		0.77424012	0.10352484	0.592502857
Q8WVC0	LEO1	LEO1 homolc	123169	Q8WVC0	-0.0219176	0.8658595	0.26248279	0.07012919	0.345355747	0.02511598	0.415753725	0.01071746	0.108710743		0.412131979	-0.1599818	0.238688298
Q9Y4Z0	LSM4	LSM4 homolc	25804	Q9Y4Z0	-0.5109323	0.2520016	-0.7036575	0.12923566	-0.645030061	0.23905082	-0.340442957	0.43294403	-0.457487554		0.300518684	0.44988972	0.308003793
O95777	LSM8	LSM8 homolc	51691	O95777	-1.2312767	0.03268035	-1.333997	0.02375234	-0.951339587	0.07932531	-0.942061763	0.08170274	-1.276407454		0.028388232	-0.641841	0.295600869
P41227	NAA10	N-alpha-acet	8260	P41227	-0.4804383	0.06250824	-0.137589	0.55287337	-0.060680373	0.79163732	-0.395694996	0.11271375	-0.349933577		0.153821553	0.24913049	0.294583988
Q9BXJ9	NAA15	N-alpha-acet	80155	Q9BXJ9	-0.1316716	0.64533098	-0.0765879	0.78796968	0.270304743	0.35504822	-0.233469303	0.42117250	-0.219835849		0.447732089	0.31529197	0.285320017
P32120	NA	NA	NA	P32120-2	1.69917743	0.01579471	1.49123402	0.02802544	-0.693441072	0.24832523	1.752086238	0.01367869	1.422364111		0.033960379	-0.3399303	0.558540867
Q9Y2X3	NOP58	NOP58 ribon	51602	Q9Y2X3	-1.0021951	0.00733131	-1.31405	0.00158958	-0.156537647	0.59272284	-0.758405965	0.02711997	-1.237653142		0.002273407	-0.4713032	0.132024537
Q14978	NOLC1	nucleolar an	9221	Q14978	-0.3116245	0.38208316	-0.3914116	0.27885238	-0.099418512	0.77545682	-0.193615101	0.58133517	-0.364560134		0.310793473	-0.6657197	0.08359096
P49790	NUP153	nucleoporin 1	9972	P49790	0.32331366	0.62160296	0.01274708	0.98718409	-0.568160441	0.39595280	1.28888006	0.14140521	0.774263035		0.25935343	-0.3247521	0.620086004
Q8N7H5	PAF1	PAF1 homolc	54623	Q8N7H5	0.35058731	0.01669288	-0.0576628	0.63333547	0.192531415	0.13639766	0.265042131	0.05214294	0.850185456		0.850185456	-0.4043464	0.008356259
O43447	PPIH	peptidylprolv	10465	O43447	0.7102702	0.04302789	-0.7224939	0.04034023	0.299644026	0.34052127	-0.639607243	0.06247489	-0.670610468		0.053049248	0.1985904	0.520723174
Q8TBX8	PIP4K2C	phosphatidyl	79837	Q8TBX8	0.20862776	0.47969213	0.22900785	0.43934169	-0.129341346	0.65804138	0.414139555	0.17934775	0.189916103		0.518805139	-0.5815108	0.07264631
Q9H814	PHAX	phosphorylat	51808	Q9H814	-0.4478676	0.16949009	-0.5400631	0.10611985	-0.288522773	0.35916771	-0.879059628	0.01804299	-0.963805295		0.011710673	-0.0755207	0.805442083
Q8TF01	PNISR	PNN interact	25957	Q8TF01	-0.8988126	0.03360872	-1.0394818	0.01810468	-0.533284008	0.16716321	-0.855632096	0.0405292	-1.295531628		0.006121471	-0.8418693	0.043278003
Q86U42	PABPN1	poly(A) bindi	8106	Q86U42	negInf	NA	negInf	NA	NA	NA	negInf	NA	negInf	NA	NA	NA	NA
O43172	PRPF4	pre-mRNA pi	9128	O43172	-0.6754522	0.07678299	-0.4762593	0.18706099	-0.083695083	0.80459446	-1.178415048	0.00853236	-1.058662706		0.014050044	-0.058897	0.886784652
O75400	PRPF40A	pre-mRNA pi	55660	O75400	-1.3972323	0.02187591	-1.8245429	0.00702267	-0.115428529	0.83330692	-1.328597688	0.01167093	-1.829982509		0.002634754	0.36491114	0.363689878

					ARR3-ARR3_372T		ARR3-ARR3_372T_CLB		ARR3-ARR3_CLB		ARR3_ISO-ARR3_372T_ISO		ARR3_ISO-ARR3_372T_CLB_ISO		ARR3_CLB-ARR3_CLB_ISO	
Protein	Gene	ProteinName	EntrezID	ProteinRef	log2FC	pvalue	log2FC	pvalue	log2FC	pvalue	log2FC	pvalue	log2FC	pvalue	log2FC	pvalue
Q9NY27	PPP4R2	protein phos	151987	Q9NY27	-0.1181773	0.77886697	0.34658587	0.42038091	0.396158457	0.450655327	0.151535268	0.719318607	-0.150061941	0.721908689	0.2771793	0.515674242
O15355	PPM1G	protein phos	5496	O15355	-1.6452936	1.63E-05	-1.8202213	7.68E-06	-0.861113163	0.001364327	-1.341060631	7.15E-05	-1.835483901	7.21E-06	-0.4499075	0.036642568
Q3YEC7	RABL6	RAB, membe	55684	Q3YEC7	negInf	NA	negInf	NA	NA	NA	-1.244646944	0.075896194	-1.548863718	0.038968412	-0.2169869	0.76345906
O60671	RAD1	RAD1 checkp	5810	O60671	Inf	NA	Inf	NA	0.032065238	0.922685897	Inf	NA	Inf	NA	-0.1371987	0.681297574
Q9NS91	RAD18	RAD18 E3 ub	56852	Q9NS91	-0.3170181	0.42980018	-0.1637272	0.67893105	0.032904664	0.933343664	-0.494456878	0.230808889	-0.437589403	0.284227017	-0.458939	0.263087208
A1A4S6	ARHGAP10	Rho GTPase	79658	A1A4S6	0.16478372	0.44670687	0.342025	0.13531508	-0.14716366	0.49515851	-0.011327852	0.957480743	-0.329742717	0.147991286	-0.1755391	0.418765851
P35268	RPL22	ribosomal pr	6146	P35268	-1.7991734	3.14E-05	-1.8738759	2.34E-05	0.056355649	0.79976622	-1.548697829	9.19E-05	-1.678442161	5.19E-05	0.43714431	0.076366493
P49756	RBM25	RNA binding	58517	P49756	-1.3836805	6.75E-06	-1.6919588	1.47E-06	-0.286432244	0.065320419	-1.121325592	3.19E-05	-1.532660478	3.12E-06	0.25053494	0.098845699
Q15287	RNPS1	RNA binding	10921	Q15287	-1.0664698	0.02497103	-1.1611807	0.01715782	0.153412958	0.702514993	-1.048057493	0.026875351	-1.355781964	0.008091979	-0.7370565	0.09365776
Q92541	RTF1	RTF1 homolo	23168	Q92541	-0.4153388	0.10105067	-0.5278438	0.04634708	-0.358204753	0.148737381	-0.52545641	0.047124011	-0.813758061	0.006684965	-0.9634017	0.00262448
P82979	SARNP	SAP domain	84324	P82979	-1.0744062	0.01684583	-1.3101417	0.00631961	-0.092076519	0.803032572	-0.61523486	0.123204554	-0.95039397	0.028740337	0.44471706	0.248233044
Q9UHR5	SAP30BP	SAP30 bindir	29115	Q9UHR5	negInf	NA	negInf	NA	NA	NA	negInf	NA	negInf	NA	NA	NA
Q14160	SCRIB	scribble plan	23513	Q14160	-0.6250304	0.01183888	-0.8817868	0.00181614	0.137893911	0.494773739	-0.771595653	0.003936289	-0.862681145	0.002069649	0.07069538	0.723342291
Q92599	SEPTIN8	septin 8	23176	Q92599	0.32909552	0.01138136	0.3431956	0.00924278	0.16038875	0.149835998	0.03657932	0.725793694	-0.113773148	0.291225074	0.11635966	0.281164648
Q8IYB3	SRRM1	serine and a	10250	Q8IYB3	2.17178657	0.00260829	2.11096752	0.00307273	-0.34273433	0.516341282	1.786938932	0.007622472	1.52335768	0.016619219	-0.8596802	0.126984697
Q9UQ35	SRRM2	serine/argini	23524	Q9UQ35	-1.6234215	0.00083098	-1.4488604	0.00168085	-0.234402985	0.47496324	-1.342425732	0.002640927	-1.274372889	0.003557252	0.10577861	0.743867967
O00422	SAP18	Sin3A associ	10284	O00422	-0.9868128	0.06393067	-1.1003649	0.04347032	-0.148657765	0.754501842	-0.777540644	0.128945769	-1.080664495	0.046480071	-0.0923441	0.845679383
Q96EB6	SIRT1	sirtuin 1	23411	Q96EB6	-0.8541958	0.00086745	-1.0631021	0.00020527	-0.098081421	0.570149288	-0.458491786	0.024382116	-0.74046254	0.002083596	0.1406157	0.42064319
Q15020	SART3	spliceosome	9733	Q15020	-0.7316117	0.01429851	-0.7382521	0.01370039	-0.0263803	0.913288072	-0.860999325	0.006327983	-0.969785682	0.003292038	-0.1248452	0.609273041
Q9Y5B9	SUPT16H	SPT16 homo	11198	Q9Y5B9	-0.6570329	0.13535925	-1.0611178	0.02783951	-0.235416437	0.568273988	-0.136465032	0.739048298	-1.264216555	0.012701022	-0.7686096	0.087981436
Q9UNE7	STUB1	STIP1 homol	10273	Q9UNE7	0.26812144	0.30824493	0.09980432	0.69607216	0.181785254	0.481758712	0.303326368	0.253297224	-0.12508876	0.625404553	0.17393785	0.500300684
P31948	STIP1	stress induce	10963	P31948	-0.1661691	0.2661917	0.03747333	0.79432151	-0.154945268	0.297392271	0.462455263	0.010436861	0.30534089	0.059323184	0.44957992	0.011984985
Q9HCN8	SDF2L1	stromal cell	23753	Q9HCN8	0.1318072	0.62175106	0.75019899	0.04761015	-0.373896145	0.186678085	0.097843307	0.713060207	0.55849915	0.065023393	-0.157831	0.55621873
Q08945	SSRP1	structure spe	6749	Q08945	-0.9500905	0.00802219	-1.1109486	0.00344623	-0.534509813	0.084112711	-0.722594732	0.028556149	-1.336840074	0.001147245	-0.6533104	0.042506846
Q13148	TARDBP	TAR DNA bin	23435	Q13148	-0.3319075	0.32041012	-0.6038782	0.09277729	-0.198089167	0.618386096	-1.322751074	0.003739543	-1.404400451	0.00271725	-1.0074652	0.014139838
O00268	TAF4	TATA-box bir	6874	O00268	0.14411002	0.5040314	0.04970841	0.81539083	0.075940967	0.721957967	0.157545693	0.466360027	0.326078142	0.152102846	0.02219147	0.916866459
Q96FV9	THOC1	THO complex	9984	Q96FV9	negInf	NA	negInf	NA	NA	NA	negInf	NA	negInf	NA	NA	NA
Q8NI27	THOC2	THO complex	57187	Q8NI27	negInf	NA	negInf	NA	NA	NA	negInf	NA	negInf	NA	NA	NA
Q96J01	THOC3	THO complex	84321	Q96J01	-0.6904881	0.08671802	-0.8736342	0.03872218	0.088736915	0.808242672	-0.476581832	0.214791253	-1.034662749	0.019142924	0.48533481	0.207282111
Q13769	THOC5	THO complex	8563	Q13769	negInf	NA	negInf	NA	NA	NA	negInf	NA	negInf	NA	NA	NA
Q86W42	THOC6	THO complex	79228	Q86W42	negInf	NA	negInf	NA	NA	NA	negInf	NA	negInf	NA	NA	NA
Q6I9Y2	THOC7	THO complex	80145	Q6I9Y2	negInf	NA	negInf	NA	negInf	NA	0.48385393	0.176351702	0.084560714	0.800268415	-0.0085308	0.97958831
Q04726	TLE3	TLE family m	7090	Q04726	-0.1596847	0.50537025	0.31037354	0.21233846	-0.13710996	0.565920611	-0.304500839	0.220287931	-0.050788438	0.830042009	-0.1400221	0.55787959
Q13428	TCOF1	treacle ribos	6949	Q13428	0.12891585	0.67674742	-0.0014874	0.99614011	-0.125099342	0.685700036	-0.013742872	0.96434968	-0.085840897	0.780638792	-0.7884258	0.029458269
P31946	YWHAB	tyrosine 3-m	7529	P31946	0.43156211	0.17717128	0.80380457	0.02481409	0.197231747	0.517900376	0.509773526	0.118578156	0.603319663	0.072356586	0.19570094	0.521067452
Q04917	YWHAH	tyrosine 3-m	7533	Q04917	0.22507817	0.29513148	0.25796535	0.23512131	0.117602691	0.574481692	0.431795281	0.063874223	0.519653941	0.032299913	0.33962364	0.129443166
P61981	YWHAG	tyrosine 3-m	7532	P61981	0.42066513	0.05531397	0.43710335	0.04824652	0.16026757	0.417993687	0.147247057	0.455331406	0.09961832	0.609996634	0.06462542	0.739480119
P49459	UBE2A	ubiquitin con	7319	P49459	-1.5760187	0.00039583	-0.9459229	0.00815722	0.487995888	0.109178267	-1.494388474	0.000561042	-0.664363307	0.039713578	0.12222373	0.663693408
O94888	UBXN7	UBX domain	26043	O94888	negInf	NA	negInf	NA	NA	NA	negInf	NA	negInf	NA	NA	NA
Q12768	WASHC5	WASH comp	9897	Q12768	-0.2106905	0.43352131	0.04954203	0.85109773	0.111633485	0.67374717	-0.100614175	0.70404497	-0.142136956	0.593245047	0.48693123	0.093155365
Q9NW82	WDR70	WD repeat d	55100	Q9NW82	1.34570466	0.09382069	1.31811453	0.09946942	-0.555869275	0.449732026	1.142867022	0.143795304	Inf	NA	-0.6212374	0.400696206
Q96B54	ZNF428	zinc finger pi	126299	Q96B54	negInf	NA	negInf	NA	NA	NA	negInf	NA	negInf	NA	NA	NA

					ARR3-ARR3_ISO		ARR3_372T-ARR3_372T_ISO		ARR3_372T_CLB-ARR3_372T_CLB_ISO		ARR3_CLB-ARR3_CLB_ISO	
Protein	Gene	ProteinName	EntrezID	ProteinRef	log2FC	pvalue	log2FC	pvalue	log2FC	pvalue	log2FC	pvalue
Q96CW1	AP2M1	adaptor related protein cor	1173	Q96CW1	-0.1514305	0.51528804	0.18590272	0.427612484	-0.020853852	0.927622478	0.01784051	0.938053574
O00203	AP3B1	adaptor related protein cor	8546	O00203	-0.0159292	0.95439453	0.00735638	0.978927802	-0.060132343	0.829314569	-0.3487463	0.232476916
O14617	AP3D1	adaptor related protein cor	8943	O14617	0.07448873	0.71829962	-0.136961	0.511376405	-0.053730282	0.794295112	-0.3778536	0.094562462
Q9Y2T2	AP3M1	adaptor related protein cor	26985	Q9Y2T2	0.04493625	0.82847559	0.05704457	0.783486859	-0.054997521	0.791037386	-0.3515255	0.118013393
Q92572	AP3S1	adaptor related protein cor	1176	Q92572	-0.0160112	0.93560784	-0.021031	0.915499337	-0.242648594	0.242009602	-0.2509205	0.22769062
P23526	AHCY	adenosylhomocysteinase	191	P23526	-0.0215368	0.96919328	0.36297647	0.520794605	0.158012088	0.777468355	0.37228955	0.510447434
O43865	AHCYL1	adenosylhomocysteinase li	10768	O43865	0.18165379	0.43060263	0.34706467	0.151444087	0.172754934	0.452664541	0.13637795	0.550541739
Q96HN2	AHCYL2	adenosylhomocysteinase li	23382	Q96HN2	negInf	NA	0.14794132	0.896116262	0.297304527	0.793582584	Inf	NA
P07550	ADRB2	adrenoceptor beta 2	154	P07550	-0.0961972	0.82026328	-0.6129506	0.172996788	-0.008713183	0.983553411	-0.2400938	0.57401811
Q8N302	AGGF1	angiogenic factor with G-p	55109	Q8N302	Inf	NA	0.0833406	0.688548843	-0.270916163	0.233634221	-0.3237451	0.301816754
Q12955	ANK3	ankyrin 3	288	Q12955	-0.1087643	0.67736975	-0.1405163	0.592304164	-0.111180357	0.670698696	-0.1916095	0.468778104
O75179	ANKRD17	ankyrin repeat domain 17	26057	O75179	-0.3808236	0.38991205	0.26882825	0.454179212	0.076741426	0.82752167	0.03937946	0.910860902
Q9UKV3	ACIN1	apoptotic chromatin conde	22985	Q9UKV3	0.08314752	0.72142295	0.3008376	0.21814824	-0.083721521	0.719596217	-0.5981071	0.028933355
P53396	ACLY	ATP citrate lyase	47	P53396	-0.0148597	0.94360971	0.08898163	0.673637555	-0.015893328	0.939696092	0.20066987	0.353190717
O75947	ATP5PD	ATP synthase peripheral st	10476	O75947	0.21176779	0.4890851	0.01007062	0.973339494	-0.276777226	0.371061992	-0.0895648	0.766939036
P25440	BRD2	bromodomain containing 2	6046	P25440	-0.2131497	0.61965878	-0.0395894	0.925973201	-0.302609726	0.484544685	-0.6080078	0.179095513
Q15059	BRD3	bromodomain containing 3	8019	Q15059	-0.1994449	0.74798814	0.05063018	0.953803661	-0.590232599	0.357851121	-0.807508	0.222051796
O60885	BRD4	bromodomain containing 4	23476	O60885	-0.1719639	0.79276917	-0.0349775	0.957291225	0.66828455	0.321946577	-0.3371977	0.608735282
Q16543	CDC37	cell division cycle 37, HSP9	11140	Q16543	0.05788824	0.73777011	0.16741383	0.345402034	0.190544223	0.286815325	0.18061136	0.310928
Q6P1J9	CDC73	cell division cycle 73	79577	Q6P1J9	-0.2340547	0.20846533	-0.1300755	0.468872232	-0.192749605	0.292538445	-0.2477162	0.185654445
Q96B23	C18orf25	chromosome 18 open read	147339	Q96B23	0.44361168	0.23032283	0.27410661	0.445564479	-0.159150178	0.653764954	-0.4495646	0.224683112
Q12996	CSTF3	cleavage stimulation facto	1479	Q12996	-0.0763264	0.74084251	-0.1807133	0.440945541	-0.295066284	0.222137106	-0.1929745	0.411818277
Q6PD62	CTR9	CTR9 homolog, Paf1/RNA	9646	Q6PD62	-0.1210037	0.53437032	0.06899157	0.720860522	-0.15933956	0.417451864	-0.221346	0.269040299
Q6UX04	CWC27	CWC27 spliceosome associ	10283	Q6UX04	-0.1966214	0.54671301	-0.1452109	0.65450417	-0.022463221	0.944452366	-0.33342	0.317070008
Q96S94	CCNL2	cyclin L2	81669	Q96S94	Inf	NA	0.36493372	0.394496942	0.34627373	0.416930614	Inf	NA
P61962	DCAF7	DDB1 and CUL4 associated	10238	P61962	0.10694328	0.74648987	-0.5619123	0.116733781	-0.253633959	0.450272485	-0.1004758	0.761247473
Q9UJV9	DDX41	DEAD-box helicase 41	51428	Q9UJV9	0.31972926	0.32660547	-0.149167	0.565750421	0.167896896	0.519360556	0.29226388	0.276258655
Q7L014	DDX46	DEAD-box helicase 46	9879	Q7L014	0.07523509	0.68456492	0.09186088	0.620804424	-0.183585559	0.333912132	0.17241921	0.362469229
Q13838	DDX39B	DExD-box helicase 39B	7919	Q13838	negInf	NA	1.06343138	0.046947046	0.26202422	0.522865409	Inf	NA
Q9NPA8	ENY2	ENY2 transcription and exp	56943	Q9NPA8	0.04480065	0.89120869	-0.4060003	0.236567233	-0.064594937	0.843768361	-0.4309983	0.211424644
P38919	EIF4A3	eukaryotic translation initia	9775	P38919	-0.2550029	0.54694736	0.07569293	0.856560526	-0.035603781	0.932187646	-0.3124537	0.463098338
O75369	FLNB	filamin B	2317	O75369	-0.0667751	0.60682507	-0.0307233	0.81156758	0.025495725	0.843080567	0.18821044	0.16960452
P35269	GTF2F1	general transcription facto	2962	P35269	-0.0175238	0.9831591	Inf	NA	-0.271744081	0.790050496	0.61740936	0.469820176
Q8IXQ4	GPALPP1	GPALPP motifs containing	55425	Q8IXQ4	0.16046839	0.69238118	0.02407307	0.95243386	-0.035896606	0.929133186	0.36834182	0.373898503
Q6Y7W6	GIGYF2	GRB10 interacting GYF prc	26058	Q6Y7W6	-0.1718636	0.50158712	0.35342228	0.185894274	-0.187962244	0.463646403	0.46577699	0.092942387
Q7Z4V5	HDGFL2	HDGF like 2	84717	Q7Z4V5	-0.1782929	0.63776708	0.07040972	0.851596954	-0.168451242	0.656190266	-0.9519181	0.031015999
Q7Z6Z7	HUWE1	HECT, UBA and WWE dom	10075	Q7Z6Z7	0.30092779	0.18741278	0.01526241	0.943513004	0.103809892	0.63237277	0.2661792	0.238068323
Q9NX55	HYPK	huntingtin interacting proti	25764	Q9NX55	-0.3154093	0.31248101	0.5540606	0.16818624	0.10032023	0.735553376	-0.0902275	0.829309101
O60921	HUS1	HUS1 checkpoint clamp co	3364	O60921	-0.0349635	0.77381303	NA	NA	NA	NA	0.48557437	0.012945248
Q96ST2	IWS1	interacts with SUPT6H, CTI	55677	Q96ST2	-0.1926652	0.75041603	-0.0928084	0.877910206	-0.018372106	0.975721964	-0.889485	0.166975601
O00505	KPNA3	karyopherin subunit alpha	3839	O00505	-0.2210933	0.15377132	-0.1855593	0.222603343	-0.12801279	0.388295451	0.00888361	0.951074923
Q07666	KHDRBS1	KH RNA binding domain co	10657	Q07666	0.03544428	0.94964131	-0.2045756	0.716607437	-0.525793067	0.362011528	0.39781104	0.48541127
Q92945	KHSRP	KH-type splicing regulatory	8570	Q92945	0.00792436	0.96701304	-0.0750103	0.696887325	-0.152582384	0.435137724	0.09366814	0.627623482
Q8WVC0	LEO1	LEO1 homolog, Paf1/RNA	123169	Q8WVC0	-0.0052192	0.96788528	0.43245205	0.008801893	-0.158991299	0.241358349	-0.5105568	0.003616914
Q9Y4Z0	LSM4	LSM4 homolog, U6 small r	25804	Q9Y4Z0	-0.176863	0.67862516	-0.0063737	0.98800893	0.06930696	0.870311575	0.91805675	0.109687149
O95777	LSM8	LSM8 homolog, U6 small r	51691	O95777	-0.1910653	0.69261464	0.09814968	0.838388708	-0.133475718	0.7817853	0.11843325	0.84073572
P41227	NAA10	N-alpha-acetyltransferase	8260	P41227	0.00325321	0.98867359	0.08799656	0.702350004	-0.209091414	0.374098804	0.31306407	0.196389366
Q9BXJ9	NAA15	N-alpha-acetyltransferase	80155	Q9BXJ9	0.16062515	0.57576101	0.05882743	0.836180717	0.017377191	0.951231672	0.20561238	0.476630691
P32120	P32120	NA	NA	P32120-2	0.0454152	0.93700873	0.09832401	0.864246689	-0.023454705	0.967438393	0.39889562	0.494199962
Q9Y2X3	NOP58	NOP58 ribonucleoprotein	51602	Q9Y2X3	0.29798284	0.31991693	0.54177197	0.090000837	0.374379734	0.219466182	-0.0167827	0.953840466
Q14978	NOLC1	nucleolar and coiled-body p	9221	Q14978	-0.4437434	0.22431363	-0.325734	0.361982364	-0.416891962	0.251060854	-1.0100446	0.01713114
P49790	NUP153	nucleoporin 153	9972	P49790	-0.382382	0.56104759	0.58318444	0.472711487	0.379133987	0.636207782	-0.1389736	0.830509179
Q8N7H5	PAF1	PAF1 homolog, Paf1/RNA	54623	Q8N7H5	-0.0332225	0.78237811	-0.1187677	0.337003402	0.001752889	0.988342881	-0.6301003	0.000632089
O43447	PPIH	peptidylprolyl isomerase H	10465	O43447	-0.1073887	0.72586484	-0.0367257	0.904212904	-0.055505262	0.855766299	0.39084571	0.222753076
Q8TBX8	PIP4K2C	phosphatidylinositol-5-pho	79837	Q8TBX8	-0.1732533	0.55524794	0.03225847	0.911567345	-0.212345062	0.472155532	-0.6254228	0.056974981
Q9H814	PHAX	phosphorylated adaptor for	51808	Q9H814	0.18669067	0.54662144	-0.2445014	0.433638615	-0.237051475	0.447242949	0.39969278	0.214718077
Q8TF01	PNISR	PNN interacting serine anc	25957	Q8TF01	-0.0223195	0.95085792	0.01986096	0.956264162	-0.278369334	0.450610333	-0.3309048	0.373401966
Q86U42	PABPN1	poly(A) binding protein nuc	8106	Q86U42	NA	NA	0.68873218	0.004465161	-0.066884219	0.604862861	NA	NA
O43172	PRPF4	pre-mRNA processing facto	9128	O43172	0.50511934	0.16487442	0.00215651	0.994901942	-0.077284047	0.819232665	0.52991746	0.225707441
O75400	PRPF40A	pre-mRNA processing facto	55660	O75400	-0.1557046	0.74374207	-0.08707	0.822404332	-0.161144202	0.679477871	0.32463503	0.502138808
Q9NY27	PPP4R2	protein phosphatase 4 regu	151987	Q9NY27	0.28406182	0.50563806	0.55377434	0.213736497	-0.212585985	0.61580391	0.16508267	0.748982444
O15355	PPM1G	protein phosphatase, Mg2+	5496	O15355	0.06738581	0.71724609	0.37161874	0.072309052	0.0521232	0.779015258	0.47859144	0.02858543
Q3YEC7	RABL6	RAB, member RAS oncoge	55684	Q3YEC7	negInf	NA	0.08008044	0.891380083	0.064073376	0.912963266	negInf	NA
O60671	RAD1	RAD1 checkpoint DNA exor	5810	O60671	0.37753394	0.29069395	NA	NA	NA	NA	0.20826997	0.538948663
Q9NS91	RAD18	RAD18 E3 ubiquitin protein	56852	Q9NS91	0.17813272	0.65279732	0.00069395	0.998592275	-0.0957295	0.808072134	-0.313711	0.434437369
A1A4S6	ARHGAP10	Rho GTPase activating prol	79658	A1A4S6	0.4627626	0.05480718	0.28665103	0.201403137	-0.209005118	0.339845536	0.43438717	0.067937014
P35268	RPL22	ribosomal protein L22	6146	P35268	-0.1482218	0.50988534	0.10225371	0.646932283	0.047211928	0.831616486	0.23256685	0.310708181

					ARR3-ARR3_ISO		ARR3_372T-ARR3_372T_ISO		ARR3_372T_CLB-ARR3_372T_CLB_ISO		ARR3_CLB-ARR3_CLB_ISO	
Protein	Gene	ProteinName	EntrezID	ProteinRef	log2FC	pvalue	log2FC	pvalue	log2FC	pvalue	log2FC	pvalue
P49756	RBM25	RNA binding motif protein	58517	P49756	-0.3361924	0.03662878	-0.0738375	0.597157644	-0.176894062	0.223895229	0.20077481	0.17295146
Q15287	RNPS1	RNA binding protein with s	10921	Q15287	0.38034841	0.35505689	0.39876068	0.333541249	0.185747195	0.644509593	-0.510121	0.224474603
Q92541	RTF1	RTF1 homolog, Paf1/RNA p	23168	Q92541	0.02947342	0.89864599	-0.0806442	0.728355072	-0.256440844	0.285724762	-0.5757235	0.033221275
P82979	SARNP	SAP domain containing ribo	84324	P82979	-0.2972835	0.42927389	0.16188784	0.662343022	0.062464249	0.865485917	0.23951007	0.521289321
Q9UHR5	SAP30BP	SAP30 binding protein	29115	Q9UHR5	NA	NA	0.28624871	0.210972159	-0.114045802	0.585181683	NA	NA
Q14160	SCRIB	scribble planar cell polarity	23513	Q14160	-0.0660176	0.74083635	-0.2125829	0.302214085	-0.046911949	0.813863018	-0.1332162	0.50910132
Q92599	SEPTIN8	septin 8	23176	Q92599	0.35039203	0.00831922	0.05787583	0.581218422	-0.106576723	0.320737788	0.30636294	0.015996424
Q8IYB3	SRRM1	serine and arginine repetit	10250	Q8IYB3	0.40077795	0.45015581	0.01593031	0.975598818	-0.186831894	0.720916364	-0.116168	0.823774966
Q9UQ35	SRRM2	serine/arginine repetitive r	23524	Q9UQ35	-0.2142433	0.51262387	0.06675247	0.83630293	-0.039755812	0.901971551	0.12593831	0.697690316
O00422	SAP18	Sin3A associated protein 1	10284	O00422	0.00584023	0.99016651	0.21511238	0.652042758	0.025540605	0.95701959	0.06215385	0.895703175
Q96EB6	SIRT1	sirtuin 1	23411	Q96EB6	-0.1618366	0.35721147	0.23386743	0.195711355	0.160802908	0.360126606	0.0768605	0.655029135
Q15020	SART3	spliceosome associated fa	9733	Q15020	0.06471328	0.78977566	-0.0646744	0.78989849	-0.166820339	0.497476979	-0.0337516	0.889225309
Q9Y5B9	SUPT16H	SPT16 homolog, facilitates	11198	Q9Y5B9	0.54797058	0.20344533	1.06853846	0.027042294	0.34487187	0.408783828	0.01477742	0.971120906
Q9UNE7	STUB1	STIP1 homology and U-box	10273	Q9UNE7	0.2134928	0.41150165	0.24869773	0.342394325	-0.011400278	0.96423331	0.20564539	0.428185695
P31948	STIP1	stress induced phosphopro	10963	P31948	-0.1347004	0.36094782	0.49392399	0.007476877	0.133167167	0.366152681	0.46982479	0.009647019
Q9HCN8	SDF2L1	stromal cell derived factor	23753	Q9HCN8	-0.0540199	0.83854104	-0.0879838	0.740633698	-0.245719753	0.457962776	0.16204526	0.546003529
Q08945	SSRP1	structure specific recogniti	6749	Q08945	0.45351381	0.13286856	0.68100957	0.036246453	0.227622326	0.425465554	0.33471319	0.251963064
Q13148	TARDBP	TAR DNA binding protein	23435	Q13148	0.72895092	0.05120252	-0.2618926	0.426702526	-0.071571294	0.82423337	-0.0804251	0.838478195
O00268	TAF4	TATA-box binding protein a	6874	O00268	0.11336012	0.59714625	0.12679579	0.555319071	0.389729857	0.095149526	0.05961062	0.779655269
Q96FV9	THOC1	THO complex 1	9984	Q96FV9	NA	NA	0.51248702	0.369181064	-0.168449383	0.756330401	NA	NA
Q8NI27	THOC2	THO complex 2	57187	Q8NI27	NA	NA	0.40526554	0.321535705	0.092761512	0.808623768	NA	NA
Q96J01	THOC3	THO complex 3	84321	Q96J01	0.11484153	0.75376343	0.3287478	0.379878123	-0.046187002	0.899336892	0.51143943	0.18622677
Q13769	THOC5	THO complex 5	8563	Q13769	NA	NA	0.58208139	0.193038474	0.035226898	0.929178498	NA	NA
Q86W42	THOC6	THO complex 6	79228	Q86W42	NA	NA	0.43698427	0.125531156	-0.143709993	0.559722522	NA	NA
Q6I9Y2	THOC7	THO complex 7	80145	Q6I9Y2	negInf	NA	0.12747726	0.703768515	0.010405201	0.975105189	-0.0163087	0.960992238
Q04726	TLE3	TLE family member 3, tran	7090	Q04726	0.01821004	0.93857343	-0.1266061	0.595468579	-0.342951937	0.172617756	0.01529793	0.948378634
Q13428	TCOF1	treacle ribosome biogenes	6949	Q13428	-0.4829372	0.14378565	-0.625596	0.06902538	-0.56729077	0.093457065	-1.1462637	0.004903343
P31946	YWHAB	tyrosine 3-monooxygenase	7529	P31946	0.10293431	0.73322658	0.18114573	0.551769634	-0.097550593	0.746592846	0.10140351	0.737017537
Q04917	YWHAH	tyrosine 3-monooxygenase	7533	Q04917	-0.1519946	0.47105898	0.05472252	0.79225116	0.109693991	0.599998027	0.07002636	0.736447777
P61981	YWHAG	tyrosine 3-monooxygenase	7532	P61981	0.2063607	0.30353989	-0.0670574	0.73012425	-0.131124331	0.504584553	0.11071854	0.571535491
P49459	UBE2A	ubiquitin conjugating enzy	7319	P49459	-0.0220937	0.93697301	0.05953651	0.831473667	0.259465918	0.365998306	-0.3878659	0.189909037
O94888	UBXN7	UBX domain protein 7	26043	O94888	NA	NA	0.25107319	0.558825945	-0.176831398	0.676976819	NA	NA
Q12768	WASHC5	WASH complex subunit 5	9897	Q12768	-0.0386929	0.88338752	0.07138334	0.787052409	-0.23037193	0.3936152	0.3366048	0.224206333
Q9NW82	WDR70	WD repeat domain 70	55100	Q9NW82	0.43763501	0.54855601	0.23479736	0.745181161	Inf	NA	0.3722669	0.608497882
Q96B54	ZNF428	zinc finger protein 428	126299	Q96B54	NA	NA	-0.3053317	0.421854455	-0.20635163	0.498337119	NA	NA

Publishing Agreement

It is the policy of the University to encourage open access and broad distribution of all theses, dissertations, and manuscripts. The Graduate Division will facilitate the distribution of UCSF theses, dissertations, and manuscripts to the UCSF Library for open access and distribution. UCSF will make such theses, dissertations, and manuscripts accessible to the public and will take reasonable steps to preserve these works in perpetuity.

I hereby grant the non-exclusive, perpetual right to The Regents of the University of California to reproduce, publicly display, distribute, preserve, and publish copies of my thesis, dissertation, or manuscript in any form or media, now existing or later derived, including access online for teaching, research, and public service purposes.

DocuSigned by:
087E9B6AD399486...
Author Signature

3/8/2022
Date